Investigating homeostatic disruption by constitutive signals during biological ageing

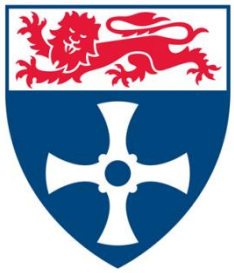

Alvaro Martinez Guimera
Institute for Cell and Molecular Biosciences (ICaMB)
Newcastle University

A thesis submitted in partial fulfilment of
the requirements for the degree of

Doctor of Philosophy

September 2017

‘If we only look at the world with a microscope, we might be able to see its structure and even its beauty, but not its goodness’ - Felicisimo Martinez Diez.

(‘Si solo miramos el mundo con el microscopio, quiza lleguemos a ver su estructura y hasta su belleza, pero no su bondad’ – Felicisimo Martinez Diez).

I would like to dedicate this thesis to my parents Belen Guimera Ferrer-Sama and Jose Maria Martinez Diaz. I hope that one day I am able to give as much as you have given me. Thank you.

(Quiero dedicar esta tesis a mis padres Belen Guimera Ferrer-Sama y Jose Maria Martinez Diaz. Ojala algun dia sepa dar tanto como me habeis dado vosotros. Gracias).

Acknowledgements

I would like to thank my supervisors Daryl Shanley, Viktor Korolchuk and Carole Proctor for giving a chance at research to an over-confident interviewee. I am thankful that our conversations over the years have encompassed so much more than just science.

I would also like to express my gratitude to Anne McArdle, Aphrodite Vasilaki, Brian McDonaugh, Malcolm Jackson and Liz Veal for continued advice and support. Having someone else display an interest in my work has been a great source of motivation.

I am thankful to the Centre for Integrated Research into Musculoskeletal Ageing (CIMA) and through them, Arthritis Research UK and the Medical Research Council for funding this PhD project.

I feel very privileged to have shared my time during the PhD with so many nice people. Thank you to Carmen Martin Ruiz, Alberto Sanz, Marina Garcia Macia, Nuria Martinez Lopez, Diego Manni, Berni Carroll, Lucia Sedlackova, Yoanna Rabanal, Rhoda Stefanatos, Glynn Nelson, Philip Hall and Dan Padgett for enriching my time at the institute. A very special thank you goes to David Hodgson, Neil McDonald, Ciaran Welsh and Gisela Otten for bringing so much to my every day. Thank you also to so many other friends that I could not possibly list here, yet have helped me so much more than they will ever know. You know who you are.

Thank you ever so much to my dearest brothers. Always knowing when to support me, when to tell me off and when to laugh at me. I could not have done this without knowing that you were there for me.

I will always be grateful to my Pija, who opened my eyes to a world so much richer than I had realised. Only you know how much I have to acknowledge you. Thank you.

Finally, I would like to say my deepest *gracias* to my parents. Nothing I could write here would ever do justice to how much of what I have done and of who I am is thanks to you. There where words fail me, I can only say thank you.

Abstract

Ageing and disease can be understood in terms of a loss in biological homeostasis. This will often manifest as a constitutive elevation in the basal levels of biological entities. Examples include chronic inflammation, hormonal imbalances and oxidative stress. The ability of reactive oxygen species (ROS) to cause molecular damage has meant that chronic oxidative stress has been mostly studied from the point of view of being a source of toxicity to the cell. However, the known duality of ROS molecules as both damaging agents and cellular redox signals implies another perspective in the study of sustained oxidative stress. This is a perspective of studying oxidative stress as a constitutive signal within the cell. In this work a computational modelling approach is undertaken to examine how chronic oxidative stress can interfere with signal processing by redox signalling pathways in the cell. A primary outcome of this study is that constitutive signals can give rise to a 'molecular habituation' effect that can prime for a gradual loss of biological function. Experimental results obtained highlight the difficulties in testing for this effect in cell lines exposed to oxidative stress. However, further analysis suggests this phenomenon is likely to occur in different signalling pathways exposed to persistent signals and potentially at different levels of biological organisation.

Table of contents

List of figures

List of tables

Abbreviations

ß-TrCP	β-Transducin repeat-Containing Protein
Akt-P(ser473)	Phospho Serine 473 Akt
AOX	Antioxidant
AP-1	Activator Protein 1
AP	Antagonistic Pleiotropy
ARE	Antioxidant Response Element
ASK-1	Apoptosis signal-regulating kinase 1
AU	Arbitrary Units
BSA	Bovine Serum Albumin
CA	Cellular Automaton
CMS	Coupled Motif Structures
CS	Constitutive Signal
DMEM	Dulbecco's Modified Eagle Medium
DMSO	Dimethyl sulfoxide
DST	Disposable Soma Theory
ECL	Enhanced Chemiluminescence
EDTA	Ethylenediaminetetraacetic acid
ETC	Electron Transport Chain
FCS	Fetal Calf Serum
FFL	Feed Forward Loop
FR	Free Radical
FRTA	Free Radical Theory of Ageing
GOX/CAT	Glucose Oxidase – Catalase enzymatic system

GPx	Glutathione Peroxidase
GSK3ß	Glycogen Synthase Kinase 3 ß
GSK3ß-P(ser9)	Phospho Serine 9 Glycogen Synthase Kinase 3 ß
H_2O_2	Hydrogen Peroxide
ssH_2O_2	Steady State H_2O_2
HD	Huntington's Disease
HIF-1	Hypoxia-Inducible Factor 1
HRP	Horse Radish Peroxidase
HSF1	Heat Shock Factor 1
HSP	Heat Shock Protein
IκB	Inhibitor of κB
IKK	IκB Kinase
JNK	c-Jun N-Terminal Kinases
Keap1	Kelch-like ECH-Associated Protein 1
LAMP1	Lysosomal-associated membrane protein 1
LSODA	Livermore Solver for Ordinary Differential Equations
MA	Mutation Accumulation
MAPK(K)	Mitogen Activated Protein Kinase (Kinase)
NADPH	Nicotinamide adenine dinucleotide phosphate
NFκB	Nuclear Factor kappa-light-chain-enhancer of activated B cells
NLS	Nuclear Localisation Signal
NO	Nitric Oxide
NOX	NADPH Oxidase

NP-40	Octylphenyl-polyethylene glycol
Nrf2	Nuclear Factor (erythroid-derived 2)-like 2
ODE	Ordinary Differential Equation
OS	Oxidative Stress
PAGE	Polyacrylamide gel electrophoresis
PAP1	Poly(A) polymerase 1
PBS	Phosphate-Buffered Saline
PBS-T	PBS + 0.1% TWEEN
PDE	Partial Differential Equation
PFL	Positive Feedback Loop
Prx	Peroxiredoxin
$PrxSO_3$	Peroxiredoxin superoxide
P/S	Penicillin/Streptomycin
RMS	Root Mean Square
ROS	Reactive Oxygen Species
SA-ß-Gal	Senescence-associated beta-galactosidase
SAPK	Stress Activated Protein Kinase
SASP	Senescence Associated Secretory Phenotype
SBML	Systems Biology Markup Language
SBGN	Systems Biology Graphical Notation
SDS	Sodium dodecyl sulfate
SOD	Superoxide Dismutase
TEMED	Tetramethylethylenediamine
TPx1	Thioredoxin Peroxidase 1
UII	Urotensin II

Chapter 1

Introduction

1.1 Biogerontology: What is biological ageing?

What is ageing? A widely accepted definition for the 'ageing' phenomenon that takes place in most living organisms is

'*the progressive loss of function accompanied by decreasing fertility and increasing mortality with advancing age*' (Kirkwood and Austad, 2000).

This definition reflects the state of knowledge in the field that aims to elucidate the underlying molecular causes of ageing, that is, the field of biogerontology. This definition reflects the current state of the field of biogerontology in both what the definition says and what it does not say. As stated in the definition, ageing occurs over time and is therefore a process. Although this remark may seem trivial, it does imply a few features worth of note. Namely the fact that there is a time window to observe and probe the phenomenon and secondly, the fact that the phenomenon involves changes which are recognisable from a reference point. Related to this is the fact that ageing is currently understood as a continuous process. As implicitly stated by the word *progressive* in the definition, the fact that ageing is viewed as a continuous process means there is no defined boundary at which an organism starts to age.

Within this setting, the definition talks about a *loss of function*. This is the very core of the definition and the understanding of the ageing process. The abstract nature of this phrase reflects the scope that is necessary to encompass the diverse observations that have been made on the ageing process. This is illustrated by the lack of a gold-standard ageing biomarker (Martin-Ruiz et al., 2011, Bürkle et al., 2015). The lack of specification regarding what *function* entails is a reflection of first of all the generality of the process. Secondly, this phrase states consequence, where the effect of the ageing process is an interference with the end purpose of a given biological system. Whatever a biological system has evolved to do to, it is somewhat less able to do it as the ageing process progresses. The effects of ageing could thus be viewed as a general dissipation of evolutionary strategies that ensure organism survival.

In an attempt to further contextualise the *loss of function* statement, two robust observations of the ageing process are more specifically defined. There is a *decreased fertility* and *increased mortality*. Note that the incorporation of these two specifications in the definition aims to make the ageing process measurable and quantifiable more than attempting to distinguish the ageing process from diseases and pathologies. It is the generality of the definition of ageing what makes this process distinguishable from diseases which may also increase mortality or decrease fertility with age. Indeed, diseases are distinguishable processes because they involve the loss of a *specific set* of functions. All humans will age, but not all humans will develop a particular disease.

The last two important points to make are on the use of the words '*accompanied*' and '*advancing*'. The former implies uncertainty regarding the underlying causality of the recurrent observations of loss of fertility and increased mortality and furthermore the relative timing of such events. It is well established that the ageing process is highly heterogeneous in, firstly, the specific functional losses that may be observed and secondly, the timing at which such dysfunctionalities may occur (Kirkwood, 2005, Passos et al., 2008, Partridge, 2010, Bürkle et al., 2015). The use of the word '*advancing*' follows from the aforementioned principle of time-dependency of the process. However, there is a reason why the word '*increasing*' may not be deemed a better choice. The reason is the fact that mortality correlates better with 'biological age' than chronological age (Bürkle et al., 2015). The ageing process may not significantly 'advance' even though time may 'increase'.

The current definition of ageing has classed some organisms as being "immortal" since they show no loss in functional markers, reproductive ability or any increase in mortality with chronological time (Archer and Hosken, 2016). Questions have been raised on whether the ageing process actually still occurs in these organisms, albeit really slowly, and whether this apparent immortality is an artefact of the current definition of ageing (Khokhlov, 2014, Archer and Hosken, 2016, Singer, 2016). In any case, the current dogmas on which the field of biogerontology rests state the *dynamic* nature of ageing, the overall *generality* of the process and the *heterogeneity* of underlying observations. Within this framework the field of biogerontology has attempted to shed light into the underlying process behind the ageing phenomenon by asking both *why* we age and *how* we age.

1.2 Theories of biological ageing

To understand the historical and current development of the field of biogerontology, it is useful to understand how biological problems are addressed in the life sciences. Tinbergen's four questions (Bateson and Laland, 2013), which are as pragmatic as they are logical, establish four facets to the investigation of a given biological problem (See Figure 1.1). Whilst a discussion on the universality of this paradigm (Bateson & Laland 2013) is beyond the scope of this work, Tinbergen's four questions provide a useful starting point to understand how evolutionary and mechanistic theories of ageing overlap with each other.

	Response	Life History
How	Mechanistic causation	Developmental causation
Why	Adaptive context	Evolutionary context

Figure 1.1 *Tinbergen's four questions. A researcher can ask how a given biological phenomenon occurs (proximate) or alternatively the researcher may be interested in the end purpose of the biological phenomenon, that is, why it takes place (ultimate). Proximate questions are associated with enquiries on the nature of mechanistic causations in themselves, whether it is an acute response, or a developmental response taking place over an organism's life. Ultimate questions are associated with enquiries on a broader (higher order) context, whether that context is a current context or part of a life history. Whilst a shift to the right on the table involves the contextualisation of the biological phenomenon in the context of time, a shift downwards involves the contextualisation of the phenomenon in the context of the environment. It goes without saying that the boundaries between the four questions are fuzzy and the questions, non-exclusive. However, they provide a pragmatic approach to understand biogerontology.*

1.2.1 Evolutionary theories of ageing

Asking *why* implies a higher order question regarding the level of abstraction, and therefore a higher order (ultimate) answer, than asking *how* (proximate answer) (Bateson and Laland, 2013). In biology, the ultimate higher level entered when seeking an explanation to observed phenomena is evolution. In trying to understand why most living organisms age, biogerontologists therefore developed evolutionary frameworks to make sense of the experimental observations available at the time.

Ageing was first expressed within an evolutionary framework by August Weismann in 1882. Weismann viewed ageing as a process selected for by natural selection which would remove the old individuals from a population to free resources for the newer generations (Weismann et al., 1891). Within this context, ageing is the result of natural selection on the population scale rather than at the level of the individual and implies a 'programmed ageing' process.

The next major breakthroughs in the evolutionary thinking on ageing came in the mid twentieth century with Peter Medawar's *Mutation Accumulation* (MA) theory of ageing (Medawar, 1952) and George William's *Antagonistic Pleiotropy* (AP) theory of ageing (Williams, 1957). Later on, in 1977, Tom Kirkwood would propose the *Disposable Soma* theory (DST) of ageing (Kirkwood, 1977). These are the three main evolutionary theories of ageing within the field of biogerontology. Central to the development of all theories was the 'Selection shadow' concept put forward by John Haldane in 1941(Haldane, 1941).

The 'selection shadow' concept refers to the decline in evolutionary selection pressure with age once an organism has passed its reproductive window. In other words, the inability of evolution to select against late-onset, deleterious, traits that do not significantly affect an organism's reproductive ability. The classical example for this phenomenon is Huntington's Disease (HD). This disease is caused by a dominant negative mutation and so it would be expected that natural selection would have selected against individuals with such mutations, yet the disease prevalence in the population is relatively high (Bates et al., 2014). However the first symptoms of HD commonly start at the age of 40, giving the individual ample time to reproduce and pass down the HD alleles. Thus, natural selection is very weak against genotypic changes that result in adverse effects later on in organismal life.

Mutation accumulation theory is based on the 'selection shadow' concept in that because germline mutations with late-onset detrimental effects cannot be removed by natural selection, a mutational load would be established on the germline which would drive the development of a variety of dysfunctionalities at older age.

Antagonistic pleiotropy theory more specifically builds from the abstract nature of the mutation accumulation theory. Williams proposed that natural selection against late-onset traits is strong enough to provide a selection pressure. This is because more subtle phenotypic changes associated with senescence, like a slightly slower pace or slightly worse immune system, can occur earlier in the decline of physiological function and affect organism survival at a much earlier age than that at which the detrimental phenotype is established. Therefore, traits with late-onset detrimental effects must have a previous beneficial effect that associates with increased reproductive ability if they are to remain within the gene pool of the population.

The Disposable Soma theory is the least abstract of all the theories in the sense that it narrows the causative molecular players to defined functional classifications. This theory argues that because organisms evolve in environments with a limited number of resources, evolution shapes a trade-off in the resource (energy) allocation between reproduction and maintenance and repair processes. The basic premise is that whilst reproduction is the ultimate goal of the evolutionary process, the organism has first to survive to the reproductive age, and perhaps a little beyond, to care for the new offspring until they become autonomous. The result of this evolved trade-off is damage accumulation throughout life history as determined by the evolved energy-allocation to maintenance and repair processes. The DST can be said to be an instance Life History Theory (Selman et al., 2012).

These three main evolutionary theories of ageing view the ageing process as an epiphenomenon, whether arising from a weaker selection past the reproductive period or from the selection of traits which maximise reproductive fitness. This is in contrast to Weismann's original view of ageing as a programmed process.

1.2.2 Mechanistic theories of ageing

In the 90s, more than 300 theories of ageing had been identified (Medvedev, 1990) but only a handful have acquired a critical weight within the field of biogerontology. In the late 1950s a number of authors related somatic mutational load to lifespan (Failla, 1958, Szilard, 1959). This somatic mutation theory (Morley, 1995) gained strength from the observed correlations between DNA repair rates and lifespan, as well as from the aged-like phenotypes of some strains of mutator mice (Promislow, 1994, Kennedy et al., 2012).

In the late 1960s the cross-linking theory of ageing (Bjorksten, 1968) proposed protein aggregation as the driving mechanism of loss of functional homeostasis with age. This theory would later be further generalised (Terman and Brunk, 2004). Around this time, Leonard Hayflick's discovery of a limited capacity for cells to undergo division (Hayflick, 1965) led to the formulation of the telomere loss theory of ageing (Kim Sh et al., 2002) out of which would stem the idea that the gradual accumulation of senescent cells in tissues can drive a progressive functional loss (Campisi, 2003). Both the somatic mutation theory and the telomere loss theory placed the concept of genomic instability at the centre of the ageing process.

By the turn of the century, the immune system and the dysregulation of inflammatory factors were introduced as the potential drivers of the ageing phenotype in the inflamm-ageing theory of ageing (Franceschi et al., 2000). Shortly after, Mikhail Blagoskonny argues for a *hypertrophy* theory of ageing (Blagosklonny, 2006) where the ageing process arises as an epiphenomenon of organism developmental programs which continue to be active in old age. The oldest and arguably the most influential theory of ageing, however, is the free radical theory of ageing.

The free radical theory of ageing (FRTA) proposed by Denham Harman (Harman, 1955) has arguably been the most influential mechanistic theory of ageing. His theory suggested that increased production of reactive oxygen species with age would drive the ageing process through increased molecular damage, with the end result of a loss of functional and structural integrity. This theory displayed the attractiveness of being based on a fundamental and irrefutable physical property of ROS molecules, their high reactivity, and the fact that they are unavoidably produced endogenously by metabolic processes. The concept that random molecular damage would drive the ageing process

intuitively fitted the observations on the variability of the ageing process and the required gradual loss of homeostasis of biological mechanisms.

The discovery of superoxide dismutases in the late 1960s by Irwin Fridovich (McCord and Fridovich, 1969) proved the evolution of mechanisms against ROS molecules. The discovery of antioxidant proteins established a paradigm on the detrimental nature of ROS and gave momentum to the FRTA. However, the eventual discovery of the physiological functions of ROS and the establishment of the field of 'Redox Biology' broke the paradigm of ROS molecules being solely a detrimental by-product of metabolism. Since the conception of the FRTA, a wealth of correlative evidence has been established in various organisms between molecular oxidative damage and lifespan, although some strong criticism of this theory has also been established (Kirkwood and Kowald, 2012, Barja, 2013, Vina et al., 2013, Liochev, 2015, Sanz, 2016).

Returning to Tinbergen's four questions, it is apparent that theories on the proximate causes of ageing are primarily concerned with mechanisms which may cause a systemic interference with cellular functions over a lifetime (Figure 1.2). Such theories originally arose as extrapolations of how lower-scale cellular observations could be relevant within a whole organism over a whole life time. Meanwhile, whilst the mutation accumulation and antagonistic pleiotropy theories arose from higher-scale observations of animal populations, the disposable soma theory emerged after a number of the main mechanistic theories of ageing had been put forwards. Consequently, DST seems more specific and refined regarding the cellular processes relevant to ageing and thus much easier to relate to experiments addressing how ageing occurs at the cellular scale.

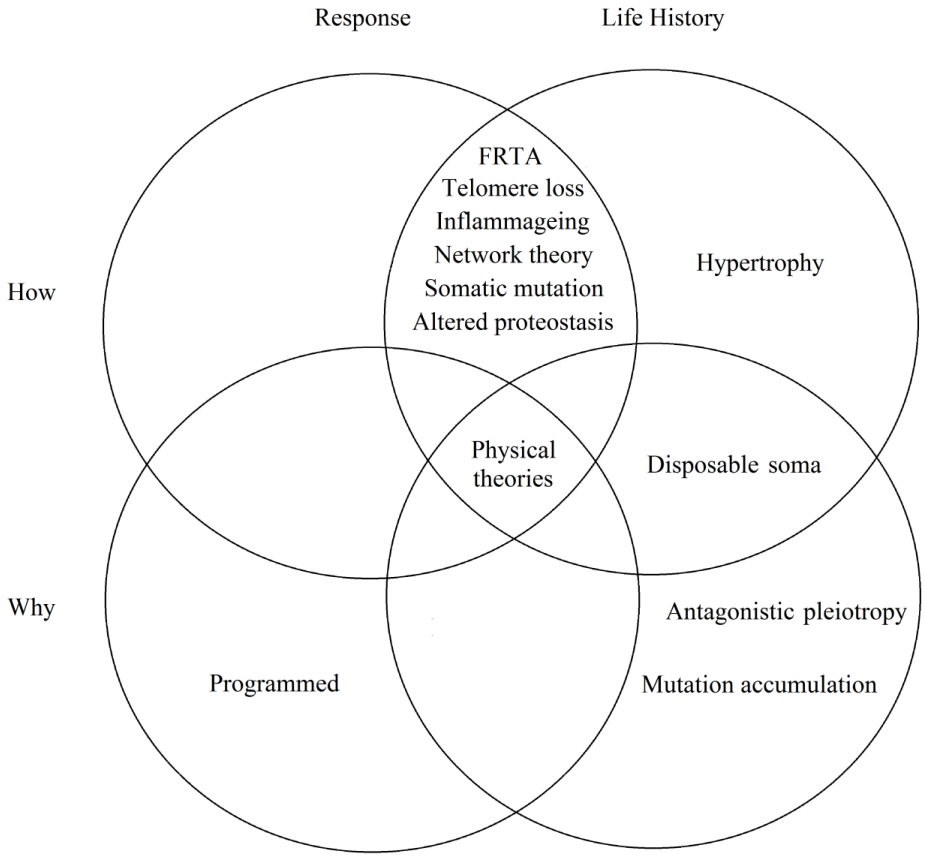

Figure 1.2. *A pragmatic classification of the main theories of ageing according to Tinbergen's four questions. Most proximal theories of ageing refer to specific mechanisms occurring and being affected over a time scale of an individual life time, but only the Hypertrophy theory is an explicitly developmental theory. The most abstract evolutionary theories can explain why ageing occurs but are not explicit about the mechanism behind the homeostatic decline observed with age. Disposable soma theory predicts both why and how ageing occurs without explicitly necessitating a specific mechanistic theory since all of them except the Hypertrophy- theories of ageing are centred around the concept of random molecular damage. The Programmed theory is the only evolutionary theory that views ageing as an acute adaptive response but makes no predictions on what the mechanism might be. Notice that the rest of the theories account for the arrow of time in some way, consistent with the notion of ageing being a continuous dynamic process. Physical theories of ageing are the most abstract and encompass all classifications.*

Whilst these are arguably the mechanistic theories of ageing that gained the most momentum, the list is by no means exhaustive (Medvedev, 1990, Tosato et al., 2007). The acknowledgement that no single mechanistic theory of ageing convincingly explained the plethora of available experimental observations led to the formulation of ageing as a network-scale phenomenon (Franceschi, 1989, Kowald and Kirkwood, 1996, Kirkwood, 2005, Mitnitski et al., 2017). The network theory of ageing arose as a prediction from the DST which places random molecular damage as the driver of the ageing process and thus would be expected to affect multiple mechanisms heterogeneously. Further attempts at the abstraction and unification of the theories of ageing materialised in the form of physical theories of ageing. The most notable examples are *loss of complexity* theory of ageing (Lipsitz and Goldberger, 1992), the *entropic* theory of ageing (Bortz, 1986) and the *reliability* theory of ageing (Gavrilov and Gavrilova, 2001).

The different mechanistic theories argue for different drivers of the ageing process. However, none of these argued drivers of the ageing process has been unequivocally resolved into being causal or consequential of the ageing process. Indeed, each theory argues that the time-dependent change in the proposed ageing-driver underlies the progression of the ageing process. However, the only explanation as to why the ageing-driver starts changing in the first place is the core concept behind both the MA and DST, which argue that random molecular damage can cause stochastic disruptions to the homeostatic organisms operating in cells. Reactive oxygen species, as argued by the FRTA, are the main molecular players with the physical properties required to cause molecular damage. Thus, exploring the mechanisms that underlie cellular redox homeostasis seems an intuitive way to understand how damage may accumulate in cells to potentially cause a functional decline.

1.3 Understanding biological ageing as a network of hallmarks

It is evident that the ageing phenomenon manifests at both the macroscopic (tissues, organ systems, life style, demographics…) and the microscopic levels (molecules and cells). All of the ageing theories explain macroscopic age-related changes in terms of microscopic age-related changes. This effectively means that the ageing phenomenon is best understood from a bottom-up approach. This does not at all dismiss the utility of top-down approaches, since these can direct and constrain research efforts directed at

the microscopic level. As a phenomenon, ageing displays a series of hallmarks that span multiple levels of biological organisation (Lopez-Otin et al., 2013). Therefore, any bottom-up approach to the study of biological ageing must eventually span multiple biological scales.

The proposed hallmarks of ageing at the microscopic level, despite being arguably mammalian-centred, provide a good starting point to understand the causal interrelations between age-related phenomena observed at the molecular and cellular level. The currently proposed nine hallmarks of ageing can be organised into a hierarchical causation scheme where primary hallmarks will cause damage, antagonistic hallmarks arise as an initial biological response to the effect of primary hallmarks and integrative hallmarks are a phenotypic manifestation of chronic changes in antagonistic hallmarks. In this scheme, primary hallmarks are exclusively pathological in nature and include *genomic instability*, *telomere attrition*, *epigenetic alterations* and *loss of proteostasis*. Antagonistic hallmarks arise as an initial compensatory response to the accumulation of damage driven by the primary hallmarks. However, antagonistic hallmarks end up contributing to the ageing process when they remain active beyond a threshold magnitude and/or time. Antagonistic hallmarks include *deregulated nutrient signalling*, *mitochondrial dysfunction* and *cellular senescence*. The sustained, deleterious state of antagonistic hallmarks over time translates into a loss of tissue homeostasis and function in the form of integrative hallmarks like *stem cell exhaustion* or *altered intercellular communication*.

This framework for understanding the ageing process is undoubtedly useful to map and contextualise experimental results. However, it is an oversimplification which seems excessively centred in a unidirectional feeding of damage through the levels of biological organisation: from individual molecules to cellular pathways, to cellular states and up to tissue properties. As the authors themselves point out (Lopez-Otin et al., 2013), the ageing hallmarks are better understood as an integrated interaction network across levels of biological organisation (Figure 1.3). With damage placed at the centre of any network perturbation in accordance with the current theories of ageing (Gladyshev, 2014).

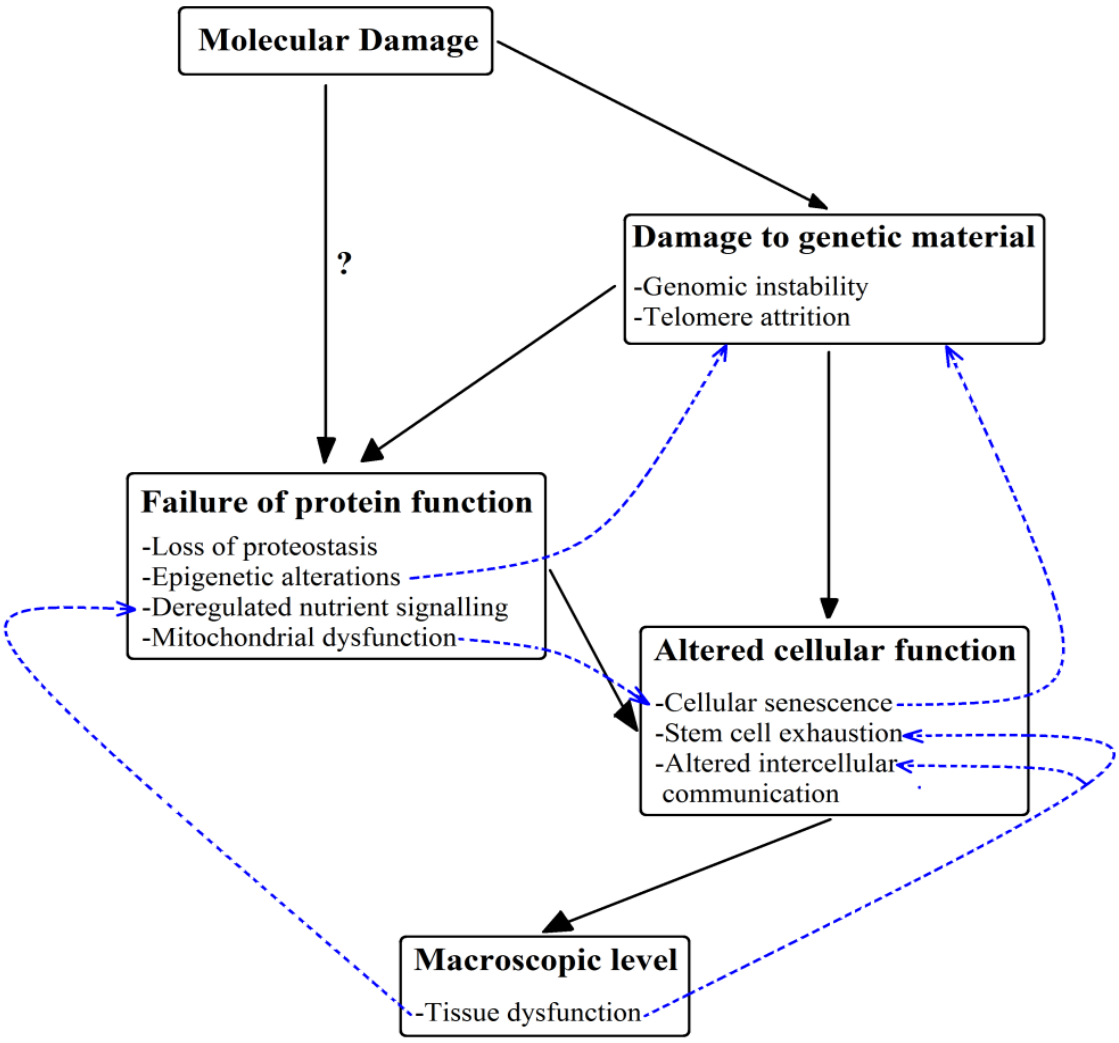

Figure 1.3. *Biological ageing as a network of hallmarks. The stochastic events of molecular damage have the potential to result in a transient or sustained network perturbation. In the case of a transient perturbation, the effect of molecular damage is diluted out by molecular turnover or cellular repair mechanisms. This perturbation will not contribute to the development of the ageing hallmarks. However, some effects of molecular damage may become permanent in the system if they are not repaired (genomic instability and telomere attrition). The robustness of the genomic structure and function allows for the effects of molecular damage to accumulate over time and gradually start feeding through the network in the form of altered protein and cellular function. When a threshold cell population becomes dysfunctional, this will become visible at the level of tissue structure, function and integrity. The interactions amongst hallmarks can be complex and self-amplifying/self-stabilising…(continues next page)*

…For example, mutations or an altered local genomic structure can result in proteins being unable to perform epigenetic modifications which in turn increases genomic instability and promotes aberrant gene expression. Mitochondrial dysfunction can drive the cells into a senescent state which is stabilised through the constitutive generation of DNA damage foci by increased ROS production. Furthermore, interactions are not exclusively bottom-up. Altered tissue structure/function can result in an altered cell niche which can interfere with intercellular communication or stem cell differentiation. Another example could be an altered hormone secretion within an organ system which results in a deficient activation of the necessary responses within tissues of distal organs.

But where do ROS and oxidative stress fit in this framework? As previously mentioned, ROS have the capacity to cause molecular damage due to their intrinsic reactivity. Therefore, oxidative stress would feed into the network at two levels: *i)* A transient stochastic occurrence (acute network perturbation) corresponding to the 'Molecular Damage' classification. *ii)* As a sustained input (chronic network perturbation) through self-amplifying or self-stabilising loops (Figure 1.3). Examples of the latter could be the ROS-mediated stabilisation of the senescent state or the promotion of mitochondrial damage by ROS generated by dysfunctional mitochondria. The nature of both of these types of homeostatic interference are fundamentally different and indeed assume a role for ROS and oxidative stress to be as a primary causative agent (i) or a as a secondary consequence (ii). In any case, ROS molecules are not the only entity which can promote a self-feeding within the network (Figure 1.3). In fact, ROS molecules are not the only potential source of stochastic molecular damage (e.g. advanced glycation end-products, unfolded proteins, infections, toxic metabolites, radiation…). However, current thinking within the field of biogerontology do place ROS as the most plausible source for the majority of molecular damage associated with the progression of the ageing process.

1.4 Redox signalling

Reduction/Oxidation (redox) reactions involve an electron transfer from a donor molecule to a recipient molecule resulting in the oxidation of the donor and the reduction of the recipient. In biological organisms there are few molecules that are nucleophilic enough to autonomously trigger a redox reaction. These molecules typically contain an oxygen atom which may have an unpaired electron (free radical) or may have a non-uniform distribution of paired electrons which results in partial changes within the molecule (Lushchak, 2014). The general term reactive oxygen species (ROS) encompasses small molecules that are autonomously involved in redox reactions mediated by the electronegative properties of the oxygen atom within them (Winterbourn, 2008).

The main free radicals (FR) present in biological systems are the superoxide- ($O_2^{\cdot}$), nitric oxide- ($NO^{\cdot}$), hydroxyl- ($OH^{\cdot}$) and peroxynitrite- ($ONOO^{\cdot}$) radicals (Winterbourn, 2008, Marengo et al., 2016, Wang and Hai, 2016). Of these, only the first two are actively produced by the cell. $OH^{\cdot}$ is produced as the accidental by-product of the reaction of free cellular iron with hydrogen peroxide (H_2O_2) and $ONOO^{\cdot}$ is generated as an accidental by-product of the reaction of $NO^{\cdot}$ with $O_2^{\cdot}$ (Schieber and Chandel, 2014, Wang and Hai, 2016). H_2O_2 is the main non-FR ROS found within cells and is involved in two-electron transfer reactions as opposed to the single-electron transfer reactions of FRs (Winterbourn, 2008,Veal and Day, 2011, Marengo et al., 2016). Due to the lack of an unpaired electron, H_2O_2 is less reactive than FRs and consequently has a longer half-live and diffusion distance (Winterbourn, 2008). These physical properties lie behind the association of FRs with unspecific molecular damage and the association of non-FR ROS molecules with physiological signalling functions.

ROS have been long-known to be constitutively produced by the electron transport chain (ETC) during respiration as a result of an electron leak from the ETC to the high oxygen environment of the mitochondrial matrix (Lushchak, 2014, Marengo et al., 2016, Wang and Hai, 2016) . However, the discovery of the ubiquity of NADPH oxidases across cell types and the evolutionary tree established that cells contain enzymes dedicated exclusively to the production of ROS, namely superoxide and hydrogen peroxide (Jiang et al., 2011, Holmstrom and Finkel, 2014). A paradigm shift occurred where ROS stopped being viewed as an inevitable and unwanted by-product of respiration (Veal and Day, 2011, Lushchak, 2014, Schieber and Chandel, 2014). It

became apparent that cells had evolved to use ROS as signalling molecules which can activate pathways and trigger cellular responses through the chemical modification of amino acid residues within target proteins. It is commonly cysteine residues within proteins which will react with ROS in the cellular environment, with a nucleophilic attack to the thiol/thiolate group resulting in the formation of a short-lived sulfenic group which will then resolve into a chemical bond (Holmstrom and Finkel, 2014, Schieber and Chandel, 2014).

Despite the currently accepted role of ROS as signalling molecules, it is still established that excessive levels of these molecules can cause cellular damage and death (Lushchak, 2014, Wang and Hai, 2016,). This is in accordance with the observation that cells contain many families of abundant antioxidant proteins (Marengo et al., 2016, Wang and Hai, 2016). Catalase scavenges hydrogen peroxide as so do peroxidase enzymes such as peroxiredoxin isoforms and glutathione peroxidase isoforms. Peroxidases are electron donors that rely on their subsequent reduction by the concerted action of cellular reducing systems involving glutathione and NADPH molecules as well as thioredoxin and reductase proteins. Superoxide dismutase isoforms convert superoxide into the less reactive hydrogen peroxide molecule. There are, additionally, non-enzymatic antioxidant compounds like Vitamins C/E or Coenzyme Q or uric acid. The variety of antioxidant protein families that have evolved within cells and the abundance at which they have evolved to be expressed reflects the importance of maintaining low basal ROS levels to maintain cellular function and survival. Also emphasising this is the observation that a common downstream consequence of a redox signalling event is the overexpression of antioxidant proteins (Espinosa-Diez et al., 2015, Marengo et al., 2016) .

The double-edged nature of ROS molecules is reflected by both the number of processes these molecules regulate and the number of pathologies that are associated with deleteriously-elevated levels of these molecules (Holmstrom and Finkel, 2014), a state loosely referred to as oxidative stress (Sies, 2015).Whilst redox signalling modulates a wide variety of physiological processes including insulin signalling (Rains and Jain, 2011), the inflammatory response (Lei et al., 2015), apoptosis (Sinha et al., 2013), vasodilation (Madamanchi and Runge, 2013), proliferation (Truong and Carroll, 2012), migration (Schroder, 2014), the stress response (Jiang et al., 2011)… high basal ROS levels are associated with cancer (Manda et al., 2015), diabetes (Wang et al.,

2013), cardiovascular disease (Madamanchi and Runge, 2013), neurodegenerative diseases (McBean et al., 2015), and ageing (Sanz, 2016).

1.5 Redox signalling pathways in mammalian cells

In mammalian cells, there are a variety of signalling pathways that have been shown to respond to changes in the intracellular levels of ROS. However, in most cases, the redox sensor molecule that acts as the starting point of the signal transduction process is not yet identified (Winterbourn, 2015). This is significant since the identification of the upstream ROS sensor clarifies whether the pathway in itself senses ROS molecules in the environment, and is therefore a redox signalling pathway, or alternatively if it is activated via crosstalk with other redox signalling pathways.

Within pathways that directly sense changes in intracellular ROS levels through the direct oxidation of signalling molecules, a further distinction can be made between pathways that are redox-modulated and pathways that are redox-activated (Oliveira-Marques et al., 2009). In redox-activated pathways, changes in intracellular ROS levels are a sufficient stimulus to activate the pathway and trigger a response. In redox modulated pathways this same stimulus is not in itself enough to cause pathway activation but may facilitate or enhance signalling caused by a second stimulus. Changes in ROS levels are thus an insufficient requisite for signalling to occur in redox-modulated pathways.

In some cases, the redox sensor molecule is a signalling node, a protein which cannot be assigned to any one particular signalling pathway according to current knowledge but rather lies at the intersection of multiple signalling axes. Such would be the example of Ref-1 (Thakur et al., 2014). Without any canonical regulatory structure to associate these proteins to, it is not always feasible to investigate systemic properties involving signal processing and homeostatic disruption.

The main redox signalling pathways in mammalian cells which are arguably redox activated and related to canonical structures with identified redox sensors can be said to be the ASK1-, NFκB-, HIF1- and Nrf2- signalling pathways.

1.5.1 ASK1 signalling pathway

Apoptosis signal-regulating kinase 1 (ASK1) is a MAPKKK family cytosolic protein involved in cell-survival signalling (Hayakawa et al., 2012, Soga et al., 2012). ASK1 is able to homo-oligomerize into high molecular mass structures through homophilic binding between its C-terminal coiled-coil (CCC) domains and homophilic binding between N-terminal coiled-coil (NCC) domains to form the ASK1 signalosome. Although ASK1 is able to oligomerize constitutively, it can only do so through its CCC domains since the binding of thioredoxin molecules to the NCC domains prevents the alignment and oligomerisation at the N-terminal of the protein. Such binding provides steric hindrance to the activatory phosphorylation required to activate the ASK1 signalosome.

Upon a rise in intracellular oxidant levels, two active cysteines in the thioredoxin molecules will undergo oxidation to form a disulphide bond. The formation of this disulphide bond promotes the detachment of the thioredoxin molecules from the ASK1 NCC domains which will now become free to align and homo-oligomerize. This activatory homo-oligomerisation event will promote further oligomerisation of ASK1 molecules into more stable higher-mass signalosomes and furthermore result in the autocatalytic phosphorylation at the NCC domain throughout the ASK1 signalosome.

This active signalosome can then recruit a variety of proteins depending on the cellular context of the oxidative signal. For example, whether the oxidative stress is part of an inflammatory response or occurs in conjunction with calcium signalling. The outcome of ASK1 activation is the subsequent phosphorylation of stress-associated protein kinases (SAPKs) like JNK or p38 which then feed the signal through integrated kinase networks that ultimately result in a cell decision process of whether the cell survives or undergoes apoptosis.

Once the oxidative stress disappears from the cellular environment through antioxidant scavenging, reduced thioredoxin molecules will be replenished by the action of reductases and will be able to bind the NCC domains to destabilise and disrupt the ASK1 signalosome so that it is no longer active. Additionally, a negative feedback loop has been identified where ASK1 activation by an oxidant stimulus results in a subsequent increase in protein phosphatase 5 (PP5) levels which actively dephosphorylates the activatory phosphor/threonine residue in the ASK1 NCC domain to destabilise and render the signalosome inactive (Morita et al., 2001).

1.5.2 NFκB signalling pathway

The combinatorial binding between the members of the nuclear factor kappa-light-chain-enhancer of activated B cells (NFκB) family of proteins gives rise to a variety of multi-protein complexes referred to as NFκB transcription factors. These transcription factors are involved in cellular responses to stress and inflammation (Hoesel and Schmid, 2013, Cildir et al., 2016). At rest, these transcription factors are kept inactive in the cytosol by the binding of members of the IκB protein family. Such binding event will not only sequester the nuclear localisation sequence (NLS) of the transcription factor but will also promote its ubiquitination and subsequent proteosomal degradation.

Whilst the signalling pathway can be activated by a variety of stimuli through various growth factor and inflammatory receptors, activation signals will converge on the activation of the IKK protein complex in the canonical pathway of NFκB. The IKK complex is an IκB kinase which promotes the ubiquitination and subsequent degradation of its IκB substrate. The phosphorylation of IκB proteins will lead to the release of NFκB allowing the recognition of the NLS and its import into the nucleus. Amongst the transcriptional targets of NFκB are genes that encode IκB proteins, which become upregulated. The transcriptional upregulation of IκB genes by NFκB creates a negative feedback loop through the ability of IκB proteins to bind nuclear NFκB and sequester it back into the cytosol to reset the signalling system. The transcription of other proteins like A20 will also contribute to the strength of the negative feedback loop.

This negative feedback produces NFκB oscillations which allows the pathway to encode information in the frequency domain as well as in the magnitude domain (Wang et al., 2012b). Whilst a non-canonical mechanism of NFκB signalling has been identified, it is comparatively less-well characterised (Cildir et al., 2016).

There is abundant evidence in the literature that the NFκB pathway can be affected by H_2O_2 treatment. It is unclear, or at least context-dependent, whether increased oxidant levels have an inhibitory or activatory effect on the pathway (Morgan and Liu, 2011). Some authors argue the pathway not to be redox-activated but redox-modulated (Oliveira-Marques et al., 2009). ROS have been proven to be able to affect the phosphorylation status of IKK and IκB in addition to the binding affinity of the NFκB transcription factor to its target genes. It is thus apparent there remains substantial

uncertainty on how the oxidant signal feeds into the NFκB signalling network and what is the resulting outcome.

1.5.3 Nrf2 signalling pathway

The nuclear factor (erythroid-derived 2)-like 2 (Nrf2) protein is a basic leucine zipper domain transcription factor considered to be the master-regulator of the cellular detoxification response (Tebay et al., 2015, Loboda et al., 2016). In its basal state, it is bound by Keap1 molecules in the cytosol to form a protein complex which promotes the ubiquitination and proteosomal degradation of Nrf2. The Keap1 molecule has a high number of cysteine residues along the length of the protein that are prone to oxidation by intracellular ROS.

An oxidation event causes a change in the conformation of the Nrf2-Keap1 complex so that Keap1 can no longer detach from Nrf2 after its ubiquitination. Consequently, under conditions of elevated oxidant levels in the cellular environment there is a lesser abundance of free Keap1 inhibitors to bind the constitutively – synthesized Nrf2 protein. This will result in a greater proportion of free Nrf2 molecules in the cytosol which will be translocated into the nucleus through the recognition of the NLS sequence which has been argued to be facilitated by a prior phosphorylation event. Within the nucleus it will transcribe a plethora of genes coding for proteins with antioxidant and detoxifying functionalities.

GSK3β has been established to be a negative regulator of nuclear Nrf2 levels via promoting its recognition and degradation by the TrCP protein (Hayes et al., 2015). It is still unclear, however, if this negative regulation via TrCP is mediated by GSK3β directly or through an intermediate molecule like Fyn (Cuadrado, 2015). Under conditions of oxidative stress, GSK3β is temporarily inhibited by a phosphorylation in its serine 9/serine 21 residues by activated Akt. It is hypothesized this inhibition may occur through the deactivation of PTEN by ROS (Cuadrado, 2015). This temporal deactivation facilitates the accumulation of Nrf2 in the nucleus. The eventual relief in the inhibition of GSK3β, presumably through a delayed phosphorylation in its tyrosine 216 residue (Zhang et al., 2013), promotes the degradation of free Nrf2 through TrCP.

Whilst Nrf2 has been reported to be able to increase the expression of Keap1 (Kaspar and Jaiswal, 2010), which in turn has been reported to translocate to the nucleus and

extract Nrf2 back into the cytosol (Niture and Jaiswal, 2009), the cell- and stimulus-specificity of these observations are still unclear. It is thus apparent that whilst the activation of the Nrf2 pathway is relatively well-characterised, there is still considerable uncertainty regarding the molecular basis and relative importance of the negative regulatory loops in this pathway.

1.5.4 HIF1 signalling pathway

Heat Inducible Factor 1 (HIF-1) is a transcription factor involved in the cellular response to hypoxia (Masoud and Li, 2015, Balamurugan, 2016). Under normal oxygen conditions (normoxia), the HIF1 alpha subunit is actively hydroxylated in its proline-564 residue by prolyl-4-hydroxylase (PHD) protein isoforms 2 and 3. This post-translational modification will be recognised by VHL proteins which will bind to HIF1a and promote its ubiquitination and subsequent proteosomal degradation. Furthermore, there is a second regulatory layer involving the hydroxylation of the TAD domain in HIF1a by FIH which prevents the binding of cofactors CBP and p300 to the HIF1 protein.

Both FIH and PHD2/3 are hydroxylase enzymes that contain a catalytic iron centre that reacts with the oxygen substrate. Under oxygen-limiting conditions (hypoxia), these reactions are believed to become substrate-limited to the point where HIF1a hydroxylation is relieved. It has additionally been suggested that the ROS generated by mitochondria under hypoxic conditions can react with the iron catalytic centres of the hydroxylase proteins to inhibit their activity (Chandel et al., 2000). Indeed, ROS generation by NOX proteins can be a positive feedback mechanism in HIF activation through the inhibition of the iron catalytic centres of hydroxylase proteins (Nanduri et al., 2015, Balamurugan, 2016). The reduced hydroxylation allows HIF1a proteins to escape VHL-binding and translocate to the nucleus. There, HIF1a will form a transcriptional complex with HIF1b, CBP and p300 and transcribe target genes.

Amongst the genes transcribed by HIF1 are those coding for PHD2/3 proteins, thus creating a negative feedback loop (Bagnall et al., 2014). Additionally, HIF1 activation has been reported to increase the expression of a range of micro-RNAs which reduce the translation of HIF1 protein (Bartoszewska et al., 2015). Although a large number of positive and negative feedback loops have been reported in this pathway (Prabhakar and

Semenza, 2012), most of them remain to be established as conserved, canonical mechanisms which apply across cell lines and experimental contexts. Additional complexity arises from the observation that HIF1 may be activated in the absence of hypoxia through the mTOR pathway (Masoud and Li, 2015), which in itself can be modulated by ROS. This activation occurs through increased HIF1 protein expression by elF-4E which may also be induced through the MAPK pathway.

1.5.5 Common features

An apparent feature of all of the main redox signalling pathways (Figure 1.4) is that the oxidant signal results in the disruption of an inhibitor-activator complex that would otherwise result in the degradation of the activator molecule. The result of this disruption is an increased abundance of free activator which needs to be stabilised by a subsequent posttranslational modification and/or molecule binding. In most cases the executed function results in a delayed negative feedback loop through the increased transcription of the inhibitory molecule. In the case of Nrf2 signalling however, the main negative regulator acts through post-translational modification and is activated independently of Nrf2, in a negative feedforward loop (Figure 1.4a).

It is useful to stress at this point that multiple post-translational feedback mechanisms have been reported for all pathways. Indeed, it has been argued that stress signalling pathways require both fast-acting post-translational feedback loops and late-acting transcriptional feedback loops for successful adaptation to the environmental conditions experienced by cells (Zhang et al., 2015b). However, these reported mechanisms have still not been established as part of the canonical signalling axis of these pathways.

The fact that the signalling systems need to reset to pre-stimulus conditions in order to allow for the next signalling event in the cell requires that the inhibitor-activator complex is restored to basal levels. This can require the modification of the activator into a form that can be identified by the inhibitor (HIF1) or the regeneration of the inhibitor (ASK1, NFκB, Keap1).

It is of interest to note that the HSF1 pathway which responds to cellular stress through the sensing of misfolded proteins or through its activation by other upstream pathways, follows similar conserved principles to the redox signalling pathways in Figure 1.4 (Jiang et al., 2015b, Masoud and Li, 2015). Under unstimulated conditions HSF1 is also

kept within an inhibitory complex with HSP70/90 which promotes its degradation. Under the presence of unfolded proteins in the cellular environment, HSP70/90 molecules will preferentially bind to them making HSF1 escape the HSP70/90-mediated degradation. After a subsequent phosphorylation, HSF1 translocates to the nucleus and will increase the expression of HSP70/90 inhibitor proteins.

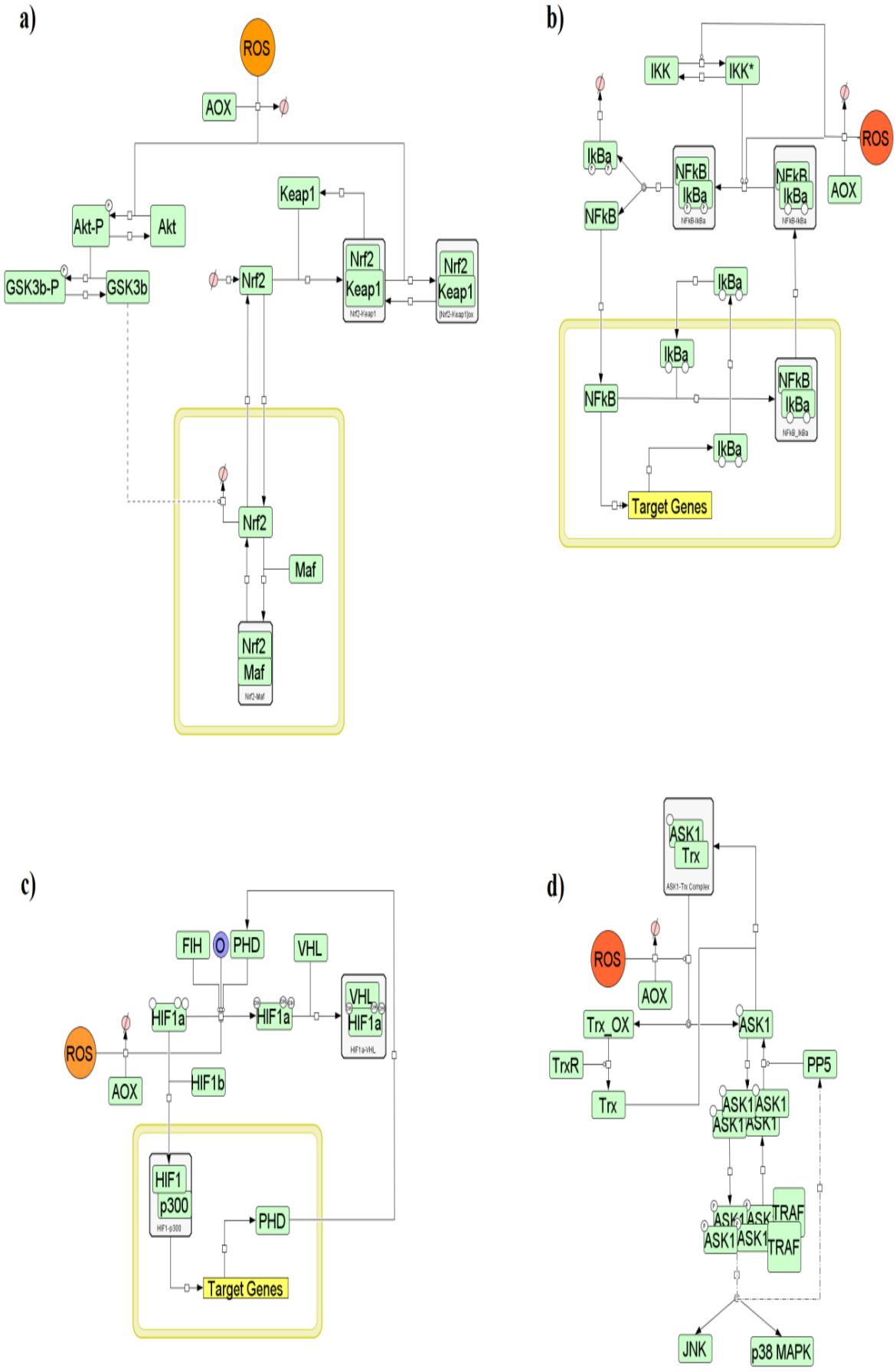
a)
ROS
AOX
Keap1
Akt-P
Akt
Nrf2
Keap1
GSK3b-P
GSK3b
Nrf2
Keap1
Nrf2
Maf
Nrf2
Maf
b)
IKK
IKK*
ROS
IkBa
NFkB
IkBa
NFkB
IkBa
AOX
NFkB
IkBa
IkBa
IkBa
NFkB
IkBa
NFkB
IkBa
Target Genes
c)
FIH
O
PHD
VHL
HIF1a
HIF1a
VHL
HIF1a
ROS
AOX
HIF1b
HIF1
p300
PHD
Target Genes
d)
ASK1
Trx
ROS
AOX
Trx_OX
ASK1
TrxR
PP5
Trx
ASK1
ASK1
ASK1
ASK1
TRAF
ASK1
ASK1
TRAF
JNK
p38 MAPK

Figure 1.4. *(Previous page). Canonical interaction networks for four major redox signalling pathways in mammalian cells. AOX = Antioxidant.* ***a)*** *Nrf2 signalling pathway.* ***b)*** *NFκB signalling pathway. Note that asterisk indicates activated form of a molecule.* ***c)*** *HIF1 signalling pathway. Note that O = oxygen.* ***d)*** *ASK1 signalling pathway.*

1.6 Redox homeostasis and ageing

Whilst the loss of redox homeostasis manifested as oxidative stress has been proven to occur with age in a variety of tissues (Dai et al., 2014, Cunningham et al., 2015), the functionality of redox signalling within an ageing context has received scarce attention. Redox signalling, at least through some pathways, can be seen to become dysfunctional in multiple tissues with age (Zhang et al., 2015a). However, the most comprehensive investigations seem to have been performed in aged skeletal muscle tissue in the context of exercise and sarcopenia.

1.6.1 ROS in exercise and skeletal muscle ageing

A good physiological example of the complex role of ROS in health and ageing is seen in skeletal muscle during exercise and the process of sarcopenia. Physical exercise is a powerful, positive lifestyle intervention where ROS are thought to play a pivotal role in the resulting beneficial effects (Radak et al., 2008). Skeletal muscle produces ROS and reactive nitrogen species (RNS) during contraction (Powers and Jackson, 2008, Jackson, 2015, Ji, 2015) which are not only necessary for force generation (Reid et al., 1993, Jackson, 2015) but also mediate an adaptive response involving the upregulation of antioxidants and heat shock proteins via redox-sensitive transcription factors (McArdle et al., 2001, Vasilaki et al., 2006b, Jackson and McArdle, 2011, Jackson, 2015). The observation that elevated ROS have also been associated with muscle wasting during inactivity (Kondo et al., 1993, Powers et al., 2012) and ageing (Aoi and Sakuma, 2011), illustrates the recurring paradigm in redox biology regarding the double-edged nature of these molecules.

The characterization of this behaviour is of special relevance to sarcopenia, a condition defined as the loss of muscle mass and function with age, which affects a very

significant proportion of the older population (Fielding et al., 2011). Such pathology is associated with several comorbidities and resulting high healthcare costs (Janssen et al., 2004). Whilst on the one hand chronic oxidative stress is a hallmark of sarcopenia (Fulle et al., 2004), physical exercise is the only available intervention which to some degree ameliorates this condition (Fielding et al., 2011, Cobley et al., 2015, Joseph et al., 2016).

Previous work on the redox-mediated adaptive responses during exercise in skeletal muscle revealed such signalling axes became aberrant with age in mice (Vasilaki et al., 2006b, Jackson and McArdle, 2011, McDonagh et al., 2014b, Ji, 2015) and humans (Cobley et al., 2015, Done et al., 2016). Although redox signalling dysfunctionality in skeletal muscle is well-established, the underlying mechanistic basis remains to be elucidated (Jackson, 2016). The reported redox signalling aberrancies in aged skeletal muscle and indeed many other tissues can be classed as a lack of response activation, reduced response activation or a constitutive response activation. However, the resolution provided by these observations is very limited since readings of redox activation are almost exclusively single time-point measurements. Thus, if a redox response is triggered more slowly but to the same magnitude, this will translate into a no-response or reduced-response conclusion if a single time-point measurement is taken (Figure 1.5). Conversely, studies reporting no change in response activation based on single time-point measurements could be misreporting an underlying stronger and faster activation that has decayed substantially by the time of measurement. In fact, the time of measurement itself is often arbitrarily chosen. Alas, there is a substantial uncertainty over the exact nature of the age-related redox dysfunctionalities.

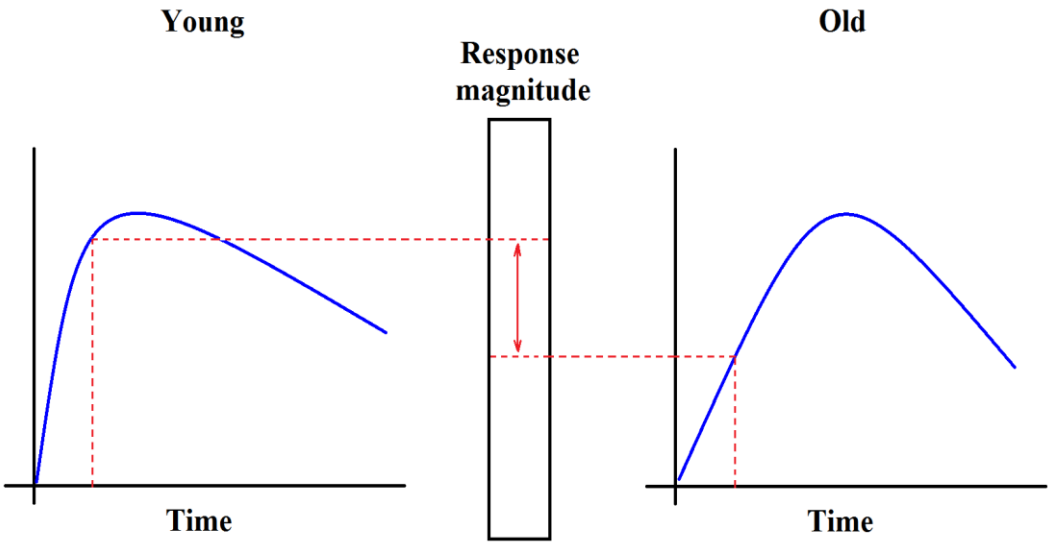

Figure 1.5. *Misleading conclusion derived from single time-point measurements. Redox activation in many aged tissues has been reported to be dampened or altogether abolished. However these readings are taken from single time-point measurements that could actually be reporting a fundamentally different behaviour, in this case, no change in activation magnitude but a delayed activation. Thus, current resolution into the nature of redox dysfunctionality is very limited.*

1.6.2 Redox homeostasis in cellular senescence

Cells are the basic units of life, the most fundamental level at which life arises as a phenomenon (Mazzarello, 1999). It follows from this that the simplest model of the ageing phenomenon is the 'ageing cell'. Cellular senescence, a state of irreversible cell-cycle arrest induced under conditions of cellular stress, has been recurrently employed as a model of cellular ageing (Campisi, 2013, Bhatia-Dey et al., 2016, Lujambio, 2016). Not only have senescent cell populations been proven to display a gradual accumulation of damaging molecules and molecular damage (Lawless et al., 2012, Dalle Pezze et al., 2014), but they have also been shown to display an increased heterogeneity in a variety of functional markers (Passos et al., 2007) . Cellular senescence has been linked to a number of age-related dysfunctionalities in a variety of tissues (Childs et al., 2015). However it was only recently that the accumulation of senescent cells was explicitly proven to actively promote the decline of physiological function and limit organism

life-span (Baker et al., 2011, Baker et al., 2016). As with any model, the question remains as to how representative it is of the process under study. It is important to note that non-dividing post-mitotic cells like neurons also undergo cellular ageing without entering a senescent state. Indeed, one can find in the literature references to a 'senescent-like state' of post-mitotic cells (van Deursen, 2014).

Being a stress-induced response, entry into cellular senescence can be promoted by elevated levels of ROS or DNA damage, amongst others (Campisi, 2013, Correia-Melo and Passos, 2015) . Thus, understanding cellular senescence as a simple model of cellular ageing requires a perspective that includes the maintenance and disruption of redox homeostasis (Correia-Melo and Passos, 2015, Chandrasekaran et al., 2016). Indeed, elevated ROS levels have been shown to be key drivers of the state of cellular senescence within a cell and the inter-cellular induction of senescence (Correia-Melo et al., 2014). In the former case, ROS can form a positive feedback loop through the constitutive induction of DNA damage that stabilises the senescent state of the cell. ROS are also part of the senescence-associated-secretory-phenotype (SASP) which can also form a positive feedback loop at the cellular scale through the senescence-induced senescence of bystander cells. Like with many aged tissues (Maher, 2005), senescent cells display a disrupted redox state (Correia-Melo and Passos, 2015, Chandrasekaran et al., 2016). However, how the cell transitions into a state of redox imbalance is unclear. Recent efforts to back-track this homeostatic disruption point towards mitochondria being the causal agents (Correia-Melo et al., 2016). Although the underlying question remains as to how mitochondria lose their functionality over time.

In any case, cellular senescence is a consistent model of gradual homeostatic disruption, of relevance to the ageing process, which can be understood through the dysregulation of ROS levels. Unfortunately, the mechanistic resolution provided by experimental data so far does not allow the untangling of the chicken-or-egg conundrum of whether ROS are the driver or the result of the age-related loss or cellular homeostasis.

1.7 Understanding ageing through systems biology

1.7.1 Systems biology

Systems biology is a discipline that evolved around the concept that certain biological observations can only be explained by considering the interactions between the elements of the biological system. This is as opposed to the so-called reductionist approach that has predominated in biological research, involving the explanation of biological phenomena in terms of the activity of single molecular players. Systems biology is thus a contrasting holistic approach which arose when the reductionist approach had generated enough knowledge on the elements of biological systems to start linking them together into networks. Such networks were revealed to be able to display new properties that none of the individual constituent molecular entities displayed alone (Kitano, 2002b, ElKalaawy and Wassal, 2015).

Biological systems tend to be intrinsically complex, involving a myriad of molecular interactions that ensure that a biological response occurs with the right strength, at the right place, the right time and with the right duration. Thus, the complexity of biological systems does not come exclusively from a complicated topology of interactions but also from a complicated behaviour of these interactions in time and space (Kholodenko, 2006, Ganesan and Zhang, 2012). Although there has been a long-standing appreciation of the necessity of studying biological systems holistically, it was not until computational methods evolved that systems biology was able to address this level of complexity as a discipline (Janes and Lauffenburger, 2013).

The development of network inference algorithms allowed the analysis of medium- and high- throughput experimental data to establish statistical relationships between measured biological entities and shed light on the underlying interaction topology of biological systems (de Silva and Stumpf, 2005, Kirk et al., 2015). For the first time, a biological response could be studied comprehensively through 'Omic' technologies. To account for the dynamic properties of the system in addition to the underlying topology, a different type of methodology is required. Namely, one that allows the simulation of the biological system in time and space (Mast et al., 2014). Within systems biology, the adoption of these techniques is referred to as systems modelling (Aldridge et al., 2006, Ganesan and Zhang, 2012).

1.7.2 Systems modelling

Systems modelling aims to reproduce the behaviour of the biological system being studied in an abstracted computational framework. This computational framework can be mathematical, where simulation involves solving the equations that model the biological system; algorithmic, where simulation involves the execution of a set of rules aiming to represent causal elements of the biological system; or a hybrid framework involving both of such approaches (Fisher and Henzinger, 2007). Within these classifications, there are a wide variety of modelling frameworks, each with specific conveniences and drawbacks (Machado et al., 2011, ElKalaawy and Wassal, 2015). The evolution of both simulation platforms and computational performance has allowed for the simulation of increasingly complex biological systems, a notable example being simulation across levels of biological organisation in what is termed multi-scale modelling (Dada and Mendes, 2011).

Any model, be it computational or not, is an abstraction of the real system under study and as such relies on a number of assumptions. In systems modelling these assumptions often abstract uncertainty on parameter values, topological arrangements or spatial distributions (Kirk et al., 2015). Whilst the first requirement for a computational model is that it reproduces the available experimental observations relevant to the biological system under study, it should additionally aim to provide an explanation for the data and ultimately generate novel predictions to be further tested experimentally. This iteration between experiments informing computer models which generate new predictions to be tested experimentally has been referred to as the systems biology cycle (Kitano, 2002b).

1.7.3 Network motifs

Pioneering work led by Uri Alon uncovered specific interaction patterns amongst network components which occurred at a much higher frequency than observed in randomly-generated networks (Milo et al., 2002, Alon, 2007). These ‘network motifs’ were not only seen in the *E.coli* transcriptional regulation map (Shen-Orr et al., 2002), but also in other biological and non-biological networks (Milo et al., 2002). This work shed light into the convergent evolution of “design principles” which mapped directional interaction topologies to specific dynamic, information-processing, properties. It furthermore suggested the possibility that the intricately complex

biological networks could be dissected and understood in terms of simple interaction circuits coupled together (Beber et al., 2012).

Networks motifs were originally identified from the analysis of bacterial transcriptional networks and comprised simple regulations (SRs), feedforward loops (FFLs), single input modules (SIMs) and dense overlapping regulons (DORs). Simple regulations refer to auto-regulatory loops, i.e. self-activation or self-inhibition. This would be the case of a transcription factor that activates or inhibits its own transcription. Feedforward loops were identified as three-node motifs with an upstream network element which has a time-separated dual interaction with a downstream network element (Figure 1.6). Because of the each of the node-interactions in this network topology can either be activatory or inhibitory, eight-classes of FFLs can arise. Different types of FFL have been attributed different information-processing properties such as response acceleration, pulse generation and delay introduction to confer memory. SIMs and DORs refer to the regulation of a group of functionally-related target genes by a single transcription factor or a combinatorial set of transcription factors respectively.

Because the initial analysis of network motifs took place in the transcriptional regulation network of *E.coli*, FFLs were formalised as three-node motifs. This is because interaction distance between gene regulatory elements in prokaryotes tends to be small. However, theoretical and experimental analysis has demonstrated such structures can still display the same information-processing properties when elongated to include more nodes (Sauro and Kholodenko, 2004, Alon, 2007, Ferrell, 2013, O'Hara et al., 2016). This is of particular relevance to protein-modification based signalling networks in cells (Cloutier and Wang, 2011, Kolch et al., 2015). Coupled motif structures (CMS) have also been identified to be overrepresented in biological networks and furthermore associated with biological status in case of cancer (Hsieh et al., 2015).

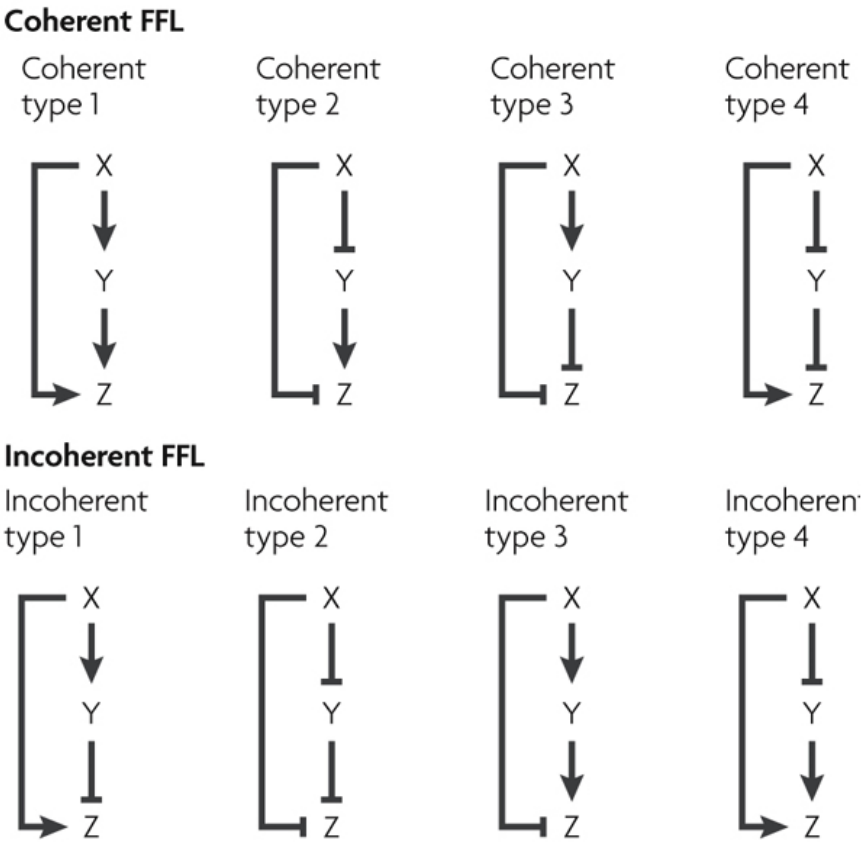

Figure 1.6. *Types of feedforward loop (FFL) motifs. Adapted from Alon (2007).*

Whilst the work undertaken by Uri Alon was the first systematic identification of network motifs in biological networks, and it introduced the concept of FFLs, it was not the first identification of simple circuits underlying the functional dynamics observed in biological systems. Indeed, previous theoretical work on understanding biological systems as self-regulating cybernetic systems led to the prediction and subsequent validation of interaction circuits, the most notable example being the repressilator (Elowitz and Leibler, 2000). These types of circuits are based on the concept of feedback, a sequential and directional interaction of a downstream network element with the upstream input network element. Again, this interaction can be activatory (positive feedback) or inhibitory (negative feedback) and can give rise to a number of dynamic properties like oscillations, pulses, accelerators, amplifiers and bistability (Brandman and Meyer, 2008). Feedback loops underlie higher order network properties such as robustness, adaptive behaviour and memory (Brandman and Meyer, 2008, Ferrell, 2013, Kolch et al., 2015).

The concept of network motifs can be criticized for establishing an *a priori* causal relationship between topological structure and function based on an insulated network representation (Ingram et al., 2006, Beber et al., 2012). In this context, "insulated" refers to the fact that network motifs do not exist in isolation but as part of dense interaction networks with cross talk at multiple levels and timescales in addition to intrinsic and extrinsic noise in the signalling systems. Indeed, some of the functionalities attributed to some network motif structures depend on the underlying parameters (Ingram et al., 2006), which are a significant source of uncertainty in themselves. In this context, the functionality attributed to a network motif, ex. response accelerator, can be altered or non-existent within the context of a larger network with multiple signals and noise (Ingram et al., 2006, Hsieh et al., 2015).

It seems apparent that insights can be gained by abstracting complex processes into network motifs or motif-like structures despite their underlying uncertainties. An example is the abstraction of the entire mTOR network into a simple topology that retained the relevant dynamic observables (Dalle Pezze et al., 2014). Their employment is useful from a theoretical perspective in that they provide a good exploratory starting point to begin to answer questions which remain unaddressed due to the limited resolution of current experimental methodologies.

1.7.4 Systems modelling of ageing processes

The acknowledgement of the multi-factorial nature of the ageing process (Kirkwood, 2011, Lopez-Otin et al., 2013, Gems, 2015) calls for methods that address this level of complexity. Namely, those that fall within the field of Systems Biology (Kitano, 2002a, Kirkwood, 2011, Kriete et al., 2011). Indeed, concepts like health, disease and ageing refer to homeostatic states which by definition encompass an interaction network. As previously discussed, ageing can only be understood as a time-evolving process, pointing to systems modelling as a potential approach to further our understanding of the homeostatic dysfunctionalities observed to develop with age.

There are a number of methodological advantages on adopting a systems modelling approach. The development of a computational model requires the researcher to be rigorous in the formalisation of the underlying biological knowledge and this often allows the identification of knowledge-gaps in the literature. By accounting for multiple

factors and making qualitative as well as quantitative predictions, computer models can potentially also inform experimental design and additionally provide a quick and low-cost 'exploratory-platform' as an alternative to doing so through more costly and lengthy experimental protocols. Furthermore, some emergent system behaviours, such as oscillations, hysteresis or robustness, can only be explained through modelling formalisms (Janes and Lauffenburger, 2013, Mast et al., 2014).

The main argument, however, for the employment of computational models is that there is no other methodological alternative that explicitly accounts for the complexity of system-level biological interactions in time and space. Indeed, it is notoriously difficult to keep track of so many molecular interactions and operating feedback mechanisms over time and space through experimental protocols or the human mind alone. Computer models provide a standardized and extendable method for formalising existing knowledge or mapping new information onto. Moreover, computational models do not only provide comprehensive simulation platforms to further our mechanistic understanding of biological systems, but can also advance our conceptual understanding of the biological problems and observations of interest (Mast et al., 2014, Mc Auley and Mooney, 2015, Mc Auley et al., 2017). The range of computational models of ageing processes developed to date reflects how systems modelling has found its place within biogerontological research (Kirkwood, 2011, Kriete et al., 2011, Mc Auley and Mooney, 2015, Mooney et al., 2016, Mc Auley et al., 2017).

1.7.5 Computational models of redox signalling

There are a number of computational models in the literature which explicitly model redox signalling processes in a variety of biological contexts (Pillay et al., 2013). The majority of these are kinetic models. These models represent reactions as a series of mathematical relationships between parameters like molecule abundances and kinetic constants (K_m, V_{max}, $K_{forwards}$, $K_{backwards}$…). The mathematical relationships are usually established kinetic equations, or mathematical derivations thereof, of which the most known examples are the Michaelis Menten equation and the mass action equation (Sauro, 2011).

Redox signalling models in the literature can be broadly divided into Ordinary Differential Equation (ODE) -based models (Adimora et al., 2010,Gauthier et al., 2013,

Benfeitas et al., 2014, Tomalin et al., 2016), which are the majority , and Partial Differential Equation (PDE) -based models (Sobotta et al., 2013, Lim et al., 2016), which are a substantial minority. Indeed, available computational models of the main mammalian redox signalling pathways are based on coupled ODEs (Bagnall et al., 2014, Pronk et al., 2014, Williams et al., 2014, Khalil et al., 2015). This methodological bias is likely to reflect the computational limitations arising from the higher dimensionality of coupled PDEs as opposed to coupled ODEs (Materi and Wishart, 2007).

Computational models of redox signalling have benefited from the conserved kinetic properties of antioxidant enzymes across eukaryotes (Netto and Antunes, 2016), which allows for the cross-applicability of the computational models in different biological settings. Parameters derived from the work of Adimora *et al* (Adimora et al., 2010) have been used in almost a dozen redox signalling models. It is worth noting, however, that the abundances, interactions and rate constants of redox sensors are mostly unknown and likely to have a much higher variation between species and cell lines (Brito and Antunes, 2014, Netto and Antunes, 2016). Indeed, the kinetic rate constants of the oxidation of transcription factors and phosphatase enzymes are only crudely estimated (Brito and Antunes, 2014, Marinho et al., 2014).

In fact, the oxidation rate constants of redox effectors by physiological oxidants is surprisingly low, most being within a range of 10-200 M/s (Brito and Antunes, 2014, Marinho et al., 2014, Winterbourn, 2015). If the calculated rate constants of redox effector oxidation hold true, then the question is immediately raised of how can an oxidant ever reach its redox effector target if it must survive scavenging by a much more abundant and faster-reacting antioxidant system. In other words, how can a redox effector activation reaction by an oxidant compete with oxidant scavenging reactions by an antioxidant system which is $10^2 - 10^4$ times more abundant and reacts $10^3 - 10^6$ times faster? (Marinho et al., 2014, Winterbourn, 2015, Pillay et al., 2016).

Although it has been argued that effective redox signalling can still occur despite the competition with the antioxidant system (Marinho et al., 2014), from a kinetic perspective, this 'competitive oxidation' paradox seems difficult to reconcile as a generic signalling strategy by the cell. Looking at redox computational models, it is evident that estimated redox effector oxidation parameters are likely to be an overestimation arising from the parameter estimation procedure. The fitting of simulation output to experimental data means that the estimated rate constant is

phenomenologically accurate but at the expense of losing mechanistic resolution. The underlying real reaction processes become encoded in an estimated rate constant which although models one reaction within the model, it does so at a rate which corresponds to multiple reactions in the real biological system.

The literature has proposed as a solution to this "low reactivity paradox" two possible, but not mutually exclusive, explanations. The first one proposes the targeting of redox effector proteins to the vicinity of ROS generation sites (Winterbourn, 2015). The consequence of this is that at small cellular locations (for example the vicinity of NADPH Oxidases) there is a higher local concentration of reactants. Under these conditions, the reaction for the activation of the redox effector becomes more significant and can compete with oxidant scavenging. Whilst there is ample evidence of this localised redox signalling (Fisher, 2009, Woo et al., 2010) there are numerous proteins which are redox-regulated and yet show no sign of specific localisation within the cell.

Another mechanism put forward as an explanation for this apparent paradox is the existence of redox-relays (Sobotta et al., 2015, Netto and Antunes, 2016) where peroxidases will oxidize a redox effector upon becoming oxidized themselves. In this case, these scavenging systems do not compete with redox effectors for a reaction with oxidants but rather facilitate these reactions. This is since such scavenging molecules are more abundant and more reactive with ROS and so act as better ROS sensors. This elegant mechanism has been known to occur in prokaryotes and recently proved to occur in mammalian cells (Sobotta et al., 2015). However, there is yet no proof for redox relays being responsible for the oxidation of most of mammalian transcription factors. This may be due to the experimental difficulty of stabilising and isolating unstable oxidation intermediates which are involved in such redox relays.

It is thus evident that redox signalling models encode a substantial uncertainty regarding both the parameter values and the topological structure of the network. Although this uncertainty can be reduced through the use of parameter estimation procedures, in both parameter calibration and model structure selection, it does render the models specific to the experimental setup the data was derived from. In this context, there are no published models of redox signalling that explicitly deal with an ageing system.

1.8 Aims

It is evident that within the field of biogerontology, available experimental data does not provide a high enough resolution to separate many observations into primary or secondary causality and break the chicken-and-egg conundrum. At the very limit of experimental resolution, computational simulation can be used as an explanatory and exploratory tool of rational scientific enquiry that draws on available knowledge to provide new insights.

A theoretical effort could provide a means to educate our intuition on the ageing process and make sense of current experimental data, as well as potentially direct new experimental efforts. The critical question at the cornerstone of ageing research concerns why do biological homeostatic systems fail with age. Current ageing theories point towards the abstract concept of stochastic damage as the cause, but this generalisation may prove too vague to understand ageing at a higher mechanistic resolution (Gladyshev, 2014).

Oxidative stress has the potential to drive a loss of system homeostasis, whether as a primary cause or as a secondary consequence of the ageing process. It is the main line of enquiry of this work to theoretically examine mechanisms in which oxidative stress might interfere with the regulatory machinery of cells. Further to this, an examination of the ability of any identified molecular dysregulations to percolate through levels of biological organisation would provide an important contextualisation. Furthermore, it is an aim of this work to test, once interferences with homeostatic function have been characterised, whether such dysfunctionalities can be fully or partially reversed in principle. The objectives of this work are thus as follows:

i) Investigate how oxidative stress can feed into biological networks to disrupt homeostatic function.

ii) Investigate how such loss of homeostatic function could percolate across biological scales (molecules to pathways to cells to tissue).

iii) Investigate whether such homeostatic disruptions could be, to some degree, reversed.

The work undertaken as part of this thesis has been organised into the following structure. After the introductory Chapter 1, Chapter 2 presents the Materials and Methods used and developed to perform the research presented in the thesis. Chapter 3 presents the main theoretical observation from which all other work in the thesis stems from. Chapter 4 presents work that theoretically aims to test for the generality of the observation. Chapter 5 presents work that aims to experimentally validate the observation. Chapter 6 presents work that aims to theoretically contextualise the observation in the complexity of *in vivo* biology. Chapter 7 and Chapter 8 are a discussion and conclusion, respectively, on all of the presented work. The entirety of the work presented in this thesis, both experimental and theoretical, has been carried out by the author although there is once instance of published work being used in this thesis as indicated in the supplementary text (Section 9.3).

Chapter 2

Materials and Methods

2.1 Computational Methods

2.1.1 Cellular Automaton (CA) framework

When modelling the interactions between biological entities, be it molecules or cells, it is often informative to capture the inherent stochasticity in the system. This uncertainty at a given point in time often arises from the probabilistic nature of the interaction between system components in a spatial context. For example, there is stochasticity in reactant A and reactant B colliding together due to random motion and there is a separate source of stochasticity on whether they will react together once they collide. At the cellular level, a cell might undergo a state-change with differing probabilities depending on its spatial position within a lattice or depending on the nature of neighbouring cells. Cellular automata have been successfully used in the past to stochastically model both molecular and cellular interactions (Schnell and Turner, 2004, Dada and Mendes, 2011). Furthermore, this methodology is intuitive to couple to a system of differential equations in order to create a multi-scale model (Dada and Mendes, 2011).

Molecular simulations were carried out in a purpose-built simulator named CASSMI (Cellular Automaton – based Spatial Simulator of Molecular Interactions). However, both the molecular dynamics simulations and the cellular population simulations were modelled through the use of a core cellular automaton framework. Such framework is implemented as follows.

Grid definition. An initial grid of three dimensions is specified as a three-dimensional matrix of zeroes with each dimension defined by vectors of length N where the number of total cells in the grid corresponds to N^3. This three dimensional matrix is the grid structure of the cell automaton (CA matrix). In CASSMI, the N-value is derived so that a user-defined spatial occupancy is reached by the total number of molecules to be simulated. In the multi-scale model, N is manually assigned.

Cell assignation. When the modelled entities are to be distributed uniformly across the CA grid, they are encoded as vectors of a length corresponding to their initial amount, with all entries in each vector being the corresponding unique entity identifier. In all cases an identifier of zero corresponds to empty space. Random seeding of entities into the N^3 zeroes matrix is performed via Matlab's *randperm* function which allows the random permutation of a target matrix *A* using the elements of a given matrix *B* in the following form:

A(randperm(numel(A), numel(B))) = B

The localised assignation of entities within the CA grid requires the definition of a constraining factor *C*, where $C<N$, to define the spatial constraint in the seeding to $\frac{C}{N}$ over one dimension. This results in a localisation defined by $\frac{C^3}{N^3}$ corresponding to the fraction of the total space in the CA grid where the entity can be found at generation = 0. CASSMI automatically derives C from the user-defined percentage localisation for the relevant species. It is important to note that in all cases of localised assignation, the randomly selected matrix coordinate has to be unoccupied. Thus, no explicit overwriting is allowed within the initial cell assignation steps.

The main loops. Once the starting grid structure of the CA has been defined, the simulation proceeds to enter the main loop (termed 'Generation loop') which defines the rule-updating iterations in the model. The generation loop models time implicitly. In CASSMI, each iteration corresponds to one movement (rule-defined update) for all molecules in the grid. In the multi-scale model, the generation loop corresponds to days. The generation loop contains in its structure a second loop which allows for the selection of each individual cell to apply the update rules. At the end of each generation loop, a complete scan of the whole CA grid is performed and the counters for each identifier updated and stored.

Neighbour selection. As in all CA models, the update of the state of each individual cell is dependent, in one way or another, on neighbouring cells. With regards to the definition of which cells are classed as being 'neighbours', Moore's neighbourhood with an $r = 1$ distance was adopted in the CA, where any neighbouring cell in touch with the reference cell is considered a neighbour. In a two dimensional matrix represented as a grid this would mean a given selected cell would have 8 neighbours as shown in Figure 2.1. This number would be 26 in a 3D matrix (See Figure 2.2).

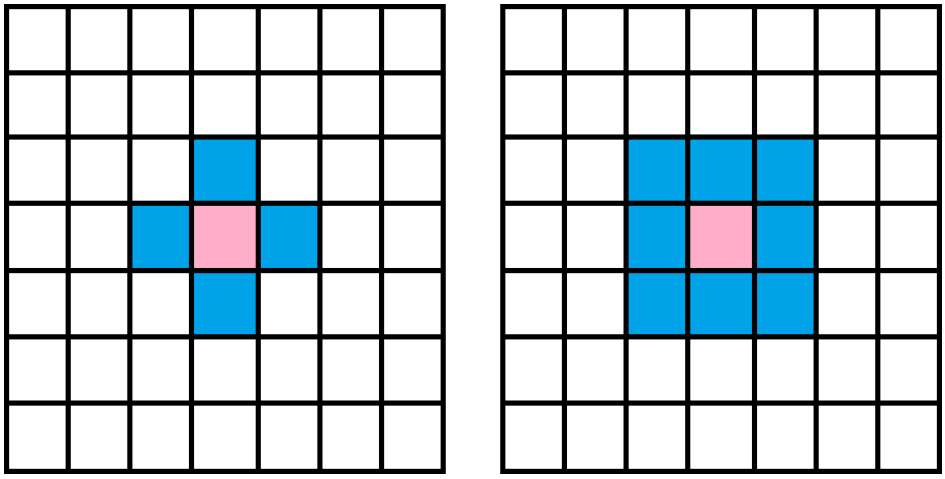

Figure 2.1. *2D representation of cell neighbourhoods most commonly employed in Cell Automaton models. Left Panel shows the von Neumann neighbourhood which defines as neighbours (blue) the cells with significant contact with the reference cell (pink). Right panel shows the Moore neighbourhood which defines as neighbours any cell which is in contact with the reference cell.*

The Moore neighbourhood was adopted over the von Neumann neighbourhood to allow for a wider range of potential interactions between individual entities and their surroundings. The greater degree of interaction freedom makes the simulation of the random motion of particles more realistic in CASSMI. Furthermore, with regards to the multi-scale model, cells in such close proximity should be expected to influence each other despite having a minimal surface-surface contact.

If a given cell in a 3D CA is defined by coordinates CA(h, i, j) any neighbour will be defined by CA($h \pm s$, $i \pm s$, j $\pm$ s) where s is a coordinate translation that can be a 0 or a 1. This geometric relation arises because a neighbour cell has to be in contact with the reference cell so it can only have a maximal coordinate separation of 1 coordinate unit in any given dimension. Because the neighbour cell may be on the same plane as the reference cell, the coordinate shift in a given dimension can be 0. The plus and minus signs of s represent any two opposite arbitrary planes in which a neighbour cell can be located with respect to a reference cell. These geometrical relations are illustrated in Figure 2.2.

On every iteration of CASSMI's generation loop, after a random cell is selected, a random neighbour of the selected reference cell is then chosen. This is achieved by creating an array with all possible coordinate updates, CA($h \pm s$, $i \pm s$, $j \pm s$) which define the neighbour coordinates as a translation from the coordinates of the reference cell (as shown in Figure 2.2). Such matrix would contain 26 coordinate updates that define Moore's neighbourhood in a 3D space and thus be as follows:

Neighbour= [-1 -1 -1; 0 -1 -1; 1 -1 -1; 1 0 -1 ; 1 1 -1;

0 1 -1; -1 1 -1; -1 0 -1; 0 0 -1; -1 -1 0;

0 -1 0; 1 -1 0; 1 0 0; 1 1 0; 0 1 0;

-1 1 0; - 1 0 0; -1 -1 1; 0 -1 1; 1 -1 1;

1 0 1; 1 1 1; 0 1 1; -1 1 1; -1 0 1; 0 0 1];

The selection of a random neighbour thus simply involves selecting a random set of coordinate updates ($\pm s$ $\pm s$ $\pm s$) from the *Neighbour* matrix and transforming the reference cell coordinates by the s translation values contained within. The selection of a random neighbour simulates the random movement of a randomly selected molecule in CASSMI. Once the neighbour is known then a set of rules are applied to update the state of the reference cell and/or the neighbour cell depending on their respective states (identifiers). In the multi-scale model, each cell has the potential to affect all of its neighbours and so instead of selecting a single neighbour coordinate at random, all coordinates are iterated through.

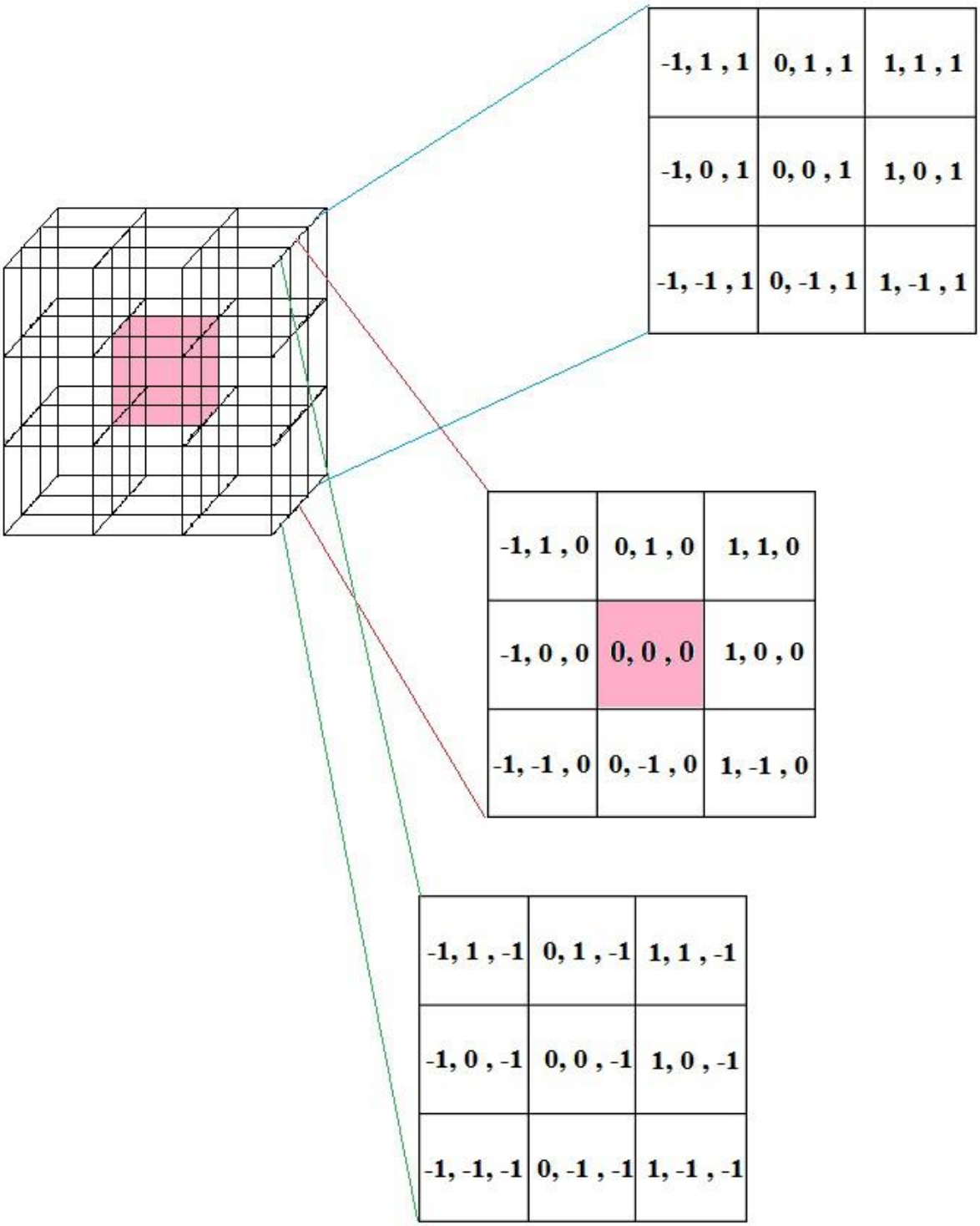

Figure 2.2. *Moore Neighbourhood defined in 3D space. The translation of the reference cell (pink) into any of the 26 neighbouring (white) cells is defined by a fixed set of coordinate updates* ***(s s s)*** *specified in the individual grids. Hence, a cell movement would be modelled as the random selection of one of the 26 possible coordinate transformations to then update the reference cell location from CA(h ,i , j) to CA(h±**s** ,i±**s** , j±**s**).*

Neighbour-dependent rules. These rules are commonly applied as a function of the states of neighbouring cells after a specific cell has been randomly selected. In CASSMI, which simulates Brownian motion of particles, there are three general rules that can be applied once a reference cell and a neighbouring cell have been randomly selected.

i) If the neighbour cell is empty, the molecule moves into neighbour cell. This rule is executed by the swapping of identifiers between the neighbouring cell and the reference cell. This models molecule movement in space.

ii) If the neighbouring cell is not a reactant, there will be a 180^{o} collision ≠

iii) If the neighbouring cell is a reactant, a reaction will occur with a probability defined by the corresponding rate constant.

≠ This collision is modelled through a 180° change in direction by multiplying the selected neighbour update coordinates ***s*** by -1. This can be readily seen by choosing any set of coordinate updates (±***s*** ±***s*** ±***s***) from Figure 2.2 and multiplying them by -1. The resulting coordinate updates will correspond to a neighbouring cell on the opposite side of the 3D square. A collision thus results in the selection of another neighbouring cell, non-randomly this time, and applying the same set of rules with the only change that should the new neighbour cell still be a non-reactant, the reference cell would retain its identifier (i.e. the selected molecule would not change position) for that generation. Because the distance moved by a particle is always 1 grid, there is a perfect momentum conservation upon collision.

Neighbour-independent rules. These rules are applied independently of the states of neighbouring cells. In CASSMI, there are three main general rules which fall under this category.

i) Zero-order reactions. Involve the seeding of new molecules into empty spaces of the CA grid every iteration with a user-defined probability. These rules are executed at the start of the generation loop.

ii) First order reactions. Executed after a cell has been randomly selected. Involve the conversion of the selected cell into a single, multiple or no products with a given probability.

iii) Events. The alteration of molecular abundances or reaction rate constants (probability of occurrence) to model an acute perturbation of the system at a user-defined generation.

Note that for any reaction that produces products, these can take the place of the neighbouring cell, the reference cell, both or alternatively a randomly chosen empty space in the CA grid in the case of zero-order reactions or Events. If no products result from a reaction then the reactant cell(s) are assigned a state of 0 (empty space). The rules of the multi-scale model are manually specified (see Section 6.2.2).

Other rules. It is important to note that CASSMI models molecules in a closed system. That is, upon reaching the edges of the N^3 space that defines the CA grid, if a molecule moves outside the grid, it will undergo a 180^o collision. Molecular simulations in CASSMI are thus simulated as an ideal gas enclosed in a container. In the multi-scale model, cells outside the CA grid are simply ignored as neighbours.

Random selection. There are five main settings in which CASSMI will perform a random selection:

1. To select the indices of a reference cell.

2. To select a random neighbour of a given reference cell.

3. To select the random indices for the seeding of new molecules produced by zero-order reactions and Events.

4. To establish whether a molecule moves at any given iteration.

5. To establish whether two neighbouring cells will affect each other (i.e. whether molecules react at any given collision).

Settings 1, 2 and 5 also apply to the multi-scale model.

In setting number 1) a 'Reference Matrix' of ascending numbers with the same dimensions as the CA (N^3) is created and permutated with a zeroes matrix of the same dimensions using Matlab's *randperm* function as described. The objective of this was to create a matrix of unique, randomly distributed, integers. On a further step Matlab's *datasample* function would be used to randomly select numbers, without replacement, from the 'Random Matrix' created and the *find* and *ind2sub* functions used to retrieve the indices of the selected number from the original 'Reference Matrix'. This last test was iterated in a loop to generate a matrix of randomly selected indices that would encompass all the coordinates of the CA and not repeat. The resulting 'Random Indices' matrix is generated inside the generation loop of the CA and thus changes in each simulation iteration. The secondary, cell-selection loop just involved iterating through the elements of this generated matrix of random indices. This method was also employed to randomly select seeding indices within constrained regions of the CA grid.

In setting number 2), Matlab's *rand* function is used to allow for a uniform probability of selection amongst all possibilities. A random number q would be generated between 0 and 1. Because there are 26 different neighbours in a Moore neighbourhood, different conditions are specified:

$$if \begin{cases} 0 \leq q < \frac{1}{26}, & neigh = 1 \\ \frac{1}{26} \leq q < \frac{2}{26}, & neigh = 2 \\ \frac{2}{26} \leq q < \frac{3}{26}, & neigh = 3 \\ \frac{3}{26} \leq q < \frac{4}{26}, & neigh = 4 \\ \vdots & \\ \frac{25}{26} \leq q < \frac{26}{26}, & neigh = 26 \end{cases}$$

Where the value for the *neigh* parameter is the array entry of the aforementioned *Neighbourhood* matrix.

For setting number 3) if the molecules were being seeded uniformly this would simply involve performing a random permutation of the already generated 'Random Indices' matrix and sampling from the resulting permuted matrix. Such a permutation would be performed every iteration of the main generation loop to vary the location of the ROS seeding. Otherwise, the same method as setting 1) is used.

In CASSMI, settings number 4 and 5 aim to model the relative mobility and reactivity of the molecules involved in the simulation. The upper reference value for mobility is one movement with probability $p = 1$ every generation iteration. The upper reference value for reactivity is instantaneous reaction (rule-update) with probability $p = 1$ upon collision between reactant molecules. Relative probabilities for molecule mobility P_m and reactivity P_k are derived from the normalisation of user-defined rate constants. Thus, for any given molecule, at any particular iteration, a movement or a reaction upon molecule encounter in space is modelled through a uniform random number generator function *rand* producing a number M such that a movement event or a reaction event will occur if:

$$0 < M \leq P_m$$

$$0 < M \leq P_k$$

In the case of the multi-scale model, this format of uniform random number generation will also determine the occurrence of interactions (the execution of rules) between cells (if neighbour dependent) or within cells (if neighbour-independent).

2.1.2 CASSMI – Cellular Automaton based Spatial Simulator of Molecular Interactions

CASSMI is a 3D Lattice Gas Cellular Automaton (LGCA) simulator developed in Matlab (MathWorks Inc., Natick, MA, 2016) which simulates biochemical reactions as the result of the Brownian motion of reactant species. Equal-sized molecules are simulated by a single-unit step-size random walk in a Moore neighbourhood under perfect elasticity within closed boundaries. Upon encounter in space molecules react with a probability derived from the normalisation of rate constants. Encounter of non-substrate molecules results in 180° collision. Input arguments allow for the individual or combined simulation of relative movement speed, percentage overcrowding, and percentage spatial localisation.

CASSMI Input

CASSMI is called as a seven-argument function from the Matlab command window (Figure 2.3). Following this, further interfacing is required with CASSMI through the command window to specify the number of molecular movements to be run in each simulation and whether visualisation of the simulated molecules is desired (Figure 2.4). The simulator requires a template excel file as an input specifying:

Mandatory information (columns A to J)

i) Molecule names
ii) Initial abundances
iii) Diffusion constant
iv) Diffusion normalisation
v) Reactants (max: 2)
vi) Rate constant
vii) Rate constant normalisation
viii) Products (max: 2)

'Molecule names' must be consistent throughout the simulation information template. CASSMI is case-sensitive to this input and errors may arise from the presence of blank spaces. 'Initial abundances' refers to particle numbers and so must be zero-inclusive integers. Diffusion normalisation intakes a numerical input [1|2|3] where [1] will normalise the values by the diffusion rate of an "average protein", $10\mu m^2/s$ (Schnell and Turner, 2004), [2] will normalise the values to the highest diffusion constant provided and [3] will intake the provided values directly without any normalisation. The resulting diffusion constants become the probabilities that the specified molecules will move on a particular generation. Rate constant normalisation has the same normalisation format as the diffusion normalisation with the sole difference that for input [1], the provided rate constant values are normalised by a diffusion-limited rate ($10^8 M^{-1} s^{-1}$). Note that to employ normalisation type [1] the defined constants should be of the same units as specified. A maximum of two reactants and two products are allowed, with first and zeroth order reactions requiring empty cells to be defined as 0 (See Figure 2.5 for an example).

Optional information (columns K to P)

i) Localised species
ii) Percentage localisation
iii) Spatial end (max: 2)
iv) Events
v) New Value for Event
vi) Generation of Event

The percentage localisation of the defined localised species refers to an axial percentage so that the initial position of such molecules will be randomly assigned to indices within the grid enclosed by $(C \cdot N)^3$; where C is the user-defined percentage localisation and N is the axial length of the entire grid. Note that the default setting involves molecules having a random uniform distribution across the entire CA grid. 'Spatial End' requires a numerical input [1|2] which correspond to opposite but symmetrical ends of the lattice. The last three columns correspond to information on 'Events' within the simulation settings. CASSMI only supports Events in the format of an addition of molecules of a given species into the grid or the alteration of a rate constant value. The alteration of a

rate constant value in an Event must be referenced through the reaction number (Figure 2.6), where the reaction number is the row number in the excel sheet minus one.

Note that even if information is provided within the input excel template on relative diffusion speeds, localised molecules or Events, these will not be incorporated into the simulation settings unless the corresponding input arguments on calling the CASSMI function activate these settings (ie; are defined as 1). By default, the probability of a one-step movement for a molecule in any given generation is 1 and molecules are seeded with uniform probability across all the possible sites within the entire grid.

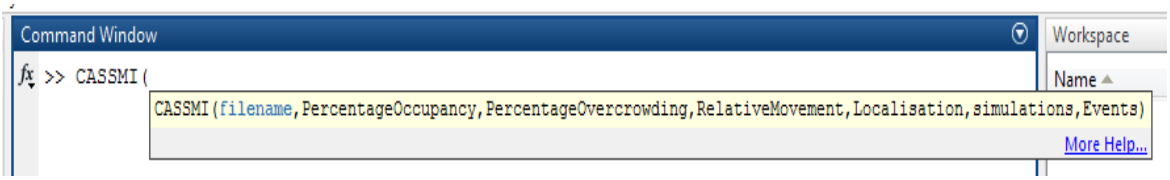

Figure 2.3. *CASSMI input arguments. 'Filename' must be a string referring to the name of the template excel file containing information on all the reactions to be simulated. This file must be located in the same directory. 'PercentageOccupancy' intakes a numerical input in the range* $[0< x \leq 100]$ *and determines the size of the 3D lattice relative to the total number of molecules to be simulated. 'PercentageOvercrowding' intakes a numerical input in the range* $[0 \leq x < 100]$ *and determines what percentage of the resulting 3D lattice will be occupied by non-reactant (overcrowding) molecules. 'RelativeMovement' intakes a numerical input* [0|1] *for the respective deactivation/activation of heterogenous probabilities of molecule movement every generation. 'Localisation' intakes a numerical input* [0|1] *for the respective deactivation/activation of constrained initial molecule distributions as defined in the input file. 'Simulations' intakes a non-zero integer as a numerical input to set the number of repeats of each simulation to be run. 'Events' intakes a numerical input* [0|1] *for the respective deactivation/activation of generation-dependent changes defined in the input file.*

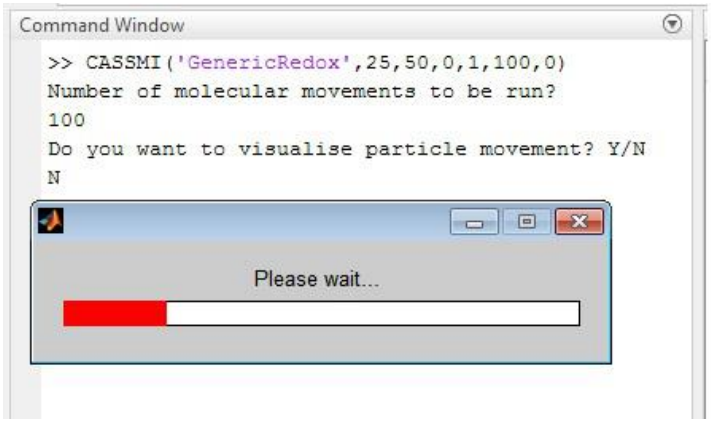

Figure 2.4. *An example of a CASSMI run. In this case, CASSMI will read the reactions specified in the template excel file 'GenericRedox' and simulate them100 times with each individual molecule undergoing 100 random movements at a 25% percentage occupancy, 50% molecular overcrowding, no relative diffusion, accounting for initial spatial localisation defined in the input file without taking into account any Events.*

GenericRedox - Microsoft Excel

File Home Insert Page Layout Formulas Data Review View Add-Ins Team

D21

	A	B	C	D	E	F	G	H	I	J
1	Molecule	Initial Abundance	Diffusion	Diffusion Normalisation	Reactant 1	Reactant 2	Rate Constant	Rate constant Normalisation	Outcome 1	Outcome 2
2	Oxidant	100	2	2	Oxidant	Sensor	1	3	SensorOX	Activator
3	Sensor	10	1		Activator	Relay	1		Function	RS
4	SensorOX	0	1		RS	0	1		Relay	Activator
5	Reductant	100	1		SensorOX	Reductant	1		Intermediate	0
6	Intermediate	0	1		Intermediate	0	0.1		Inhibitor	ReductantOX
7	ReductantOX	0	1		ReductantOX	dummy1	1		Reductant	dummy1
8	Function	0	1		Oxidant	AOX	1		AOX	0
9	Relay	10	1		Inhibitor	Activator	1		Sensor	0
10	RS	0	1		Function	0	0.05		0	0
11	AOX	100	1		0	0	0.1		Oxidant	0
12	dummy1	100	1							
13	Inhibitor	0	1							
14	Activator	0	1							
15										

Figure 2.5. *Example of mandatory input required for a simulation in CASSMI.*

K	L	M	N	O	P
Localised	Percentage Localisation	Spatial End	Events	NewValue	Generation
Relay	25	1	Oxidant	100	500
Sensor	25	2	Reaction_9	0.01	1000
Oxidant	10				

Figure 2.6. *Example of optional input required for a simulation in CASSMI.*

CASSMI Output

CASSMI saves the simulated time courses for all user-defined species as both a matlab figure (.fig) and a .jpeg file. Default plots display the mean molecule abundance ± standard deviation for each generation. However, commenting-out line 308 in the *CASSMI.m* file and uncommenting line 309 in the same file will plot individual simulation trajectories. Eight output arguments can be obtained from CASSMI.

CASSMI Output Arguments

[1] Mapped Identifiers
[2] Raw Simulation Data
[3] Abundances
[4] De Novo Reactions
[5] Second Order Reactions
[6] Localised Molecules
[7] First Order Reactions
[8] All Reactions

The first CASSMI output argument is an array listing the molecules in the model with the corresponding unique numerical identifiers automatically assigned by CASSMI. These identifiers will be used in the rest of the function output. The second output argument is a Matlab structure containing the raw simulation data for all species for each individual run. For each individual simulation, columns correspond to individual generations and rows correspond to individual species in the same order as specified by the user (can be seen in Output argument [1]). The third function output provides the starting abundances for each individual species. Outputs 4, 5, and 7 are matrices which list reactions as partitioned into zeroth order-, second order- and first order- reactions respectively. The column format of Outputs 4, 5 and 7 is as follows: *[Reactant1, Reactant2, Output1, Output2, Rate Constant, Reaction Number]*. Output 6 lists the identifiers of the molecules defined by the user to be seeded locally within the grid along with the corresponding initial abundance and percentage localisation. Output argument 8 lists all of the reactions simulated. Note that whilst output argument 2 is provided to facilitate any further analysis of the simulation data, the remaining of the output arguments intend to facilitate troubleshooting.

CASSMI validation tests

The random movement of particles within the simulation can be visually appreciated by plotting the trajectories of the first 100 movements in space of 10 given molecules (Figure 2.7). This was followed by the tracking of a molecule over $1 \cdot 10^6$ movements within the CA grid to confirm that every point in the CA grid was reachable by a particle given enough random movements (Figure 2.8). A further test was performed to assess if the random movement simulated in the CA script could represent simple particle spreading and equilibration over a container when particles are localised in space at the start of the simulation (Figure 2.9). Confirmation that the CA model could reproduce recognisable kinetic profiles for different order reactions was undertaken Figure 2.10). Overcrowding, localisation and relative diffusion was confirmed visually and through simulation (Figure 2.11). An example of the logic processing behind the simulation of a simple CASSMI model is illustrated in Figure 2.12.

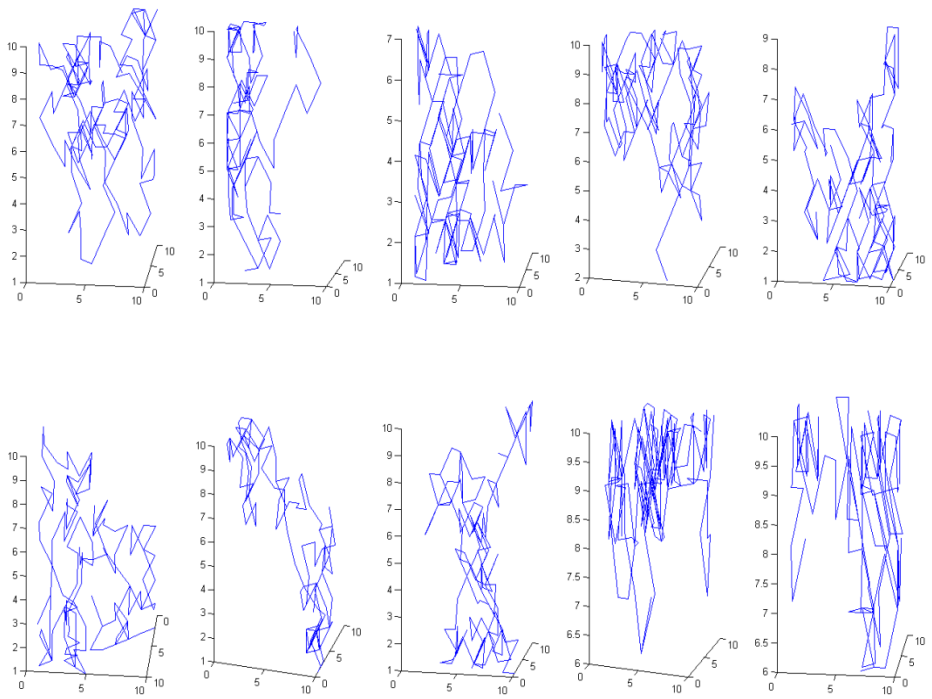

Figure 2.7. Trajectories for the first 100 movements of 10 different particles in an N^3 space where N=10.

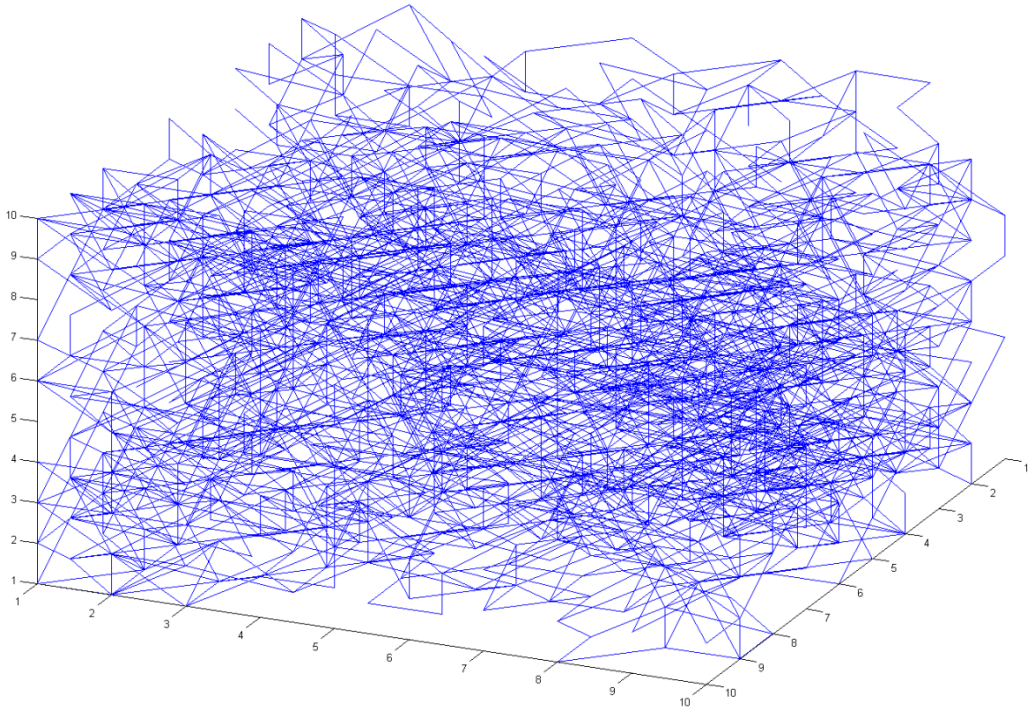

Figure 2.8. All spaces in the grid are reachable for a randomly moving particle given enough movements. Simulation parameters are N=10 and 1 000 000 movements for a single particle.

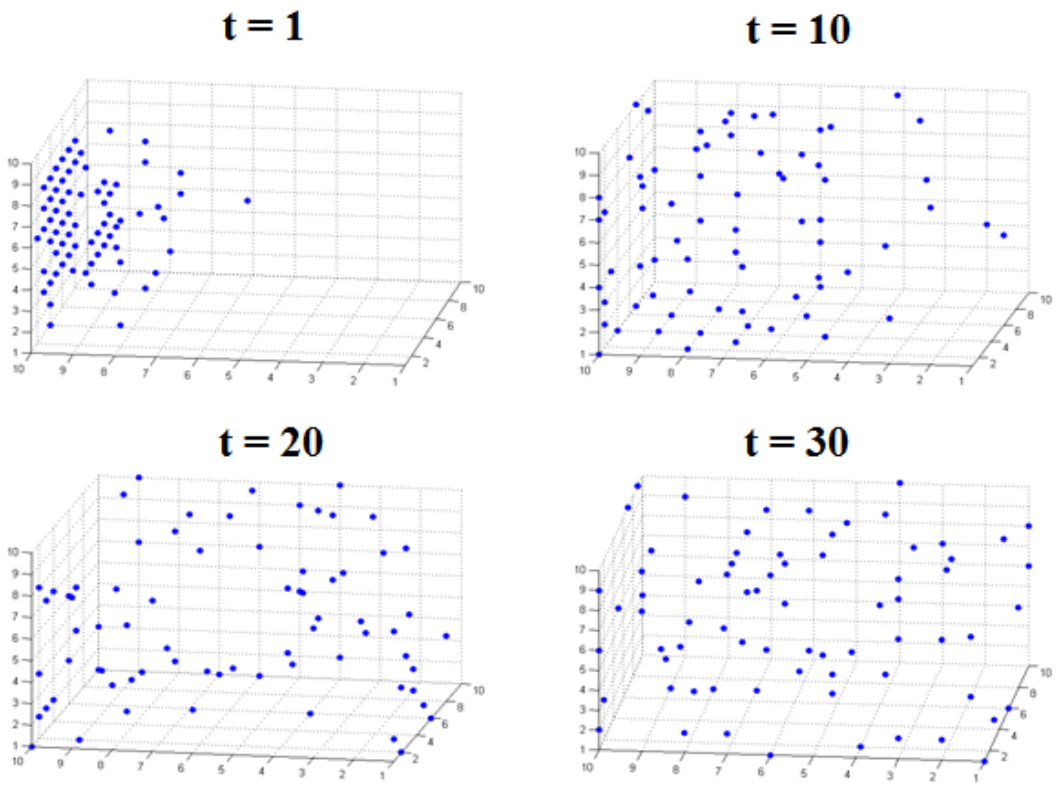

Figure 2.9. Cellular automaton model reproduces equilibration behaviour of a perfect gas in an enclosed container. Time corresponds to arbitrary units.

Figure 2.10. (Next page). Validation of CASSMI simulation output for elementary kinetic reaction profiles. **a)** Zero-order reaction $/ \rightarrow A$. **b)** First-order reaction $A \rightarrow B$. **c)** Second-order reaction $A + B \rightarrow C + D$.

a)

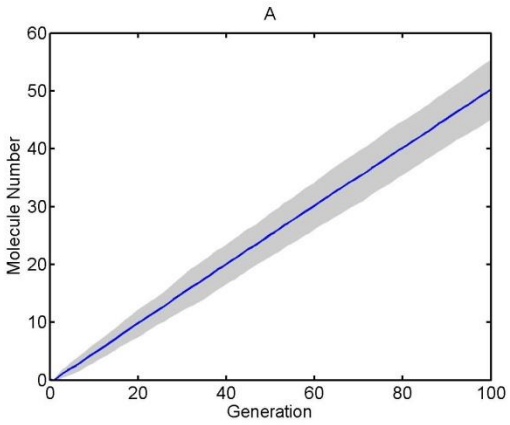
A
Molecule Number
Generation
0
10
20
30
40
50
60
0
20
40
60
80
100

b)

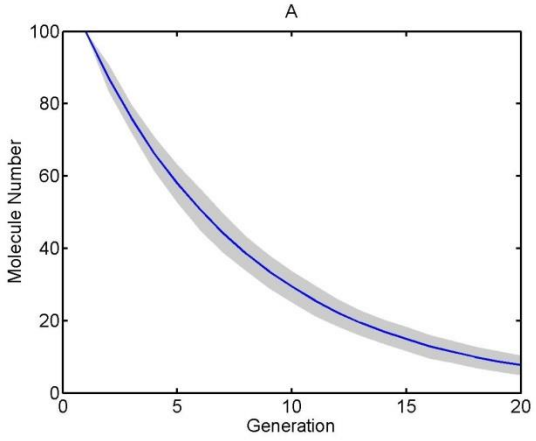
A
Molecule Number
Generation
0
20
40
60
80
100
0
5
10
15
20

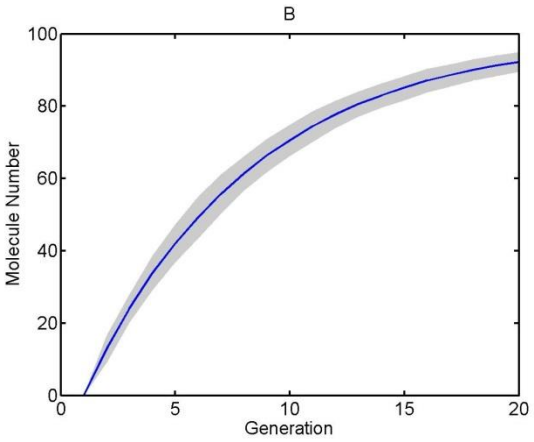
B
Molecule Number
Generation
0
20
40
60
80
100
0
5
10
15
20

c)

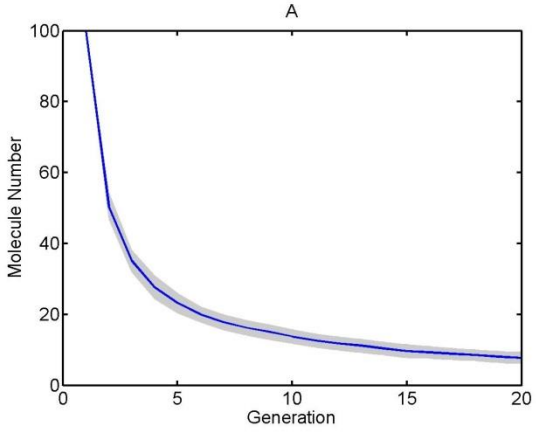
A
Molecule Number
Generation
0
20
40
60
80
100
0
5
10
15
20

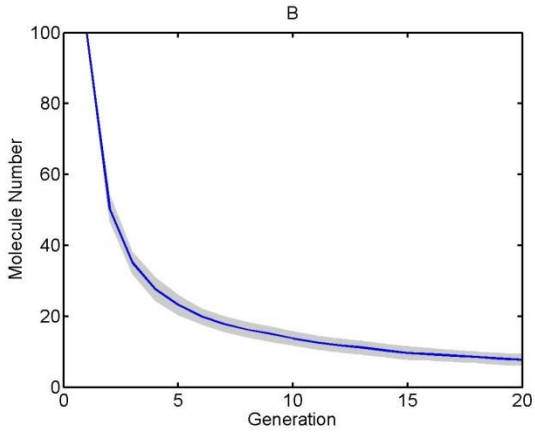
B
Molecule Number
Generation
0
20
40
60
80
100
0
5
10
15
20

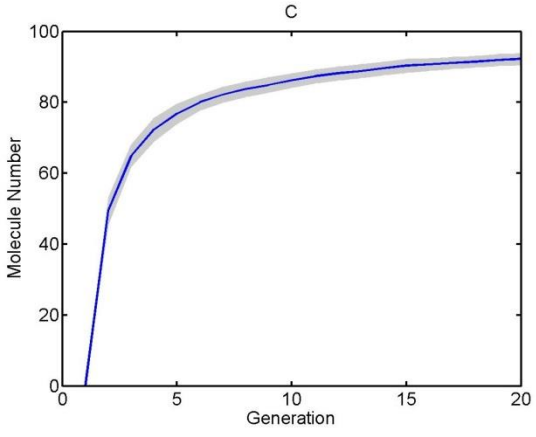
C
Molecule Number
Generation
0
20
40
60
80
100
0
5
10
15
20

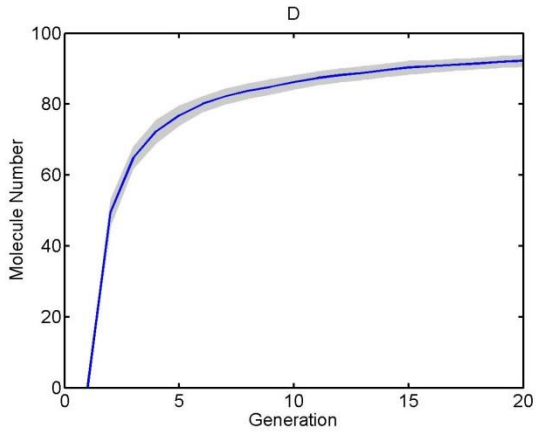
D
Molecule Number
Generation
0
20
40
60
80
100
0
5
10
15
20

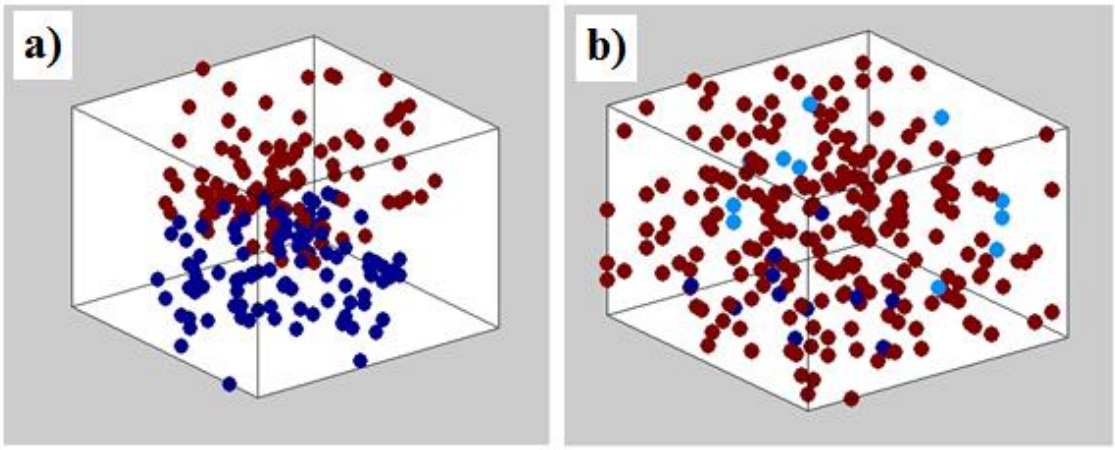

Figure 2.11. Visual validation of localisation and overcrowding of molecules during a CASSMI simulation. **a)** Localisation of molecules at separate ends of the grid. **b)** Inclusion of overcrowding molecules (brown) amongst reactant molecules (blue).

The following is a simplified pseudocode of CASSMI

Create a N x N x N matrix (grid with N^3 cells)

Assign a defined number of unique identifiers to randomly selected cells in the grid (seeding)

FOR generations:

FOR all cells in the grid:

Choose a random cell

IF cell is > 0 (not empty space – a molecule)

Choose a random neighbour

IF neighbour is 0 then neighbour switches identifier with the cell (movement) with corresponding probability

IF neighbour is not a reactant then collision occurs

IF neighbour is a reactant react with corresponding probability

Choose another random cell until all cells have been chosen.

Seed new molecules in the grid from Events or zero-order reactions

Scan CA grid and update counters of all identifiers in the grid

Next generation

Figure 2.12. *(Next page) Simplified logic flowchart representing how a simple redox signalling model can be simulated by CASSMI. Main loops in the script structure are shown in blue. CA(h,i,j) is the individual cell defined by coordinates h, i, j within the cell automaton (CA) grid.* ***(s)*** *corresponds to a coordinate translation value for each h,i,j coordinate which defines the neighbouring cell coordinates with respect to the moving cell coordinates as defined in Figure 2.2. Identifiers: Empty space=0, ROS=1, antioxidants=2, glutathione=3, redox sensor=4. In this example the number of oxidation events is being tracked. Note that scavenge involves the updating of the ROS identifier from 1 to 0 (empty space).*

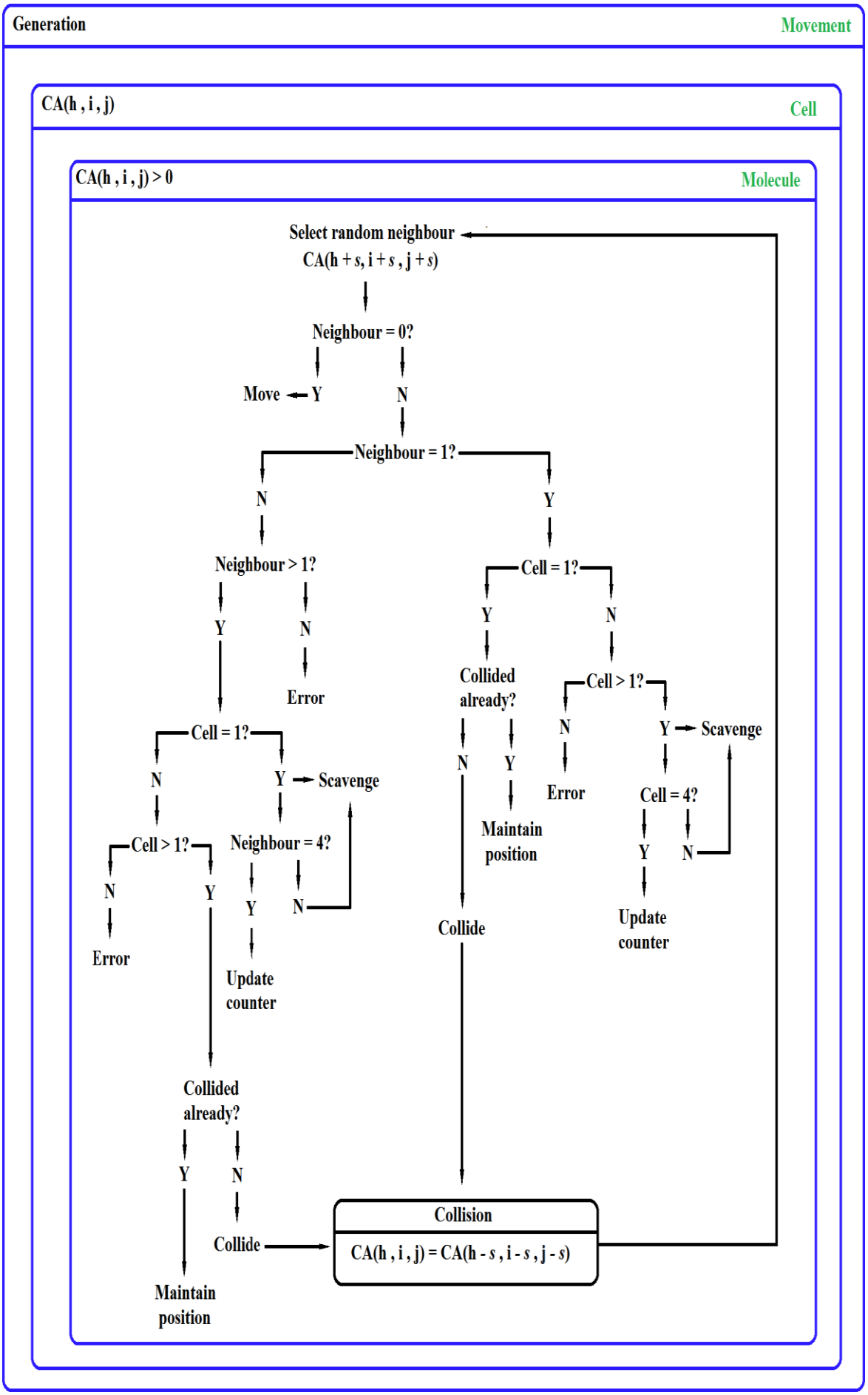
Generation
Movement
CA(h , i , j)
Cell
CA(h , i , j) > 0
Molecule
Select random neighbour
CA(h + s, i + s , j + s)
Neighbour = 0?
Move
Y
N
Neighbour = 1?
N
Y
Neighbour > 1?
Y
N
Error
Cell = 1?
N
Y
Scavenge
Cell > 1?
N
Y
Error
Neighbour = 4?
Y
N
Update counter
Collided already?
Y
N
Maintain position
Collide
Cell = 1?
Y
N
Collided already?
N
Y
Maintain position
Collide
Cell > 1?
N
Y
Error
Scavenge
Cell = 4?
Y
N
Update counter
Collision
CA(h , i , j) = CA(h - s , i - s , j - s)

2.1.3 Ordinary differential equation (ODE) – based simulations

Ordinary-differential equation-based models are commonly employed to model systems of biochemical reactions (Aldridge et al. 2006). The connectivity and structure of a biological network arises from the fact that the product of one reaction will often be the substrate or modifier for another reaction. In such a way, the different elements of a biological system are coupled to each other. This is modelled by the coupling of variables in a system of coupled differential equations. The use of the ODE modelling framework thus intuitively fits the nature of the system being modelled when it comes to biochemical networks.

Constructing an ODE-model of a biochemical network firstly requires the identification of the key components in such a system of interest. Once the relevant molecular interactions are defined, these can be formalised into a static SBGN network (Sorokin et al., 2015) and an SBML model (Hucka et al., 2003) through CellDesigner 4.4 (Funahashi et al., 2003). The resulting interaction network can then be imported into COPASI (Hoops et al., 2006) where kinetic equations are assigned to each molecular interaction and preliminary values for abundance and kinetic parameters are specified. Note that all molecular interactions in the model follow elementary mass action kinetics. The resulting model is thus a system of coupled ordinary differential equations where the rate of change in a given molecule abundance A at a given time point is determined by the sum of the rates of the reactions R_i which involve that given molecule as a substrate $(v_{\_A})$ or as a product (v_A). The latter two rates are themselves the product of individual abundances (A_i) of the reactants (r) involved in the reaction.

$$A = \sum_{R=1}^{R=N} v_A - \sum_{R=1}^{R=N} v_{-A}$$

where N = total number of reactions and the rate of a given reaction (v_R) corresponds to

$$v_R = k \prod_{r=1}^{r=n} A_r^s$$

where n = total number of reactants, r= reactants, k = rate constant for reaction R, s = stoichiometric amount.

Simulation involves the solving of the system of coupled differential equations that constitute the model through the LSODA algorithm within COPASI. The equations are solved for a given time interval with a configuration for Relative Tolerance of $1e^{-6}$, Absolute Tolerance of $1e^{-12}$ and maximal internal steps of 10000. Before the simulation, initial molecule abundance parameters were fixed to values which resulted in a steady state at $t = 0$ that otherwise would have been reached at $t > 0$ as the simulated reactions equilibrated. Signals are introduced into the model as 'Events' that act on a signalling system that is already at a homeostatic steady state. Stochastic simulations were performed using the direct Gillespie algorithm in the Matlab R2017a (Mathworks, Natick, MA) SimBiology toolbox.

2.1.4 Sensitivity analysis

Local sensitivity analysis was carried out in COPASI. This method systematically and sequentially alters parameter values by a user-defined magnitude (as a percentage of the parameter value) and examines how simulation output is changed by such alteration. Sensitivity analysis indicates which model parameters the simulation output is sensitive to. This indicates which elements of a biological system may be tightly regulated to provide a robust response and/or to furthermore establish at which points in the model can parameter uncertainty affect simulation output and the conclusions derived thereof. Sensitivity analysis was performed on the *Time Series* of *non-constant concentration of species* and configured with parameter values of 0.001 and 1e-12 for the delta factor and the delta minimum respectively. Sensitivity analysis was performed on all parameters and initial values.

Local sensitivity analysis suffers from the limitation that it does not comprehensively explore the parameter space since the perturbations used to probe model behaviour only involve varying the values of one parameter at a time. To explore perturbations of

groups of parameters in different combinations a global sensitivity analysis would be required (Saltelli et al., 2008). Such methods resemble optimisation algorithms in that they are a heuristic approach to a combinatorial problem and thus tend to be computationally intense. Emulators can be used as an alternative to local or global sensitivity analysis where a function is derived that reproduces the simulation output of the model (i.e. a meta-model) (Ratto et al., 2012). However, because the sensitivity analysis is carried out on models that already represent abstractions of signalling pathways in themselves, the use of emulators seems a too-far a departure from the original biological system. Amongst all the alternatives, local sensitivity analysis was undertaken for convenience, since it is already embedded in the COPASI environment and it is not computationally intense.

2.1.5 Information theoretic analysis

When investigating the function (or loss of function) of signalling pathways it is necessary to consider what their function is. A signalling pathway can be said to function to transmit information from the cellular environment, whether it's the internal or external environment. But what exactly is meant by information? Can it be systematically quantified?

Information has been defined by Claude Shannon as being a function dependent on a probability of occurrence (Shannon, 1997). Intuitively, if one is certain about the outcome of an event, nothing would be learnt once that event takes places. If an event outcome has very low probability of happening, and it does, one would expect surprise at the outcome and new information on the uncertain state of the event outcome would have been gained. This conceptual relationship between the information content H_X of event X and the probability of occurrence $p(X)$ of event X can be formalised into the following axioms:

1. Information content, H_X, is a decreasing function of the $p(X)$. i.e. More unlikely events provide more information than more likely events.

2. $H_X = 0$ when $p(X) = 1$. No information will be gained if there is certainty on the outcome of the event.

3. $H(X \cap Y) = H_X + H_Y$. If two events X and Y are independent of each other, their combined information content should be the sum of their individual information contents.

Shannon's information content equation, also termed Shannon's entropy equation, satisfies all of these axioms in the following format.

$$H_X = \log \frac{1}{p(X)} \tag{1}$$

Thus, information is intrinsically linked to uncertainty. Upon a closer examination of axiom 3, it becomes apparent that if two events are dependent on each other, then $H(X \cap Y) < H_X + H_Y$ since there would be an expected overlap in information content between both events if knowing the outcome of one provided information on the likely outcome of the other. This is intuitive since, for example, whilst the event probability of a randomly drawn card being a king of hearts is $\frac{1}{52}$, this probability would increase if the outcome of the event of the card being red was known to be true. In this case, knowing about event Y reduces the information needed to describe X. This reduction in information content is actually information gained on the state of X by narrowing down the state probabilities when knowing state Y. The information event Y provides on event X can therefore be said to be:

$$I(Y \rightarrow \mathrm{X}) = H_X - H(X|Y)$$

Shannon proved this through formal mathematical derivation to provide the mutual information equation between two discrete random variables X and Y.

$$I(X;Y) = \sum_{x \in X} \sum_{y \in Y} p(x,y) \cdot log \frac{p(x,y)}{p(x) \cdot p(y)} \tag{2}$$

However, in practice, the joint distribution $p(x, y)$ is not a direct observable. Thus we can derive:

$$p(x|y) = \frac{p(x \cap y)}{p(x)}$$

$$p(x, y) = p(x \cap y) = p(x) \cdot p(y|x)$$

Substitute into equation (2) so then mutual information becomes:

$$I(X;Y) = \sum_{x \in X} \sum_{y \in Y} p(x) \cdot p(y|x) \cdot log \frac{p(y|x)}{p(y)} \quad (3)$$

In this format, equation (3) can be used to quantify how much information can downstream molecule y provide about upstream molecule x. If x is a signalling molecule and y is downstream enough, the mutual information between both random variables would correspond to the information flow through the signalling pathway. Note that both x and y can be considered random variables due to the inherent stochasticity in biomolecular signalling pathways. The corresponding probabilities would thus be derived theoretically through the stochastic simulation of a given kinetic model.

For any given abundance value of x in a model simulation, a probability distribution can be derived for molecule y through the running of a large number of stochastic simulations to derive $p(y|x = x_i)$. From the latter distributions it is possible to derive $p(y)$ by obtaining the marginal probabilities of y over all values of x. Whilst $p(x)$ is usually unknown, if assumed to be uniformly distributed, then the mutual information becomes systematically normalised (Uda and Kuroda, 2016). This means that $I(X;Y)$ values cannot be interpreted in absolute terms (i.e. in terms of the number of signal states that the pathway can distinguish between) but still allows for the relative comparison of information flow across a signalling pathway under different simulated conditions but the same underlying topological structure. Figure 2.13 shows a simplified flowchart of the algorithm developed in Matlab to calculate the theoretical mutual information between molecular species in signalling pathways simulated in SimBiology.

Figure 2.13. *(Next page). Logic flowchart of the developed algorithm for the calculation of the mutual information between model species. The algorithm is composed of four modules. The first module generates p(x) by creating a uniform or normal distribution around an inputted mean value for x. The second module generates data through the iterative stochastic simulation of the model for each value of the user-defined range of x. The third module tabulates the data generated from the second module to derive p(y) across all values of x. The final module draws from the derived p(y) and p(x) generated from the previous modules to compute the local mutual information for each value of x which is then summated to derive the global mutual information between the two variables x and y.*

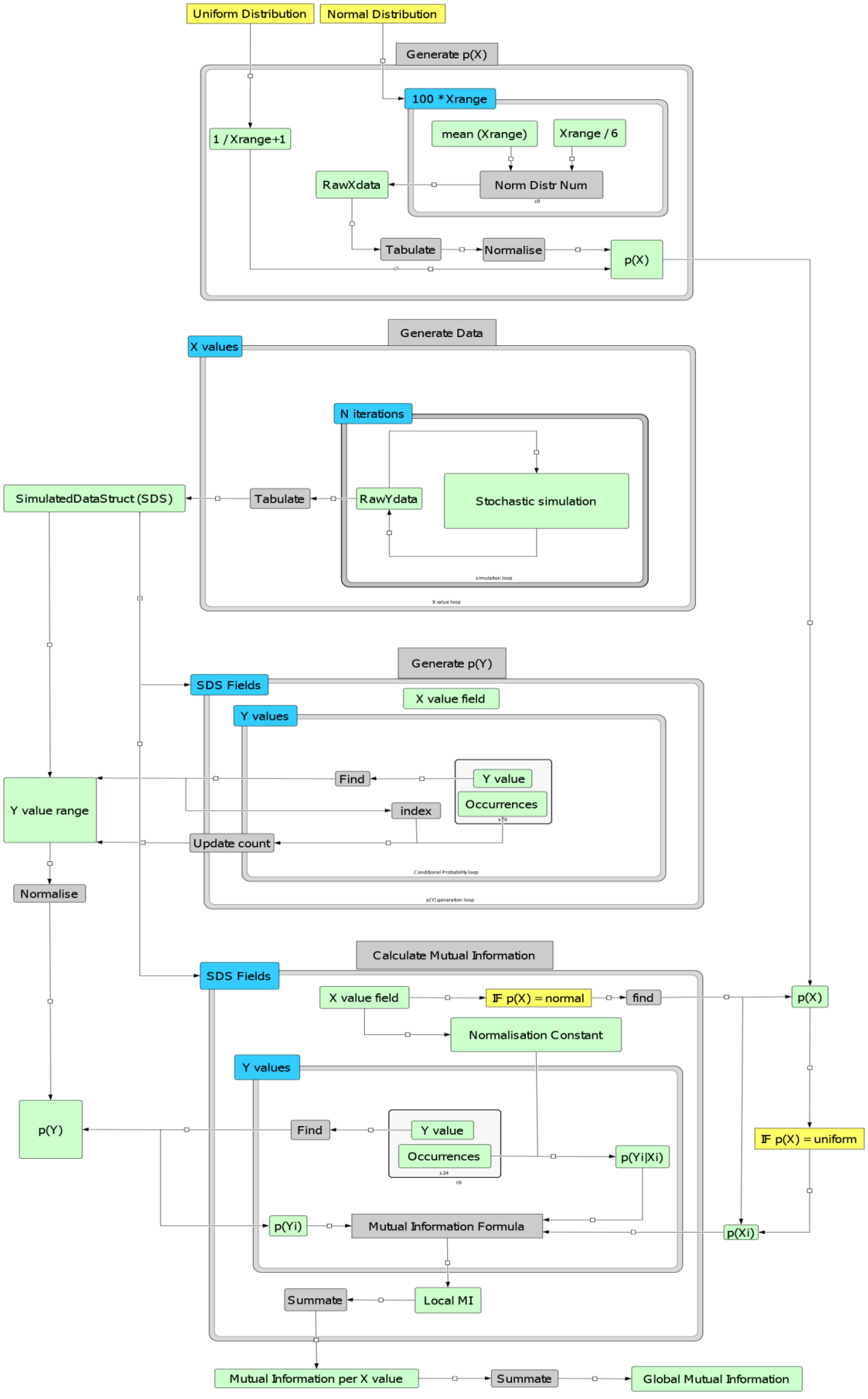
Uniform Distribution
Normal Distribution
Generate p(X)
100 *Xrange
1 / Xrange+1
mean (Xrange)
Xrange / 6
RawXdata
Norm Distr Num
Tabulate
Normalise
p(X)
Generate Data
X values
N iterations
SimulatedDataStruct (SDS)
Tabulate
RawYdata
Stochastic simulation
simulation loop
X value loop
Generate p(Y)
SDS Fields
X value field
Y values
Find
Y value
Occurrences
index
Y value range
Update count
Conditional Probability loop
Normalise
p(Y) generation loop
Calculate Mutual Information
SDS Fields
X value field
IF p(X) = normal
find
p(X)
Normalisation Constant
Y values
p(Y)
Find
Y value
Occurrences
p(Yi|Xi)
IF p(X) = uniform
p(Yi)
Mutual Information Formula
p(Xi)
Summate
Local MI
Mutual Information per X value
Summate
Global Mutual Information

2.1.6 Random network generation algorithm

The properties of mathematical models often exist in a finite area of the parameter space. Stochastically probing the parameter space can provide a heuristic approximation of how robust the model-derived observations are to the underlying parameters. However there still remains an uncertainty regarding the accuracy of the model structure and whether model-derived observations might depend on a specific model architecture. In this case, testing for alternative topologies alongside the parameter space will probe the main sources of uncertainty which the model behaviour depends on. Stochastically generating an entirely new model architecture and parameter set is an "extreme" example of the heuristic exploration of the combined parameter-topological space. This approach can be useful to test for the overall generality of an observation if it is suspected to occur as a general property of a given type of systems.

An algorithm was developed in Matlab for the systematic exploration of model topologies. This algorithm requires the specification of 15 input parameters. Seven of these parameters must be defined as scalar values: *Repetitions, Basal level of constitutive signal, Simulation Time, Signal Strength, Signal Time* and *Minimum Relay Length*. The latter specifies the minimum number of activation profiles that must be identified within a simulated network in order to be taken forward for further analysis. This is to discard cases where the signal feeds directly to downstream network elements. The rest must be defined as vectors defining the lower and upper boundaries between which the algorithm will randomly sample a value with a uniform probability. Should any of these parameters be desired to be clamped to a specific value, both the lower and upper bounds should be assigned to the desired value. Input parameters specified as vectors include:

- Number of reactions (Rn)
- Range of initial abundances
- Number of positive auto-regulation loops
- Number of positive feedback loops
- Percentage inhibitory reactions
- Percentage of competing reactions
- Percentage of degradation reactions

- Range of rate constant values

A reaction stoichiometric matrix is specified as a zeroes matrix of dimensions (Rn x Rn). To this matrix, an additional row (r_d) and a column (c_d) are further added for the incorporation of a generic degradation reaction. The algorithm randomly selects a row *i* and a column *j* of the reaction matrix. Both of these random selections are performed using the *datasample* function without replacement. To maximise uncertainty over which element of the reaction matrix will be selected by the randomisation procedure, the randomly selected row and column will be accepted with a probability of 0.5, else another column will be randomly selected without replacement. If a set of coordinates from a matrix are accepted, the zero-entry will be changed to a value of ±1 with the value sign randomly assigned with probability of 0.5 but restricted by counters in the case of (-1) assignations. Once a single assignation has taken place, the algorithm then moves to the next randomly selected row. This first round of interaction definitions ensures every reaction (row) will uniquely feed into another reaction (column). Thus, the directionality of the interactions follows the rows in the matrix.

A positive value indicates a network interaction where the product of the reaction defined by row *i* feeds into the reaction defined by column *j*. Therefore, all values of row r_d will remain as zero since the degradation reaction is an end-point in the network (Figure 2.14). A negative value within the reaction matrix indicates a network interaction where the product of the reaction defined by row *i* will inhibit the substrate of the reaction specified by column *j* without being itself utilised by the reaction. Modelling of inhibition in this way requires of three further specifications be included in the algorithm. Firstly, that if an inhibitory interaction arises there must be a substrate feeding into the reaction (i.e. at least one positive value in the column for reaction *j*). If none have yet been assigned, then a row within the reaction column is randomly selected and its value changed from zero to one. Secondly, the inhibitor must undergo a first-order degradation. Thirdly, the number of inhibitory reactions that are randomly assigned cannot surpass the randomly chosen percentage from the user-defined input range.

The algorithm will then move on to scan the created reaction matrix. It will firstly scan the diagonal of the reaction matrix where $i=j$. In this case, a positive matrix entry would correspond to a self-activation reaction where the product of the reaction denoted by row *i* will feed as a substrate into the same reaction denoted by a column with the same

identifier value for *j*. The number of self-activating reactions can be user-defined. If the first round of interaction definitions did not randomly create a number of self-activation reactions that matches those specified by the user then indices where *i=j* will be selected in a random order and be removed (assigned to 0) or incorporated (assigned to 1) to match the counter.

At this point, the reaction matrix encodes an interaction network where every reaction uniquely feeds into another reaction. The algorithm then undergoes a second round of defining interactions. The procedure of this round is identical to the first one except that conditions are set so that *i)* only matrix entries with a value of 0 which are not part of the diagonal can be changed into a 1 *ii)* the maximum number of new interactions included is limited by a counter determined by the user-defined input on percentage competing reactions. The result of this second round is that the products of some reactions (rows) will feed into multiple other reactions (columns), creating a branching-off scenario of competition between two reactions for the same substrate.

Further additions to the reaction matrix are made where entries in c_d are randomly selected to be assigned a value of 1 for a number of reactions constrained by the user-defined percentage of reactions whose products are degraded. Note that substrates that are not assigned to be degraded are assumed to have a half-life substantially longer than the time-scale of the simulation. At this point the algorithm performs various scans of the reaction matrix. The first one ensures that there is at least one column in the matrix with all-zero elements. This means no reaction feeds into that particular reaction and thus it is an input point in the network. If no input reactions are found, a column (not c_d) is selected at random and assigned all-zero values. A second scan is then performed that looks for the occurrence of positive feedback loops (PFLs) in the generated reaction matrix. A PFL is defined as the condition where *matrix(i,j)* and *matrix(j,i)* are both 1. The number of PFLs can be user-defined.

If the first round of interaction definitions did not randomly create a number of PFL s that matches the minimum number specified by the user then indices will be selected in a random order and PFLs will be incorporated to match the specified minimum value. To avoid PFLs to be defined at the ends of the network, when these have been identified or defined, one of the two reactions involved in the PFL will be selected at random along with another reaction not involved in the PFL and a positive interaction link will be established between them. This is to ensure the PFL product feeds into the network and will only be incorporated if it does not already exist in the network topology. An

additional condition was introduced that a positive feedback loop must contain an inhibitory reaction that feeds into one of the two reactions. If this condition was not satisfied it was added through the random selection of a zero-entry of a randomly selected row in the reaction column. This inhibition would feed into one of the two reactions involved in the positive feedback loop selected at random.

Once the reaction matrix has been defined, a product matrix of size (Rn x Rn) is defined where rows correspond to species and columns correspond to reactions. The same procedure will be employed as in the first round of defining interactions in the reaction matrix to assign species as products of randomly selected (without replacement) reactions. The only difference being that such assignation involves only positive values within the matrix.

In the next step the algorithm iterates through every reaction and its product, then extracting its substrates from the products of the reactions that feed into the given reaction. This involves cross-checking between the *reactions* and *products* matrices. Unique reactions are defined because the algorithm generates a list of species names *Si* where *i* is the number of unique products. Thus, the extraction of the reactant and products of each reaction can be sequentially mapped to a species name and a string created in the form '*S3 + S7 -> S2'* using the function *strcat*.

In addition to unique species names, unique rate constant names *Kr* are defined for each reaction *r* in the network. A randomly chosen value constrained by the user-defined input will be assigned to every rate constant and every species initial abundance. It is worth noting that inhibitory reactions are generated separately so that when the algorithm encounters an interaction defined as -1 in the matrix it will retrieve the product of that reaction and a randomly selected a substrate of the reaction it feeds into and define two reaction strings in the form: '*NegReg + Si -> NegReg' and 'NegReg -> Degraded'*. Where *NegReg* is the negative regulator species performing the inhibitory interaction. Species that are substrates for the degradation reaction are defined in a format *'Si -> Degraded'* thus following first- order kinetics.

The nature of the algorithm makes it possible that multiple input reactions (reactions with no other reactions feeding into them) may arise. A scan is performed to locate these input reactions in the reaction matrix and to randomly select one and assign a '*Signal*' species to the reaction so that the reaction string becomes '*Signal -> Si'*. The *Signal* species is the variable that will be altered in strength and timing according to

user-defined inputs to simulate a stimulus going through the network architecture. Because only one signal is simulated through one input network branch, large parts of the network may remain unused/unaltered by the stimulus.

Once the reactions have been defined as strings, in addition to species names and initial abundances and alongside rate constant names and values, a simbiology model can be created through the *addspecies*, *addparameter* and *addreactions* functions. Models are simulated deterministically using the ODE15s solver. Note that the simulation time is set to be determined by $1/K_s$, where K_s is the slowest rate constant in the model. The acute stimulus is introduced at $1/2K_s$ in order to allow for the equilibration of the system. If the simulation of the generated model yields a minimum user-defined number of activation curves within the network species, a new reaction will be incorporated into the model for the constitutive synthesis of the *Signal*. The rate constant for the constitutive synthesis is set to a default of double that of the rate constant of the reaction of the *Signal* with the sensor molecule in the network.

Once this modification is introduced into the model, an identical acute stimulus will be fed through and the resulting activation profiles will be compared with those previously generated by the acute stimulus alone. This comparison is made through the use of the *findpeaks* function.

If the peak identified in the constitutive signal model displays a smaller magnitude than the peak identified in the simulations without a constitutive signal, that species will be catalogued as 'blunted' if this reduction in magnitude is at least 10%. If a defaulted minimum of three species in the network display a reduced activation magnitude in the presence of a constitutive signal (Blunted) then the model information will be extracted and stored for further analysis of its structural properties. Conversely, if the peak identified in the constitutive signal model displays a larger magnitude than the peak identified in the simulations without a constitutive signal, that species will be catalogued as 'additive' if this increase in magnitude is at least 10%. If a defaulted minimum of three species in the network display an increased activation magnitude in the presence of a constitutive signal then the model information will be extracted and stored for further analysis of its structural properties.

The number of conditions in the network generation procedure, both user-defined and otherwise, means that the smaller the network being simulated, the less random its underlying architecture will be. This is why the minimum number of reactions within

the randomly-generated networks is set to 50. All reactions are simulated following first-order kinetics with the exception of inhibitory reactions which will follow second order kinetics. The 'standard' run of the algorithm refers to configuration settings for a minimum network size of 50 reactions with percentage inhibitory reactions, percentage degradation reactions and percentage competing reactions assigned through the uniform random sampling from value vectors [25-50], [10-25] and [10-25] respectively. Initial abundances were assigned to 10 (AU) and the basal signal was set to arise from a synthesis reaction of the signal following a zero-order rate constant of twice the value of the rate constant for signal reaction with its sensor. Standard algorithm settings were used throughout.

The node connectivity of the resulting networks was tested (Figure 2.15). The distributions reveal low connected nodes (1-3 degrees) with a relatively high occurrence and the presence of high connected nodes (10-15 degrees), also called hubs, with a relatively high occurrence. This is a feature of scale-free network topologies that have been argued to realistically represent biological networks (Barabasi and Oltvai, 2004).

Figure 2.14. *(See next two pages). Illustration of the generation of a biochemical interaction network.* ***a)*** *Reaction matrix. 0 = no interaction, 1 = product of row reaction feeds as a substrate to the column reaction, -1 = inhibitory interaction. Note that there is one self-activation reaction (blue) and one positive feedback loop arising from the mutual activation of reactions 3 and 7 (green). Reactions with no other reactions feeding into them (Inputs) are all-zero columns (R1, R6 and R8). Reactions are selected at random to feed into an added reaction column that corresponds to a degradation reaction (red). Because the degradation reaction is an end-point, it will not feed into any reactions (all-zeros in R9 row). However, should recycling occur as a result of the degradation process, this could be included into the network by allowing 1s to be seeded into the last row of the reaction matrix.* ***b)*** *Interaction network topology corresponding to the reaction matrix in A.* ***c)*** *Product matrix. Every reaction generates one unique product.* ***d)*** *Bipartite network representation of the network corresponding to the reaction matrix and the product matrix. Red= degradation reactions.*

a)

	R1	R2	R3	R4	R5	R6	R7	R8	R9
R1	0	1	0	0	0	0	0	0	0
R2	0	0	1	-1	0	0	-1	0	0
R3	0	0	0	0	1	0	1	0	1
R4	0	0	0	1	-1	0	0	0	0
R5	0	0	0	0	0	0	0	0	1
R6	0	0	0	0	0	0	1	0	0
R7	0	0	1	0	0	0	0	0	1
R8	0	0	0	1	0	0	0	0	0
R9	0	0	0	0	0	0	0	0	0

b)

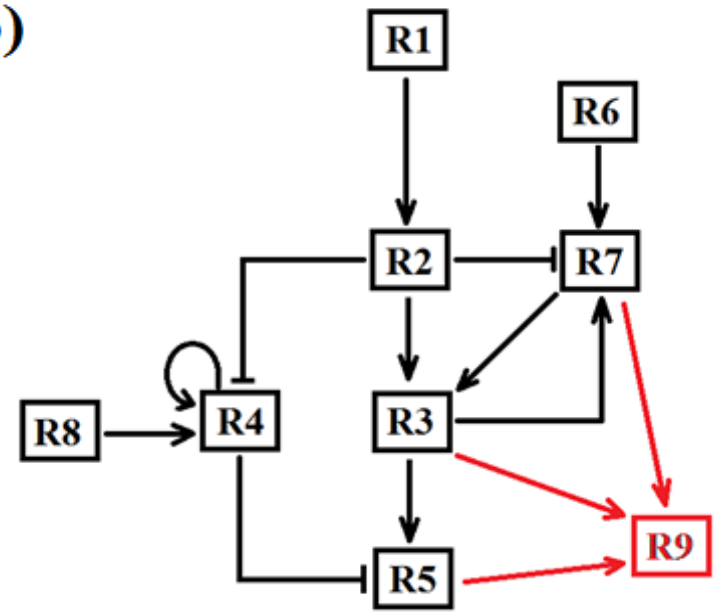

c)

	R1	R2	R3	R4	R5	R6	R7	R8
S1	0	0	0	1	0	0	0	0
S2	0	0	0	0	0	0	0	1
S3	0	0	0	0	0	1	0	0
S4	0	0	0	0	1	0	0	0
S5	1	0	0	0	0	0	0	0
S6	0	0	0	0	0	0	1	0
S7	0	0	1	0	0	0	0	0
S8	0	1	0	0	0	0	0	0

d)

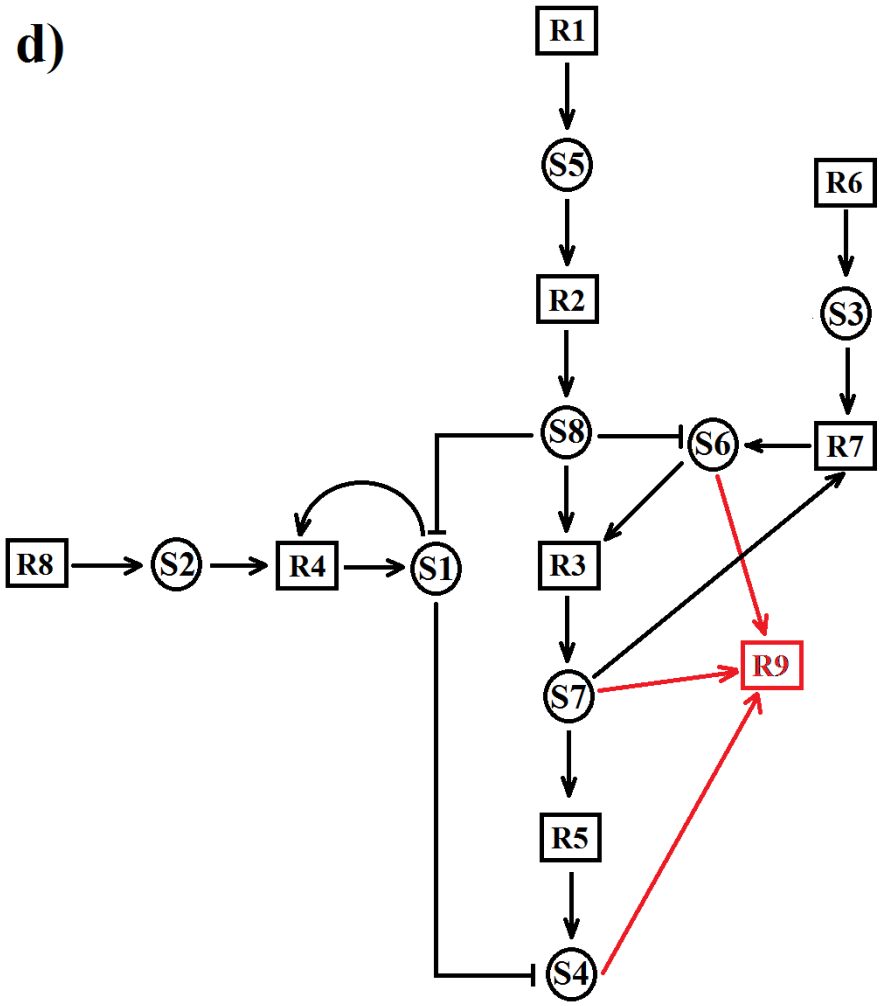

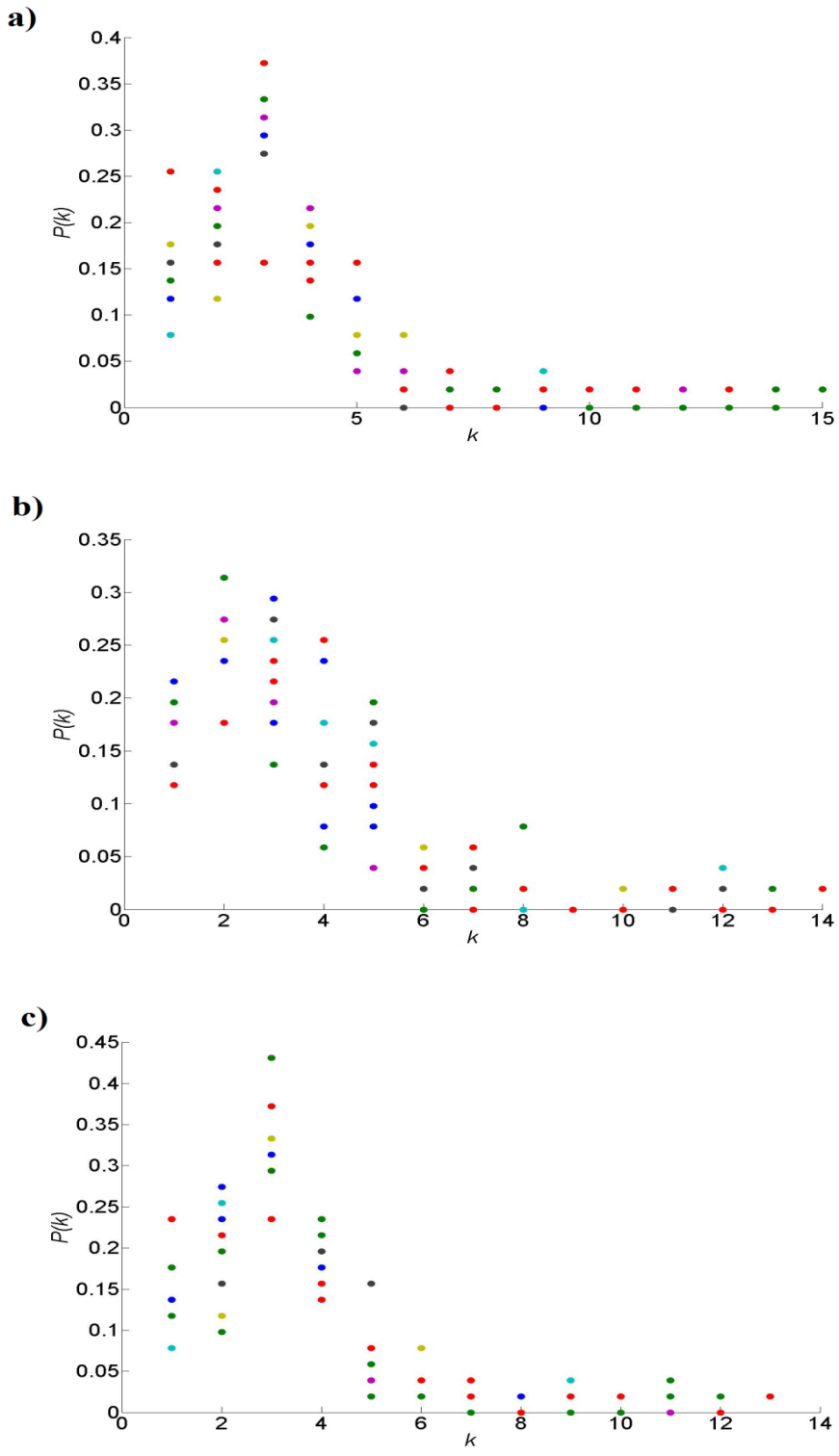

Figure 2.15. *Node degree distribution for networks displaying* ***a)*** *'Additive' behaviour,* ***b)*** *'Blunting' behaviour and* ***c)*** *under conditions of no model selection criteria. Data shown for 10 models. K = node degree, P(k) = probability of observing a degree k in the model. Additive behaviour refers to an increased network activation by an acute stimulus in the presence of a basal signal. Blunting behaviour refers to a decreased network activation by an acute stimulus in the presence of a basal signal.*

2.1.7 Multi-scale simulations

The maintenance of biological homeostasis often involves processes encompassing multiple levels of organisation. For example, damaged mitochondria are kept in check by mitophagy in order to avoid damage accumulation. However, if this mechanism fails, mitotic cells can arrest their cell cycle and enter a state of senescence which can be recognised and cleared by immune cells. By taking into account both levels of organisation, an intuition can be developed as to how biological dysfunctionality may be compensated or propagated across scales. Furthermore, it potentially allows the mechanistic bridging between molecular alterations during age and loss of tissue homeostasis.

The multi-scale model of senescent cell populations was developed as a Matlab script that simulates cells as interacting agents within a cellular automaton framework. 2D and 3D multi-scale models were constructed to simulate a regular lattice occupied by resting cells at 100% confluency. All cells thus begin in a resting state (*R*). Other states the grid cells can enter include; pre- senescent (PS), senescent (S) and empty (E). A single simulation of the model will involve a probabilistic updating of cell states according to defined rules. A single simulation, referred to as a generation, corresponds to a unit time of 24hrs. At each generation, each randomly-selected cell will be mapped to the following rules:

i) If state is (*R*) then transition to (*PS*) with probability P_{ind}
ii) If state is (*PS*) and has been for <10 days then state is retained
iii) If state is (PS) and has been for 10 days then transition to (S)
iv) If state is (*S*) then neighbouring (*R*) agents transition to (*PS*) with probability P_{Bys}
v) If state is (*S*) then transition to (E) with probability P_{clr}
vi) If state is (E) then transition to (R) with probability P_{new}

Note that neighbouring agents are defined as those within the Moore neighbourhood of the selected agent. This corresponds to 26 neighbours in a 3D grid and 8 neighbours in a 2D grid. Rule *i)* models the entering of a cell into the senescence program whilst rules *ii)* and *iii)* correspond to the progression of the senescent phenotype. Rule *iv)* models the senescent-induced-senescence bystander effect. Rule *v)* models senescent cell

clearance by the immune system. Rule *vi)* models the replacement of empty spaces with new cells.

The model becomes multi-scale in the definition of the probability of induction, P_{ind}. Instead of assigning a numerical value to P_{ind}, whenever rule *i)* is applied a single stochastic run of the Dalle Pezze model (Dalle Pezze et al., 2014) of cellular senescence induction is performed. The end-level of four variables is then collected: ROS, p21, DNA damage and SA-β-GAL. If the levels of these four molecules are above their average end-levels derived from a previous deterministic simulation of the model then the transition defined by rule *i)* will take place. Thus, the Dalle Pezze model can be said to be employed to gain a sneak-peak into the future as to whether a cell will become senescent or not.

When the multi-scale model simulates irradiation-induced senescence, rule *i)* is only applied at day 1. When the multi-scale model simulates the stochastic induction of senescence it does so by running a single molecular dynamics simulation in CASSMI for every resting cell at every generation. The CASSMI run simulates an actively inhibited positive feedback loop that has the potential to undergo a runaway process with a low probability (conceptually explained in Section 6.2.1). In the cases when a runaway process occurs it is detected when the damaging molecule reaches a spatial occupancy of >50% of the total space in the grid. If this occurs it will be interpreted as a substantial amount of damage having taken place in the cell and the Dalle Pezze model will be run stochastically once to determine if that single cell will undergo senescence as a result of this damage perturbation.

The multi-scale model can thus be summarised as a macro-solver (i.e. the resolving of the states of the cells in the model) coupled to a micro-solver (an ODE-model) that simulates a timescale which is fast compared to the macro-solver. The micro-solver is the Matlab SimBiology toolbox simulating the Dalle Pezze et al. (2014) model to capture molecular changes that are fast compared to the cell transitions modelled in the cellular automaton generations. Model simulation involves a grid with 10 arbitrary units in any dimension simulated (10^3 cells in a 3D model and 10^2 cells in a 2D model). The arguably low number of cells simulated aims to represent an arbitrary section of an arbitrary tissue and was limited by computational time. The simulation time of the multi-scale model was approximately 1.2 days in the case of a 30 day simulation of irradiation-induced senescence and approximately 3.9 days in case of a 30 day stochastic-induced senescence.

2.2 Experimental methods

2.2.1 General information on cell culture

C2C12 myoblasts are a mouse skeletal muscle cell line commonly employed as an *in vitro* model of skeletal muscle (Burattini et al., 2004, Manabe et al., 2012). The culture of these cells involves their maintenance in a 5 % CO_2 humidified incubator (Thermo Forma^{TM} Steri-Cycle^{TM} CO_2 Incubator) at 37ºC. All references to incubation throughout this work will involve these same conditions. Undifferentiated, mitotic, C2C12 myoblasts are grown in high glucose Dulbecco's Modified Eagles Medium (Sigma Aldrich - D5671), supplemented with 10 % fetal calf serum (Sigma Life Sciences – F9665). This growth medium will be referred to as 'non-differentiating' medium. Note that all media used in cell culture procedures contains 1% Penicillin/Streptomycin (Sigma Life Science P4333) and 1% L-Glutamine (Sigma Life Science G7513). Furthermore, all cell culture reagents are previously warmed up to 37ºC in a water bath (Grant OLS200). All cell culture work takes place in an alcohol-treated, sterile tissue culture hood (CAS BioMet2 TriPASS CII). Additionally, serum free medium also refers to the high glucose DMEM (D5671) medium with P/S and L-Glutamine but without serum supplementation.

2.2.2 C2C12 differentiation

To trigger C2C12 myoblast differentiation into post-mitotic myocytes and then myotubes (Manabe et al., 2012), cells are plated on 0.1% gelatin-coated dishes. Their culture medium is modified to High Glucose DMEM (D5671) supplemented with 2% Horse Serum (Sigma Aldrich – H1270). This medium will be referred to as 'differentiating' medium. Differentiation is started at 80% cell confluency and lasts for 7 days. Such a prolonged differentiation period aims to promote homogeneity at the population level since there is a high variation in the time taken by each cell to differentiate into myotubes.

The dishes are coated through the addition of Attachment Factor Protein (Life Technologies S-006-100) to cover the whole plate surface and left in the incubator for 30 minutes. Any medium is changed every two days and $2 \cdot 10^5$ C2C12 myoblasts seeded per 75cm^2 flask (CellStar) or $5 \cdot 10^4$ myoblasts seeded per well in a 6-well plate

(Thermo Fisher Scientific -130184). The apparent low seeding density in the 25cm^2 flask is necessary since differentiation in C2C12 myoblasts is triggered by cell-cell contacts and so splitting has to be performed at roughly 60% confluency.

2.2.3 Cell splitting

Cell splitting involves a series of steps, the first one being the removal all of the medium in the flask followed by washing the cells in serum-free medium in order to remove any serum which may quench the trypsin. Cells are then trypsinized by covering the surface of the flask with Trypsin-EDTA (Sigma Life Science – T3924) and left in the incubator for 5 minutes. Following this, the trypsin is quenched by the addition of an equal volume of non-differentiating medium. The resulting mixture containing the trypsinised cells is then transferred into a centrifuge tube (Starlab) and centrifuged (Eppendorf Centrifuge 5804R) at 900rpm for 5 minutes.

After the centrifugation step, all the cells are found as a pellet at the bottom of the falcon tube. The medium is removed and the pellet re-suspended in non-differentiating medium. A volume of 10μL of the re-suspended cells is taken for a cell count in the haemocytometer (Assistent®). The number of cells within the central grid corresponds to roughly 1/10000th of the number of cells per ml of the re-suspended pellet mixture. The volume of this mixture added to each plate/flask is then calculated so that an aforementioned corresponding number of cells are seeded. After such a volume of re-suspended cells is added it is important to mix well the flask/plate contents to ensure an even seeding of the cells across the plate, especially since differentiation is triggered by cell-cell contact.

2.2.4 Cell cryopreservation

Cryopreservation of cells involved the centrifugation (900rpm for 5 min) of a volume of re-suspended cells that corresponds to $1 \cdot 10^6$ cells. The resulting pellet is re-suspended in 1ml of 'freezing' medium. Such medium consists of 60% serum free medium, 30% FCS, and 10% DMSO (Sigma Life Science – D8418). The resulting cell suspension is then transferred to a cryotube (Thermo Scientific Cryotube™ 1.8ml vial) and kept in a -20ºC freezer for two hours. Then its transferred to a Mr Frosty™ freezing container

(Nalgene – 5100) and kept in a -80ºC freezer for two days. Following this period, the cryotube is then transferred to liquid nitrogen storage (CBS Isothermal V3000-AB). Such a step-wise freezing protocol ensures gradual freezing and improved preservation of the cryopreserved cells. Note that cryopreservation of C2C12 cells can only be undertaken in their mitotic myoblast form.

2.2.5 Cell defrosting

Defrosting of cells involves a brief (approx. 30sec) warming up in a 37ºC water bath and a quick transfer to a centrifuge tube containing non-differentiating medium. After a gentle mixing, centrifugation at 900rpm for 5min follows and then the resulting pellet is re-suspended again in non-differentiated medium and ready for seeding. These steps ensure the quick removal of DMSO which can be toxic to cells.

2.2.6 General information on cell treatments

In all cases, upon completion of a treatment, the plate surface is covered in ice-cold 1xPBS (98085 Cell Signalling) and cells are scraped off the surface through the use of a cell scraper (Sarstedt – 83.1830) and transferred to ice-cold micro-centrifuge tubes (Starlab – S1615) kept on ice. During time course measurements in 6-well plates, all cells are scraped at the same time so that later time points are subjected to the treatment the earliest and the earliest time points are treated last.

Note that in all cases where an H_2O_2 treatment was performed on cells, be it in the form of an acute bolus addition or a steady state treatment for 24 hours, cells had their medium changed into high glucose DMEM (Life Technologies – 21063-029) serum free medium with no phenol red. This 'treatment' medium avoids H_2O_2 scavenging by serum factors or the phenol red present in the other media used in cell culture. All H_2O_2 treatments occurred in 6-well plates where 1ml of the treatment media is added to each well, including in the control well. This ensures a medium depth is established that allows enough oxygen to be dissolved in the medium to be used by the cells and also act as an abundant substrate for the GOX/CAT system.

2.2.7 Acute H_2O_2 treatment

For acute H_2O_2 bolus treatments, the desired H_2O_2 concentration is achieved via the dilution of a 1M stock (Sigma Aldrich - 323381) in sterile H_2O (MilliQ® - Thermo Scientific Barnstead™ Nanopure™ - 7146) to a concentration that accounts for the volume of medium in the plate the cells are being grown in.

2.2.8 Sustained H_2O_2 treatment

For steady state H_2O_2 treatments the GOX/CAT enzymatic system is used (Mueller et al., 2009, Sobotta et al., 2013). Such a system involves the enzyme glucose oxidase from *Aspergillus niger* (Sigma – G0543-50KU) and catalase from bovine liver (Sigma – C1345-10G). The relative concentrations of these two enzymes in the medium will determine the steady state concentration of H_2O_2.

Glucose oxidase converts glucose and oxygen in the medium to H_2O_2 and gluconolactone. The catalase in the medium will then scavenge some the H_2O_2 produced (depending on the relative level) to produce water and oxygen. Because oxygen is a substrate of the glucose oxidase enzyme the cycle adjusts to a given flux. It is important that the medium employed is high glucose to ensure that this substrate is in abundance for both the cells and the enzymatic system. The choice of medium, steady state H_2O_2 concentrations and treatment duration are in line with previously characterised treatments based on the GOX/CAT system (Mueller et al., 2009).

Different steady states of H_2O_2 production were established as described previously (Mueller et al., 2009) with glucose oxidase being kept at a constant concentration and catalase concentrations being altered by different dilutions in PBS. The highest rate of steady state H_2O_2 generation used, 0.1μM/sec, caused no cell death after 24hr treatment compared to controls. However, this steady state concentration did trigger redox signalling as so did all of the lower steady state concentrations used. The steady state concentrations of H_2O_2 produced by the GOX/CAT system were thus deemed to be physiological.

2.2.9 GOX/CAT preconditioning

The preconditioning of cells for 24 hours with a given steady state level of H_2O_2 precedes a given treatment at the 24hr time point. Prior to the addition of the treatment agent, the preconditioned cells are thoroughly washed with 'treatment' medium to remove the glucose oxidase and catalase enzymes. This is especially since the catalase in the medium can scavenge the posterior H_2O_2 bolus treatment.

2.2.10 Urotensin II treatment

Mouse Urotensin II (071-08 - Phoenix Pharmaceuticals) was diluted in sterile H_2O to a stock concentration of 100µM. The treatment concentration used is 500nM achieved through dilution in 'treatment' medium. Treatment duration is 1hr for all experiments.

2.2.11 Nuclear fractionation

Note that all steps in this procedure must take place within ice-cold micro-centrifuge tubes. Defined volumes in this protocol are for 1.5ml micro-centrifuge tubes containing cells scraped from a well in a 6-well plate. Thus the volumes detailed can be scaled according the surface area of the plate on which cells are treated. Following a given treatment, cells in 500µL ice-cold 1xPBS are scraped into micro-centrifuge tubes. To obtain the nuclear fraction of the scraped cells, the first step requires a pop spin involving a 20 second centrifugation at 4ºC (Eppendorf centrifuge 5415R) to collect the cell pellet. Following this the PBS is discarded with care not to disrupt the pellet.

The pellet is re-suspended in 0.1% NP-40 detergent (Sigma-Aldrich IGEPAL® CA-630) in PBS at a volume of roughly 200µL per micro-centrifuge tube if cells were treated on a 6 well plate. Resuspension involves constant up-and-down pipetting for 5 minutes per sample with a P200 pipette. After resuspension each sample should be maintained at rest for at least 10 minutes to allow the mild NP-40 detergent to disrupt the cell membranes and allow for a better separation of the nuclear fraction. Next, 75µL of each resuspension is transferred to a separate micro-centrifuge tube to be used as a

sample for the whole cell lysate. These 'whole cell' samples can be left on ice until the final stages of the protocol. The re-suspended samples can then be centrifuged for 20sec at 4ºC (pop-spin) to collect the nuclear pellet.

The supernatant corresponds to the cytosolic fraction and can be collected (~150µL) into separate tubes at this point if desired. The nuclear pellet is then gently washed in 500µL of 0.1% NP-40 by detaching the pellet as a whole from the tube by jetting the 500µL of NP-40 into the side of the tube. Once the whole pellet is suspended in the detergent, gently tilt the tube 3-5 times. After this step the nuclear samples are pop spinned and the supernatant is discarded. For the resulting samples, the cytoplasmic fractions and the whole cell lysates are mixed in one volume of 4 x sample buffer (SDS plus 10% β-mercaptoethanol [Sigma – M6250]) per three volumes of sample. In the case of the nuclear pellets, these are re-suspended in 100µL of 1 x sample buffer (diluted in MilliQ water).

The samples for the nuclear fractions and the whole cell lysates are then sonicated (Microson ultrasonic cell disruptor XL, MISONIX Inc.) for 2 x 5sec intervals per sample at 2 watts (RMS) whilst ensuring the sonicator tip is wiped in ethanol and dried between the sonication of different samples. The use of the sonicator aims to disrupt the nuclear membranes. The final step involves the boiling (Grant QBD1) of all samples at 100ºC for 5 minutes to allow for the denaturation of proteins in the samples and their thorough reduction by the sample buffer added. Samples are then chilled on ice for 5-10 minutes and stored in the -80ºC freezer for further use or directly run on acrylamide gels for western blotting.

2.2.12 Western immunoblotting

This technique is based on polyacrylamide gel electrophoresis (PAGE) where proteins are separated by size as determined by their migration distance over an acrylamide gel at a constant voltage. The higher the percentage of acrylamide in the (running) gel through which proteins in each sample migrate, the slower the protein migration will be for a given voltage. Thus, lower percentage acrylamide gels (ex. 6.5% PAGE) are used to separate high molecular weight proteins since at such low percentage acrylamide low molecular weight proteins run over the gel quickly and the slower moving proteins are separated over the whole gel. Conversely, 15% PAGE allows for a good separation of

low molecular weight species but not high molecular weight species which will not migrate great distances over the running gel. In this work, all gels were SDS-PAGE gels unless otherwise stated. Thus proteins are separated solely by size and not their native conformation.

The reagent proportions used in the formation of the PAGE gels are defined in Tables 2.1 and 2.2. Note that in the making of the gels, the running gel is introduced into an upright standing 1.5mm cassette (ThermoFisher Scientific Novex® - NC2015) which is toped up with sterile H_2O and left to polymerise for approximately 30 minutes. The H_2O is then discarded by tipping over the cassette with the solidified gel and the stacking gel is added to fill up the cassette to the top. The comb to define the wells within the stacking gel is added into the cassette so that a slight excess of stacking gel overflows the cassette. This is left for 15 minutes to allow for the polymerisation of the stacking gel.

Gels were run on an XCell SureLock^{TM} (Invitrogen) tank at 125V and 29mA for 90 minutes on Tris-Glycine running buffer. Precision Plus Protein^{TM} Dual Color Standards ladder (BioRad – 161-037LI) was used as a reference of protein molecular weight. The running buffer was made by making a 3% and 14.4% dilution of Tris (Sigma Life Science – T1503) and Glycine (Sigma Life Science - G8898) respectively in sterile H_2O with a further addition of 1:200 volume of 20% SDS. The gels were then laid on a methanol-activated nitrocellulose membrane (Merck Millipore - IPVH00010) and 'sandwiched' in between blotting pads (VWR® - 28298) in a semi-dry transfer tank (Trans-Blot SD – BioRAD). The blotting pads, membranes and gels had been previously soaked in transfer buffer, which is a running buffer without any SDS addition. Protein transfer from the gel to the membrane is performed at 17V for 60 minutes.

After the transfer step the membrane is washed in PBS to remove any transfer buffer and washed for two minutes in Ponceau reagent (Sigma Life Science 78376). The latter will stain protein bands in the membrane in red, thus facilitating the trimming of the membrane to blot different membrane sections with different antibodies. The membrane sections are then washed for 10 minutes in PBS-T (PBS with 0.1% TWEEN®20 Sigma Aldrich -P1379) to remove the Ponceau staining. Membrane strips are then washed in 5% Milk (Marvel original dried skimmed milk diluted in PBS-T) for 60 minutes in order to block protein binding sites that may promote non-specific binding of antibodies. After this time period, membranes are rinsed with PBS and incubated on a

see-saw rocker with the target primary antibody in a 4ºC cold room overnight.

Following incubation with the primary antibody, the membranes undergo a triple sequential wash of PBS, PBS-T and PBS for 5 minutes each wash before being incubated with the secondary antibody for 60 minutes. The secondary antibody consists of a species-specific anti-Horse Radish Peroxidase (HRP) antibody diluted in 5% Milk. Following this incubation period another triple wash follows. The membranes are then kept in the dark with the chemiluminescence ECL mixture (Immun-Star™ WesternC™ kit BioRad 170-5070) for 5-10 minutes. The membranes are then ready for exposure in a Fujifilm LAS-4000 Raytech developer machine. Image processing and quantifications were performed with ImageJ software (Schneider et al., 2012).

Note that throughout this protocol all 'washing', 'blocking' and 'incubation' procedures involve the incubation of the membranes inside a petri dish with the desired reagent, at room temperature, on a see-saw rocker (Stuart SSL4) unless otherwise specified.

To blot for more than one protein in the same membrane when the migration distance between proteins is too small to physically separate them by trimming the membrane, a stripping buffer is used (Blot Stripping Buffer RestoreTM PLUS Western 46430 Thermo Scientific) to ensure there is no chemiluminescence signal overlap between two proteins sequentially blotted for. After developing the latest protein of interest, membranes are washed in PBS for an hour and then incubated for 1hr in stripping buffer. The next steps involve the blocking of the membranes in 5% milk for one hour before rinsing with PBS and re-incubating with another primary antibody overnight in the 4ºC cold room see-saw rocker.

Table 2.1. *Running gel reagents*

Reagent*	6.5% PAGE	8% PAGE	10% PAGE	12% PAGE	15% PAGE
Sterile distilled H_2O	4.5ml	4.6ml	3.4ml	2.9ml	2.0ml
30% Acrylamide (Severn Biotech Ltd 20-2100-10)	2.0ml	2.4ml	3.0ml	3.6ml	4.5ml
1.5M Tris, pH 8.8 (Sigma Aldrich T6066)	2.3ml	2.4ml	2.4ml	2.4ml	2.4ml
10% SDS (Sigma Aldrich L4390)	90.0µl	90.0µl	90.0µl	90.0µl	90.0µl
10% Ammonium Persulphate (Sigma Aldrich 215589)	90.0µl	90.0µl	90.0µl	90.0µl	90.0µl
TEMED (Sigma Aldrich T9281)	7.2µl	3.6µl	3.6µl	3.6µl	3.6µl

*Volumes correspond to one (9ml) gel

Table 2.2. *Stacking gel reagents*

Reagents*	5% PAGE
Sterile distilled H_2O	1.4ml
30% Acrylamide (Severn Biotech Ltd 20-2100-10)	0.43ml
1.5M Tris, pH 8.8 (Sigma Aldrich T6066)	0.33ml
10% SDS (Sigma Aldrich L4390)	26.5µl
10% Ammonium Persulphate (Sigma Aldrich 215589)	26.5µl
TEMED (Sigma Aldrich T9281)	2.65µl

*Volumes correspond to one (2ml) gel

2.2.13 Antibodies

The antibodies used in this work are listed in Table 2.3 (next page). Note that 5% milk refers to Marvel Original Dried Skimmed milk diluted in PBS-T and 5% BSA refers to Bovine Serum Albumin (Sigma Life Science - 05482) diluted in PBS-T. All antibody dilutions contain 1:500 concentration of sodium azide (NaN_3) for antibody conservation. All antibodies are stored in a -20ºC freezer.

Table 2.3. List of antibodies used.

Antibody	**Species**	**Concentration**	**Company**	**Catalogue Number**
Anti-Nrf2 (D1Z9C)	Rabbit	1:500 in 5% BSA	Cell Signalling Technology	#12721
Anti-GAPDH (D16H11)	Rabbit	1:10000 in 5% BSA	Cell Signalling Technology	#5174
Anti-Lamin B1	Rabbit	1:1000 in 5% milk	Abcam	ab16048
Anti-Keap1	Rabbit	1:500 in 5 % BSA	Abcam	ab66620
Anti-Phospho GSK3ß-Ser9	Rabbit	1:500 in 5% BSA	Cell Signalling Technology	#9336
Anti-GSK3ß (27C10)	Rabbit	1:1000 in 5% BSA	Cell Signalling Technology	#9315
Anti-Akt	Rabbit	1:1000 in 5% BSA	Cell Signalling Technology	#9272
Anti-Phospho Akt (Ser473)	Rabbit	1:1000 in 5% BSA	Cell Signalling Technology	#9271
Anti-$PrxSO_3$	Rabbit	1:2000 in 5% milk	Abcam	ab16830
Anti-Catalase	Rabbit	1:1000 in 5% milk	Genetex	GTX110704

Anti-SOD1	Rabbit	1:5000 in 5% BSA	Abcam	Ab13498
Anti-β-actin	Rabbit	1:1000	Cell Signalling	#4967
Anti- HRP	Rabbit	1:5000 in 5% milk	Sigma	A0545

2.2.14 Protein quantification

The BioRad DC Protein Assay (BioRad – 500-0113 [Reagent A] – 500-0114 [Reagent B] – 500-0115 [Reagent S]) was employed following the instructions provided by the manufacturer. Absorbance values as measured through by a Fluostar Omega plate reader (BMG Labtech) were recorded for each cell lysate sample and for four known concentrations of BSA diluted in sterile H_2O. A standard curve is made out of the absorbance values of the known protein concentrations and the protein concentration of each sample calculated by mapping the absorbance value into the standard curve. A desired uniform protein concentration across samples was then achieved by performing the appropriate dilution of the sample with loading buffer (2xLaemmli buffer [BioRad – 161-0737] with 10% β-mercaptoethanol added to the final mixture). Samples are then boiled at 100ºC for 5 minutes in a heating block (Grant QBD1 Boiler) and then chilled on ice for 5-10 minutes. The samples can be then taken straight to western blotting analysis or frozen at a -80ºC freezer (Eppendorf New Brunswick^{TM}– U725-G).

2.2.15 X-ray irradiation

Differentiated C2C12 myotubes were irradiated with a 20 Grey (225kV) X-ray dosage through the use of an XRAD-225 X-ray irradiator. The media was immediately replaced after irradiation to avoid secondary damage by chemical species that may form during the irradiation of the medium. Cells were then cultured for 15 days post-irradiation.

2.2.16 Hyperoxia exposure

C2C12 myotubes were cultured (HERAcell^{TM} 150i incubator – Thermo Scientific) at 40% Oxygen / 5% CO_2 at 37^{o}C. Incubation period under hyperoxic conditions was of 7 days with the 'differentiation' medium renewed every 2 days.

2.2.17 Reverse Protein Phase Array (RPPA) measurements

Samples were sent to the Newcastle University Protein and Proteome Analysis (NUPPA) facility for the systematic quantification of protein abundances through RPPA (Charboneau et al., 2002, O'Mahony et al., 2013). Sample preparation for this procedure involves the scraping of cells grown in a six-well plate into 40µL of lysis buffer (1.5% SDS) after a double wash in PBS. Samples are then frozen and sent to the NUPPA facility. The basic RPPA procedure involves the sonication of samples in a rotatory sonication bath followed by a centrifugation step to collect the supernatant. A sample processing step follows involving the quantification of protein abundance through the use of the Bradford assay and appropriate volume dilutions to an optimised protein concentration of 0.2mg/ml in each sample. Alkaline phosphatase treatment is then employed to remove phosphate groups from proteins in the samples in order to validate any phospho-antibodies to be employed during the procedure.

Samples are then ready to be robotically printed in quantities of 400pL into a chip at four different dilutions. The printing procedure involves the printing of multiple repeats of the same sample dilution in different "seals" within the chip that will allow the washing with different primary antibodies after a previous blocking step with vaporised blocking agent. The secondary antibodies are coupled to an Alexa-647 fluorescent dye. Measurements are taken by the excitation of samples with four different laser intensities and readings involve the integration of the four different laser intensities over all sample dilutions. Output readings are thus relative fluorescence intensity (RFI) values.

Chapter 3

‘Molecular habituation’ as a potential mechanism of gradual homeostatic decline with age

3.1 Introduction

The chemical properties of reactive oxygen species confers these molecules the ability to cause molecular damage, but despite this, they also participate in essential cellular signalling functions (Winterbourn, 2015, Wang and Hai, 2016). For example, redox signalling has been established to be involved in the modulation of insulin signalling (Besse-Patin and Estall, 2014), the stress response (Jiang et al., 2011), cell survival (Trachootham et al., 2008) and tissue regeneration (Sen and Roy, 2008), to name but a few. The dual nature of ROS as signalling molecules and damaging agents is thought to depend on abundance, where low levels of these molecules will perform signalling functions and higher levels will promote molecular damage (Schieber and Chandel, 2014). Indeed, various pathologies (Barbieri and Sestili, 2012, De Marchi et al., 2013, Sosa et al., 2013, Besse-Patin and Estall, 2014, Kim et al., 2015, Brioche and Lemoine-Morel, 2016, Lepetsos and Papavassiliou, 2016) and the ageing process itself (Kirkwood and Kowald, 2012, Sanz, 2016,) display increased markers of oxidative stress. The nature of the homeostatic dysregulation that causes cells to transition from a state of controlled ROS production that serves essential signalling functions to a state of oxidative stress that causes molecular damage over time remains to be elucidated.

Oxidative stress is defined as a cellular state involving a mismatch between the abundance of oxidant molecules and the antioxidant capacity of the cell, favouring the former (Sies, 2015). Oxidative stress is thus characterised by an increase in the basal levels of ROS. This increase can be transient or constitutive (Pickering et al., 2013). Whilst transient (acute) oxidative stress is associated with controlled ROS generation during redox signalling, constitutive (chronic) oxidative stress is commonly viewed as an uncontrolled process that drives molecular damage. Chronic oxidative stress thus involves longer time-scales of cellular exposure to ROS. As such, chronic oxidative stress becomes relevant to chronic diseases, age-related diseases and the ageing process. Oxidative stress shall hereon refer to chronic oxidative stress. The intrinsic reactivity of

ROS has made oxidative stress a very attractive research target when trying to explain a variety of homeostatic disruptions in terms of the unspecific molecular damage caused by these molecules (Winterbourn, 2015). It is thus of interest to explore weak points in the mechanisms that maintain redox homeostasis in the cell in order to examine how such mechanisms may become dysfunctional so that intracellular oxidant levels increase.

The role of ROS as potential causal agents of homeostatic disruption through molecular damage has meant that chronic oxidative stress has been studied almost exclusively as a source of toxicity to the cell. However, the established function of ROS molecules as cellular redox signals points towards a largely neglected perspective in the study of the consequences of chronic oxidative stress. That is, studying sustained oxidative stress as a constitutive signal within the cell. Examples of this perspective include the study of chronic oxidative stress as a constant inhibitory signal in both calcium signalling (Roedding et al., 2013, Gorlach et al., 2015) and T cell activation (Fulop et al., 2014). With regards to redox signalling, however, the potential consequences of an oxidant signal being constantly present are unclear. The following enquiry could be formalised when addressing this gap in the literature: how are redox signalling pathways likely to respond to an acute ROS signal when in the presence of a constitutively elevated oxidant level in the cellular environment? The physiological significance of such an enquiry becomes apparent when considering that redox signalling pathways have been shown to become dysfunctional in a variety of tissues in contexts where oxidative stress is also present in the cell (Vasilaki et al., 2006b, Sohal and Orr, 2012, McDonagh et al., 2014a, Claflin et al., 2015, Cobley et al., 2015, Zhang et al., 2015a, Done et al., 2016, Jackson, 2016).

One could further abstract the enquiry into the following form: does the constitutive presence of a signal in the environment affect a signalling pathway's ability to transduce a subsequent acute pulse of the same signal? In the case of ROS monitoring, current experimental methods have a limited molecular resolution (Woolley et al., 2013, Ribou, 2016). Moreover, most studies on redox signalling have focused on acute ROS stimuli rather than treatments involving the long-term exposure of cells to controlled oxidant levels (Millonig et al., 2012, Covas et al., 2013, Sobotta et al., 2013, Tan et al., 2015a). It is thus unsurprising that very few studies explicitly examine the consequences of a long-term oxidant exposure on redox signalling processes. A notable exception is the work undertaken by Pickering *et al.* who demonstrate that a sustained oxidant treatment

can affect the activation of redox-mediated adaptive responses in the cell (Pickering et al., 2013).

When a scientific enquiry becomes as general as that postulated here, it becomes challenging to address it by experimental means alone. Computational simulation can provide a means to explore the 'mechanistic space' as to how oxidative stress may interfere with redox signalling processes within the cell. This work reports that a constitutive signal in the cellular environment can potentially reduce the responsiveness of a given signalling pathway via the sustained activation of negative regulators. This phenomenon seems to occur in a variety of signalling pathways and potentially at different levels of biological organisation.

3.2 Rationale for a generic model of redox signalling

The main challenge regarding the study of how oxidative stress may affect redox signalling concerns the variety of different redox signalling pathways there are in a cell. Different pathways will have different regulatory structures and will be likely to display different dynamics to the same stimulus. Hence, it would be informative to study the effect of oxidative stress on individual pathways one at a time. However, an alternative and less time-consuming approach would be an attempt to abstract the conserved regulatory features of such pathways. This is the most appropriate approach if any phenomenon is suspected to be generalizable. A close inspection of the major redox stress response pathways in mammalian cells, i.e. NFκB, Nrf2, ASK1, HIF1 and HSF1, reveals a number of conserved regulatory features. In all of these cases pathway activation involves the interference of the cellular stress with an inhibitor-activator complex (Soga et al., 2012, Hoesel and Schmid, 2013, Jiang et al., 2015a, Masoud and Li, 2015, Tebay et al., 2015).

The disrupted complexes are IκB – NFκB in the NFκB pathway (Hoesel and Schmid, 2013), Keap1 – Nrf2 in the Nrf2 pathway (Tebay et al., 2015), Thioredoxin1 – ASK1 in the ASK1 pathway (Soga et al., 2012), VHL – HIF1α in the HIF1α pathway (Masoud and Li, 2015) and the HSP70/90 – HSF1 complex in the HSF1 pathway (Jiang et al., 2015a). Whilst the disruption of the IκB – NFκB inhibitory complex by oxidant molecules to activate the NFκB response has been called into question (Oliveira-Marques et al., 2009, Morgan and Liu, 2011) the notion of an oxidant-mediated

disruption of an inhibitory complex is well established for the ASK1, Nrf2 and HIF1 pathways (Chandel et al., 2000, Nanduri et al., 2015). The activation of the HSF1 pathway by oxidative stress is different to the other pathways in that oxidants are thought not to be sensed directly but rather through changes in the abundance of misfolded folded proteins or alternatively the activation of other upstream pathways (Yoo et al., 2014, Swan and Sistonen, 2015).

The disruption of the inhibitor-activator complex by oxidants in these pathways results in an increase in the levels of free activator. In all cases, the free activator undergoes a post-translational modification or a binding event with a second molecule. This stabilising step involves the binding to other co-factors in the case of the Nrf2, NFκB, HIF1 and HSF1 pathways or the dimerization of ASK1 molecules upon the activation of the pathway. Furthermore, in all the redox signalling pathways the activated molecules have been reported to undergo phosphorylation upon pathway activation.

The mechanistic basis of the resetting of the different signalling pathways has been elucidated to different extents. However, in all cases, the signalling pathway must return to the starting point, i.e. an activator being actively bound by a protein to form an inhibitory complex. This necessitates the complex to be regenerated. This may require the re-activation of the inhibitor molecule through a post-translational modification or alternatively the *de novo* synthesis of the inhibitor molecule.

These conserved features were formalised into a core generic redox model (Figure 3.1), hereafter referred to as Model 1. Missing from this model are mechanisms of negative regulation that promote the disruption of the activator stability so that the system can be reset. However, as mentioned previously, there is considerable variation regarding the number of elucidated mechanisms of negative regulation in each pathway and their relative importance. Another common feature arises in all pathways, however, and that is the existence of a transcriptional negative feedback loop resulting from the activity of the activator which results in an increased expression of the inhibitor molecules. The resetting of the redox signalling pathways can thus be said to follow a common two-step process involving an initial destabilisation of the activator molecule followed by the subsequent formation of the inhibitor-activator complex.

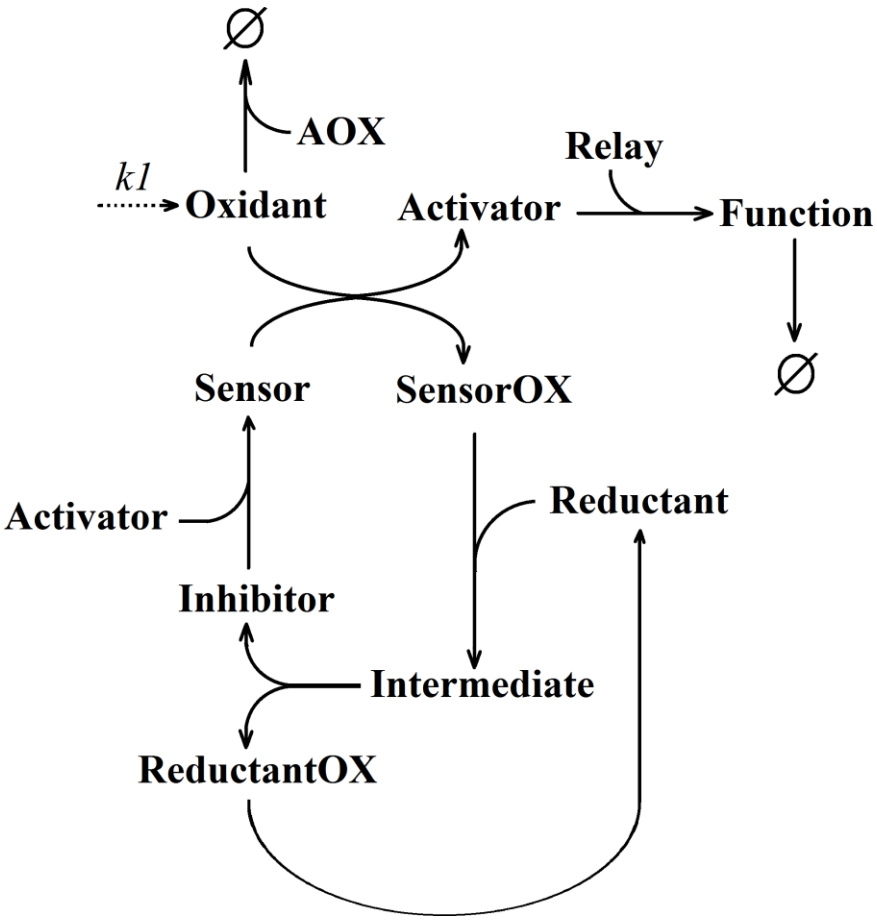

Figure 3.1. *Generic redox signalling Model 1. Basal oxidant levels are modulated through the value of k1 which defines the flux of oxidant generation. The pathway is activated by an oxidation reaction of the inhibitor-activator complex that acts as a redox sensor. This oxidation reaction will result in an increase in the free levels of activator molecules which will further go on to perform a function after being stabilised by a binding event with a relay molecule. The initial redox-sensing reaction will result in the modification of the inhibitor that makes it unable to continue inhibiting the activator. The inhibitor must undergo a two-step regeneration process to be returned to a chemical state that allows its binding to the activator molecule to recreate the inhibitory complex (Sensor). AOX=Antioxidant. OX = oxidized. Dashed circle = degradation.*

The activator destabilisation step would refer to the transcriptional complex disruption and subsequent nuclear export of the NFκB, Nrf2, HSF1 and HIF1 transcription factors or the disruption of the ASK1 signalosome. Model 2 expands on Model 1 by including such an element negative feedback (Figure 3.2a). Despite negative feedback being a common means for the shutdown of biological responses, it is not the only regulatory mechanism that allows for this. This is exemplified by the Nrf2 signalling pathway, which is deactivated by the delayed action of GSK3β (Cuadrado, 2015, Tebay et al., 2015). Because the delayed activation of GSK3β is ROS-dependent but Nrf2-independent (Kaspar et al., 2009, Cuadrado, 2015), this is an example of an incoherent feedforward loop or negative feedforward loop.

A negative feedforward loop requires an upstream branching point where further downstream one arm of the network will feed back into the other arm. Such a parallel topology introduces negative regulation independently from the levels of the activator molecule. This contrasts with the in-series structure of negative feedback loops where the introduction of negative regulation is dependent on the state of the activator. Model 3 expands on Model 1 to include a system in which negative regulation occurs primarily through a negative feedforwards loop (Figure 3.2b). Models 2 and 3 thus aim to be abstract representations of redox signalling pathways. These are employed to explore how the presence of a constitutive signal in the form of oxidative stress can affect the ability of these pathways to transduce an acute redox signal.

It is worth noting that Models 2 and 3 are extensions from the core Model 1. The main difference between Models 2 and 3 with Model 1 is that the former two involve the introduction of a negative feedback molecule (NegReg) after a time delay which is modelled by reactions involving 'Relay' molecules. In Model 2, 'NegReg' molecules are introduced downstream of the 'Function' molecule. In Model 3, 'NegReg' molecules are introduced independently of the activation of the 'Activator' and 'Function' molecules. Therefore, the activation dynamics of the three models are directly comparable through the 'Activator-Function' branch, which is conserved across models, when investigating different topologies of negative regulation.

The mathematical formalisation of Models 1- 3 can be found in Supplementary Tables 1-9. Note that in all of the ODE-based models in this work, the parameter *k1* will correspond to a zero-order rate constant for the synthesis of the *Signal* molecule in the model. Simulation of the models is carried out in COPASI through the LSODA algorithm under default settings. The largest model simulated was the Schilling et al.

(2009) model which consists of 33 species participating in 42 reactions. The simulation of such a network of 33 nodes and 42 edges took less than two seconds to simulate. Model 1 consists of 12 species and 9 reactions. Model 2 consists of 15 species and 12 reactions. Model 3 consists of 17 species and 14 reactions. Models 1 – 3 took less than 2 seconds to simulate.

Figure 3.2. *(Next page). Network representations of a genetic redox signalling model incorporating* ***a)*** *a negative feedback loop (Model 2) or* ***b)*** *a negative feedforward loop (Model 3). Basal oxidant levels are modulated through the value of k1 which defines the flux of oxidant generation. AOX=Antioxidant. OX = oxidized. Dashed circle = degradation.*

a)

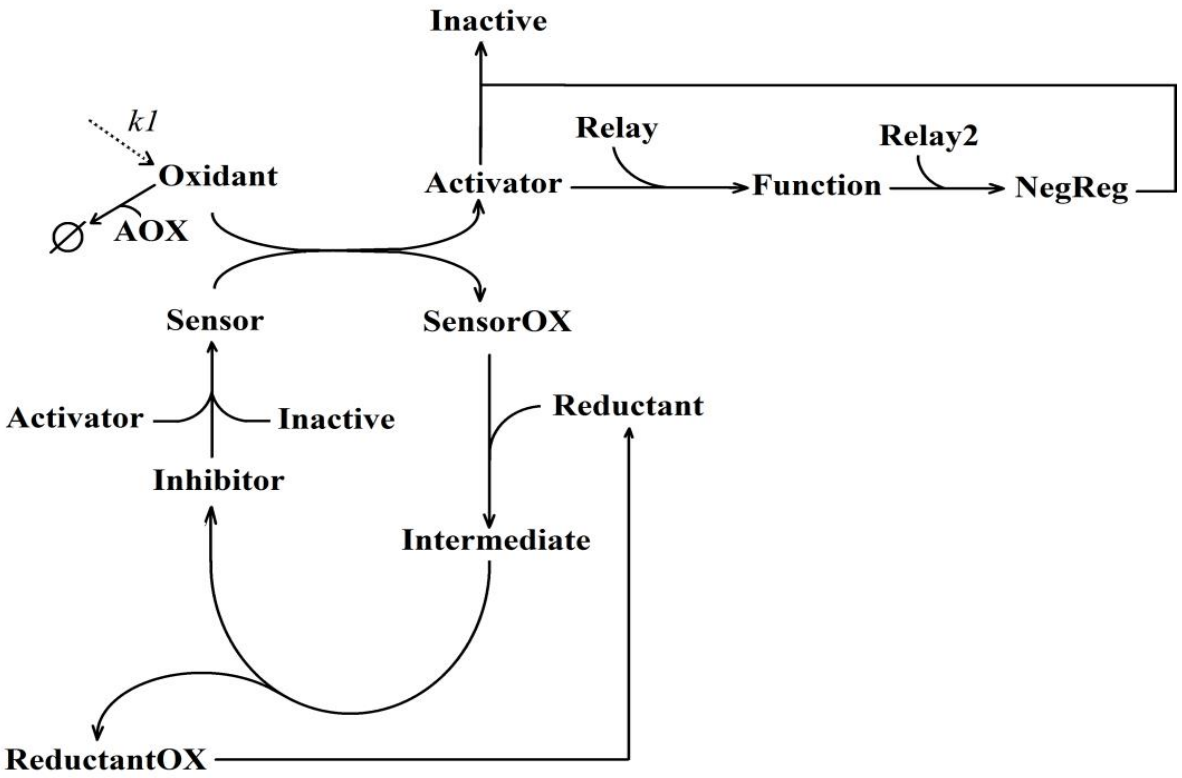
Inactive
k1
Oxidant
AOX
Relay
Relay2
Activator
Function
NegReg
Sensor
SensorOX
Activator
Inactive
Reductant
Inhibitor
Intermediate
ReductantOX

b)

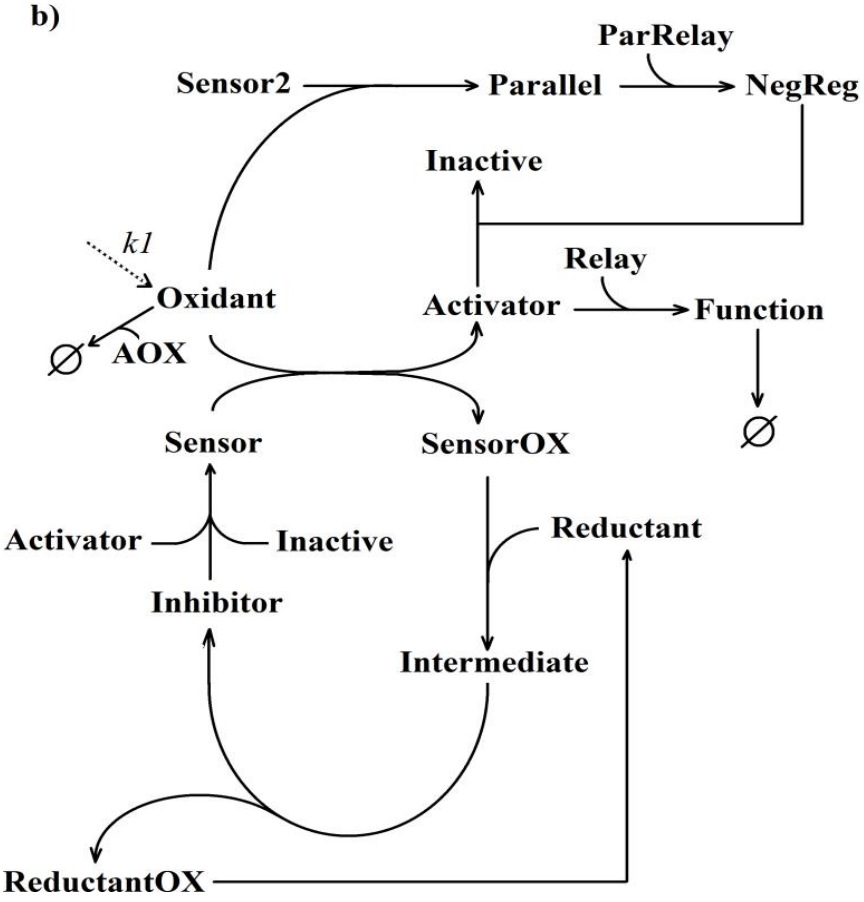
ParRelay
Sensor2
Parallel
NegReg
Inactive
k1
Oxidant
AOX
Relay
Activator
Function
Sensor
SensorOX
Activator
Inactive
Reductant
Inhibitor
Intermediate
ReductantOX

3.3 Results

3.3.1 Oxidative stress reduces the magnitude of pathway activation in response to an acute redox signal

When the basal rate of oxidant generation (*k1*) is increased in both Model 2 and Model 3, the activation profiles display a significantly reduced peak stimulation magnitude (Figure 3.3). This observation was systematically explored in a parameter scan for a range of values of *k1* (Figure 3.4). Of note is the observation that the *negative regulator* species in Model 3 actually displays an increased magnitude of activation at increasing values of *k1*. Another consequence of increasing the value of *k1* is an observed increase in the steady-state levels of the *activator*, *function* and *negative regulator* molecules (Figure 3.3). The reduction in the activation magnitude of Model 2 and Model 3 at higher *k1* values contrasts with the saturation profiles obtained in Model 1 under the same parameter changes (Figure 3.5). In these saturation profiles, the peak activation magnitude reached by the species within the pathway actually increases with increasing values of *k1*.

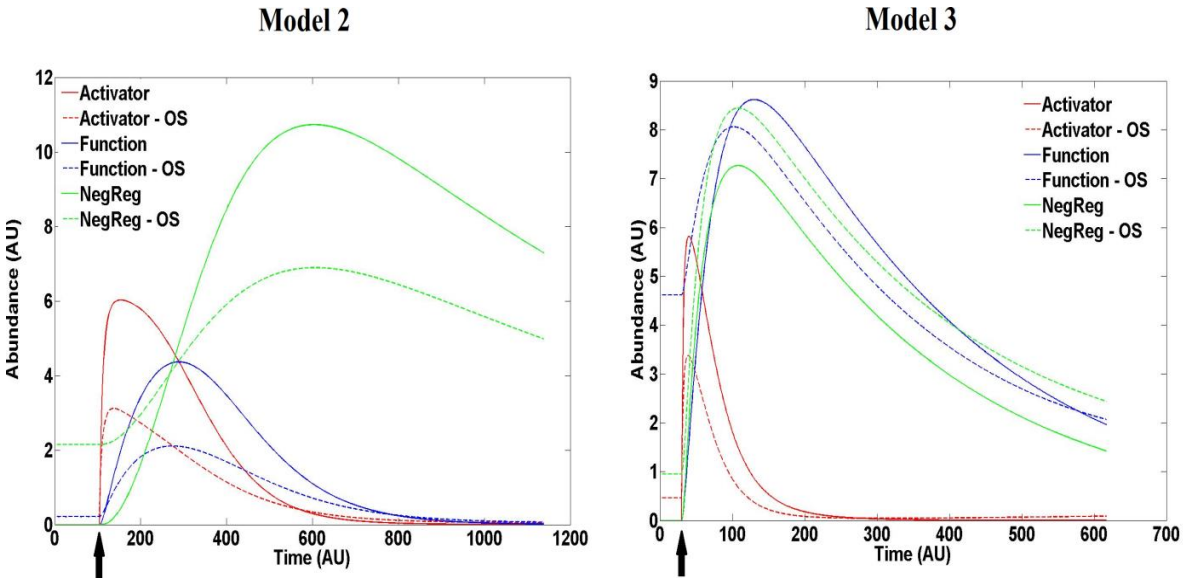

Figure 3.3. *Simulated profiles for Models 2 and 3 for different k1 values. OS = oxidative stress where k1 = 1 (else k1 = 0). Stimulus strength = 100 at time point marked by black arrow.*

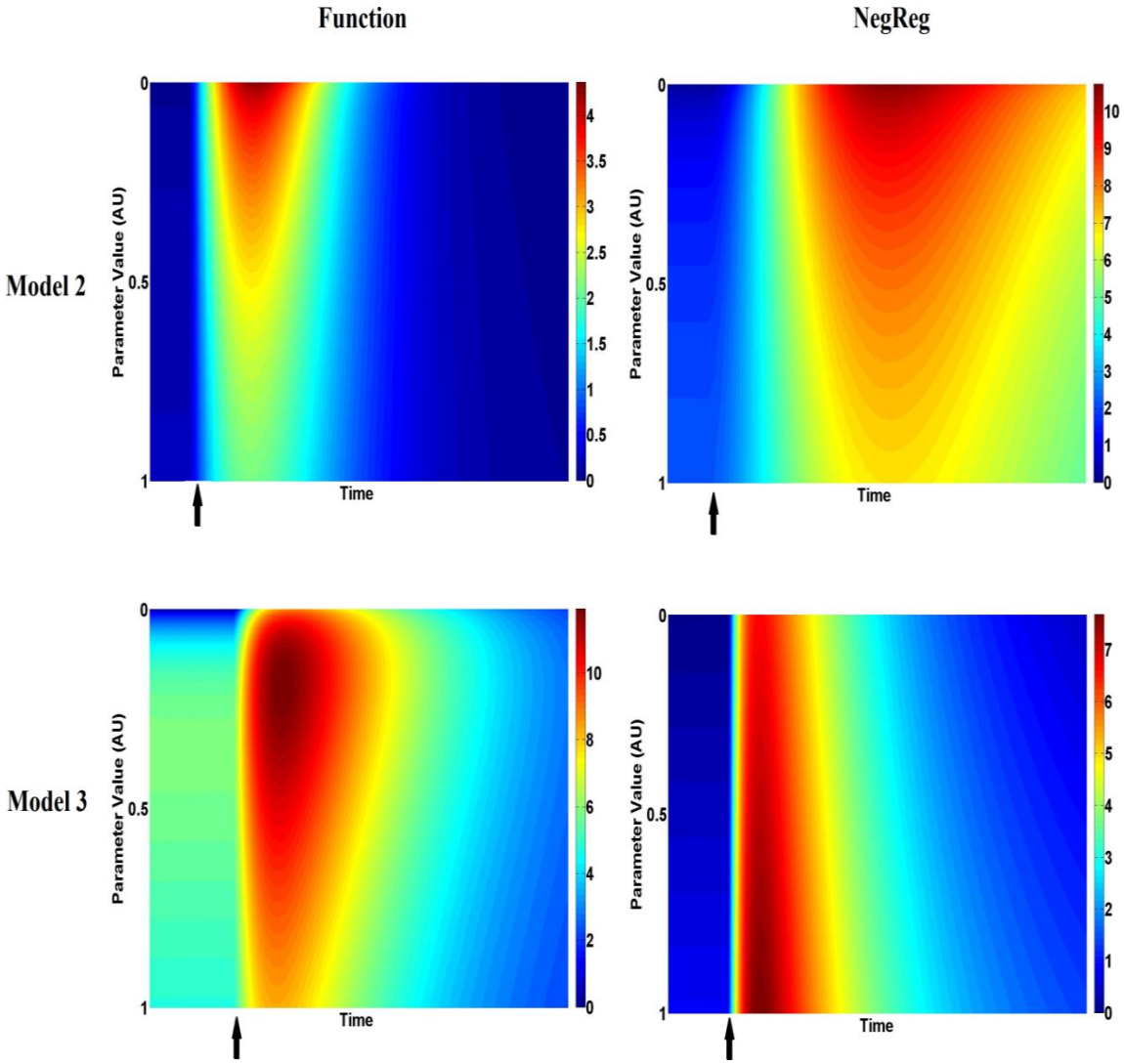

Figure 3.4. *Parameter scans of Models 2 and 3 for k1 values. Scan involves a regular step-wise increase for 1000 intervals between 0 and 1. Colour-bar = arbitrary units of molecular abundance. Stimulus strength = 100 at time point marked by black arrow.*

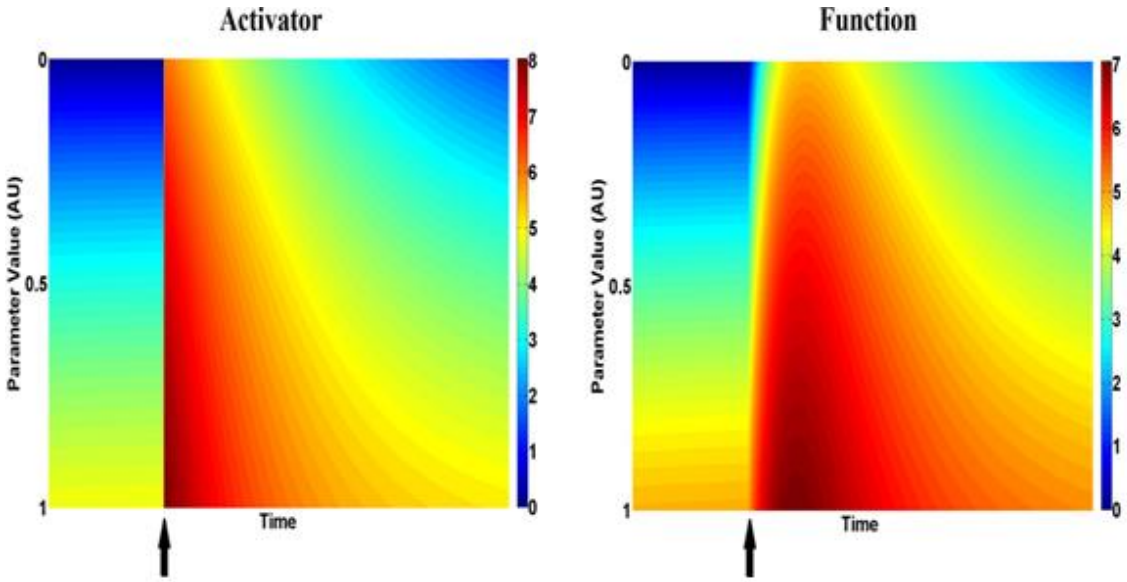

Figure 3.5. *Parameter scans for k1 values in Model 1. Parameter scan involves a regular step-wise increase for 1000 intervals between 0 and 1. Colour-bar = arbitrary units of molecular abundance. Stimulus strength = 100 at time point marked by black arrow.*

The stable elevation in the levels of the pathway species indicates that the continuous oxidant flux is stabilising a new steady state in both models. It is thus a possibility that the reduced responsiveness of the pathway is the result of a network-wide loss in sensitivity (Dalle Pezze et al., 2014). To examine the effects of the *k1* value on the network-wide sensitivity of Models 2 and 3, sensitivity analysis was performed on all three models (Figure 3.6). The sensitivity analysis reveals some conserved gains in sensitivity across all three models under conditions of oxidative stress. These include an increase in the overall network sensitivity to the rate of oxidized inhibitor reduction (*k6* in Model 2 and *k7* in Models 1&3). It is of interest that oxidative stress seems to increase the sensitivity of *Activator* and *Function* molecules to parameters that directly control the *negative regulator* entities (*k10* / *k12* in Model 2 and *k10* / *k11* / *k12* in Model 3). Oxidative stress thus causes a shift in the model sensitivities rather than an network-scale reduction in sensitivity.

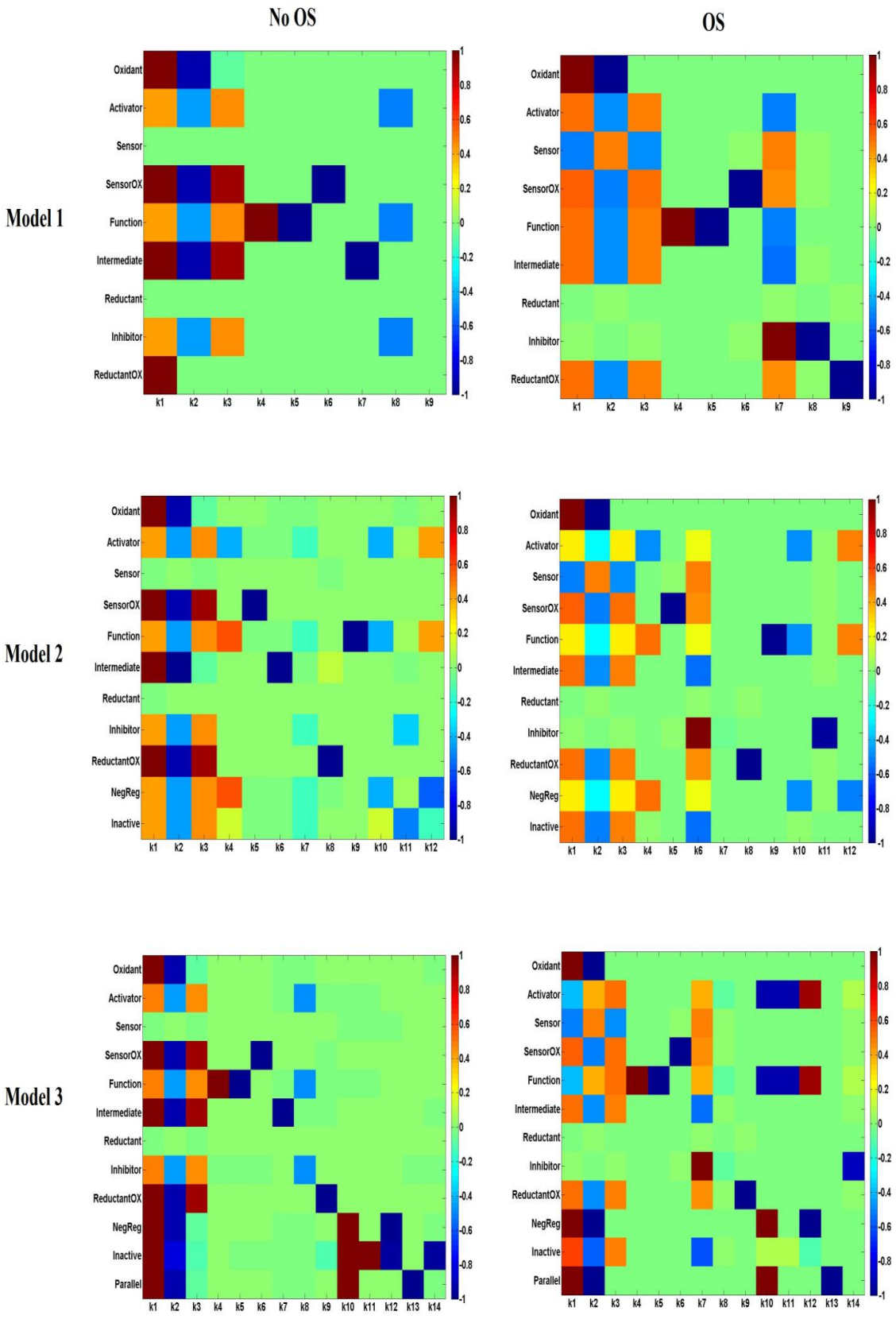

Figure 3.6. *Sensitivity analysis heat maps for Models 1, 2 and 3 in the presence (k1 = 1) and absence (k1 = 0) of oxidative stress (OS). Delta factor = 0.001, Delta minimum = 1e-12. Analysis run in COPASI and plotted in Matlab.*

3.3.2 A sustained increase in the basal levels of negative regulators causes a loss of pathway responsiveness under conditions of oxidative stress

The fact that Model 1 displays a saturation pattern under increasing levels of signal (oxidative stress) and Models 2 and 3 display a blunted response suggests that their main topological difference, i.e. the presence of a negative regulator, lies behind such difference in behaviour. The basally increased level of *negative regulator* molecules in the new steady state promoted by oxidative stress appears as a potential source of dampening of the acute redox signal. If this possibility holds true, then a gradual increase in the basal levels of the *negative regulator* molecules should result in a loss in pathway responsiveness to an acute redox signal even in the absence of oxidative stress. This *in silico* experiment was carried out by clamping the negative regulator levels at increasing values, which resulted in a subsequent reduction in pathway activation (Figure 3.7). The robustness of these observations was tested by re-running the simulations at different values of the parameter defining the strength of inhibition by the *negative regulator* molecules (Figure 3.8). Furthermore, to confirm that this behaviour was not an artefact of how inhibition by the *negative regulator* was modelled (second-order mass-action degradation reaction) the *in silico* experiment was repeated with the negative regulator acting through competitive inhibition (Figure 3.9).

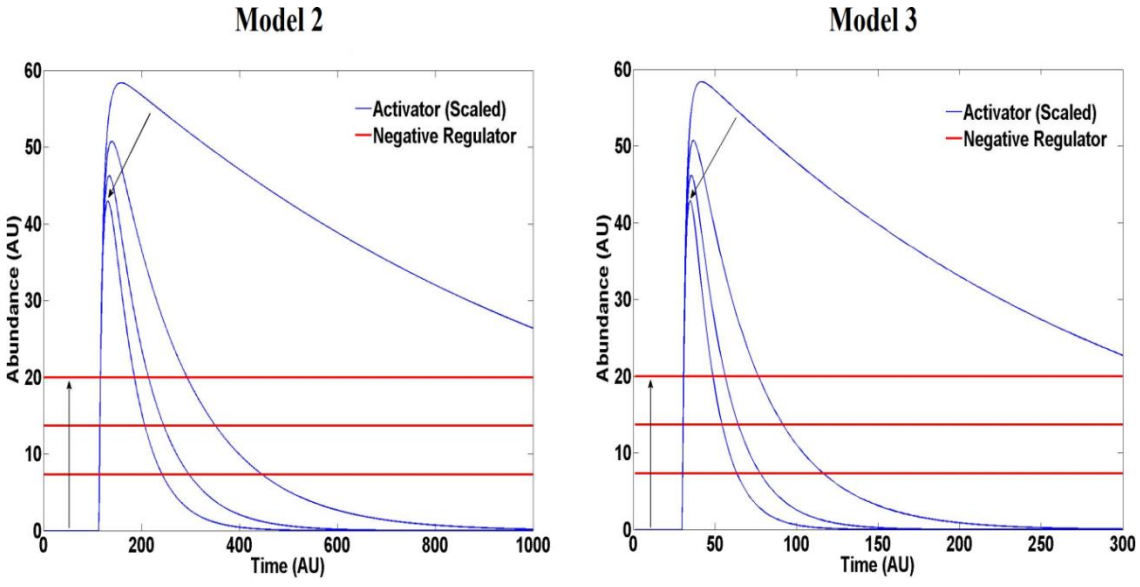

Figure 3.7. *Simulated profile for 'Activator' molecules in Models 2 and 3 under increasing resting levels of negative regulator molecules. k1=0 and stimulus strength =100. Arrows illustrate curve shifts with increasing negative regulator basal levels.*

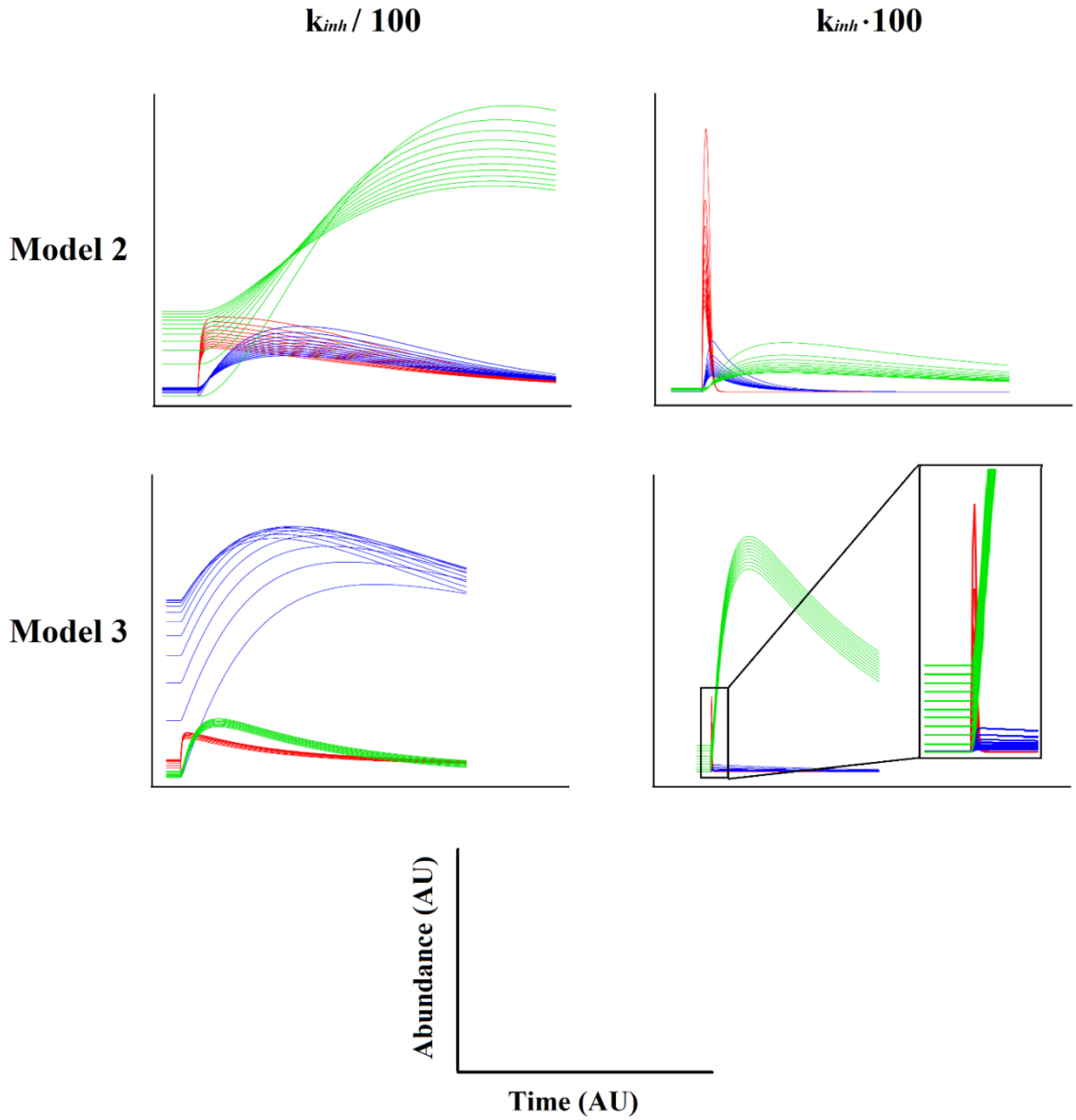

Figure 3.8. *Parameter scan for k1 at different inhibition strengths.* k_{inh} *= inhibition rate constant. Green = negative regulator, Blue = Function, Red = Activator. Scan is 10 intervals between 0 and 1.Time courses shown for* k_{inh} *values10000 orders of magnitude apart.*

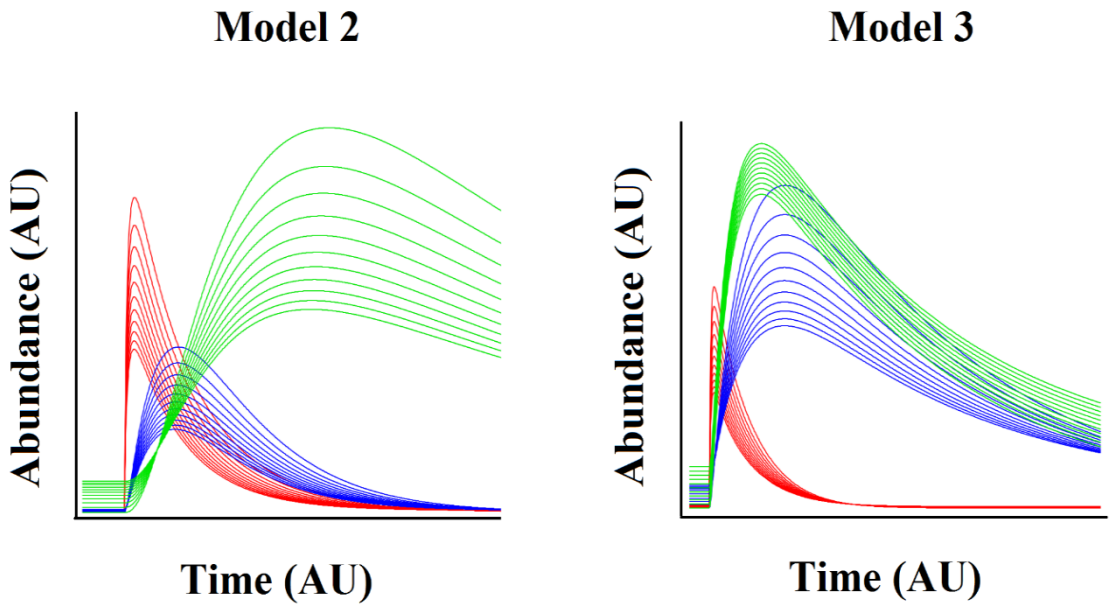

Figure 3.9. *Parameter scan for k1 with negative regulator molecules acting on activator molecules through competitive inhibition kinetics. Inhibition parameters:* K_m*=10,* K_i*=10,* V_{max}*=10. Green = negative regulator, Blue = Function, Red = Activator. Scan is 10 intervals between 0 and 1.*

The generic redox models employed to explore the effects of oxidative stress are kinetic models based on ordinary differential equations. This modelling framework effectively simulates the signalling pathways as molecular fluxes being distributed across reaction branches. However, this is not the only way these biological systems could be modelled. To gain confidence that the theoretical observations are not an artefact of the modelling framework employed, Models 2 and 3 were simulated using a Molecular Dynamics approach. Models 2 and 3 were simulated in a three-dimensional cellular automaton simulator (CASSMI – See Section 2.1.2) as equal-sized particles undergoing Brownian motion within an enclosed container. Simulations in this modelling framework confirms the existence of a reduced pathway activation under conditions of oxidative stress which is caused by an elevation in the resting levels of *negative regulator* molecules (Figure 3.10).

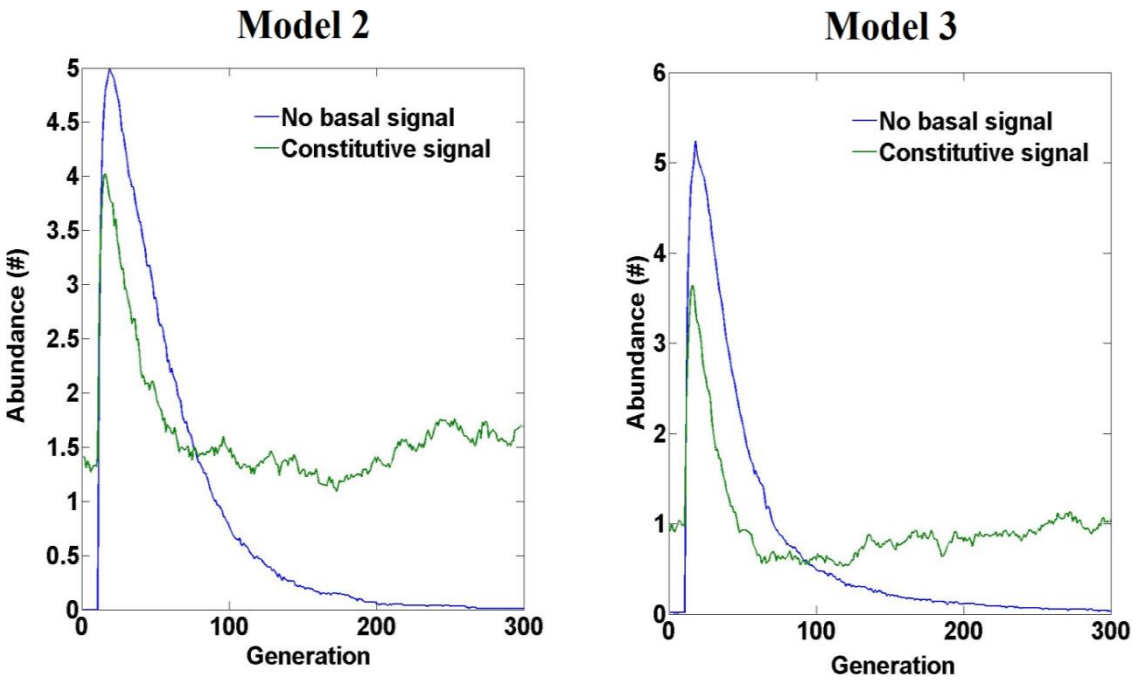

Figure 3.10. *'Activator' profiles for Models 2 and 3 simulated through a Molecular Dynamics framework. Averages computed from 1000 model runs. Initial molecule species match the values defined in Supplementary Tables 6 and 9. For reactions of order greater than one, the probability of the reaction firing upon the encounter of substrates in space was set to 1. First order reactions were set to fire every generation. The probability of firing for first order reactions was set to 0.1, 0.01 and 0.05 for the resolving of the 'Intermediate' species, degradation of the negative regulator and the degradation of 'Function' respectively (latter reaction unique to Model 3). Spatial occupancy by the simulated molecules was set to 50% and the stimulus strength set to 100.*

3.3.3 Constitutive signals reduce pathway responsiveness across multiple model topologies

The formalisation of *in silico* models of biological systems always involves a degree of uncertainty with regards to how representative the network structure is of the underlying modelled process. If a given theoretical observation is specific to a given model topology then the more weighting the structural uncertainty will have on the acquired insights. Testing for the robustness of theoretical observations against model topology can also be viewed as testing for the generality of an observation. To this end, the effects of a constitutive signal were investigated in models with both simpler and more complex topologies.

Models 2 and 3 were further abstracted to Models 4 and 5 respectively (Figure 3.11a&c). Models 4 and 5 are thus network motif-like structures which could correspond to an interaction pattern within any biological system. Model 4 consists of 6 species and 9 reactions. Model 5 consists of 8 species and 13 reactions. Both Models 4 and 5 showed a loss in the magnitude of pathway activation by an acute signal when in the presence of basally elevated levels of the same signal (Figure 3.11). The observation was once again back-tracked to the constitutive elevation of the resting levels of negative regulator *N*. Models 4 and 5 also display a similar shift in network-sensitivities in response to a constitutive signal as do Models 2 and 3 (Figure 3.12).

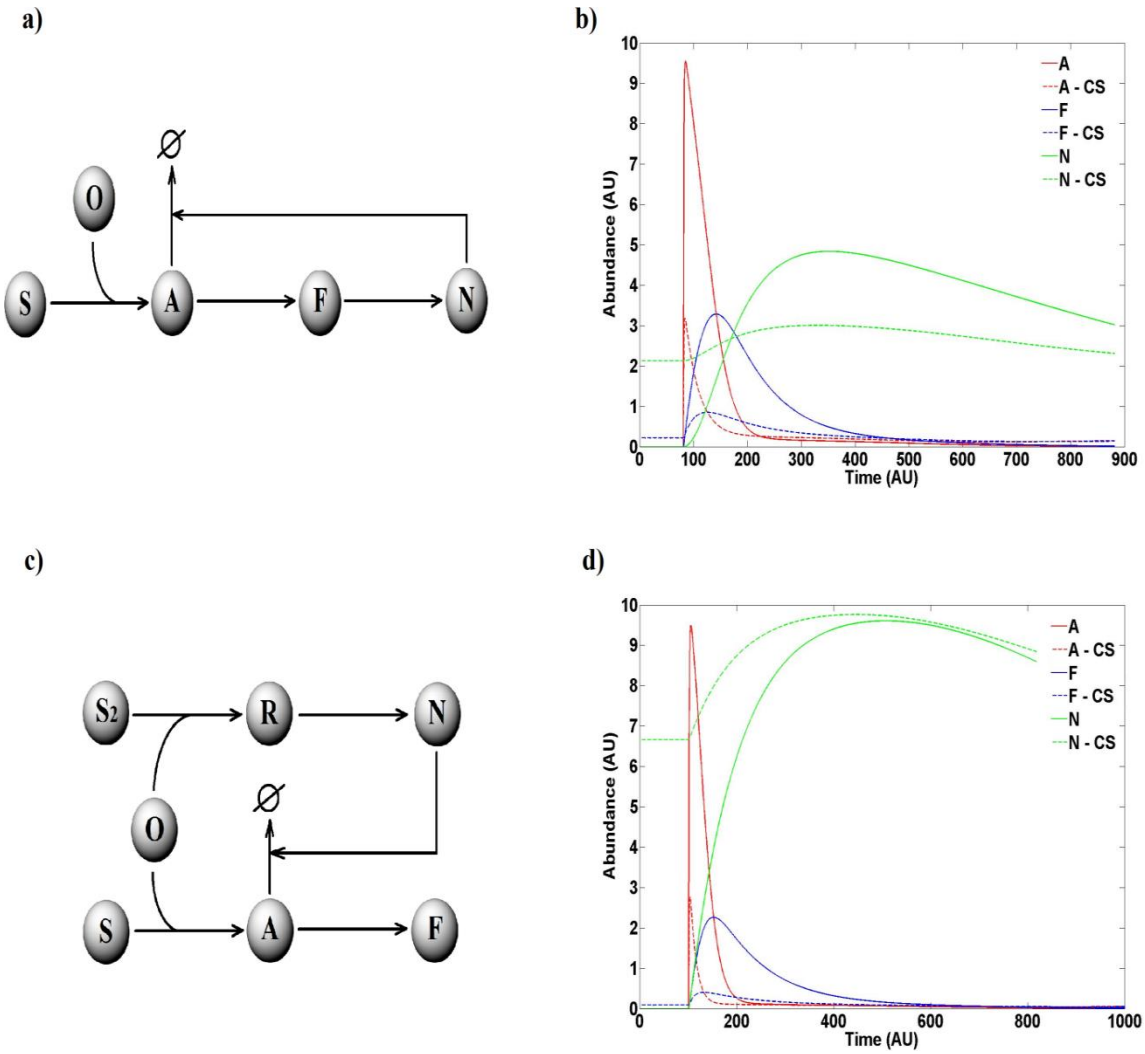

Figure 3.11. *Simulated activation profiles of Models 4 and 5 at different values of k1.* ***a)*** *Model 4 topology.* ***b)*** *Simulation output of Model 4 at k1 = 0 (continuous line) and k1 = 0.02 (dashed line).* ***c)*** *Model 5 topology.* ***d)*** *Simulation output of Model 5 at k1 = 0 (continuous line) and k1 = 0.02 (dashed line). CS = constant signal (k1 = 0.02). k1 is the parameter for O generation. Dashed circle = degradation. Stimulus strength =100.*

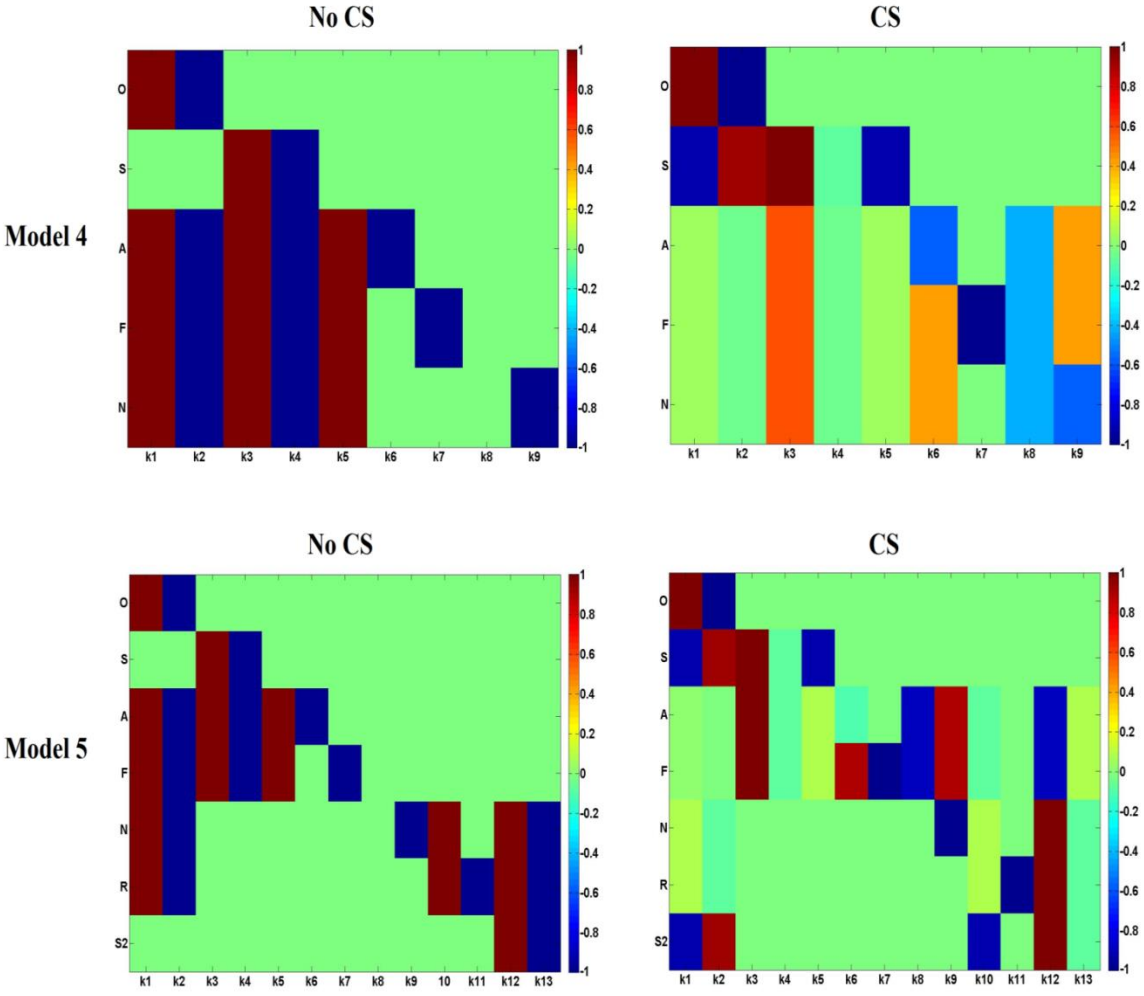

Figure 3.12. *Sensitivity analysis heat maps for Models 4 and 5 in the presence (k1=0.02) and absence (k1=0) of a constitutive signal (CS).*

When testing for the effects of a constitutive signal on a more complex model topology, a published model was chosen of a non-redox signalling pathway which has been calibrated with experimental data. Such model also satisfies a requisite of requiring just minor alterations to the published structure (i.e. the incorporation of an input reaction to provide a steady-state for the signal). The ERK signalling model published by Schilling *et al.* (Schilling et al., 2009) was selected for this purpose and slightly modified by adding two reactions, one for Epo synthesis following zero-order kinetics (*k1*) and another for Epo degradation (first order kinetics with rate constant value of 0.1). The incorporation of these two reactions increases the steady state level of Epo in the model, on top of which the same published acute addition of Epo is then introduced. Once again, negative regulator molecules are observed to enter steady state of higher resting abundance and this is accompanied with a reduced magnitude of activation of the ERK pathway to the same Epo stimulus (Figure 3.13).

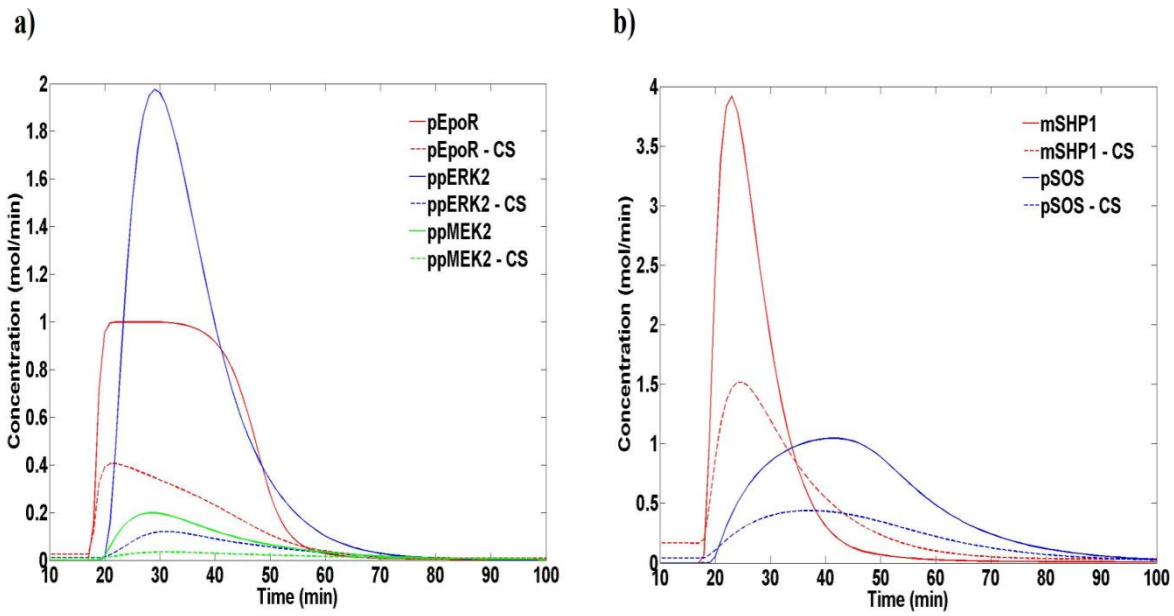

Figure 3.13. *Simulated activation profiles of the Shilling et al ERK signalling model (Schilling et al., 2009) when subjected to an acute Epo stimulus in the presence or absence of a sustained Epo signal.* ***a)*** *Pathway species that can be classed as 'Activators'.* ***b)*** *Pathway species that can be classed as 'Inhibitors'. CS = constitutive signal (k1 = 0.1).*

3.3.4 The sustained presence of a signal leads to a diminished information flow through the signalling pathway

What does it mean to the cell that a pathway is activated at a reduced magnitude? What are the functional consequences? Is the reduced magnitude still enough to trigger the desired response? When there is not enough experimental data available, these questions are non-trivial to answer theoretically. It can be conceived that a requirement for a cell to trigger a response to a stimulus is that the most downstream species of the stimulus-sensing pathway experiences a sufficient enough change from its basal state. The functional cellular response to the signal can thus be said to depend on how reliable the most downstream species in the sensing-pathway (Y) is in reflecting any alterations in the state of the most upstream species (X) that senses the stimulus.

It is possible to quantify the amount of information that the state of species Y would provide on the state of species X via the calculation of the mutual information between both variables (Shannon, 2001). In the case of Models 4 and 5, species X would be the O signal the system is responding to and species Y could be any species downstream of

it. Analysing the mutual information between these variables reveals a reduction in information flow through both Models 4 and 5 at increasing levels of the constitutive signal (Figure 3.14). A reduction in information flow of the same nature is also observed when the same mutual information analysis is repeated for Models 2 and 3 (Figure 3.14).

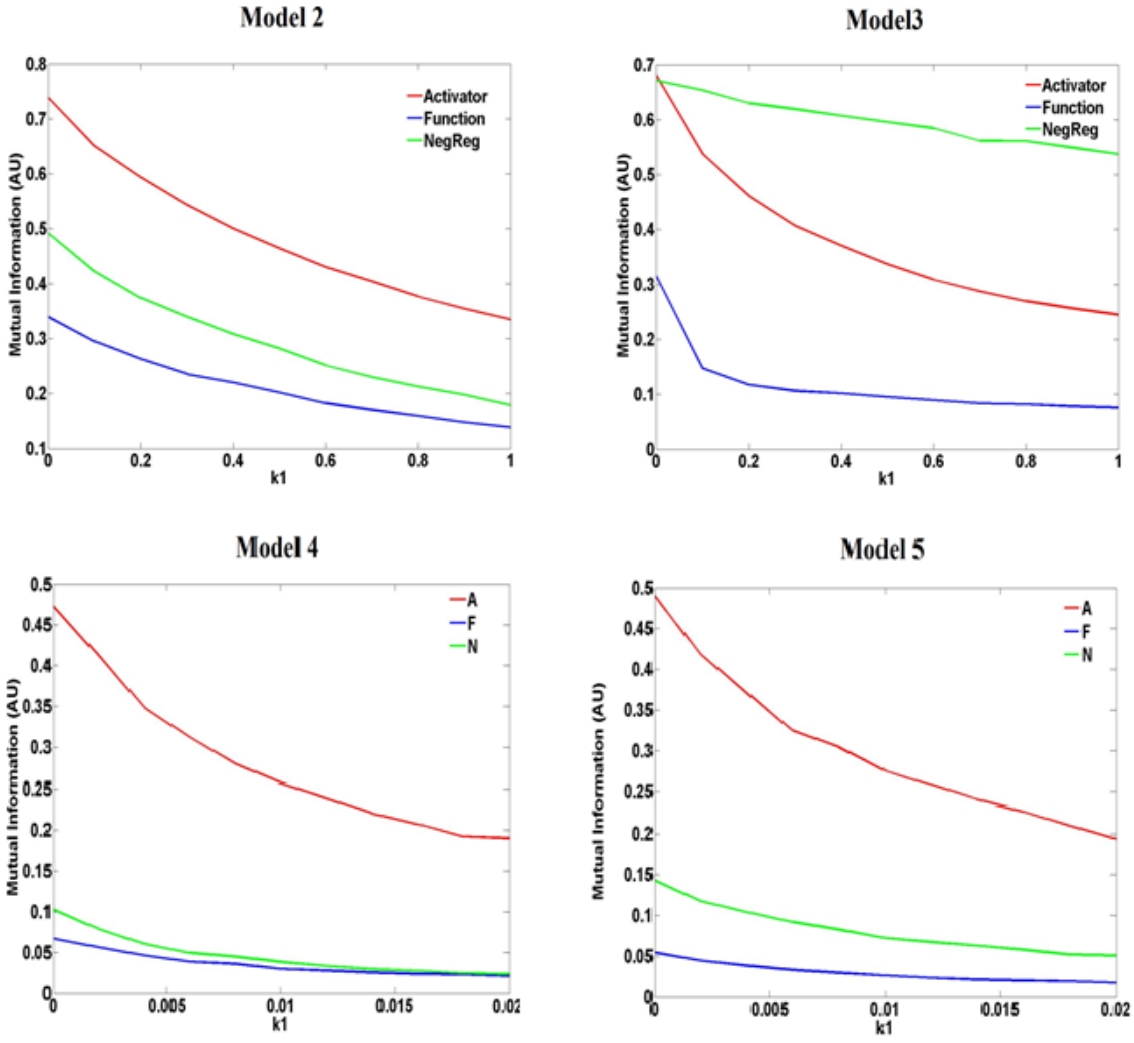

Figure 3.14. *Mutual information analysis in Models 2-5 for different values of k1. Mutual information was derived from the molecular abundance distributions at the time point of the maximal response peak. Mutual information value derived from 1000 stochastic simulations. Stimulus strength =100.*

A reduction in mutual information between molecules X and Y translates into a greater uncertainty on whether a change in the levels of stimulus X will be reflected by changes in downstream molecule Y so that the cell can mount a response. This uncertainty will thus manifest at the cell population level, where a greater proportion of the cells will not display a phenotype associated with the stimulus they have been exposed to. Indeed if one were to observe the cells and guess whether they have been treated or not it will be more difficult to do so. Such a consequence of sustained cellular signals resulting in reduced information flow is evidenced in the dose-response profiles of Models 4 and 5 (Figure 3.15). It can be appreciated in these dose-response curves that at higher levels of the constitutive signal the magnitude of stimulation maps to a larger range of possible abundance values of molecule *F*.

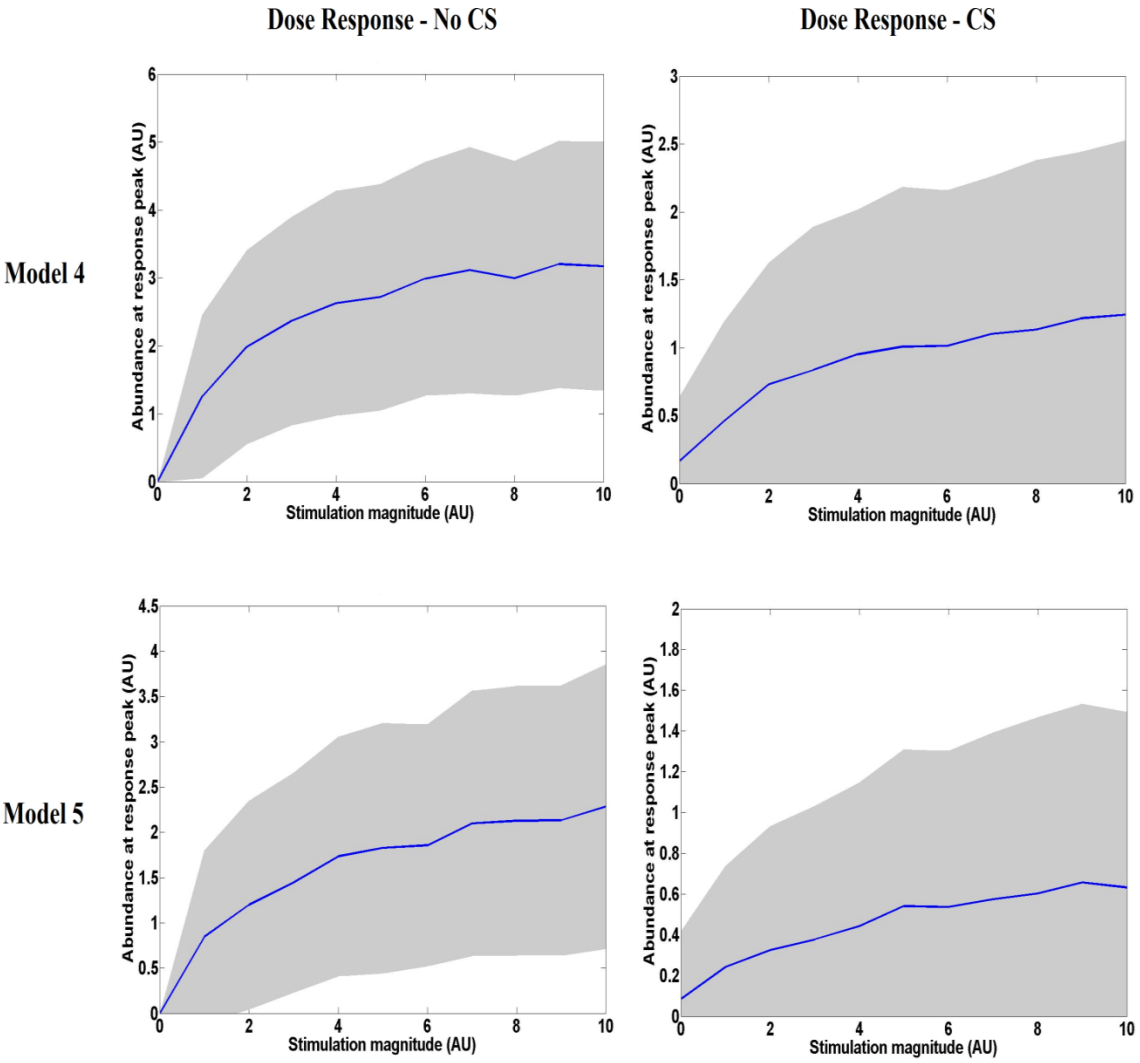

Figure 3.15. *Simulated dose-response profiles of molecule F in the presence and absence of a constitutive signal. Mean (blue) and standard deviation (shaded) are derived for the time point of maximal response peak of molecule F. Data derived from 1000 stochastic simulations. CS=constant signal (k1 = 0.02). Stimulus strength =100.*

3.3.5 Reduced responsiveness can occur across levels of biological organization

The observation that the 'blunting' phenomenon is robust to the complexity of the underlying network structure hints at the possibility that this behaviour could occur beyond the level of intracellular signalling. Indeed, the abstract nature of Models 4 and 5 could well refer to animal or cellular populations. To test this possibility, a cellular automaton framework was employed to define a three-dimensional agent-based model formalised as follows.

Agents were randomly seeded across a regular lattice to account for a final 50% occupancy. The initial state of all agents is resting state (*R*). Simulation involves the probabilistic transition of agents to a number of potential other states, namely, to a perturbed state (*P*), to a negative regulator state (*N*) or to a state of non-existence (*E*). Agents are selected in a random order each generation and run through the following update rules:

i) If state is (*R*) then transition to (*P*) with probability P_{ind}

ii) If state is (*P*) then n_i neighbouring (*E*) agents transition to (*N*) with probability P_{rec}

iii) If state is (*N*) then neighbouring (*P*) agents transition to (*R*) with probability P_{res}

iv) If state is (*N*) and state has existed for G_i generations then (*N*) transitions back to (*E*)

Note that neighbouring agents are defined as those within the Moore neighbourhood of the selected agent. Also of note is that rule G_i represents the duration of the presence of a negative regulatory state and n_i encodes the strength of negative regulation.

The model can be thus summarised as follows. The transition of agents from resting state (*R*) to perturbed state (*P*) leads to the recruitment of negative regulator agents agents (*N*) that will promote the transition back to the resting state and subsequently disappear after a certain number of generations (Figure 3.16a). The lifetime of the *N* state is the only model parameter that is not probabilistic in nature. A stimulus is modelled as a transient change in P_{ind} which results in a shift in the agent populations. The magnitude of such a shift in the agent populations is seen to be smaller when the basal P_{ind} probability is elevated (Figure 3.16). This observation is seen alongside an

increase in the steady state population of *N* agents. These results provide further evidence for the robustness of our observations to the underlying modelling framework and topology. Furthermore, they suggest that the blunting phenomenon could be observed at higher biological scales, such as intercellular interactions.

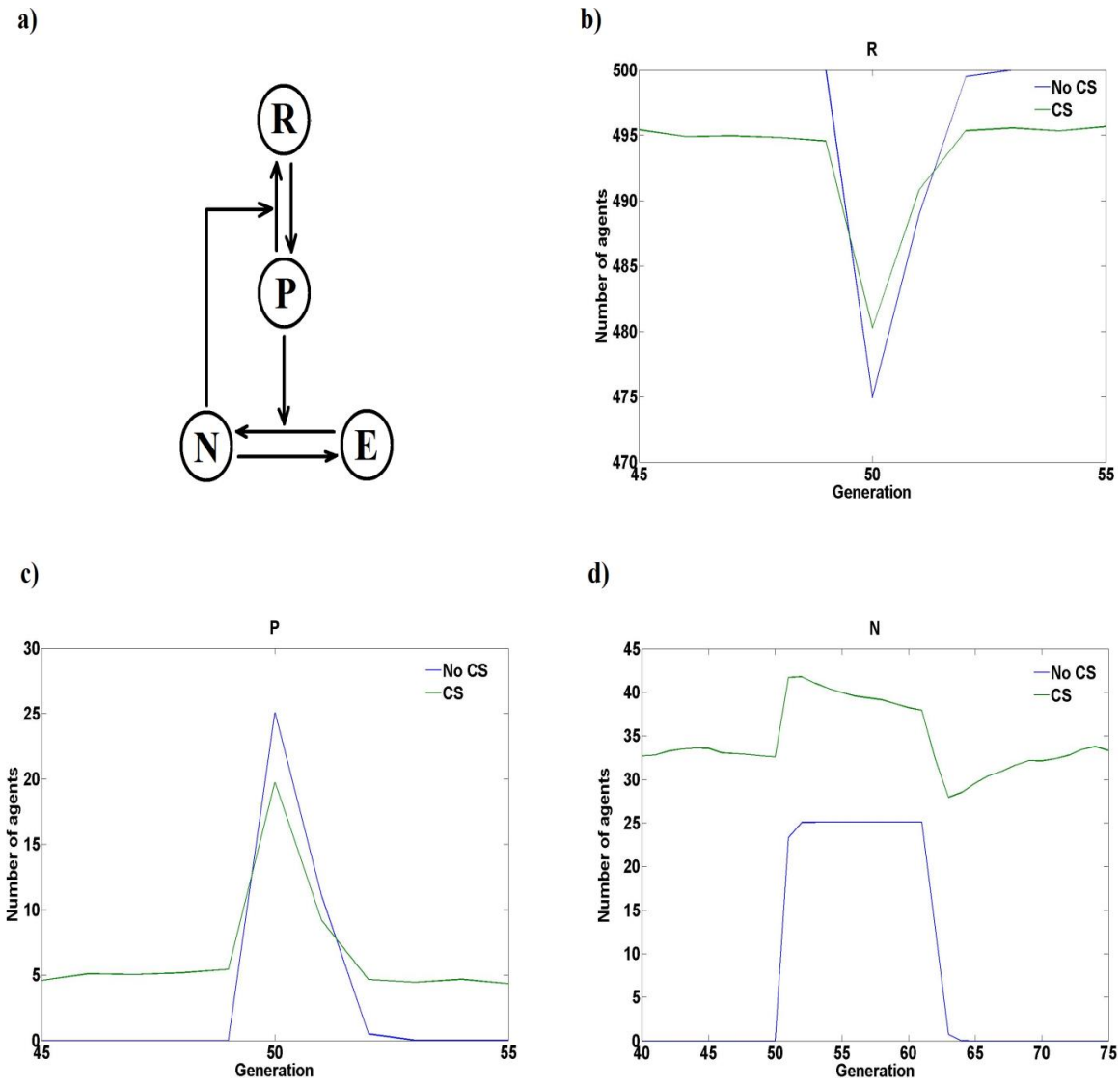

Figure 3.16. *Agent-based simulation in three dimensional space.* ***a)*** *Diagram of agent interactions.* ***b)*** *Simulated profile for R agents.* ***c)*** *Simulated profile for P gents.* ***d)*** *Simulated profile for N agents. CS=constant signal (P_{ind} = 0.01). Stimulation length = 1 generation. Stimulation strength: P_{ind} = 0.05. No CS: P_{ind} = 0. Plotted averages derived from 1000 simulation run at G_i=10, n_i=1, P_{rec}=1, P_{res}=0.9.*

3.4 Discussion

Both ageing and disease conceptually involve a departure from an optimal functional state, i.e. a loss of biological homeostasis. It can thus be argued that research into ageing and disease is essentially a quest for the causation and reversal of such homeostatic disruptions. But how is such loss of homeostasis recognised in the first instance? It commonly manifests as the constitutive elevation or reduction in the levels of a given biological entity. Most theories of ageing argue for stochastic damage as the cause of homeostatic loss during age, without specifying mechanistically how stochastic perturbations may weaken the robust biological systems. The perspective of considering the ageing process as a network-phenomenon suggests that loss of homeostasis in one cellular process could feed into other cellular sub-systems, potentially priming for a larger scale homeostatic loss. For example, age-related frailty has been described in terms of damage propagation across a biological network (Mitnitski et al., 2017).

In the process of biological ageing, it is not established how cells transition from a state of being able to control proposed molecular drivers of ageing like ROS, damaged proteins or inflammatory factors, to being in a state where such molecular entities are constitutively present. However, in this work we show that regardless of the underlying cause of the constitutive signal, it can potentially make biological systems more vulnerable to suffer a more widespread homeostatic dysregulation by reducing the responsiveness of signalling pathways that control regulatory responses. Work by Dalle Pezze *et al.* (Dalle Pezze et al., 2014) demonstrates how a system-wide loss in sensitivity can lead to a loss in biological functionality without the need for damage or mutation since *'the global decrease in sensitivity upon kinetic rate constants indicated that the semantics of these model parameters, e.g. promoter or inhibitor, became more uncertain. As a consequence, this uncertainty increased system noise and decreased network robustness, which, in the context of a cell, translated into weak signalling regulations and therefore poor intervention effectiveness'.*

Furthermore, a case is made for constitutive signals potentially being able to drive a homeostatic imbalance at the cellular level. We observe that constitutive signals do not result in a homeostatic collapse, but a rather more subtle loss in responsiveness. This can mean that, at the tissue level, cellular populations would mount physiological responses of weaker strength, at an altered time or even an altered duration. Such a

quasi-functional state can be expected to prime a tissue for a gradual accumulation of damage and a functional decline.

The reported loss in pathway responsiveness under the presence of a constitutive signal can be back-tracked to a sustained elevation in the basal levels of negative regulator molecules. Previous work has demonstrated that cells can actively modulate the responsiveness of their signalling pathways via the steady state levels of negative regulator entities (Toyoshima et al., 2012). In fact, the prolonged elevation of negative regulators has been long argued to be a mechanism of physiological habituation to an environmental signal (Grissom and Bhatnagar, 2009, Herman, 2013, Lee et al., 2013, Ramaswami, 2014).

Further to this, the sustained activation of SAPKs in *Candida albicans* has been recently shown to result in a sustained elevation in the basal levels of the PTP negative regulators which stabilise a state of constitutive low-level Hog1 activation which promotes the survival of the organism under stressful conditions (Day et al., 2017). Additionally, a systematic testing of stress-resistance during the life cycle of *C. elegans* revealed a loss in the responsiveness of all organismal stress responses, although not caused by an increased activation with age (Dues et al., 2016). The idea of the observed blunting effect of constitutive signals being an adaptive response would mean that a homeostatic disruption arising from such signals could be a pleiotropic effect.

It is interesting to note that the reduction in information flow observed in Models 2-5 when in the presence of a constitutive signal (Figure 3.14) follows a very similar profile to a previously reported reduction in synaptic transmission efficacy during habituation (Prescott and Chase, 1999). At the cellular scale, the prolonged presence of negative regulators in the cellular environment has been characterised as a refractory mechanism to further stimuli (Vizan et al., 2013, Adamson et al., 2016). Such body of evidence gives support to the possibility that cells may have adapted to enter a state of reduced sensitivity.

Further evidence for the biological plausibility of a dampening effect caused by basally elevated levels of negative regulators comes from computational simulations of the cell cycle which indicate that the weak activation of negative feedback can lock the cell cycle an a stable intermediate state which needs of a stronger signal to induce a response (Rahi et al., 2016). An interesting observation from the mutual information analysis is that the negative regulator molecules can provide the highest amount of

information on the state of the environmental stimulus. This seems in line with the observation that negative regulators can display a better correlation with lifespan than the regulated activating molecules (Lewis et al., 2015).

It is interesting that the sustained presence of a stimulus can be a source of response heterogeneity within a cell population. It could be expected that pre-conditioning cells with the same stimulus would synchronise cells or even prime them for a response. However, different cells could also become desensitized to the signal at different rates. The interplay between habituation and sensitisation has been long known to affect response plasticity (Prescott and Chase, 1999). At least theoretically, a chronic signal in the cellular environment can be a source of uncertainty to a cell or tissue when discerning the presence of an acute stimulus and whether a consequential response should be mounted. This would translate into an increased percentage of cells that do not respond to a physiological stimulus. This illustrates the potential of a signalling dysregulation at the molecular level to percolate into the tissue scale in the form of populations of cells that fail to mount an appropriate response to a given physiological signal.

It is unlikely that the reported effect of constitutive signals is the sole driver of loss of responsiveness in biological systems. Factors such as altered binding affinity due to genetic mutation or a sub-optimal cellular environment, altered gradients across cellular compartments or altered basal levels of sensor molecules could also play major contributions to a loss in pathway responsiveness. For instance, a beneficial redox signal produced in the mitochondria (Scialo et al., 2016) would experience a decreased driving force as a result of a reduced gradient between the mitochondrion and an increasingly oxidized cytoplasm with age. This would be expected to manifest in a reduced flux of H_2O_2 across the mitochondrial membrane and consequently a reduced mitohormetic response. Alternatively, a sustained low-level hyperoxidation of cysteine residues in redox sensor proteins would also be expected to reduce the responsiveness of redox signalling pathways to acute ROS stimuli.

Dynamic computational models can often be criticised for being overly-simplistic representations of biological systems, which are known to have a much higher complexity than that represented in the model structure. This is apparent upon comparison of the dense interaction networks generated by bioinformatics approaches and the “insulated” chains of reactions that compose dynamic models. Such comparative simplicity is the result of the parsimonious approach to the construction of

dynamic models that need to be smaller than static models since they require many more parameters to capture the temporal dimension of the modelled system. Additionally, wherever model structure is related to function, there remains the uncertainty of whether any observed model behaviour is constrained to a small region of the parameter space. Such are the criticisms of network motifs (Ingram et al., 2006). It is likely that, in the same way as network motifs, some cases of signalling dysfunctionality will possibly be mapped onto constitutively elevated levels of negative regulators and others will not.

3.5 Concluding Remarks

Overall this work proposes that, at least in principle, sustained signals in the cellular environment can promote a state of unresponsiveness arising from an increase in the basal abundance of negative regulators. It is likely this will be a useful concept for researchers to bear in mind when coming across biological systems displaying aberrant signalling in the context of ageing and disease.

Chapter 4

A systematic exploration of network structures that display an altered activation in the presence of constitutive signals

4.1 Introduction

A criticism of the bottom-up approach to modelling biological systems is that the model structures are often too simplistic. These model structures contrast with the complexity of top-down interaction networks of biological systems which define statistical relationships between biological entities (de Silva and Stumpf, 2005, Gunawardena, 2014, Villaverde and Banga, 2014). A contrast between the network structures created by these two complementary approaches highlights that kinetic models are often simulated in "insulation" from the actual interaction network they are embedded in through multiple crosstalk points. This is the result of the modelling parsimony required to capture the temporal dimension of a biological system through the use of a more computationally-intense framework, i.e. the solving of systems of coupled differential equations.

The attempt to reproduce *in silico* the time-evolution of a biological system thus conveys *i)* an uncertainty regarding the consequences of simplifying the network complexity and *ii)* an uncertainty regarding the values of the model parameters. In both of these cases it is of interest to systematically test the robustness of model predictions to unbiased but realistic changes in both its structure and underlying parameter values. The systematic generation of pseudo-random network structures would provide an unbiased method to explore the generality of an observed system behaviour and furthermore the structural properties that support the behaviour of interest. This approach would aim to establish a relationship between structure and function.

The use of random number generators in establishing the network structure and parameter values not only reduces the bias in the model-construction process, but also accounts for structural and parametric uncertainty. Bias in this context refers to the subjective choices the modeller must undertake in the formalisation of the model. However, the exploratory space resulting from the random assignation of both structural interactions and parametric values is vast. Furthermore, it is well established that

biological networks are not random (Barabasi and Oltvai, 2004). It is thus necessary to account for prior biological information to some degree in order to not only constrain the exploratory space, but to create a more realistic model of a potential biological system.

For instance, should a positive-feedback loop arise in a randomly generated model it would be expected that a negative interaction should feed into at least one of the species involved since otherwise a runaway process would arise. Furthermore, a signal being fed through the network should result in a minimum number of recognisable activation/inhibition profiles in the form of peaks and/or troughs easily identifiable from the background pre-stimulation levels. Such conditions will reduce the computational search time and increase the biological relevance of a systematic analysis of these characteristics.

An algorithm was developed that permits a systematic analysis of pseudo- randomly-generated model structures (see Supplementary Figure 1) with the aim to explore the topological features that might promote a 'blunting' effect and to furthermore assess the generality of this observation. The algorithm was run under 'standard' settings (see Section 2.16) throughout unless otherwise indicated. The execution of the algorithm for random network generation involved a parallelisation of the algorithm work flow so that 1000 jobs would be run each creating and simulating 1000 models. Algorithm running time under standard settings involving the generation of networks with >50 nodes was 3.3 hours in a Sungrid Engine computer cluster.

4.2 Results

4.2.1 Response 'blunting' by constitutive signals requires inhibitory interactions to be activated

Randomly generated networks were examined for both 'additive' and 'blunting' behaviour in the presence of a constitutive signal (Figure 4.1). In this work, the magnitude of such additive/blunting effects was respectively quantified as the percentage increase/decrease in peak magnitude under the presence of a constitutive signal. The generation and simulation of one million networks yields models with recognisable activation profiles for a minimum of three species for ~42% of them. Of

these, ~1% displayed a blunting behaviour and ~63% displayed an additive response. A 10% minimum departure from the peak response magnitude was set as the threshold to define whether 'blunting' or 'additive' effects occurred. This arbitrary value was chosen to be the minimum change in responsiveness that could conceivably be expected to be measured through experimental methods. Frequency analysis of the generated networks that display a blunted response in the presence of a constitutive signal reveals that the extent of blunting can be quite severe for a substantial number of model topologies, especially with increasing the basal levels of the signal (Figure 4.2).

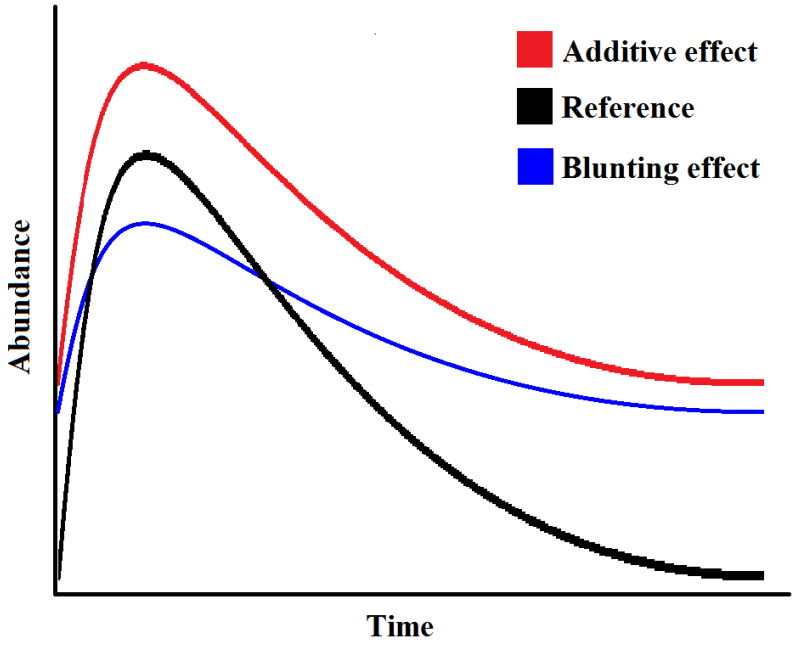

Figure 4.1. *Representation of an 'additive' behaviour (red) and a 'blunting' behaviour (blue) for a species activation in the presence of a constitutive signal. Note that both effects usually arise from an elevated basal level of the molecule.*

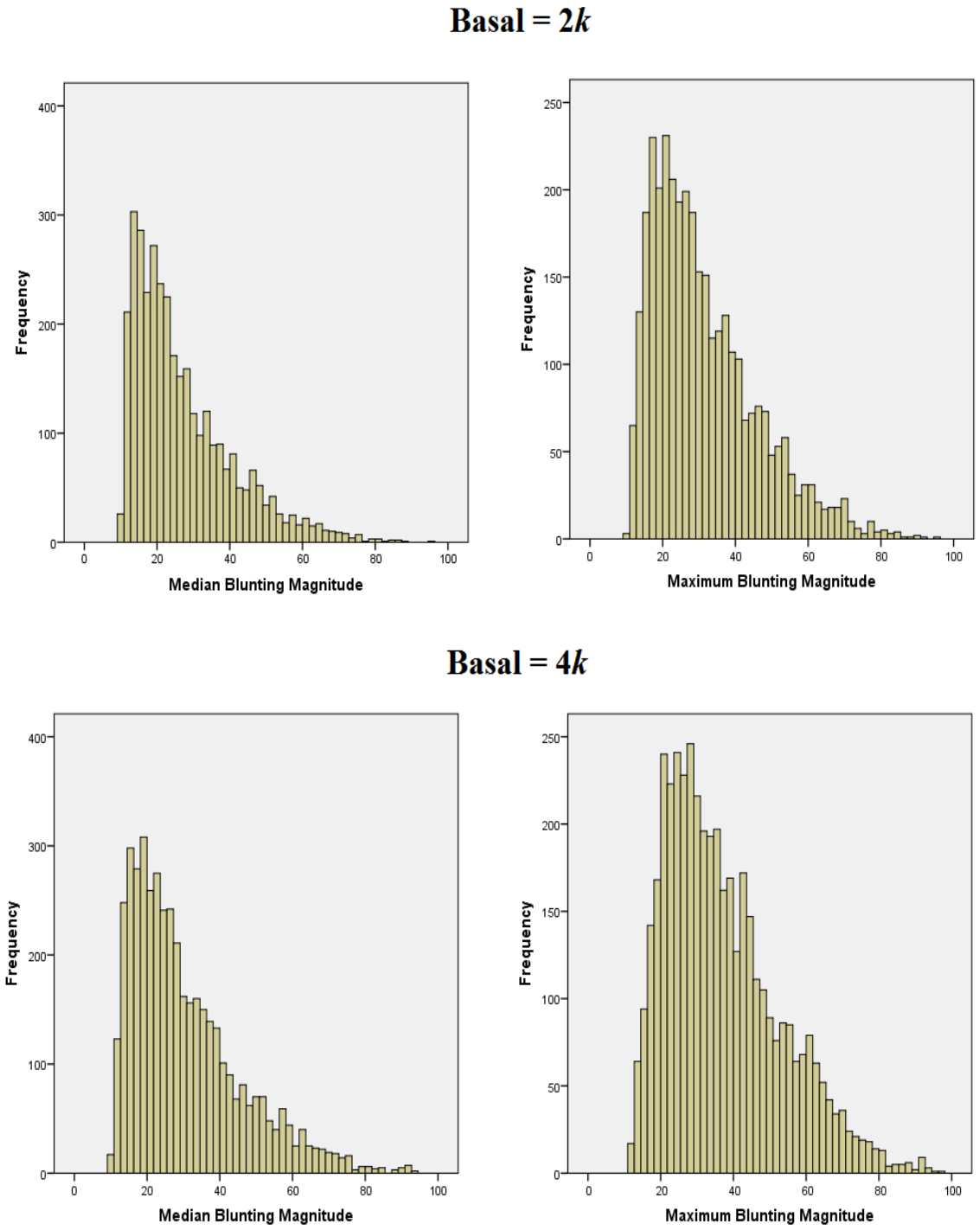

Figure 4.2. *Distributions of the extent of the 'blunting' effect for different levels of the constitutive signal. 'Basal' refers to the value of the zero-order rate constant of the synthesis of the constitutive signal. k refers to the rate constant of signal utilisation. Blunting magnitude refers to the percentage reduction in peak response abundance under the presence of a constitutive signal.*

When looking at the distribution of inhibitory properties displayed by the networks shown to become blunted, a number of features arise. Firstly, that the inhibitory properties of the activated portions of the networks are normally distributed, indicating that entropy has been maximised. However, upon the examination of the distribution of the number of activated reactions in the network, it becomes apparent that there is a pronounced departure from the normal distribution at lower values of this variable (Figure 4.3). Although this distribution also showed a departure from Gaussian for networks displaying an 'additive' behaviour (Figure 4.4), it is visibly a more substantial deviation in the case of networks displaying 'blunting' behaviour.

Another noticeable feature is the fact that the networks that display 'blunting' behaviour will always have a minimum of one activated inhibitory interaction whilst when analysing networks displaying an 'additive' behaviour there is an overrepresentation of networks with no activated inhibitory interactions. This would seem to suggest that negative regulators are a requirement for the 'blunting' effect to occur. Interestingly, networks displaying an 'additive' effect tend to have more positive feedback loops than networks displaying blunting behaviour, with more than half of the networks displaying 'additive' behaviour containing one or more positive feedback loops (Figure 4.4). The algorithm for random network generation involves a process of model-selection where only models displaying recognisable activation profiles in response to an acute stimulus are taken forwards for further analysis. To examine whether this selection process was shaping the distributions of network properties these were re-derived with such model selection being abolished. The distributions obtained (Figure 4.5) still display a slight departure from a normal distribution with regards to the number of activated reactions. This seems to suggest that the algorithm implementation results in a slight bias towards the analysis of smaller activated sub-networks.

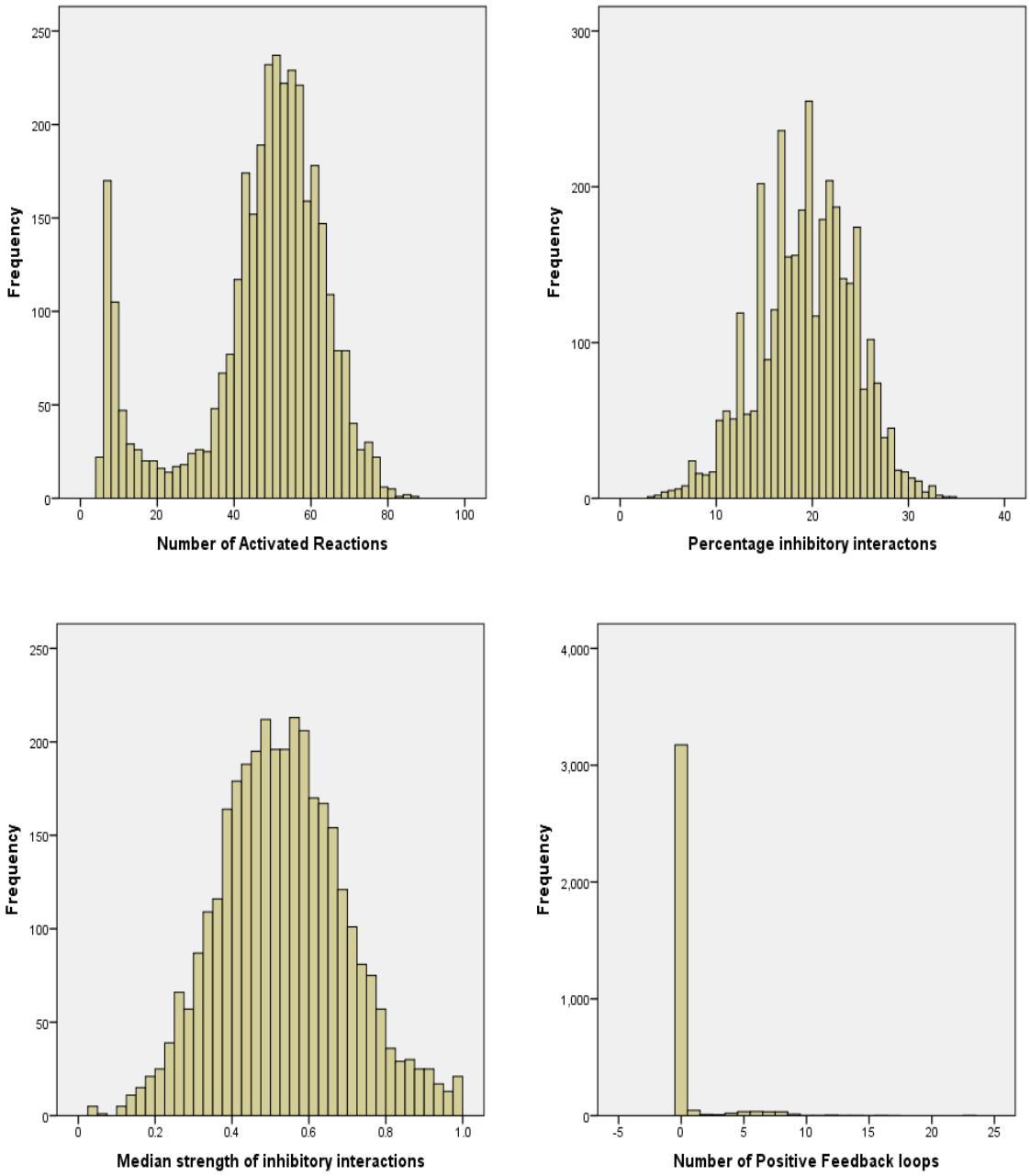

Figure 4.3. *Distributions for models that display a 'blunting' behaviour in the presence of a constitutive signal. Percentage inhibitory interactions refers to the number of inhibitory interactions in the portion of the network that was activated by a stimulus. Inhibitory interaction strength refers to the second-order rate constant of the reaction between the inhibitor and its target. PFL= Positive feedback loop defined as a topology where the product of a given reaction acts as a substrate for the reaction that synthesised its substrate.*

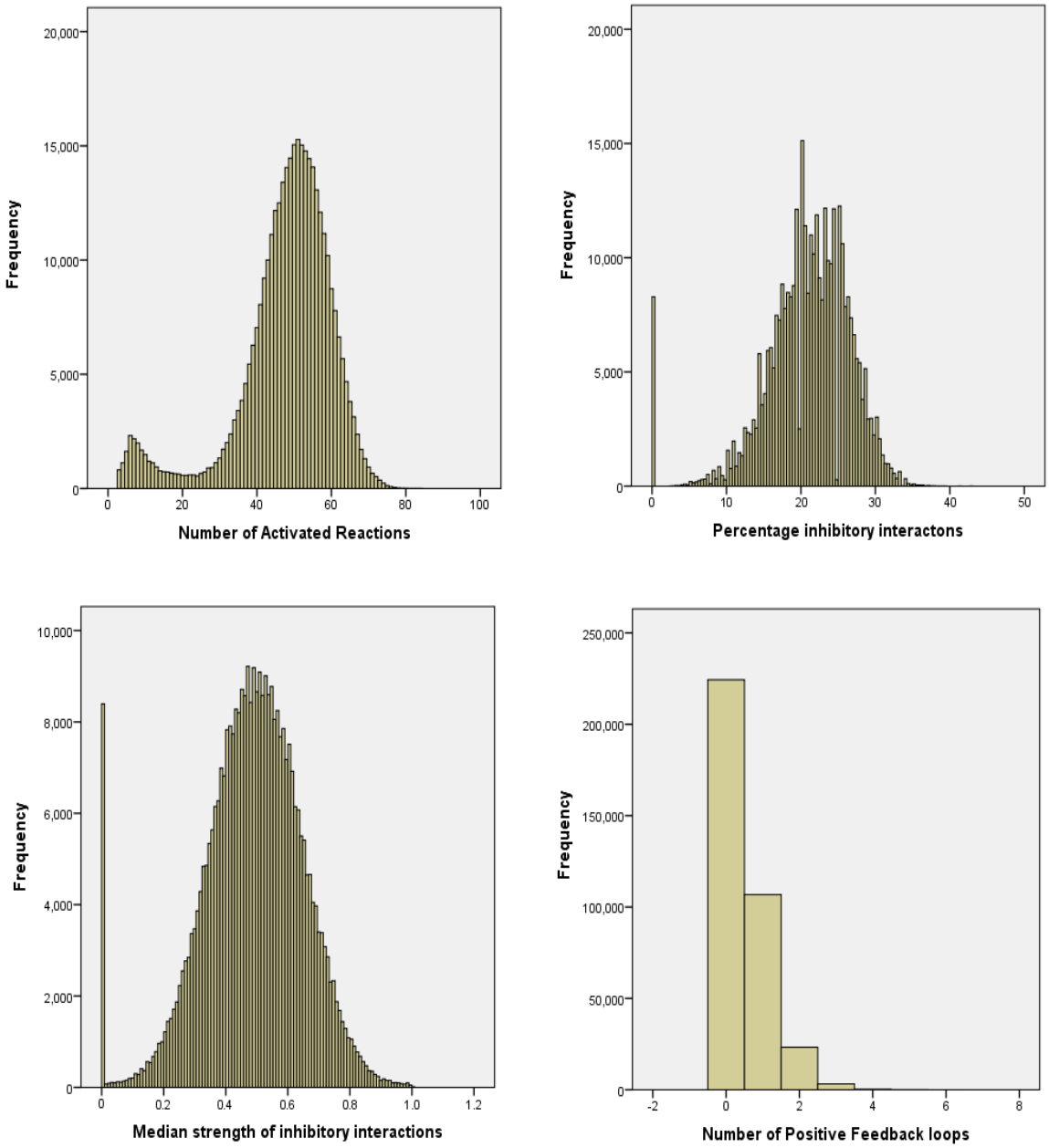

Figure 4.4. *Distributions for models that display 'additive' behaviour in the presence of a constitutive signal. Percentage inhibitory interactions refers to the number of inhibitory interactions in the portion of the network that was activated by a stimulus. Inhibitory interaction strength refers to the second-order rate constant of the reaction between the inhibitor and its target. PFL= Positive feedback loop defined as a topology where the product of a given reaction acts as a substrate for the reaction that synthesises its substrate.*

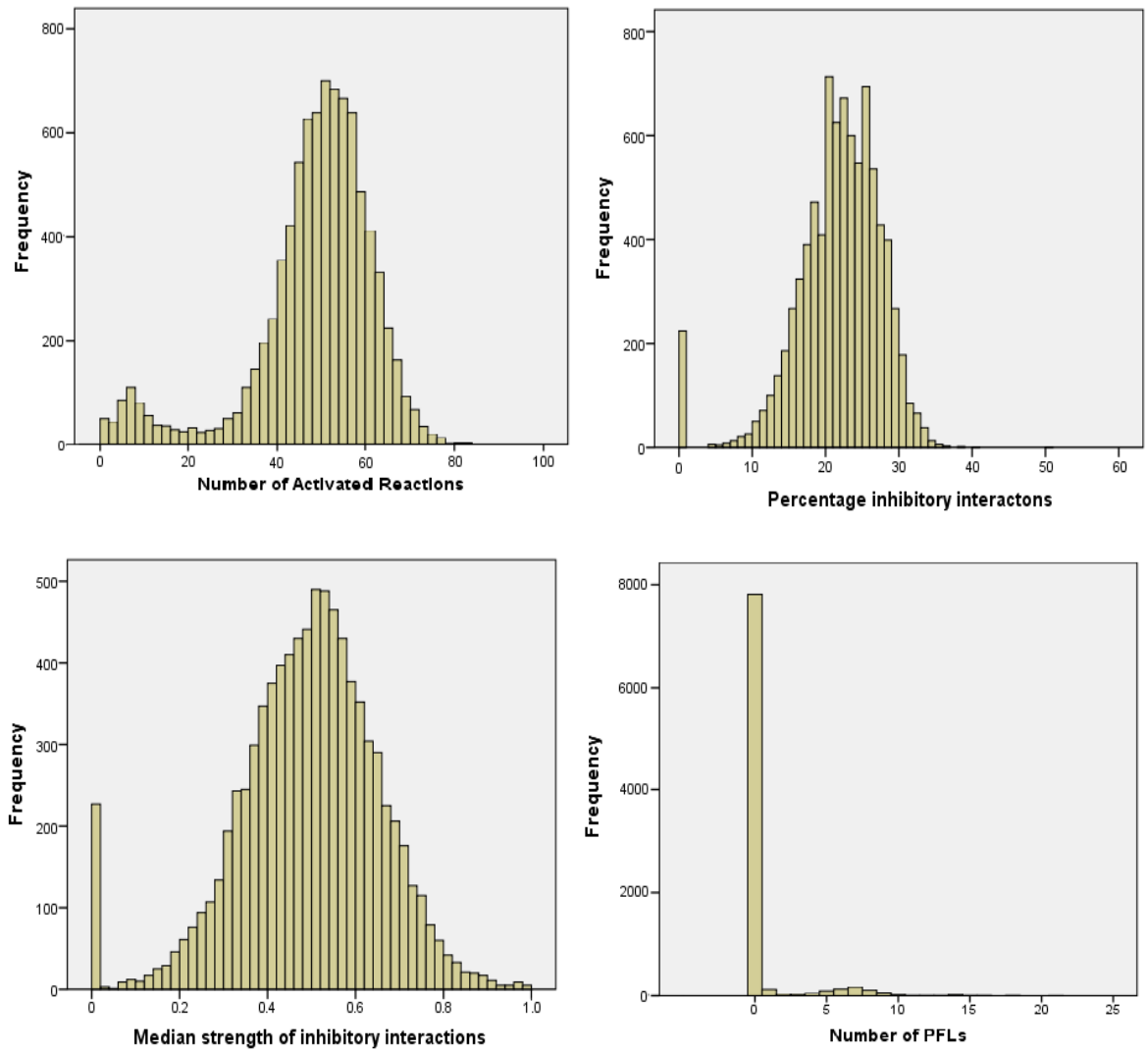

Figure 4.5. *Distributions for all simulated models without being selected for the display of recognisable activation profiles upon an acute stimulation. Percentage inhibitory interactions refers to the number of inhibitory interactions in the portion of the network that was activated by a stimulus. Inhibitory interaction strength refers to the second-order rate constant of the reaction between the inhibitor and its target. PFL= Positive feedback loop defined as a topology where the product of a given reaction acts as a substrate for the reaction that synthesises its substrate.*

4.2.2 A 'blunting' phenomenon is more likely to be observed in smaller networks

As specified in Section 2.1.6, a set of configuration parameters for the random network generation algorithm was established as the reference setting. This configuration involved input ranges for percentage inhibitory reactions, percentage competing reactions and percentage degradation reactions of *[25-50]*, *[10-25]* and *[10-25]* respectively. Initial abundances were set to 10 (AU) for all molecules, rate constants sampled from a value range of *[0.001 to 1]* and networks were set to have a minimum number of 50 reactions. The basal level of the signal was set to arise from a zero-order rate constant of value $2k$ where k is the rate constant of utilisation of the signal. The algorithm was then run under different variations of these parameters (*ceteris paribus*) to examine changes in the frequency of occurrence of the 'blunting' phenomenon.

Increasing the degradation reactions in the network by shifting the sampling range to *[25-50]* markedly decreases the number of networks displaying the blunting behaviour, whilst this is not obviously seen for networks displaying an 'additive' behaviour (Figure 4.6). Increasing the number of competing reactions within the network to *[25-50]* results in a small increase in the occurrence of 'blunting' but a more pronounced increase in the occurrence of 'additive' behaviours. Increasing the basal level of the constitutive signal to $4k$ results in a large increase in the networks identified to display both behaviours. The parameter with the largest effect on the number of retrieved networks displaying 'blunting' behaviour is network size.

A reduction in the size of the randomly generated networks from a minimum of 50 reactions to a minimum of 20 reactions results in an almost three-fold increase in the number of networks displaying a 'blunting' effect. This confirms the previous observation regarding the pronounced bias of networks displaying a 'blunting' behaviour towards smaller sub-networks (Figure 4.3) and hints at the possibility that such an effect would be most likely be observed in smaller and possibly simpler biological sub-systems. Interestingly, decreasing the number of inhibitory reactions in the network actually increased the instances in which the generated models displayed any of both behaviours. The number of positive feedback loops in the network did not seem to affect the frequency of occurrence of any of the two effects of the constitutive signal. The data does not seem to suggest that a reduced occurrence of the 'blunting' phenomenon in the randomly generated networks translates into an increased

occurrence of networks displaying an 'additive' effect in the presence of a constitutive signal or vice versa.

It is worth noting that a substantial number of simulated networks displayed a 'blunting' behaviour for all simulation settings. Again, indicating the robustness of the 'blunting' observation. Interestingly, when all of the rate constant parameters are set to be 0.1 in the network, the generation of a million model structures does not retrieve any 'blunting' behaviour. This seems to suggest it is not a phenomenon that arises solely from the network topology alone but by a combination between model structure and the parameter space. In order to confirm that the algorithm bias towards smaller networks would not influence these results, the data was cropped for networks containing less than 20 reactions. The same overall pattern of behaviour occurrence under different algorithm settings was observed with the exception of a reduction in the occurrence of 'additive' behaviour when the algorithm was run under increased basal level of the signal (Figure 4.7).

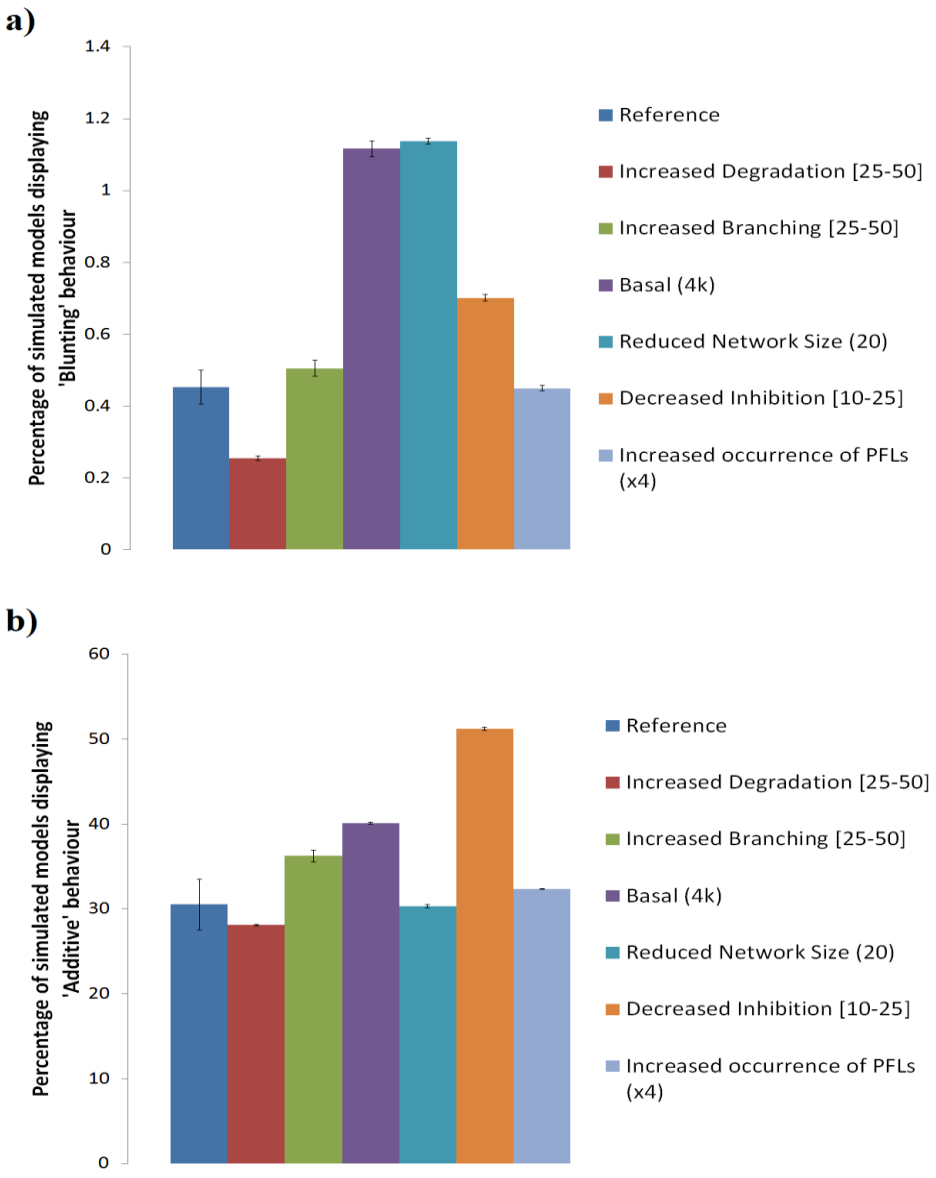

Figure 4.6. *Effects of the configuration parameters for random network generation on the frequency of occurrence of the 'blunting'* ***(a)*** *and 'additive'* ***(b)*** *effects. 'Reference' refers to configurations settings of initial abundance = 10, rate constant range = [0.001-1], percentage inhibitory interactions range = [25-50], percentage degradation reactions range = [10-25], percentage competing reactions range = [10-25], minimum network size = 50 reactions and Basal = 2k where Basal refers to the value of the zero-order rate constant of the synthesis of the constitutive signal. k refers to the rate constant of signal utilisation. PFL= Positive feedback loop defined as a topology where the product of a given reaction acts as a substrate for the reaction that synthesises its substrate. Configuration parameter changes undertaken ceteris paribus. Error bars correspond to standard deviation of the data. N=3.*

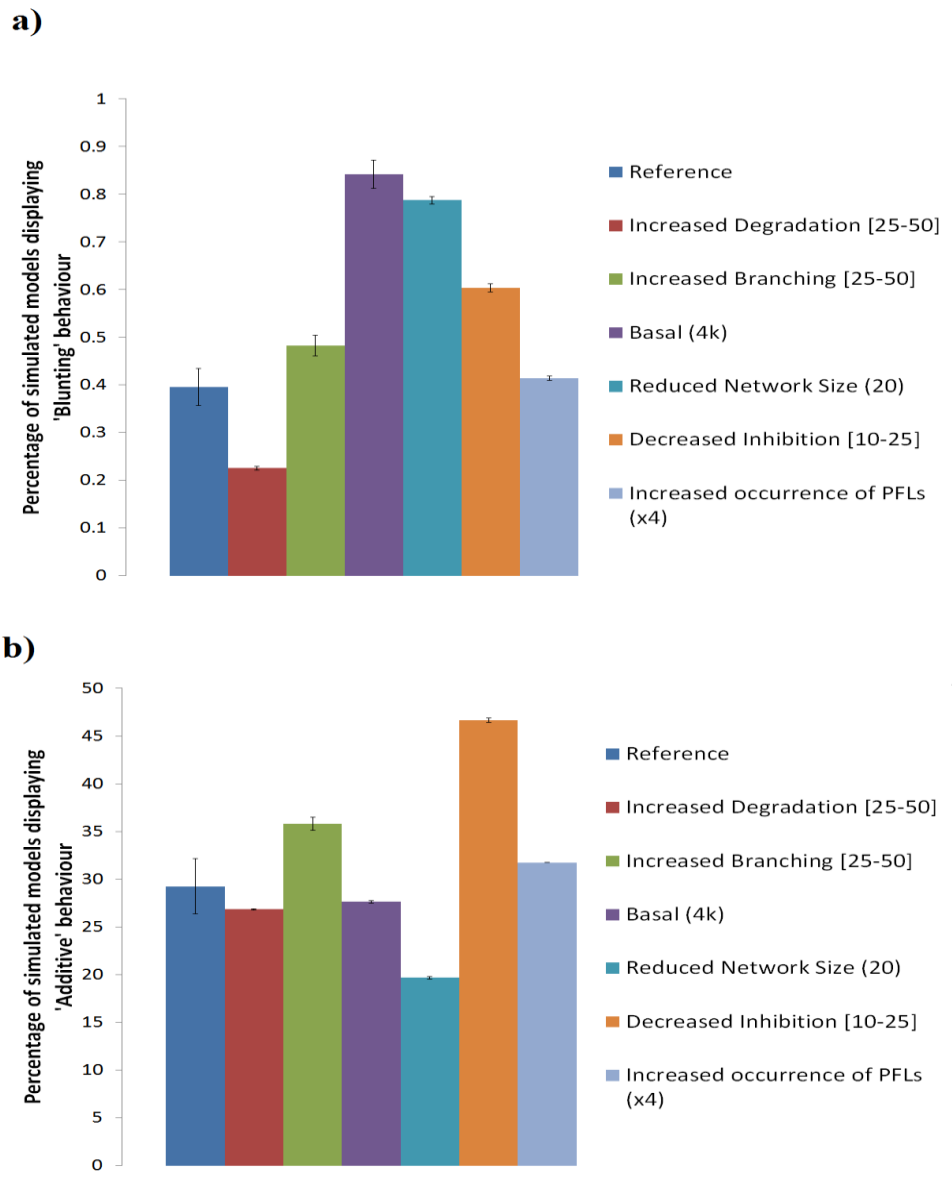

Figure 4.7. *Effects of the configuration parameters for random network generation on the frequency of occurrence of the blunting* ***(a)*** *and additive* ***(b)*** *effects using the dataset cropped for networks displaying less than 20 activated reactions. Reference refers to configurations settings of initial abundance = 10, rate constant range = [0.001-1], percentage inhibitory interactions range = [25-50], percentage degradation reactions range = [10-25], percentage competing reactions range = [10-25], minimum network size = 50 and Basal = 2k where Basal refers to the value of the zero-order rate constant of the synthesis of the constitutive signal. k refers to the rate constant of signal utilisation. PFL= Positive feedback Loop defined as a topology where the product of a given reaction acts as a substrate for the reaction that synthesises its substrate. Configuration parameter changes undertaken ceteris paribus. Error bars correspond to standard deviation of the data. N=3.*

4.2.3 The magnitude of 'blunting' does not correlate with network inhibitory properties

Upon examination of the relationship between the extent of the 'blunting' or 'additive' responses in a network and the inhibitory properties of the network it becomes apparent that there is no correlation between these variables as determined by a two-tail Spearman correlation analysis (Figure 4.8). This also holds true when both inhibitory properties are combined into a single metric (data not shown) and for when the 'blunting' magnitude of individual variables are plotted against the strength or distance of the nearest inhibitory reaction in the network (Figure 4.9). Thus, the activation of an inhibitory reaction is required for 'blunting' to occur but the number or collective strength of negative interactions in the network will not provide an indication of the extent of the loss of pathway responsiveness. As evidenced in the *hex* plots of Figures 4.8 and 4.9, there is a wide value range of network inhibitory properties that allow for a wide range of blunting-extents to occur. This reinforces the observation that a blunting phenomenon arising from a constitutive signal is a well-supported behaviour within the network "possibility-space". The plots for networks displaying an 'additive' behaviour again reveal the overrepresentation of models where inhibitory interactions are not activated, with no cases of this feature being observed for models displaying a 'blunting' behaviour (Figure 4.8).

Figure 4.8. *(next page) Relationships between the extent of a blunting/additive effect and the inhibitory properties of the network. Percentage inhibitory interactions refers to the number of inhibitory interactions in the portion of the network that was activated by a stimulus. Inhibitory interaction strength refers to the second-order rate constant of the reaction between the inhibitor and its target. The magnitude of an additive/blunting effect respectively corresponds to the percentage increase/decrease in response peak magnitude in the presence of a constitutive signal.*

Blunting effect

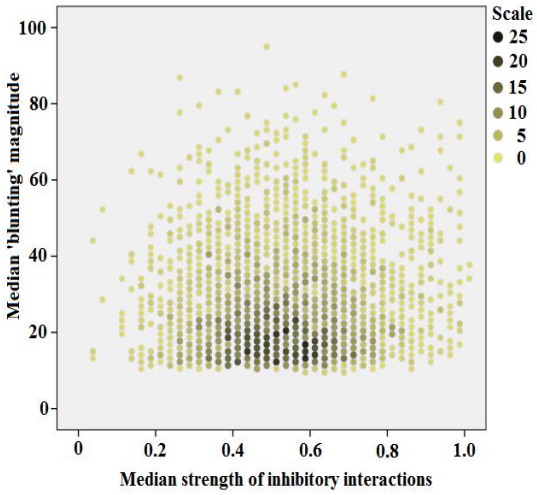

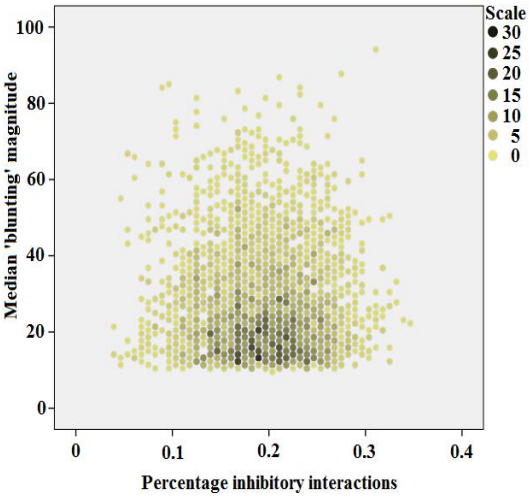

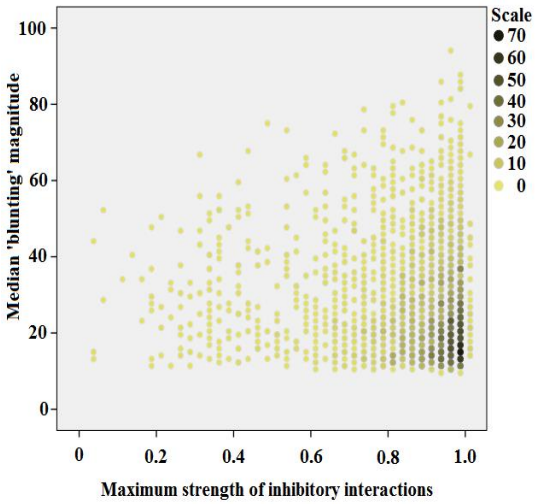

Additive effect

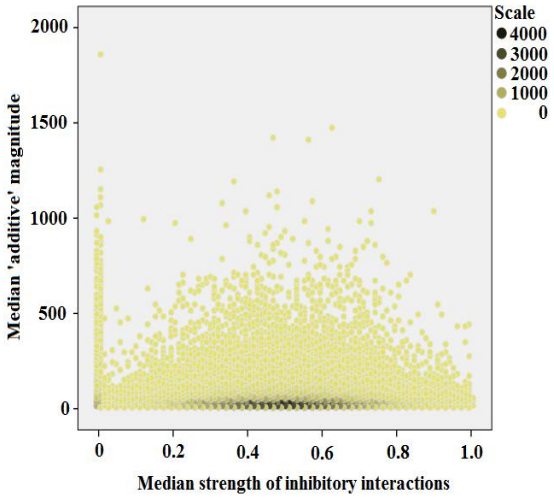

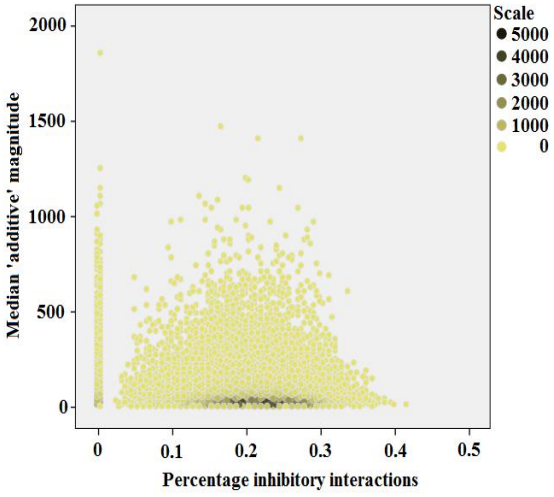

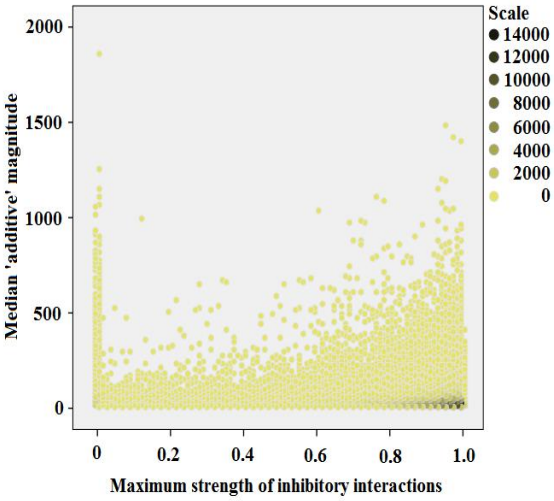

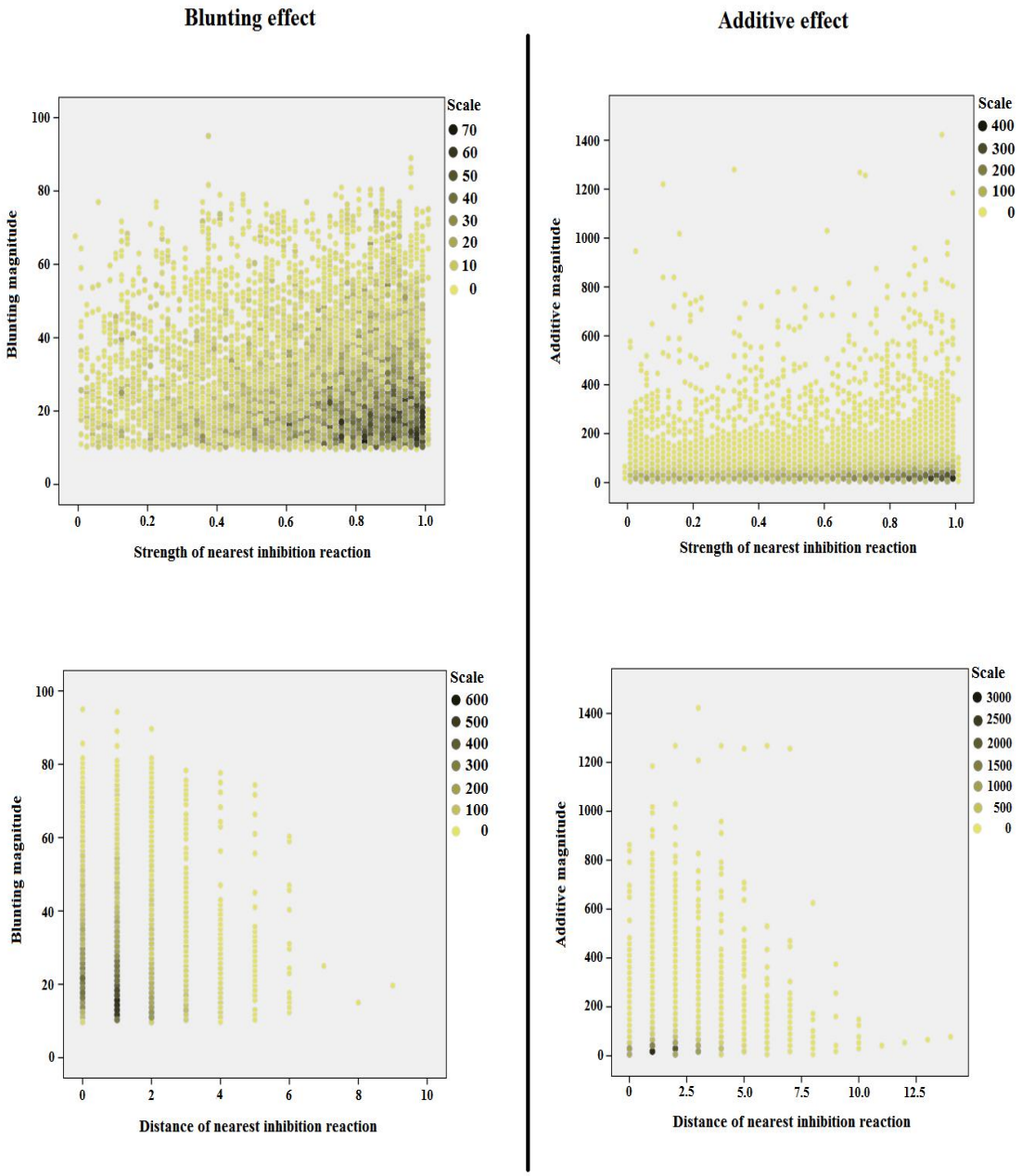

Figure 4.9. *Relationship between the change in response magnitude displayed by a given variable and the inhibitory properties (distance and strength) of the nearest inhibitory reaction. Hex plots show 'blunting' magnitude data for 18229 variables derived from 3429 networks and additive data for 17907 variables derived from 4685 networks. Interaction 'strength' refers to the reaction rate constant. Network distance refers to the number of reactions (nodes) between two given variables.*

A comparison of the collective inhibitory properties between models that display a 'blunting' behaviour and those that display an 'additive' behaviour reveals that models that display a 'blunting' behaviour consistently have a slightly higher median inhibitory strength across the network than those displaying an 'additive' behaviour, whilst the reverse situation is true regarding the percentage inhibitory reactions (Figure 4.10). The differences in these inhibitory metrics between networks that display both types of behaviour seems too small to use any of them as an *a priori* predictor of the effects of a constitutive signal on a given biological network. At the level of individual variables, however, molecules that display a 'blunted' response are more likely to be found closer to an inhibitory reaction that is also more likely to be stronger compared to if the variable displays an 'additive' response (Figure 4.11). It is thus apparent that the presence of an inhibitory reaction is the sole and sufficient requirement for a wide range of networks to be potentially able to display a reduced response to an acute stimulus when in the presence of a constitutive signal.

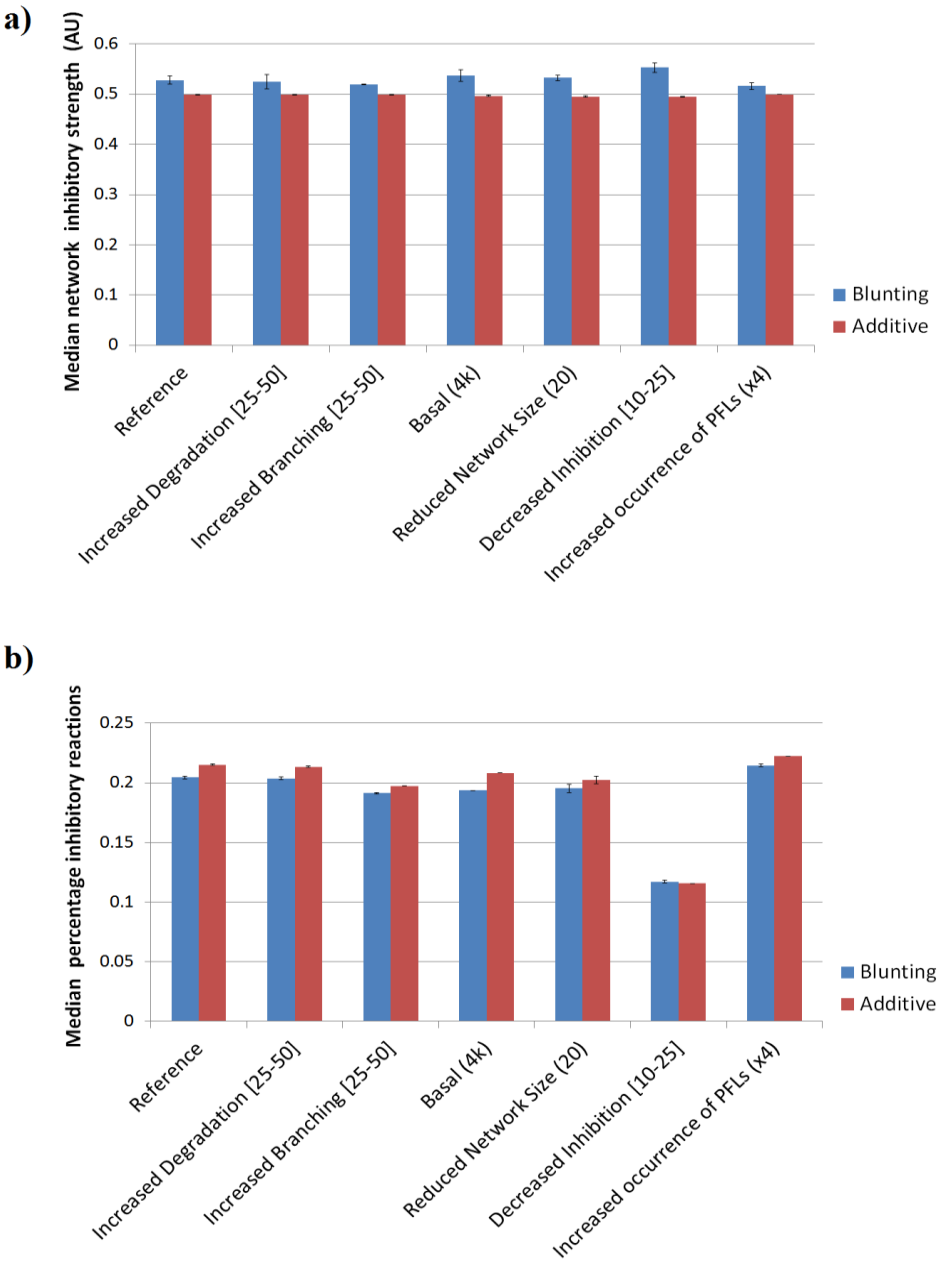

Figure 4.10. *Comparison of network properties between models displaying a 'blunting' behaviour and models displaying an 'additive' behaviour in the presence of a constitutive signal using the dataset cropped for networks displaying less than 20 activated reactions. Inhibitory interaction strength refers to the second-order rate constant of the reaction between the inhibitor and its target. Percentage inhibitory interactions refers to the number of inhibitory interactions in the portion of the network that was activated by a stimulus. PFL= Positive feedback loop defined as a topology where the product of a given reaction acts as a substrate for the reaction that synthesises its substrate. Error bars correspond to standard deviation of the data. N=3.*

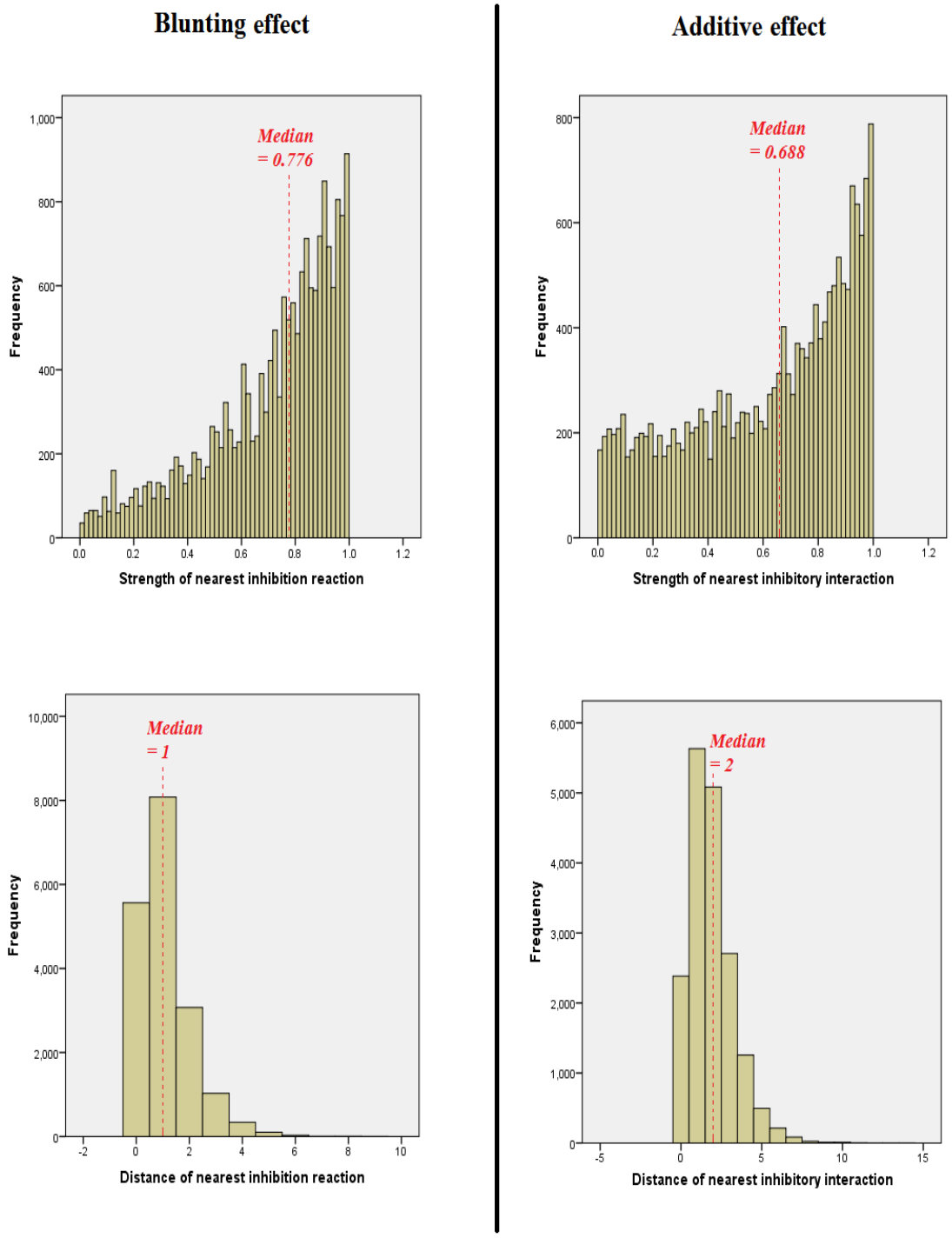

Figure 4.11. *Distributions for the strength and distance of the nearest inhibitory reaction to variables displaying a 'blunting' or 'additive' effect. Blunting data displayed for 18229 variables derived from 3429 networks. Additive data displayed for 17907 variables derived from 4685 networks. Interaction 'strength' refers to the reaction rate constant. Network distance refers to the number of reactions (nodes) between two given variables.*

4.2.4 Examining the tendency of networks to lose responsiveness under constitutive signals

The random network generation algorithm can allow for the systematic testing of *in silico* interventions that aim to restore system responsiveness. This involves simulating a series of network perturbations on those randomly generated models that are identified to display a 'blunting' behaviour. But what interventions should be systematically tested? The generated results suggest the blunting phenomenon is a network behaviour that cannot be solely mapped to inhibitory properties and that is indeed affected by systemic features like network branching or the number of degradation reactions. Indeed, it is not even clear from the data what would be required to transition from a 'blunted' response to an 'additive' response.

Other than the trivial observation of lowering the basal level of the constitutive signal to rescue the 'blunting' effect, it is of interest to explore the possibility of whether introducing a second constitutive signal into the network could potentially rescue network responsiveness. In an ideal setting, the signalling cascade that is experimentally seen to be unresponsive would be examined for crosstalk with other secondary pathways in order to rationally select a secondary pathway component to inhibit/overexpress or an appropriate secondary signal input to feed in in order to attempt to increase the responsiveness of the target pathway.

The obvious caveat of this approach is that introducing another constitutive signal into the network could rescue some parts of the network from a lack in responsiveness but decrease the responsiveness in other parts. To examine the proportional effects that a second constitutive signal might have on variables displaying 'blunting' and 'additive' effects within networks, the algorithm was run under standard settings and programmed to introduce a second constitutive signal after the variables displaying such behaviours had been located. A second simulation runs at this point where an acute signal pulse of the same magnitude is used to stimulate the network under the constitutive presence of the same signal and of a different signal (See Figure 4.12**c**).

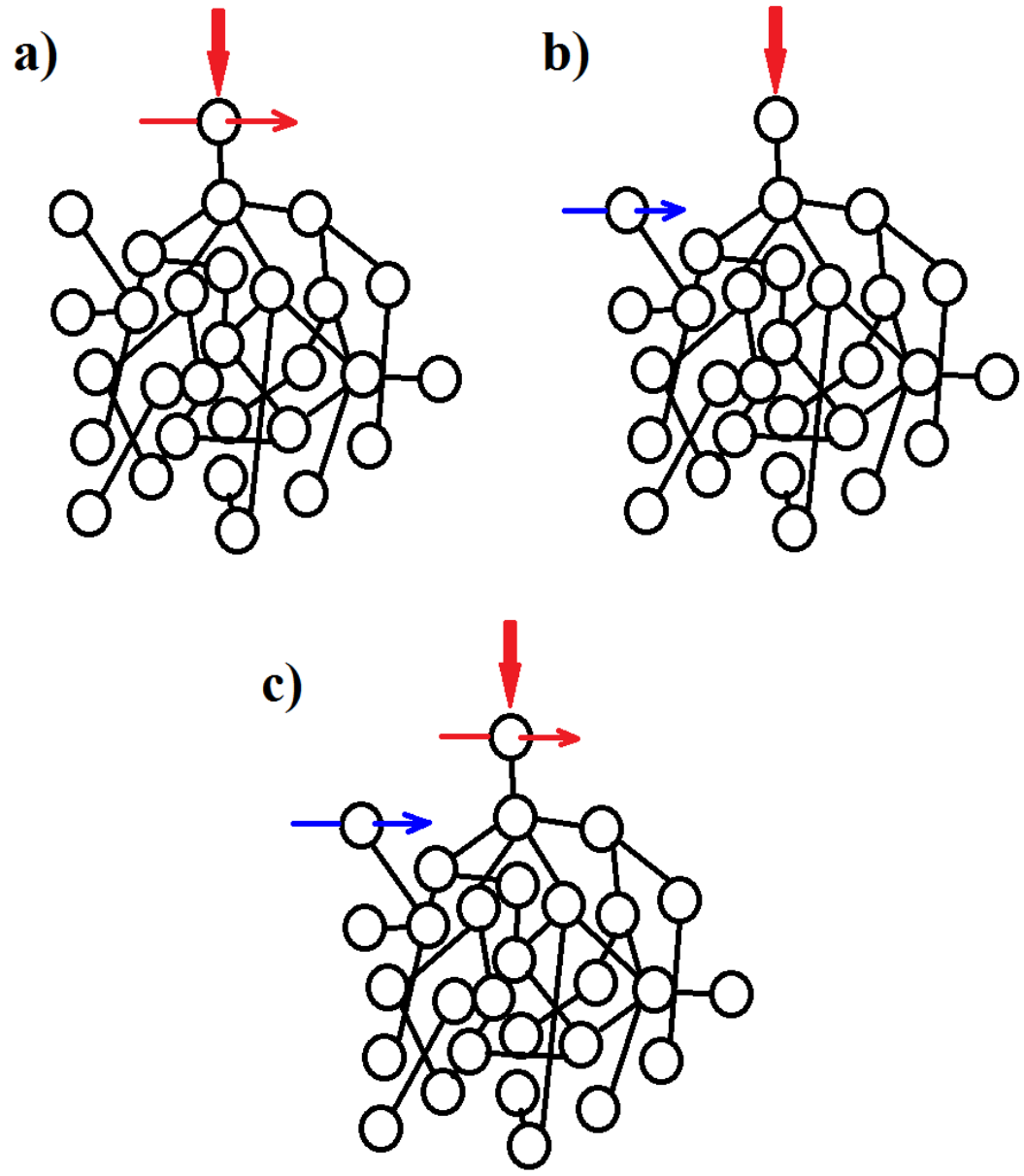

Figure 4.12. *The three systematic network interventions used to examine the occurrence of 'additive' and 'blunting' effects within the network.* ***a)*** *Examining changes in response magnitude to an acute signal under the presence of a constitutive basal elevation of the same signal.* ***b)*** *Examining changes in response magnitude to an acute signal under the presence of a constitutive basal elevation of a different signal.* ***c)*** *Examining changes in response magnitude to an acute signal under the presence of a constitutive basal elevation of both the same and a different signal. Vertical arrow = acute stimulus, horizontal arrow = constitutive signal.*

The simulation of a million models yielded 1424781 molecules displaying an 'additive' effect and 94179 molecules displaying a 'blunting' effect. Whilst 42.3% of the variables displaying an 'additive' effect displayed an increased activation magnitude when a second constitutive signal was introduced, only 10.1% had an increased activation above 0.1 arbitrary units (minimum peak magnitude for analysis is 1 a.u). In the case of variables displaying a 'blunting' effect , whilst 26.8% of the variables displaying an 'blunting' effect displayed an increased activation magnitude when a second constitutive signal was introduced, only 3.5% had an increased activation above 0.1 a.u. These statistics contrast with the 22.0% and 28.3% percentage of 'additive' and 'blunted' variables (respectively) that displayed at least a 0.1 reduction in activation magnitude in the presence of a second constitutive signal. The distribution of values for the change in peak magnitude upon the introduction of a second constitutive signal illustrates how such a perturbation tends to favour a further reduction in responsiveness in the network rather than a rescuing effect (Figure 4.13).

When the data are pooled together and normalised by the relative occurrence of both the 'additive' and 'blunting' effects, the tendency of the introduction of a second constitutive signal to further exacerbate the loss in network responsiveness can be appreciated (Figure 4.14). Almost two thirds of all the variables examined display a reduced responsiveness as a result of the introduction of a second constitutive signal. Only 1.1% of variables that displayed a 'blunting' effect transitioned into an 'additive' effect upon the introduction of a second constitutive signal. This is in contrast to the 6.8% of variables that displayed an 'additive' effect and then transitioned into a 'blunting' effect upon the introduction of a second constitutive signal.

An interesting observation arose when the algorithm was run under standard settings but with only one constitutive signal being introduced into the network through a different node to the acute stimulus as illustrated in Figure 4.12**b.** Out of a million models simulated under these settings, 7.9% displayed a 'blunted' response and only 2.1% displayed an 'additive' response. This is a stark contrast to the 0.45% and 30.5% respective occurrence of these effects when the constitutive signal is of the same nature of the acute signal (Figure 4.7). This seems to suggest that a loss in pathway responsiveness is more likely to occur if the constitutive signal is feeding into the pathway through crosstalk interactions than if feeds in through the same sensor that the acute signal is stimulating through. As opposed to constitutive signals of the same

nature of the signal, those that enter the pathway through crosstalk interactions are more likely to promote a 'blunting' effect than an 'additive' effect.

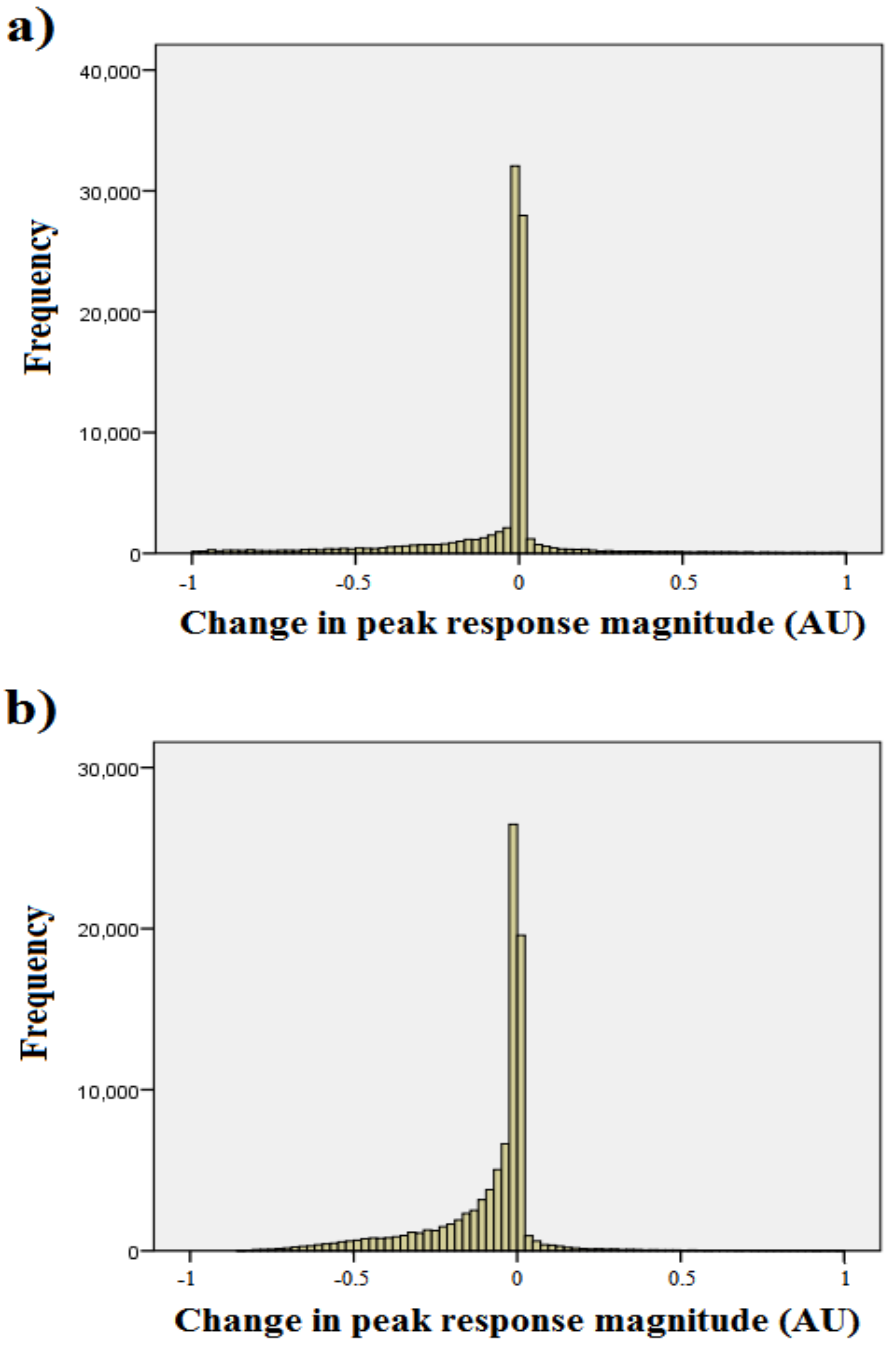

Figure 4.13. *Distributions of changes in peak response magnitude in response to a second constitutive signal feeding into the network for variables displaying an 'additive' effect* ***(a)*** *and variables displaying a 'blunting' effect* ***(b)****. N = 1424781 molecules displaying an 'additive' effect and N = 94179 molecules displaying a 'blunting' effect.*

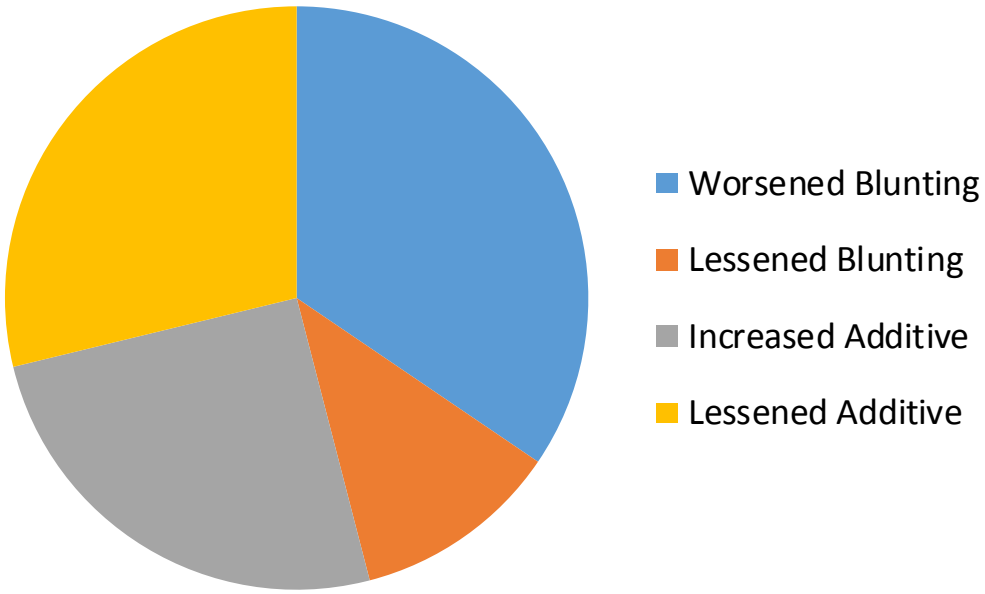

Figure 4.14. *Changes in the response magnitude of variables displaying an 'additive' or 'blunting' behaviour as a result of the introduction of a second constitutive signal into the network.*

4.3 Discussion

A fundamental question in biology asks how structure relates to function. At the molecular scale, a substantial amount of research has been undertaken to establish structure-function relationships in biological networks (Barabasi and Oltvai, 2004, Ma and Gao, 2012, Mitra et al., 2013) . One of the most successful examples of such efforts was the identification of network motifs (Milo et al., 2002). Network motifs are small network sub-structures seen to be overrepresented in biological networks and are associated with a set of dynamic properties that serve specific biological functions (Alon, 2007). Functional associations in biological networks has furthermore been extended to Coupled Motif Structures (CMSs), which have been analysed in relation to biological conditions such as cancer (Hsieh et al., 2015). Whilst the statistical analysis of the over- or under-representation of structures within a network will identify relevant structures, the mapping of dynamic data to such structures is required to capture function (Beber et al., 2012).

The *a priori* investigation of whether a given structure supports a target function requires the consideration of how much of the possible parameter space supports such function. Furthermore, depending on the specificity of the structure being investigated, different structural arrangements between the network elements will need to be considered. This results in a vast 'possibility space' (search space) to explore. Ma *et al.* simulated 16038 three-node circuits, sampling 10000 parameter combinations for each, effectively exploring 1.6×10^8 combinations to investigate which circuit structures are most likely to display an adaptive behaviour (Ma et al., 2009). Faucon *et al.* also investigated functional properties of three-node motifs but narrowed down the search space by considering only fully connected triad (FCT) structures (Faucon et al., 2014). The topological equivalencies arising from the symmetry of FCTs allowed for the further narrowing of the search space in the look for circuits that produced multi-stability. The authors tested 421,875 parameter sets for each of the 104 resulting structures, effectively requiring $\sim 4.4 \times 10^7$ simulations.

Such high-throughput computation required to establish circuit-function maps in three-node circuits exemplifies the size of the search space where a function of interest can exist in. The so-called enumeration method used by Ma *et al.* (2009) is a brute force approach involving the exploration of all possible network structures for a large set of parameters (Xi and Ouyang, 2016). However, such an approach is only feasible for

small network motifs since the consideration of all possible structures of a three node network already involves 3^9 combinations. For a four-node network this number ascends to 3^{16}, which has been estimated would take current computational systems 10 years to analyse (Xi and Ouyang, 2016).

Such figures serve as an indication of the size of the search space that needs to be explored. For large networks of at least 50 nodes, the enumeration method is simply not feasible. Heuristic methods like evolutionary algorithms have been developed in order to sample possible models from the high-dimensional search space and navigate towards functional properties of interest through model selection criteria (Warmflash et al., 2012). The adopted methodology in this work is heuristic in the sense that it makes use of random sampling in an attempt to capture a somewhat unbiased sample of the search space. It further makes use of a selection criterion to analyse the networks that display a minimum number of activation profiles of a minimum magnitude in response to an acute signal. However, the developed algorithm contrasts with evolutionary algorithms in that it stochastically samples the search space instead of stochastically navigating it through local search (Warmflash et al., 2012).

The consideration of 10^6 models per run of the algorithm is indeed a small sample of a search space encompassing both topological and parametric combinations. The use of one randomly-generated parameter set per randomly-generated model means that large numbers of model structures that could display the properties of interest would be discarded. Despite this, it is a surprisingly high frequency that ~0.5% of the generated structures displayed a 'blunting' behaviour when the constitutive signal was of the same nature as the acute signal, with this number ascending to ~8% when the constitutive signal was of a different nature to the acute signal. These results being under the algorithm configuration settings used. The substantially higher frequency of models displaying a 'blunting' behaviour when the constitutive signal feeds into the network as crosstalk suggests that although cross-talk may be a mechanism for complex signal processing (Hart et al., 2013) and robust signal transmission (Uda et al., 2013), it may be a weak-point in signalling processing when a signal is constantly present in the cellular environment.

The fact that a substantial number of the models displaying a 'blunting' effect had a loss in peak response of over 20% (Figure 4.2) emphasises that such an effect by constitutive signals is not only common, but should be experimentally-noticeable. The introduction of a second constitutive signal is more likely to further reduce the responsiveness of

variables in the networks to an acute signal but more likely to do so if the network already displays a 'blunting' behaviour (Figure 4.13). This observation emphasises how networks seem to be prone to lose responsiveness in the presence of a constitutive signal, but with some network structures being more prone than others.

Whilst it is a clear outcome of the undertaken exploration of the 'search space' that networks seem to be susceptible to losing responsiveness in the presence of a constitutive signal, no relationship was found between inhibitory properties of the network and the occurrence or extent of loss in responsiveness. This is in agreement with previous observations on the robustness of the 'blunting' observation against variations in model topology and inhibition parameters (Section 3). Indeed, the results obtained show how a wide range of 'blunting' magnitudes and occurrences are supported by a wide range of network inhibitory properties encompassing the number of inhibitory reactions in the network, their median strength and the maximum inhibitory strength present (Figure 4.8).

A flaw with the approach of trying to establish correlations between network-wide inhibitory properties and the presence or extent of the 'blunting' effect is the arbitrary definition of what constitutes inhibition. A local definition for inhibition was adopted, where an inhibitory reaction is one that reduces the availability of a reaction substrate though a second order reaction. The caveat of this definition is apparent when one considers that a double inhibition is in effect an activatory mechanism relative to the most downstream molecule involved. Thus, a theoretical arrangement of the network structure could mean that the network has more inhibitory reactions than another one, but yet be more excitable by an acute stimulus. Such a consideration could have dissipated any correlations between inhibitory strength and inhibitory presence in the network and any observed 'blunting' effect.

However, when molecules are considered individually within the networks, still no correlation is seen between the distance or strength of the nearest inhibitory reaction and the loss in responsiveness observed in the presence of a constitutive signal (Figure 4.11). Interestingly, such metrics of the distance and strength of the nearest inhibitory interaction were the only ones that allowed a discernment between variables displaying a 'blunting' effect and those displaying an 'additive' effect. This hints towards the importance of negative regulators in stabilising the loss in responsiveness. This importance is further confirmed by the observation that there are no retrieved instances

of models displaying a reduced responsiveness when there are no inhibitory interactions being activated by the acute signal (Figures 4.3 and 4.4).

Because of the relative nature of what constitutes inhibition, i.e. what is inhibitory for one variable can be activatory for another, it could be expected that feeding a second constitutive signal through the network should rescue some of the responsiveness of half of the variables and worsen the other half. However there seems to be a clear bias towards the worsening of the effect (Figure 4.14). When taken together with the high occurrence of 'blunting' in the generated networks, especially when the constitutive signal feeds into the network as crosstalk, it seems that biological networks that function to relay signals tend to be prone to lose their responsiveness in the presence of constitutive signals.

This last observation is perhaps not entirely surprising considering that the requisite for a biological system to return to its pre-stimulation state in the presence of a continued signal is that it displays perfect adaptive behaviour (Shankar et al., 2015). Adaptive behaviour allows for the sensing of fold-changes, rather than absolute changes, in the level of the signal (Goentoro et al., 2009). Although perfect adaptive behaviour has been reported for a number of biological systems (Shankar et al., 2015, Ferrell, 2016), the behaviour is usually supported by just a portion of the parameter space (Chang and Levchenko, 2013, Ferrell, 2016) . This is exemplified by the minority (365 out of 16038) of three-node structures that are able to display an adaptive behaviour (Ma et al., 2009).

Adaptive behaviour has so far been mapped to a few basic interaction structures mainly including incoherent feedforward loops (IFFLs) and negative feedback loops (NFLs) (Ferrell, 2016). However, some complex eukaryotic pathways have been indicated to be able to display adaptive behaviour (Cohen-Saidon et al., 2009, Lee et al., 2014, Thurley et al., 2014, Thurley et al., 2015, Frick et al., 2017). This suggests that even complex pathways might be able to be abstracted into simplified structures that concisely capture the network behaviour at least under certain circumstances. The study of perfect adaptation in *E.coli* chemotaxis is the prime example of this (Tu, 2013). Perfect adaptation is not established as a property of many biological systems. The generality of perfect adaptation needs to be known in order to appreciate the vulnerability of biological networks to constitutive signals. Another possibility is that initially perfectly adaptive systems could lose such ability during the ageing process and thus become vulnerable to the constitutive signals that may arise.

The inability to locate structure-function relationships in the exploration of the search space where networks display a 'blunting' behaviour raises the issue of whether the adopted methodology was a suitable search strategy. The networks generated by the algorithm follow mass action kinetics where most reactions are first-order. This effectively restricts system dynamics to the relaying of acute peaks. The representation of a biological system as mostly behaving like a signalling cascade does not capture the richness and complexity of behaviour commonly seen in biological systems. This simplicity results from a parsimonious exercise of model definition aimed to facilitate the back-tracking of the 'blunting' behaviour to network structure without the confounding effects of more complex mathematical functions.

However, this level of simplicity means that any claim made on the generality of the obtained results is thus questionable. For example, such dynamic simplicity exclusively examines negative feedback as displaying an analogue behaviour in relation to an input signal. This means that switch-like (digital) mechanisms of negative feedback are not considered. The latter would not necessarily promote a state of imperfect adaptation under conditions of a constant input signal.

The generation of random networks is an unbiased method for systematically assessing the generality of an observation and to look for recurrent properties that might be associated with the function the networks are being selected for. Indeed, it has been argued to be a useful method for exploring potential structure-function relationships in biological systems (Aho et al., 2007, Bois and Gayraud, 2015). However, an argument against this strategy of search space exploration is that biological networks do not display random architectures (Barabasi and Oltvai, 2004). It could be argued that since the 'blunting' effect is observed in random structures then such a phenomenon could transcend the case of biological networks alone and thus their use is a more-encompassing testing for generality. In any case, it is worth noting that the networks generated by the algorithm are pseudo-random in the sense that a number of rules are applied that aim to:

i) Retain biological realism of the network. For instance, positive feedback loops need to have an inhibitory reaction regulating the loop.

ii) Allow a directed exploration of the search space. Through the random or non-random user-defined assignation of the number of degradation reactions, competing reactions, inhibitory reactions, positive feedback loops…

The algorithm selection criterion of networks based on their display of suitable activation properties would be expected to introduce a departure from purely random architectures. Indeed, the distribution of the node degrees across the simulated models reveals they do not correspond to those of a random network (See Figure 2.15 in Materials and Methods). This corresponds to a scale-free degree distribution reflected by most nodes having a low degree with a few nodes with a higher number of degrees, referred to as hubs (Jeong et al., 2000, Barabasi and Oltvai, 2004).

The random number generators employed by the algorithm sample with a uniform probability in order to provide an unbiased generation of models. When a node is randomly chosen as an input for the acute signal, the signal will feed through part of the network, but rarely the entire network. This is why the distributions seen in Figures 4.3 to 4.5 tend towards a Gaussian distribution. Within a large network, an acute stimulus is expected to be less likely to stimulate just a few of the constituent nodes or most of the constituent nodes, whilst the stimulation of an intermediate number of nodes is more likely. However, a clear bias is seen within the algorithm that favours the activation of a smaller subset of nodes. The observation that such bias is seen in all models generated (Figure 4.5) indicates it originates from the algorithm workflow, although the origin could not be located. However, such bias seems to not change the observations derived from the data (Figures 4.6 and 4.7).

The fact that such bias in our algorithm was most readily apparent in models displaying a 'blunting' behaviour is suggestive of the increased occurrence of this phenomenon in smaller networks. This idea is reinforced by the increase in the retrieval of models displaying a 'blunting' behaviour when minimum network size was decreased to 20 reactions (Figure 4.6). Despite having an equal value for the median number of activated reactions, models displaying a 'blunting' behaviour had a median path length between the altered variable and the nearest inhibition reaction that was half of the that of models displaying 'additive 'behaviours. Such observations seem to indicate that the 'blunting' effect is more likely to be relevant to small biological sub-networks or circuits than as a whole-network effect. This could be because within a larger network there may be more opportunities for compensatory effects that might dilute out its occurrence.

It is of interest to note that the only network generation parameter that reduced the frequency of models displaying a 'blunting' effect was the number of degradation reactions (Figures 4.6 and 4.7). The presented results suggest that increasing network-

wide turnover would dissipate any 'blunting' effects stabilised by a constitutive signal. This possibility seems in line with the pro-longevity effects of increasing macro-autophagy activity in a number of model organisms (Martinez-Lopez et al., 2015). It could be argued that under conditions of increased degradation, fewer variables reach stimulation magnitudes over the threshold required by the algorithm. If this held true then increased degradation would be expected to also reflect as a decrease in the number of models retrieved to display 'additive' behaviour, which it does not to the same extent (Figures 4.6 and 4.7).

A striking observation in this analysis was the rarity of occurrence of models which displayed instances of both 'additive' and 'blunting' behaviour. Such occurrences where counted but discarded from further analysis in order to ease the discernment between network structure and 'blunting' occurrence and magnitude. However, such low occurrence suggests that although the generated network structures are large and complex, the network portions that are activated by the acute stimulus may not necessarily be so. This possibility reinforces the idea that the generated network structures are more relatable to signal-relaying cascades that follow simple kinetics than to more complex homeostatic networks in the cell.

4.4 Concluding remarks

The random sampling of a model 'search space' encompassing both topological and parametric combinations has revealed that the loss in network responsiveness as a result of a constitutive signal can occur in a wide range of networks. No association was established between the strength of the 'blunting' effect and the underlying inhibitory properties but its occurrence might be favoured in smaller biological systems rather than large-scale networks. Whilst concerns remain over the methodological strategy adopted, namely the generation of network structures that follow simple mass action kinetics, this work reinforces previous results on the potential ability of a wide range of biological systems to display a loss in responsiveness in the presence of constitutive signals.

Chapter 5

Sustained oxidative stress treatments do not reduce the activation response of the Nrf2 signalling pathway to an acute redox stimulus in C2C12 myotubes

5.1 Introduction

The main predictions from the theoretical exploration carried out in this work can be summarised as follows. Firstly, that a biological system exposed to a constitutive signal for a sufficiently long period of time can become less responsive to a posterior acute addition of the same signal. Secondly, that consequential to such exposure to a constitutive signal, there will be a constitutive elevation in the basal levels of negative regulator molecules which will actively promote the loss in system responsiveness. The next step is to test these predictions experimentally.

Redox signalling underlies a number of beneficial responses triggered by skeletal muscle during a period of exercise (Cobley et al., 2015, Jackson, 2015, Ji, 2015). Aged skeletal muscle is associated with a state of damage and oxidative stress where the protective responses triggered by an exercise stimulus are blunted (Cobley et al., 2015, Jackson, 2015, Ji, 2015). However, it is mechanistically unclear if oxidative stress is the direct causative agent of the impaired redox signalling (Jackson, 2015). The elucidation of the nature of this signalling dysfunctionality in skeletal muscle is a step towards improving the efficacy of exercise as a lifestyle intervention for the elderly.

Redox signalling in aged skeletal muscle thus seems an intuitive physiological context to investigate the potential occurrence of a reduced activatory response stemming from the presence of a constitutive signal (a.k.a. oxidative stress). With the aim to circumvent the impractical use of skeletal muscle biopsies to explore this redox signalling dysfunctionality, we attempt to establish an *in vitro* model that reproduces the stressed conditions observed in aged skeletal muscle. Such an *in vitro* model consists on the use of the C2C12 mouse myotube cell line.

There are a variety of ways in which oxidative stress may be induced *in vitro*. Perhaps the most popular is to expose cells to an extracellular concentration (usually $\geq$100μM) of H_2O_2. This is an acute treatment, since H_2O_2 scavenging by the cell culture will

reduce the extracellular levels of H_2O_2 quite rapidly (Gulden et al., 2010, Kaczara et al., 2010, Wagner et al., 2013) and is usually referred to as a 'bolus' treatment. Another approach that has been used in the past is to treat cells with paraquat. Paraquat is a molecule that induces oxidative stress by producing superoxide molecules, which will also further form H_2O_2 and hydroxyl radicals, whilst utilising reducing equivalent molecule NADPH (Dou et al., 2016). Cell exposure to ionizing radiation has also been used to indirectly induce oxidative stress (Passos et al., 2010, Azzam et al., 2012, Szumiel, 2015).

Hypoxia refers to the sustained incubation of cells under low oxygen conditions (<5%) and has been shown to be able to increase ROS production in some tissues including, but not limited to, heart and muscle tissue (Turrens, 2003, Clanton, 2005, Bell et al., 2007, Clanton, 2007, Klimova et al., 2009, Cervellati et al., 2014). Hyperoxia, the sustained incubation of cells under high oxygen conditions (>20%), is well established to result in increased ROS production in a variety of tissues (von Zglinicki et al., 1995, Turrens, 2003, Flandin et al., 2005, Papaiahgari et al., 2006, Klimova et al., 2009, Baez and Shiloach, 2014).

More recently, an enzymatic system was developed which involves the mixing of specific unit stoichiometries of glucose oxidase and catalase (GOX/CAT) enzymes in the cell culture medium (Mueller et al., 2009). This enzymatic system will use glucose and oxygen in the media to produce a steady state level of H_2O_2 (ssH_2O_2) for 24hr. Such system allows a controlled and sustained exposure of cells to H_2O_2 which is not possible with acute bolus treatments. Consequently, the cellular responses triggered by both types of H_2O_2 treatments are significantly different (Chandra, 2009, Miguel et al., 2009, Covas et al., 2013, Marinho et al., 2013, Sobotta et al., 2013).

The somewhat abstract definition of what constitutes oxidative stress allows for a variety of possibilities regarding the nature of the treatment that can be used to induce oxidative stress. Should the stress be reflected by a certain response magnitude of stress-sensitive proteins? Should the exposure to the stress have a minimum duration? Should it be a specific, mechanistically-defined stress or a non-specific stress? Should it cause a minimal amount of cell death? Even if there was a standardization of what constitutes oxidative stress, it would still be arbitrary and perhaps not very useful considering the cell-specificity of stress responses. All of the aforementioned experimental strategies can induce ROS production but not in the same way, with the

same specificity or to the same extent. Indeed, the exact nature of the stress observed in skeletal muscle remains undefined (Jackson, 2015).

In this work the effects of oxidative stress on redox signalling through the Nrf2 signalling pathway is examined via the use of three stress regimes. Namely, a steady state H_2O_2 treatment for 24hrs, incubation under hyperoxic (40% oxygen) conditions for a week and x-ray irradiation. These three stress regimes aim to model different scenarios on the nature of the stress that may be present in aged skeletal muscle. The steady state H_2O_2 treatment aims to model a stress caused by a mechanistically-defined interaction between elevated levels of H_2O_2 and target molecular processes. Hyperoxic incubation aims to model a longer-term, sustained exposure to high oxygen conditions and allow for more systemic changes to occur within cells. X-ray irradiation aims to model a state of generic, non-specific damage within cells.

With these defined stress regimes we model a "standard" redox signalling event to be the response produced by a 50μM H_2O_2 bolus treatment. Thus, we employ extracellular H_2O_2 boluses to investigate potential effects that the stress regimes may have on the ability of such boluses to trigger a redox response. However, this method has the caveat that although it examines changes in redox signal transduction, it overlooks the cells ability to generate the redox signal in the first place. In order to account for potential interferences of the stress regimes on redox signal generation we use a 0.5μM Urotensin II treatment as a proxy. This is because there are many potential sites for ROS production in skeletal muscle during a period of exercise (Jackson, 2015), however, recent evidence points towards NADPH oxidases being the major source of ROS production during muscle contraction (Sakellariou et al., 2014). Urotensin II has been shown to increase ROS levels through the induction of NADPH oxidases (Djordjevic et al., 2005, Yu et al., 2015) including in the C2C12 mouse skeletal muscle cell line (Wang et al., 2013).

The question remains as to how to optimise the ROS treatments so the experimental setup remains physiologically relevant and not arbitrarily high. There is evidence in the literature that ROS levels at rest in aged skeletal muscle roughly double those measured in young skeletal muscle as indicated by direct ROS measurements (Vasilaki et al., 2006a, Miller et al., 2012, Palomero et al., 2013) and by markers of protein damage (McDonagh et al., 2014b). Furthermore, it seems that the magnitude of ROS generation in young skeletal muscle during a period of contractions is 0-50% greater than the ROS levels measured at rest in aged skeletal muscle (Vasilaki et al., 2006a, Palomero et al.,

2013) and 2-3 times higher than basal ROS levels in resting young muscle (Close et al., 2005, Vasilaki et al., 2006a, Palomero et al., 2013, Pearson et al., 2014). These relative magnitudes can be used as a guideline to ensure a certain degree of proportionality in the choice of ssH_2O_2 concentrations relative to the bolus H_2O_2 concentrations (Figure 5.1).

5.2 Results

5.2.1 Sustained oxidative stress promotes sustained peroxiredoxin hyperoxidation

It is well established that different cell types can have different susceptibilities to the same stress regime. It is thus of interest to examine whether the chosen stress conditions induced changes in a molecular marker sensitive to intracellular oxidant levels. Western blot measurements were performed on the levels of hyperoxidized peroxiredoxin ($PrxSO_3$) levels in C2C12 myotubes subjected to each different stress condition (Figure 5.2). All pre-conditionings induced a statistically-significant increase in the levels of $PrxSO_3$ with respect to non-conditioned controls. The 24hr treatment with a ssH_2O_2 production rate of 0.1μM/s resulted in a 5 fold increase in $PrxSO_3$ levels with respect to controls. Hyperoxia and irradiation treatments both resulted in a roughly two-fold increase in $PrxSO_3$ levels. Such changes in the oxidative marker indicate the presence of increased levels of intracellular oxidants in C2C12 myotubes exposed to all pre-conditionings. Perhaps unsurprisingly, the 24hr ssH_2O_2 treatment resulted in significantly higher levels of $PrxSO_3$ than the other two stress regimes. This could be due to the conditioning being shorter term or more likely due to the fact that it is the only stress regime that involves the direct and controlled generation of ROS. Note that no stress regime resulted in a significant increase in cell death (data not shown).

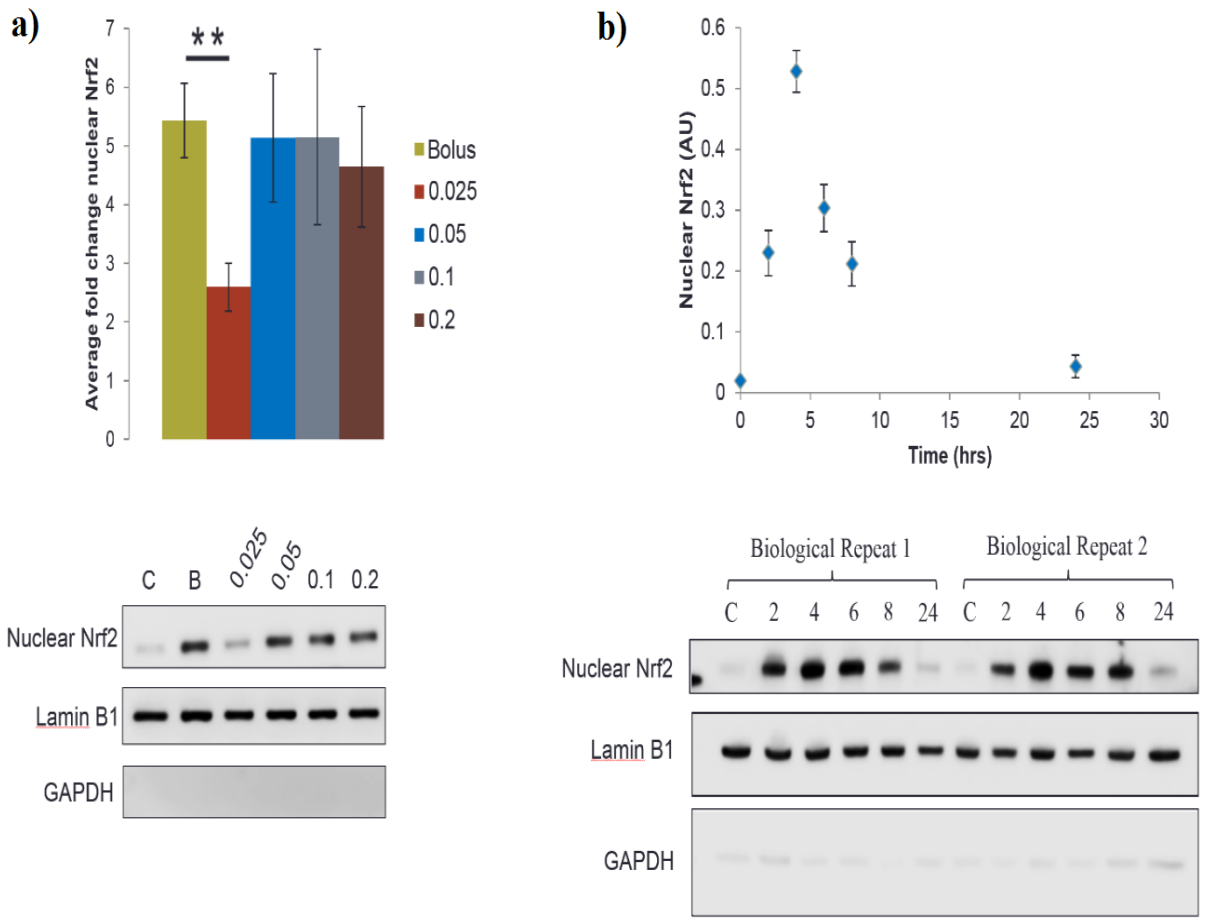

Figure 5.1. *Characterisation of Nrf2 activation by the GOX/CAT enzymatic system.* ***a)*** *Comparison of Nrf2 activation by an acute H_2O_2 bolus and by 24hr treatment with different ssH_2O_2 concentrations as produced by the GOX/CAT enzymatic system (N=4). B=Bolus=50µM H_2O_2 treatment collected at 60min. # = ssH_2O_2 production rate (µM/s).* ***b)*** *Time course profile of Nrf2 activation by 0.1µM/s ssH_2O_2 treatment for 24hrs (N=4). AU= Arbitrary Units, # = hours. C=Control, Error bars = standard deviation. * = $p<0.05$, **=$p<0.01$, ***=$p<0.001$.*

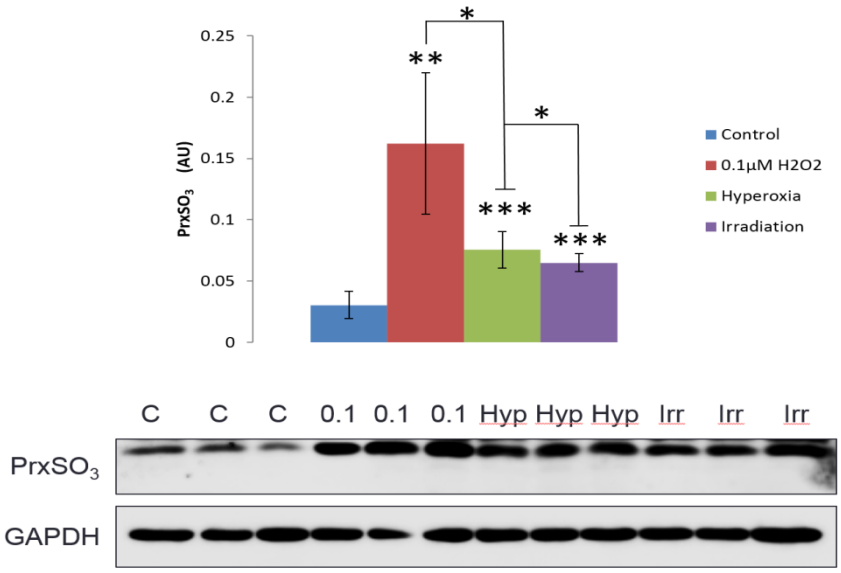

Figure 5.2. *All pre-conditionings induce peroxiredoxin hyperoxidation (N=6), C = Control, # = ssH$_2$O$_2$ production rate (µM/s), Hyp = 40% Hyperoxia, Irr = X-ray irradiation at 20G. * = p<0.05, **=p<0.01, ***=p<0.001.. Error bars = standard deviation. (AU) = Arbitrary Units.*

5.2.2 Sustained oxidative stress does not result in reduced Nrf2 activation by Urotensin II

In order to examine whether the elevated oxidant levels interfered with redox signal generation within the cells they were treated with 0.5µM of Urotensin II (UII) after they had been subjected to each stress regime. The lowest ssH$_2$O$_2$ treatment used in the 24hr pre-conditioning induced a similar level of Nrf2 activation as the UII treatment alone (Figure 5.3a). Interestingly, there was no additive effect on Nrf2 activation when cells preconditioned with higher rates of ssH$_2$O$_2$ were further treated with UII.

In stark contrast, myotubes pre-conditioned under hyperoxic conditions or irradiation displayed a statistically significant increase in Nrf2 activation after treatment with UII relative to non-preconditioned cells treated with UII (Figure 5.3b&c). For hyperoxia-conditioned cells, UII treatment caused a three-fold higher increase in Nrf2 than that induced by UII treatment alone (Figure 5.3b). This increase was four fold-higher in irradiated cells treated with UII than in non-irradiated cells treated with UII (Figure 5.3c). Note that neither hyperoxia nor irradiation induced an increase in nuclear Nrf2 levels at rest (Figure 5.5a&b). A possibility immediately arises from this data that the

longer term stress regimes of hyperoxia and irradiation may result in increased cellular levels of NADPH oxidases at rest in C2C12 myotubes, although this was not tested for.

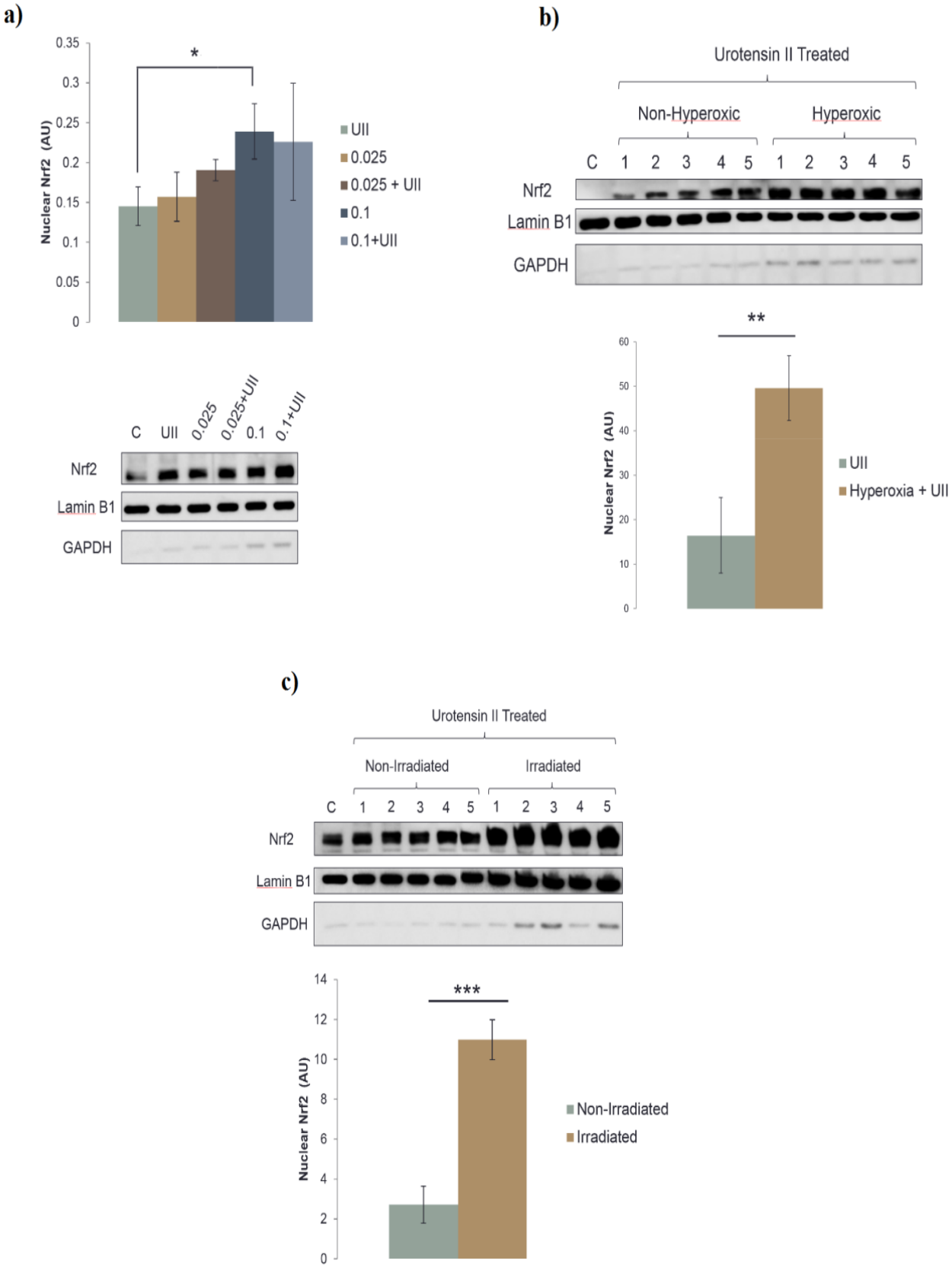

Figure 5.3. *(previous page). Nuclear Nrf2 levels in response to Urotensin II treatment.* ***a)*** *Nrf2 activation in ssH_2O_2 preconditioned cells treated with urotensin II (N=4). # = ssH_2O_2 production rate (µM/s).* ***b)*** *Nrf2 activation by urotensin II in cells subjected to Hyperoxia (N=5). # = biological repeats.* ***c)*** *Nrf2 activation by urotensin II in irradiated cells (N=5). # = biological repeats. C= Control, UII = 0.5µM urotensin II collected after 60min., * = p<0.05, **=p<0.01, ***=p<0.001. Error bars = standard deviation. (AU) = Arbitrary Units.*

5.2.3 Sustained H_2O_2 treatment, but not X-ray irradiation or hyperoxia, alters Nrf2 activation dynamics to an acute H_2O_2 stimulus

To explore whether any of the stress pre-conditionings could interfere with redox signal transduction, time course measurements were taken of nuclear Nrf2 levels after a bolus H_2O_2 treatment. Firstly, the activation magnitude of the Nrf2 response was examined in cells preconditioned at different ssH_2O_2 concentrations. Interestingly, when myotubes are pre-conditioned for 24hrs in 0.025µM/s ssH_2O_2 and a subsequent 50µM H_2O_2 bolus is added, an additive effect in Nrf2 activation is observed at the 60min time point (Figure 5.4a). This observation seems to imply that the lack of additive effect of UII treatment on Nrf2 signalling following the same preconditioning could be the result of a reduced ability of UII to trigger a redox signal under such conditions. However, when ssH_2O_2 pre-conditioning rates are increased, the additive effect gradually fades away (Figure 5.4a). This could well suggest a saturation point of the Nrf2 pathway or potentially the activation of a negative feedback loop which dampens down the response. To further confirm this observation, the same ssH_2O_2 pre-conditionings were repeated but with a subsequent doubling of the concentration of the H_2O_2 bolus to 100µM. A disappearing additive effect at higher concentrations of ssH_2O_2 was still observed (Figure 5.4b).

To further examine whether the ssH_2O_2 stress regimes could be affecting the Nrf2 response duration, time course measurements were performed following the treatment of ssH_2O_2-preconditioned cells with a 50µM H_2O_2 bolus. The only significant difference between the Nrf2 time courses obtained was a shift in the maximum peak of the response from 30min in non-preconditioned cells (Figure 5.4c) and 0.025µM/s ssH_2O_2 preconditioned cells (Figure 5.4d) to 60min in 0.1µM/s ssH_2O_2 preconditioned cells (Figure 5.4e). Otherwise, all responses were roughly half-maximal by 90min and

back to basal after 240min. The time courses generated for ssH_2O_2–preconditioned cells are lower in magnitude than those produced for non-preconditioned cells. Because no reduction in Nrf2 activation levels at the 60min time point was observed in preconditioned cells (Figure 5.4a), which is very apparent if the AU quantifications from the time courses are compared, this magnitude difference can be attributed to inter-experiment variability.

When time course measurements were performed on hyperoxic or irradiated cells treated with a subsequent 50µM H_2O_2 bolus, no difference in the Nrf2 activation profiles was observed compared to those of non-preconditioned cells (Figure 5.5a&b).

Figure 5.4 *(next page). Measuring the effect of 24hr ssH_2O_2 treatments on the magnitude and duration of Nrf2 activation by an H_2O_2 bolus.* ***a)*** *Nrf2 activation by bolus treatment on cells preconditioned at different ssH_2O_2 production rates (N=4). B=Bolus=50µM H_2O_2 collected after 60min, # = ssH_2O_2 production rate (µM/s).* ***b)*** *Nrf2 activation by a doubly concentrated bolus treatment on cells preconditioned at different ssH_2O_2 production rates (N=4). B=Bolus=100µM H_2O_2 collected after 60min, # = ssH_2O_2 production rate (µM/s).* ***c)*** *Time course of Nrf2 activation by a 50µM H_2O_2 bolus in non-preconditioned cells (N=8). # = minutes.* ***d)*** *Time course of Nrf2 activation by a 50µM H_2O_2 bolus in 0.025µM/s ssH_2O_2 preconditioned cells (N=4). 0.025 = ssH_2O_2 production rate (µM/s), # = minutes.* ***e)*** *Time course of Nrf2 activation by a 50µM H_2O_2 bolus in 0.1µM/s ssH_2O_2 preconditioned cells (N=4). 0.1 = ssH_2O_2 production rate (µM/s), # = minutes. AU= Arbitrary Units, C= Control, Error bars = standard deviation, * = $p<0.05$.*

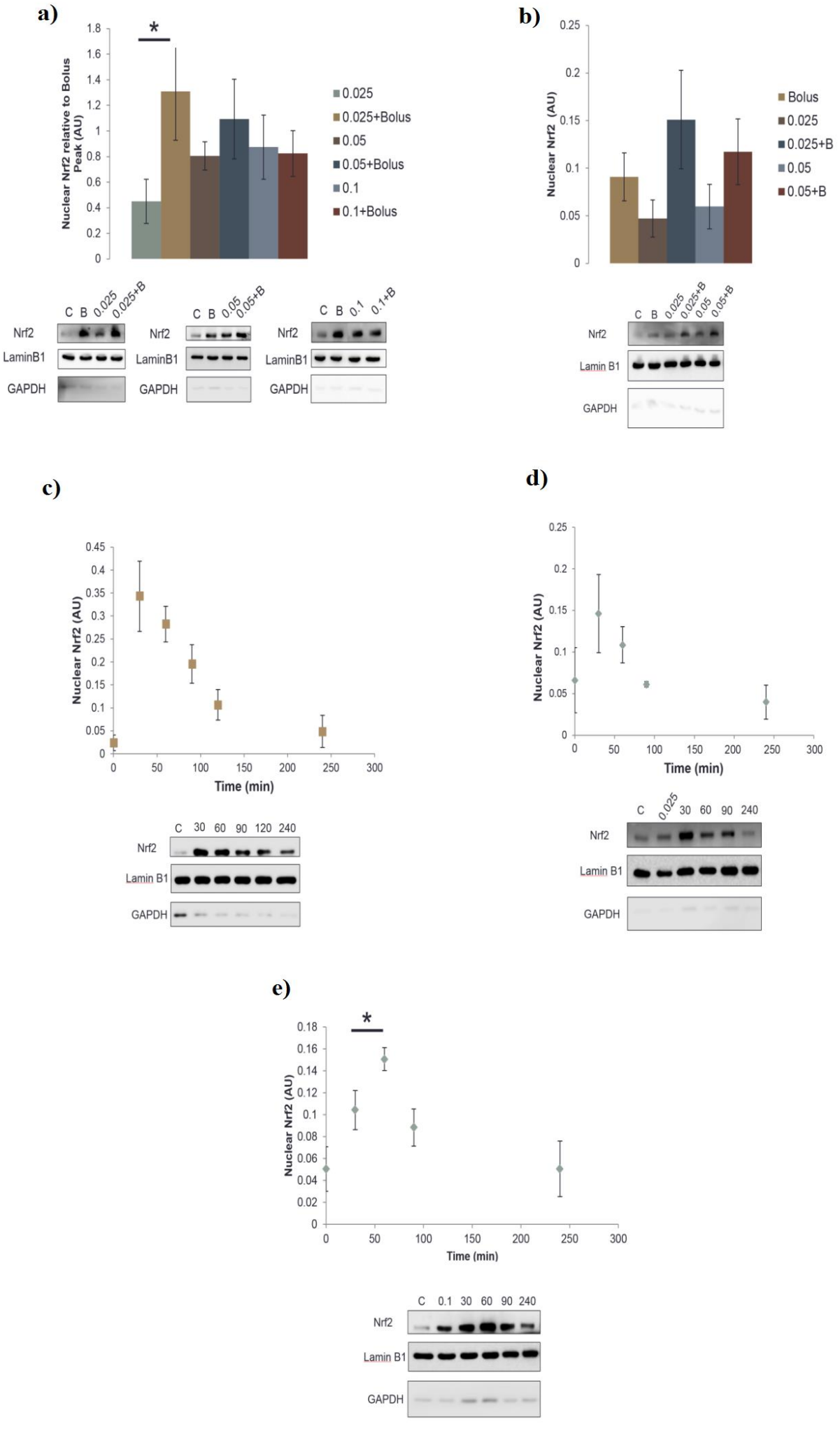
a)
Nuclear Nrf2 relative to Bolus Peak (AU)
0.025
0.025+Bolus
0.05
0.05+Bolus
0.1
0.1+Bolus
C B 0.025 0.025+B
C B 0.05 0.05+B
C B 0.1 0.1+B
Nrf2
LaminB1
GAPDH
b)
Nuclear Nrf2 (AU)
Bolus
0.025
0.025+B
0.05
0.05+B
C B 0.025 0.025+B 0.05 0.05+B
Nrf2
Lamin B1
GAPDH
c)
Nuclear Nrf2 (AU)
Time (min)
C 30 60 90 120 240
Nrf2
Lamin B1
GAPDH
d)
Nuclear Nrf2 (AU)
Time (min)
C 0.025 30 60 90 240
Nrf2
Lamin B1
GAPDH
e)
Nuclear Nrf2 (AU)
Time (min)
C 0.1 30 60 90 240
Nrf2
Lamin B1
GAPDH

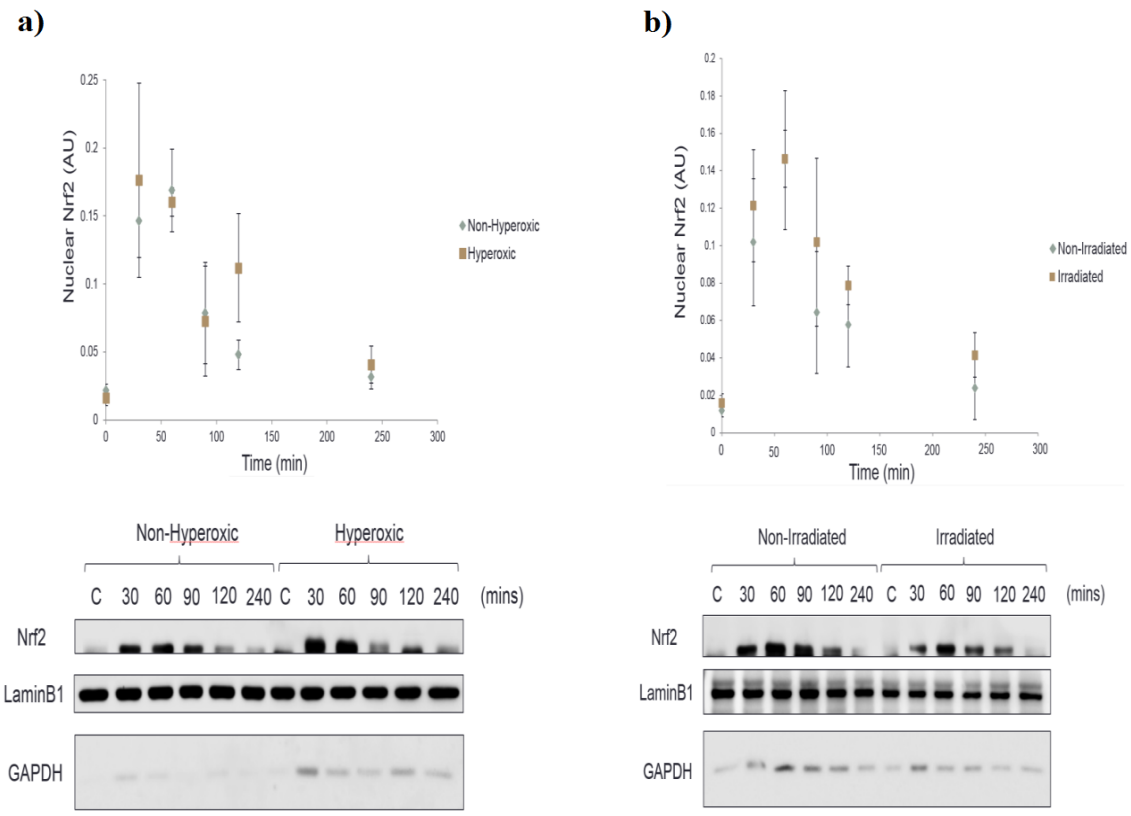

Figure 5.5. *Nrf2 activation profiles of hyperoxic and irradiated cells.* ***a)*** *Nrf2 activation profile by a 50μM H_2O_2 bolus treatment on cells cultured in hyperoxia for a week (N=4).* ***b)*** *Nrf2 activation profile by a 50μM H_2O_2 bolus treatment on irradiated cells (N=4). AU= Arbitrary Units, C= Control, error bars = standard deviation.*

5.2.4 Antioxidants could be the main negative regulators of Nrf2 activation under conditions of oxidative stress

A time course of Nrf2 activation during a 24hr steady state treatment with H_2O_2 reveals a peak in nuclear Nrf2 after 4hrs which gradually decays over the following 20hrs (Figure 5.1b). Considering the GOX/CAT system has been proven to sustain a constant H_2O_2 flux over 24hrs (Mueller et al., 2009), it is apparent that the Nrf2 system is being reset despite the ROS signal still being present in the cellular environment. The resetting of the Nrf2 signalling system to (or close to) its original state suggests the system could be displaying adaptation.

To investigate whether the basal levels of the main negative regulators of Nrf2 would remain elevated after a 24hr exposure to a steady state level of a signal, a titration

experiment was carried out with different ssH_2O_2 levels. Protein levels were measured via Reverse Protein Phase Array (RPPA) to obtain a finer resolution. The obtained results (Figure 5.6) show that a 24hr incubation with increasing concentrations of steady state hydrogen peroxide will increase the levels of both the activatory (pY216) and inhibitory (pS21/pS9) phosphorylation-modifications in GSK3β. However, the inhibitory phosphorylation in residue S9 has been shown to override the activatory effect of the Y216 phosphorylation (Bhat et al., 2000). Although the activation of Akt promotes the inhibitory phosphorylation of GSK3β (Cuadrado, 2015), there is no obvious relationship between the levels of activated Akt and the inhibitory/activatory phosphorylation group in GSK3β. This might not be entirely unexpected considering the complexity of the regulation of Akt activation by H_2O_2 at least in the C2C12 cell line (Tan et al., 2015b).

No significant change was seen in the basal levels of Keap1 after any of the 24hr treatments which is surprising when one considers the reported decrease in Keap1 half-life under oxidative conditions (Taguchi et al., 2012). Upon examination of intracellular levels of antioxidant enzymes (Figure 5.7) it is seen that upon a 24hr exposure to 0.1μM/s ssH_2O_2, C2C12 myotubes strongly upregulate intracellular protein levels of the catalase enzyme. It thus seems that the negative regulators most likely to reset the Nrf2 pathway under conditions of sustained oxidative stress are antioxidant enzymes through the scavenging of intracellular ROS molecules.

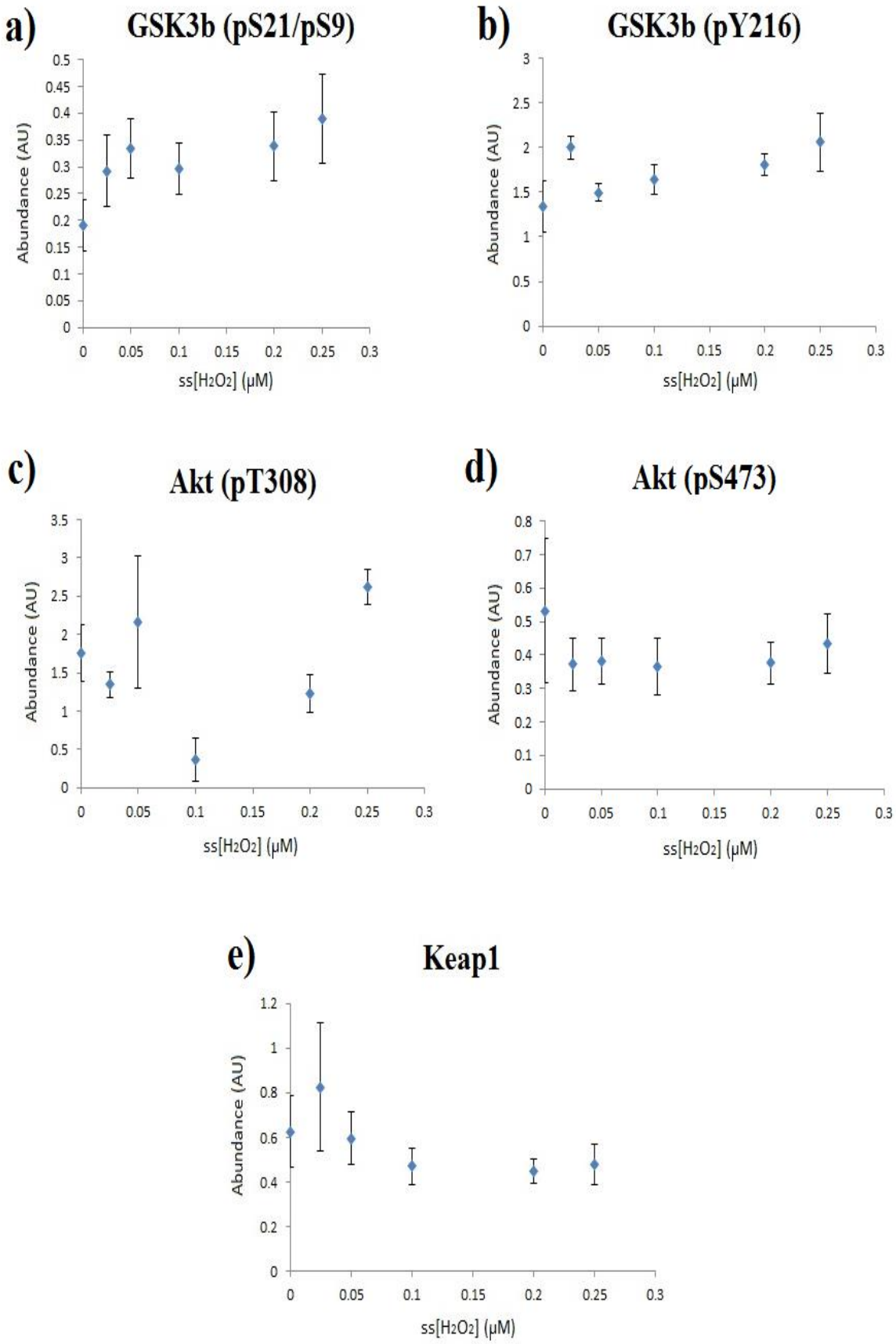

Figure 5.6. *Dose-response curves for 24hr ssH_2O_2-treated C2C12 myotube cells. (AU) = Arbitrary Units. Error bars = Standard deviation. (N=6).*

a)

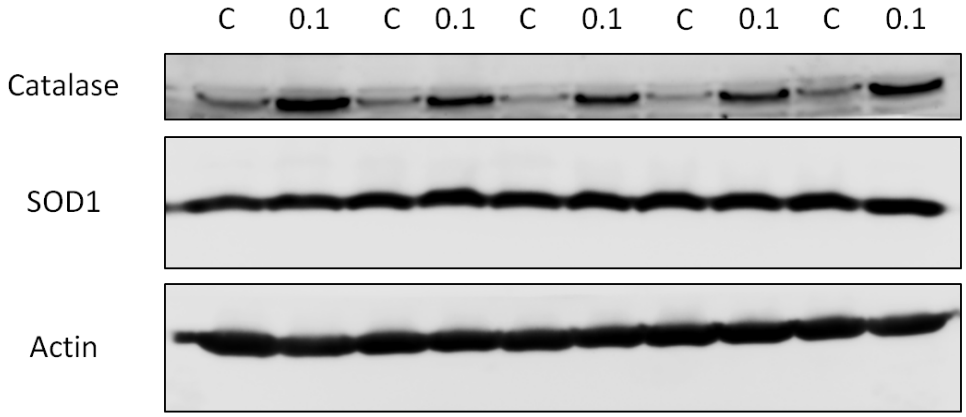

b)

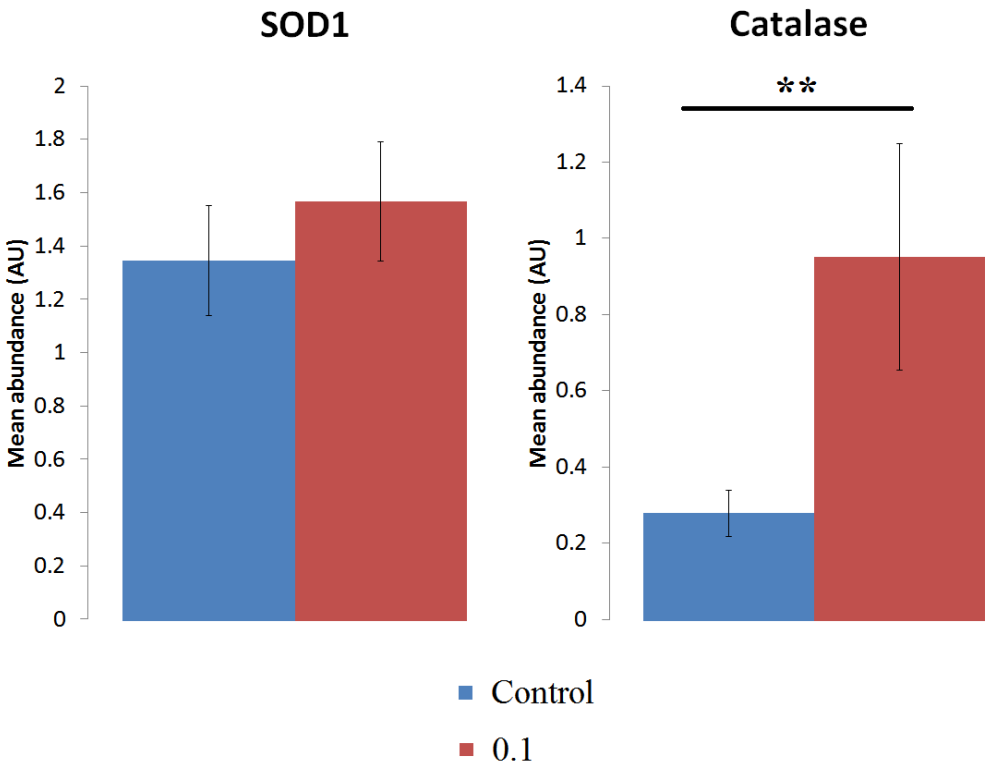

Figure 5.7. *Changes in antioxidant abundance upon a 24hr treatment with 0.1µM/s steady state (ss) H_2O_2 in C2C12 myotubes.* ***a)*** *Western blot image. C = Control. 0.1 = 24hr treatment with 0.1µM /s steady state (ss) H_2O_2.* ***b)*** *Immunoblot quantification. N=5. Error bars = Standard deviation. * = p<0.05, **=p<0.01, ***=p<0.001. AU = Arbitrary Units.*

5.3 Discussion

It is not entirely surprising that the hyperoxic and irradiation pre-conditionings did not affect the time course of Nrf2 activation (Figure 5.4). Skeletal muscle is known to have a high resistance to ionizing radiation (Jurdana et al., 2013, Hardee et al., 2014) and whilst there are very few studies involving hyperoxic incubation of skeletal muscle cells, they utilize 95% oxygen incubation for a shorter period of two days (Flandin et al., 2005, Barreiro et al., 2009). The fact that a statistically significant elevation of hyperoxidized peroxiredoxin was observed (Figure 5.2) after a week (hyperoxia regime) and 15 days (irradiation regime) indicates that cells were being successfully exposed to oxidative stress for a prolonged period of time in an attempt to more faithfully reproduce the time scale of the molecular stress present in aged skeletal muscle.

More surprising was the observation that both hyperoxia and irradiation increased the magnitude of Nrf2 activation after Urotensin II treatment (Figure 5.3). Although this observation was not further pursued, it seems likely that during the long time scales of these stress regimes, the expression of NADPH oxidases may have increased to provide for a stronger ROS signal upon activation by UII treatment (Collins-Underwood et al., 2008, Pendyala et al., 2009, Wang et al., 2017). If this observation was found to be true, it would have interesting physiological implications since NADPH-oxidase mediated signalling is an important mediator of variety of stress responses (Jiang et al., 2011).

It is difficult to infer the effect that the 24hr ssH_2O_2 preconditioning regime may be having on the activation of the Nrf2 in response to an H_2O_2 bolus addition. Initial experiments looking at the nuclear Nrf2 levels at the 60min time point reveal a response saturation pattern (Figure 5.4a). The lowest ssH_2O_2 preconditioning displays an additive effect in the levels of nuclear Nrf2 when an H_2O_2 bolus is added. As the ssH_2O_2 preconditioning concentration gradually increases however, nuclear Nrf2 levels at 60min post-stimulation do not increase beyond the Nrf2 levels triggered by the bolus alone. This pattern is also seen in the ssH_2O_2 titration (Figure 5.1) and when the H_2O_2 bolus concentration was doubled to 100µM (Figure 5.4b).

Because the nuclear Nrf2 levels at the 60min time point in ssH_2O_2 preconditioned cells never seem to go significantly below the levels triggered by a bolus alone, it can be concluded there are no indications of a blunting of the redox response under these conditions. An interesting observation is that the steady state H_2O_2 flux produced by the

GOX/CAT system results in a bolus-like profile of Nrf2 activation over the 24hr preconditioning (Figure 5.1b). There is a strong possibility that over this time period the cells are adapting to the new steady state level of intracellular oxidant by increasing antioxidant levels. This possibility is supported by the observation of a strong increase in intracellular catalase levels after a 24hr exposure to 0.1μM/s ssH_2O_2 (Figure 5.7).

Such an adaptive response would mean the apparent saturation pattern observed for Nrf2 activation could actually reflect a dampened redox response by increased antioxidant levels. This is hinted at by the fact that the bolus addition seems to have a (non-significant) decreasing activation trend in the levels of nuclear Nrf2 with higher ssH_2O_2 preconditioning concentrations (Figure 5.4a). The lack of a 'blunting' effect is in accordance with the observation of a lack of an obvious increase in the basal levels of the main negative regulators of Nrf2 (Figure 5.6). However, the Nrf2 system does seem to be reset to pre-stimulus levels even in the presence of a constant signal (Figure 5.1b). It could be that the increased expression of antioxidants is facilitating this resetting and preventing an additive response without causing a 'blunting' effect.

Having failed to observe an obvious effect of the ssH_2O_2 preconditioning on the magnitude of the Nrf2 response, time courses were performed to examine potential interferences with the response duration and the activation profile. The levels of nuclear Nrf2 at 30min relative to 60min do not reach a statistically significant difference under a stress regime of 0.025μM/s ssH_2O_2 and under no preconditioning. However, the 0.1μM/s ssH_2O_2 preconditioning does result in a statistically significant difference in the levels of nuclear Nrf2 in the 60min time point with respect to the 30min time point. This could be due to a slower response, with fewer nuclear Nrf2 at 30min compared to 60min. In any case, the nuclear Nrf2 decay from its peak seems to be happening more quickly on the 0.1μM/s ssH_2O_2 preconditioned cells.

An Nrf2 response which not only is mounted more slowly, but decays more quickly could be hinting towards some signalling abnormality in this pathway at higher levels of oxidative stress. If the activation magnitude experiments (Figure 5.4a&b) had been performed at the 30min time point instead of the 60min time point, a blunting effect may have been observed. It thus becomes a question of how the genetic programme triggered by Nrf2 is affected by both the magnitude of the response and the duration of the response. It is thus a possibility that a blunting of this redox response may be to some extent occurring within this altered time course profile of Nrf2 activation under 0.1μM/s ssH_2O_2 preconditioning. Mechanistically speaking, an adaptive response

resulting in increased antioxidant expression could explain a redox response which takes more time to mount and lasts for a lesser time.

Equally as unclear is the effect of the ssH_2O_2 preconditioning regimes on redox signal generation by urotensin II. Experiments involving an H_2O_2 bolus addition on top of 0.025µM/s ssH_2O_2 preconditioned cells (Figure 5.4a) show an additive effect, indicating the Nrf2 system has still a margin to be further activated at the 60min time point. This is also indicated by the levels of nuclear Nrf2 reached by higher ssH_2O_2 pre-conditionings (Figure 5.3a). However, no additive effect is seen when 0.025µM/s ssH_2O_2 preconditioned cells are treated with UII. Admittedly, the magnitude of Nrf2 activation after 60min caused by UII treatment is roughly half than that triggered by a bolus since it triggers the same level of nuclear Nrf2 translocation as the 0.025µM/s ssH_2O_2 preconditioning alone. If the cells adapt over the 24hr ssH_2O_2 treatment by increasing antioxidant levels, it may be a possibility that the redox signal triggered by UII treatment may not be strong enough to cause an increase in Nrf2 translocation discernible by western blotting. Another plausible possibility is that elevated H_2O_2 levels inside the cells is actively inhibiting the activation of NADPH oxidases which mediate the UII-activated signalling (Kovacic et al., 2001, Desai et al., 2014, Kovac et al., 2015).

There are a number of reasons why a reduced responsiveness in the Nrf2 pathway might not have been observed when C2C12 cells were exposed to a steady state flux of H_2O_2. As mentioned previously, this cell line is known to have a high resistance to stressors. The very use of an immortalised cell line implies that the cells used for the study are stress resistant since they are able to thrive under the non-physiological conditions of *in vitro* tissue culture.

Secondly, the exposure of cells to a steady state flux of H_2O_2 for 24hrs resulted in a three-fold increase in the intracellular catalase levels. This means that the system is responding to the constitutive signal by reducing the levels of the signal itself. This would be predicted to substantially alleviate any underlying blunted response that could arise. Looking at the standard deviations of the data obtained through immunoblotting it is necessary to consider what magnitudes of loss in system responsiveness would be necessary to occur in order to be able to be confidently discerned using this experimental technique. The observed resetting of the Nrf2 system under conditions of a constant ROS flux indicates that this pathway could be capable of perfect adaptation.

Another possibility could be that the redox signal is not being properly elicited in aged tissues as has been shown in skeletal muscle (Palomero et al., 2013).

5.4 Concluding remarks

None of the presented data conclusively demonstrates that oxidative stress mechanistically interferes with redox signalling through the Nrf2/Keap1 pathway. Indeed, a lot of molecular changes are likely to be occurring over the large time periods of the adopted oxidative stress regimes. This means a very substantial amount of work would be required to dissect the reasons behind the observed changes in the Nrf2 activation profile in response to a bolus upon a 0.1μM/s ssH_2O_2 preconditioning regime and the lack of an additive effect on ssH_2O_2 preconditioned cells by Urotensin II treatment. Rather, this work provides hints as to the nature of a potential interference of elevated oxidant levels with redox signalling. It is evident that there are statistically insignificant trends in our data such as the decreased nuclear Nrf2 levels in ssH_2O_2 plus bolus combined treatments (Figure 5.4a). Increasing the number of repeats should help discern whether these patterns have an underlying physiological importance. This work seems to provide the first evidence of the ability of the Nrf2 pathway to undergo near-perfect adaptation and thus potentially be able to sense fold-changes in ROS rather than absolute levels. It seems of particular interest the possibility that chronically elevated levels of oxidant in aged skeletal muscle might be actively inhibiting redox signal production by NADPH oxidases during a period of exercise.

Chapter 6

Testing the multi-scale robustness of biological systems to constitutive signals: A case study on cellular senescence

6.1 Introduction

Living organisms have evolved a wide range of mechanisms to maintain a tight homeostatic control over their internal environment. Negative regulators operate at different levels of biological organisation to maintain a desired homeostatic state. This includes negative regulation at the molecular level, cellular level and organ level. This multi-scale cybernetic property of living organisms makes them robust to perturbations, allowing them to maintain function in a wide range of suboptimal environments. A question then arises regarding whether any potential effects of a perturbation at the molecular level in the form of a constitutive signal can be buffered by regulatory interactions at a higher level of biological organisation i.e. cell to cell. Agent-based simulations (Section 3.3.5) have indicated that populations can be stabilised by a constitutive input in the environment. However such agent-based model is an abstract toy model with arbitrarily-assigned parameters and is therefore hardly relatable to a biological process.

The progression of cellular senescence is an example of a biological process relevant to ageing which is regulated across levels of biological organization. At the molecular level, cells will enter a senescent state if an environmental stress causes unresolvable DNA damage (Lujambio, 2016). If a ROS-mediated positive feedback loop is triggered, the senescent state can be stabilised (Passos et al., 2010). Defective mitochondria, the main source of senescence-inducing ROS, are kept in check by mitophagy. At the cellular level, a senescent cell can be recognised and destroyed by the immune cells, but also induce neighbouring cells to become senescence in a bystander-effect (Lujambio, 2016). The fact that the maintenance of senescence homeostasis involves regulatory layers at different levels of biological organisation signifies that such regulatory processes also occur at different time scales. It is thus difficult to keep track of the interplay of these processes experimentally.

Multi-scale computational models have been able to capture such level of complexity in a number of biological settings including tumour growth (Wang et al., 2015), plant development (Muraro et al., 2016), bone remodelling (Colloca et al., 2014) and heart function (Quarteroni et al., 2017). The development of a multi-scale model commonly involves the use of separate computational frameworks to model different levels of biological organisation which are then coupled together through formal methodologies (Dada and Mendes, 2011).

The theoretical work undertaken seems to suggest that constitutive signals are likely to promote network dysfunctionality at the molecular scale. However, quality-control mechanisms span levels of biological organisation. This means that there may be mechanisms at the cellular level that can compensate against the presence of constitutive signals driving a loss in homeostasis. To explore the extent to which constitutive signals like stress can drive a loss of homeostasis when considering different levels of biological organisation, a multi-scale model of a tissue undergoing cellular senescence was formalised. The aim of such a model would be to provide an exploratory platform to observe how system homeostasis may be perturbed by constitutive signals when regulation spans multiple levels of biological organisation. This is most likely to represent a more realistic view of how the ageing process might occur *in vivo*. To understand whether constitutive signals can result in the stabilisation of a senescent cell population within a tissue a multi-scale model of cellular senescence progression was developed. In this biological scenario, the constitutive signal feeding into the system will be stress.

6.2 Results

6.2.1 Understanding stochastic damage as the stochastic occurrence of runaway processes

The first issue encountered when formalising such multi-scale model is that ‘stress’ is a too abstract term. Of relevance to the ageing context, senescence is induced when environmental stress translates into stochastic damage. But how to model stochastic damage? If one is interested in a significant homeostatic disruption within the cell as a result of stochastic damage, the following rationale can be developed.

Let's consider a regulated molecular entity which could be a damaging agent or an activator molecule (*A*). Such a species will be actively degraded or inhibited by a protective or regulatory entity (*N*) to maintain a low-level homeostatic state of molecule *A*. The effective regulation of *A* is ensured by a much higher abundance of *N*. This is because effective regulation requires that entity *N* encounters entity *A* in three dimensional space through random motion and so a higher abundance of the negative regulator ensures more of the search space is covered at a given time. The robustness of biological systems to external perturbations suggests that a collapse of a homeostatic state by a stochastic event requires a failure in the regulatory mechanisms so that *i)* Entity *N* becomes less effective or *ii) A* escapes or overrides *N*.

Stochastic genetic mutations that result in changes to the binding affinity between *N* and *A* would satisfy both scenarios. Beyond genetic mutations as the sole explanation of homeostatic failure, *A* could be able to override the action of *N* should it have the ability to trigger a runaway process. In such a case, the homeostatic maintenance relies on the effectiveness of *N* in counteracting the self-amplifying property of *A*. Biological examples of such positive feedback loops include ROS-induced ROS generation (Passos et al., 2010, Zorov et al., 2014), chain reactions of free radical molecules with lipids (Pratt et al., 2011), protein aggregation processes (Holmes and Diamond, 2012), calcium-induced calcium release (Endo, 2009) and other molecules which participate in positive feedback loops for the purpose of robust signalling within cells (Mitrophanov and Groisman, 2008). Such biological entities are tightly regulated by protective molecules or negative regulators such as antioxidants, protein degradation machinery, calcium pumps or others.

At any given point, it is expected that the negative regulator is performing its function effectively, as it has evolved to. However, does the self-sustaining structure of the positive feedback provide a means for a regulatory-overriding albeit with a low probability? Does this regulatory structure provide an intrinsic reliability limit? To begin to explore the answers to such questions the interplay between a self-amplifying property that promotes accumulation and a counteracting negative regulation activity must be further formalised into a computational model. Entities *A* and *N* can be modelled as equal-sized molecules undergoing Brownian motion in three dimensional finite space. A simple molecular dynamics simulation based on a cellular automaton framework is used to model this system (Figure 6.1a).

Entities N are modelled as perfect negative regulators, meaning that upon encounter of entities A and N in space, entity A will disappear with a probability of one. In this setting, the effectiveness of negative regulation by entity N is limited by its abundance. Amongst the most abundant negative regulators operating within cells are antioxidant proteins limiting the intracellular levels of ROS molecules. Their abundance can thus be used as working value for the simulated number of N entities. The combined abundance of the main antioxidant proteins operating in mammalian cells derived from the PaxDB database (Wang et al., 2012a) yields a value of approximately 31000ppm. This value combines the abundance of all the peroxiredoxin isoforms, catalase and SOD1 and translates into a 3% percentage occupancy of the cellular space simulated in the model. The derivation of such a proxy value is in the scale indicated by abundance measurements for the peroxiredoxin 1 isoform, which reportedly accounts for 0.1-1% of the total soluble protein in the cell (Perkins et al., 2015).

Model simulation settings were configured to a 5% occupancy of N entities, with no A entities at the start of the simulation. The production of entities A is modelled by the random introduction of a single entity with a probability of 0.1 every generation. The self-amplifying ability of the A entities was formalised as a reaction $A + A \rightarrow 4A$ occurring with a probability of 0.5 upon the encounter of the two substrates in space. 1000 generations were run for 1000 cells.

The simulated profiles indicate that for a small percentage of the cells, entity A is able to override its negative regulation by entity N and cause a runaway-process that stabilises a new steady state level of the entity (Figure 6.1b). This indicates that the uncertainty arising from the encounter of molecules in space can potentially be sufficient for negative regulation to be overridden by a self-amplifying process. Following this, should both entities be segregated in space, the regulation of runaway processes would be more ineffective, with a greater percentage of cells experiencing such dysregulations. Intracellular overcrowding has been proved to be able to promote reactant segregation through volume exclusion (Schnell and Turner, 2004). Intracellular overcrowding will thus promote a spatial heterogeneity in the distribution of molecules where reactants may be transiently shielded. Such an effect could insulate the initialising steps of a runaway process so that it is more difficult to abolish by a negative regulator. When overcrowding molecules are introduced into the simulation as equal-sized molecules serving the sole purpose of providing a source of molecular collisions, there is a clear increase in the occurrence of runaway events (Figure 6.1c).

The fact that entity *N* is modelled as a perfect regulator highlights the ability to encounter regulatory targets in space as a limiting factor for system reliability. This observation is especially relevant to regulatory entities which are large macromolecules, such as SOD or catalase, which will have slow diffusion speeds and their movement will be heavily influenced by intracellular overcrowding (Papadopoulos et al., 2000). It could thus be speculated that some antioxidant proteins may have evolved to such high abundances in biological systems to retain an effective space-search for their substrates despite having hindered diffusion. It is of interest to note that the simulated profiles shown in Figure 6.1 show close resemblance to the simulated stochastic appearance of β-amyloid plaques during the progression of Alzheimer's Disease (Proctor et al., 2012). This model will hereafter be referred to as the 'runaway' model.

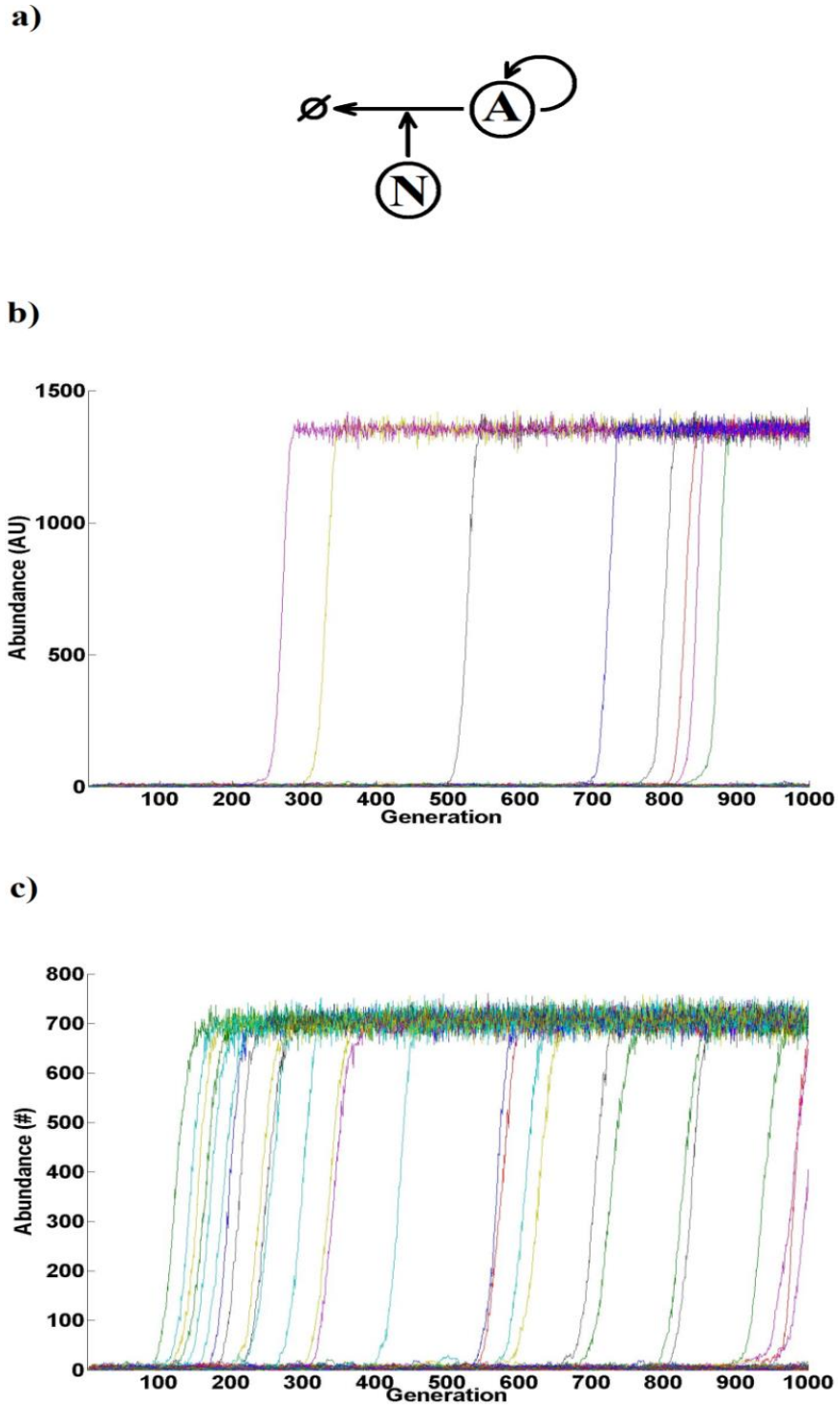

Figure 6.1. *Molecular dynamics simulation of the inhibition of a runaway process.* ***a)*** *Diagram representing the negative regulation of a self-amplifying molecule A by molecule N.* ***b)*** *Abundance of A molecules for 1000 simulations of 1000 molecular movements in the absence of overcrowding molecules.* ***c)*** *Abundance of A molecules for 1000 simulations of 1000 molecular movements in the presence of a 50% occupancy of overcrowding molecules. Dashed circle = degraded. Simulations run at 5% percentage occupancy with initial abundances A=0 and N=100.*

6.2.2 Senescence-induced-senescence can be estimated to occur with a high probability within cell populations

Having defined a toy model that represents molecular damage arising as a result of a stochastic homeostatic perturbation, it is necessary to establish a computational framework to simulate a cell population within an arbitrary tissue. A cellular automaton framework can be employed to this end where cells at rest can transition between different states, i.e. resting, pre-senescent, senescence or empty space, with different probabilities (Figure 6.2). However, such probabilities must be derived. The probability of senescence induction P_{ind} can be derived from the stochastic simulation of the experimentally-calibrated model of irradiation-induced senescence developed by Dalle Pezze *et al.* (Dalle Pezze et al., 2014). This model captures the molecular changes that occur during the progression of cellular senescence and is calibrated on data derived from human MRC5 fibroblast cells grown as a monolayer *in vitro* and x-ray irradiated at 20G. The stochastic simulation of such model reveals that not all cells will follow the molecular progression displayed on average by the population (Figure 6.3).

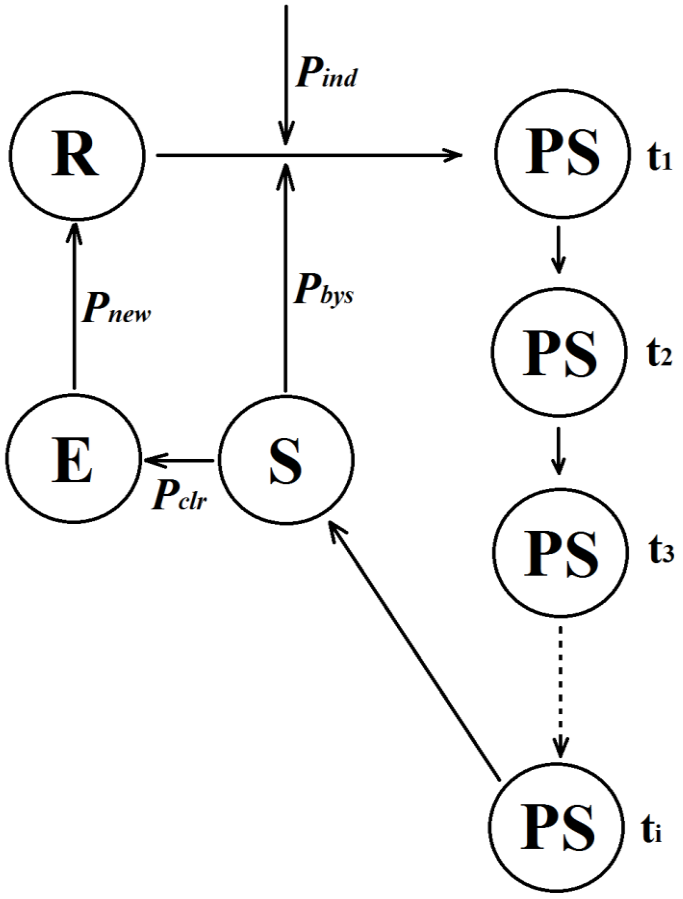

Figure 6.2.*(previous page) State transitions in the cellular automaton model of senescence progression within a tissue. R= Resting, PS=Pre- Senescence, S= Senescence, E=Empty, t=time (days),* P_{ind}*= Probability of senescence induction,* P_{bys}*= Probability of bystander effect,* P_{clr}*=Probability of clearance,* P_{new}*= Probability of new cell appearing in the tissue. Model simulation involves a grid with 10 arbitrary units in any dimension simulated (*10^3 *cells in a 3D model and* 10^2 *cells in a 2D model). The arguably low number of cells simulated aims to represent an arbitrary section of an arbitrary tissue and was limited by computational time. The simulation time of the multi-scale model was approximately 1.2 days in the case of a 30 day simulation of irradiation-induced senescence and approximately 3.9 days in case of a 30 day stochastic-induced senescence.*

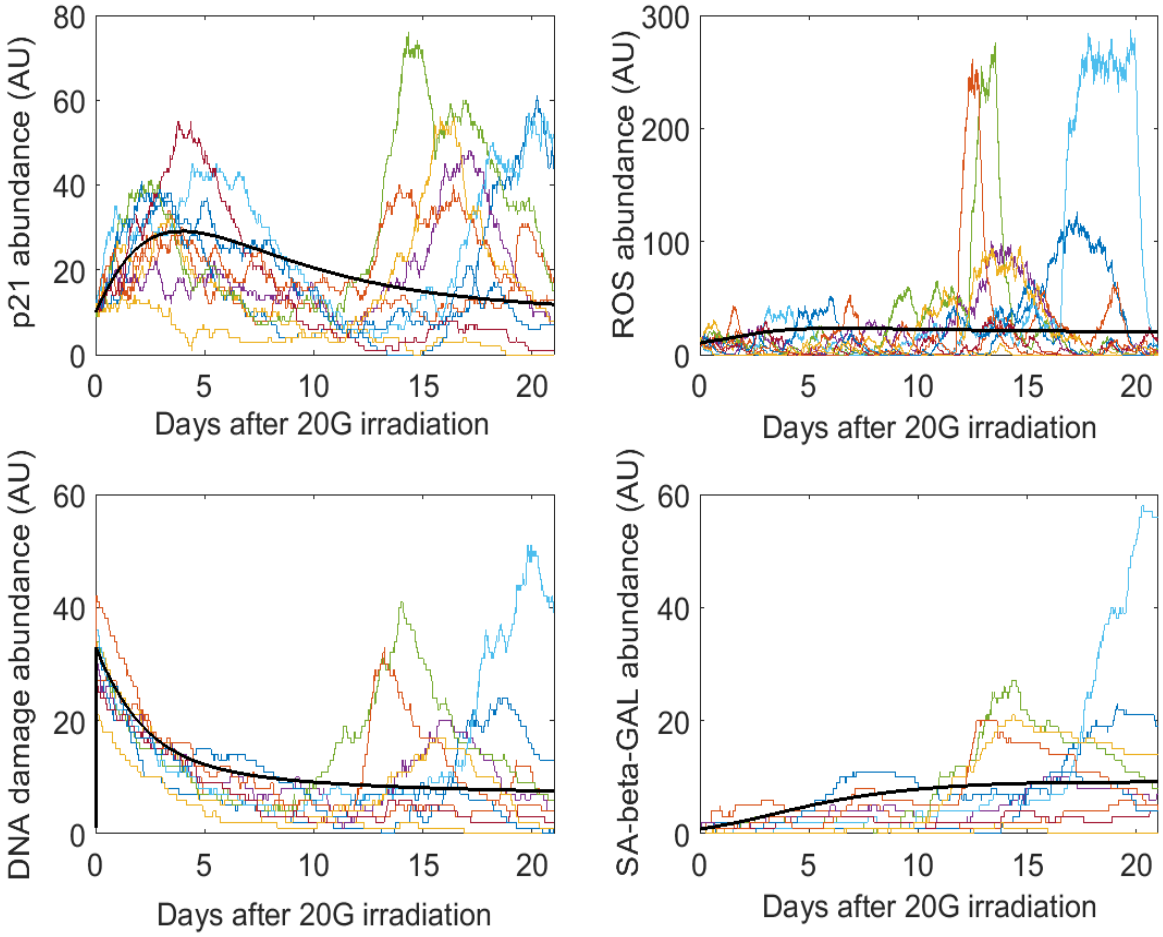

Figure 6.3. *Simulation of the Dalle Pezze et al. model of irradiation-induced cellular senescence. Individual stochastic runs (N=10) for four representative molecules are displayed as different-coloured trajectories with the deterministic simulation being overlaid in black.*

Whether a cell becomes senescent or not is a binary outcome requiring an arbitrary threshold. Such a threshold was defined as being the average molecular abundance for four molecular markers of senescence, namely, p21, DNA damage foci, SA-β-GAL and ROS. Should a single stochastic simulation result in time course profile where all four molecules display above-average levels at the 21 day time-point, the cell will be classed as having entered a senescent state. Stochastic runs of the Dalle Pezze model indicate that under such definition of a senescent state, 20G irradiation will result in a P_{ind} of ~0.12 (Figure 6.4). The stochastic running of the Dalle Pezze model was embedded into the cellular automaton framework so that at day 1 of the simulation, all cells are irradiated (i.e. undergo a single stochastic simulation of the Dalle Pezze model) and

those that meet the senescence threshold transition into a pre-senescent state within the cellular automaton grid. Note that apoptosis was not included as a potential transition state resulting from 20G X-ray irradiation since such a treatment does not induce a measurable increase in apoptotic levels in MRC5 cells (Bluwstein et al., 2013, Dalle Pezze et al., 2014).

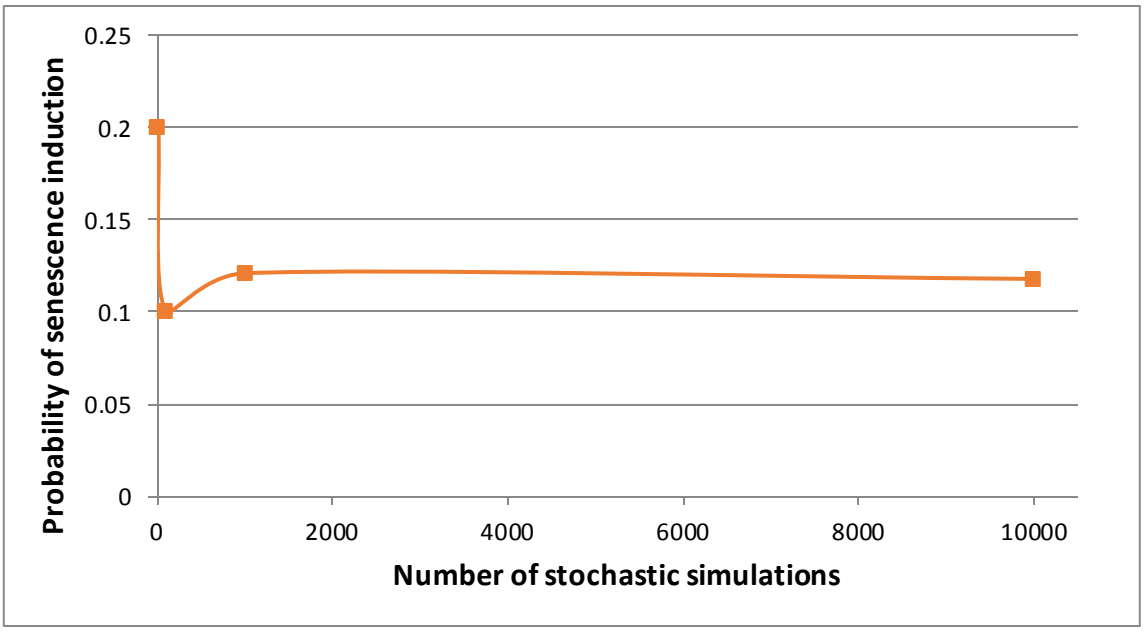

Figure 6.4. *Stochastic convergence of the Dalle Pezze et al model to the probability of senescence induction.*

It is next necessary to derive the probability of senescence-induced-senescence P_{bys}. This can be achieved through an exercise of parameter estimation using data derived from Passos *et al.* (Passos et al., 2010) on the time course of percentage senescence cells in 20G X-irradiated human MRC5 cells (Supplementary Figure 1A in Passos *et al* 2010). Not only is data obtained under identical conditions to that used to calibrate the Dalle Pezze model, but because it is performed *in vitro*, the computational model can be run as a 2D monolayer with parameters for the immune clearing of senescence cells P_{clr} and the renewal of the tissue P_{new} being set to zero. Under these conditions a scan can be undertaken for different values of P_{bys} to search for a value that minimises the discordance between the simulated data and the experimental data as quantified by the chi-squared metric. Such a parameter estimation yields multiple *minima* where different values of P_{bys} will give very similar best fits to the experimental data (Figure 6.5a).

Simulations with the derived best-fitting values for P_{bys} fail to capture the short-term dynamics of senescence induction in the population of cells. This is most likely due to the stringent definition of senescence adopted in our model as opposed to the sole requisite of SA-β-GAL staining in the experimental data. Running the irradiation simulations in a 3D cell grid gave a faster change in cellular populations than when the model was simulated for a 2D monolayer (Figure 6.6) with the same parameter set. This is expected since the bystander effect caused by senescent cells has more neighbours to act upon in a three-dimensional tissue. Interestingly, the 2D model displayed an oscillatory transition which was not displayed by the 3D model.

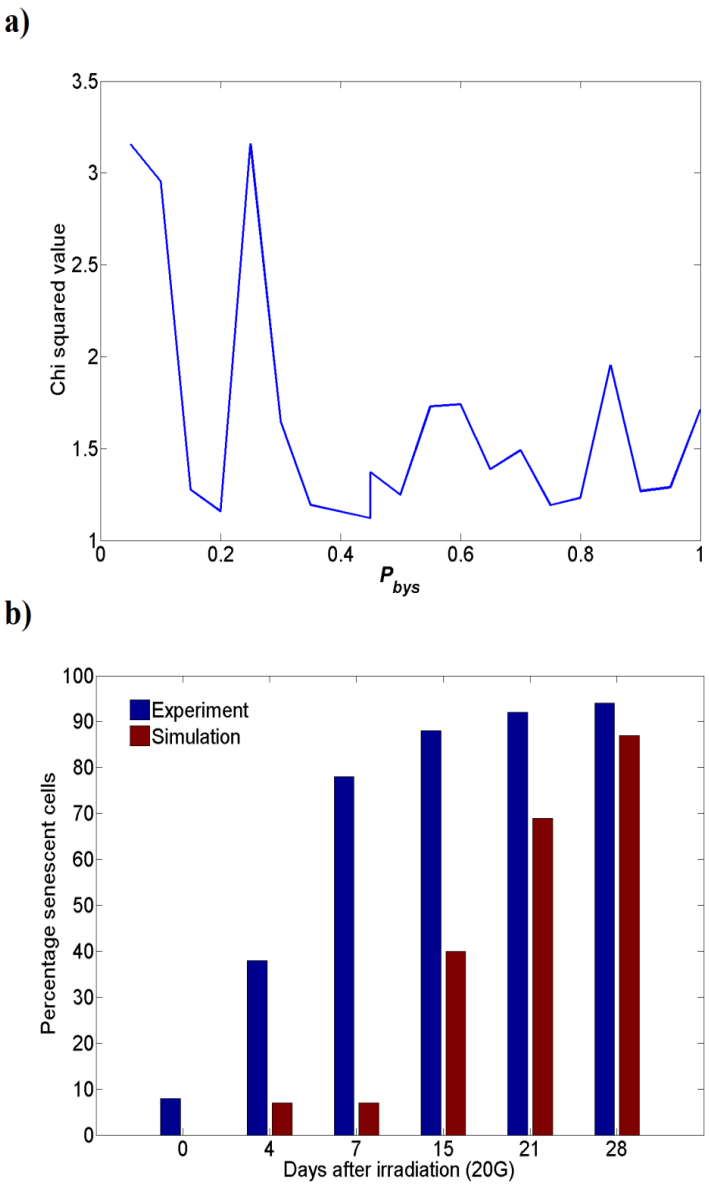

Figure 6.5. *P_{bys} parameter fitting to experimental data derived from Passos et al. (2010).* ***a)*** *Parameter fitting landscape for P_{bys}.* ***b)*** *Best-fitting time course for the number of senescence cells after irradiation. Simulated populations were derived from a P_{bys} value of 0.4 for a simulated 10 x 10 grid of cells.*

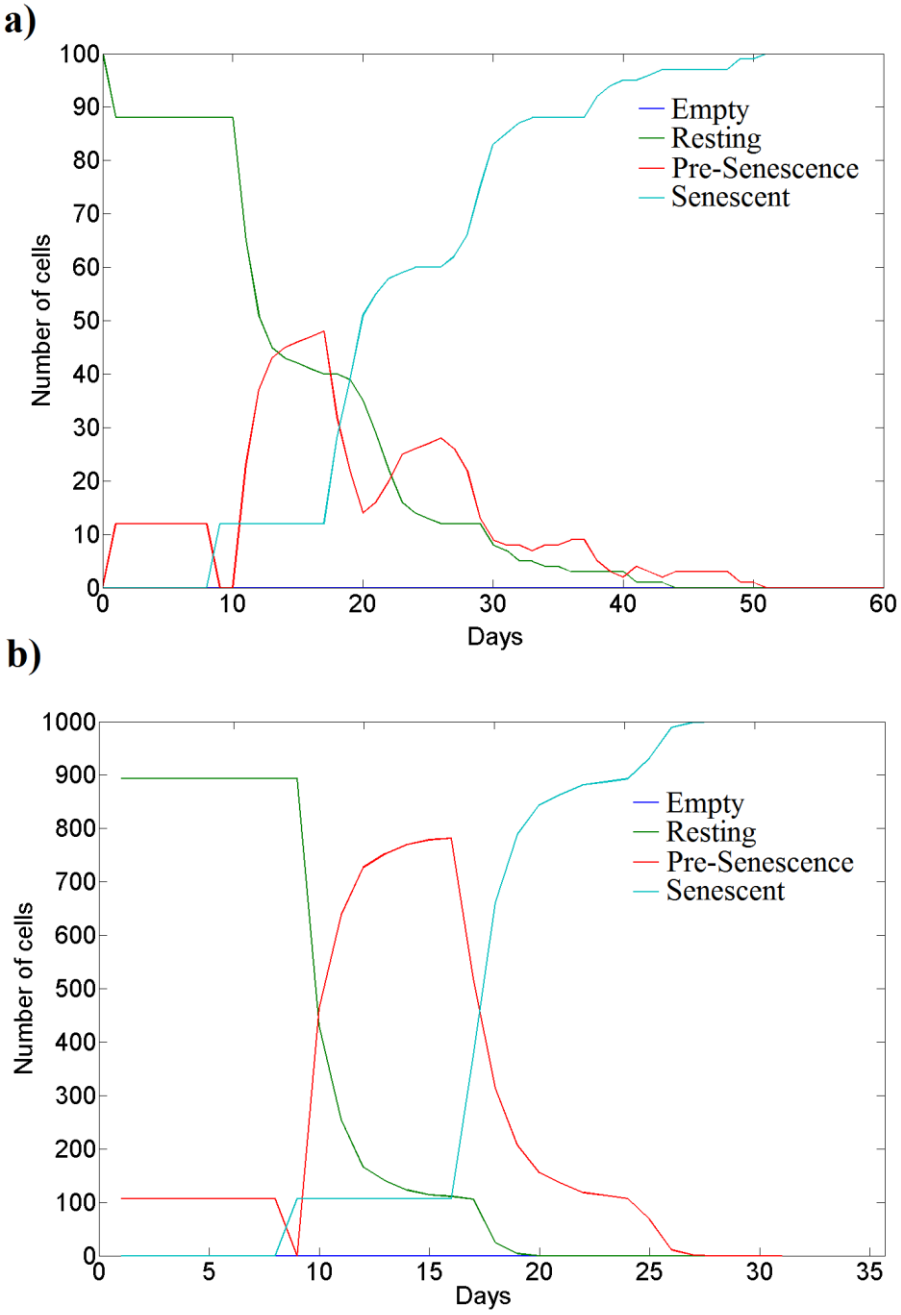

Figure 6.6. *Simulation of the cellular automaton model of irradiation-induced senescence as* ***a)*** *a 10x10 two-dimensional cellular monolayer and* ***b)*** *a 10x10x10 three-dimensional cellular grid.* $P_{bys} = 0.4$.

Hints as to the possible values of P_{bys} can be obtained by attempting to obtain an estimate for P_{clr} from the literature. Data obtained from the *in vitro* co-culture of senescent cells with natural killer cells at a 1:10 ratio suggest an upper value of 40% cytotoxicity of the immune system for the senescent cells (Krizhanovsky et al., 2008). When considering that senescent cells are rare in the tissues of young individuals it seems likely that arising senescent cells are effectively cleared by the immune system before they induce any spreading of senescence across the tissue. It can thus be assumed that $P_{bys} \leq P_{clr}$ under fully functional physiological conditions. A gradual increase in P_{ind}/P_{bys} and/or a decrease in P_{clr} could be envisioned to drive the observed accumulation of the senescent population with age. With a working value of 0.4 for P_{clr}, the potential values for P_{bys} are thus constrained to ~0.2 or ~0.4. Work published by Nelson *et al* (Nelson et al., 2012) shows that the 1:1 co-culture of senescent and non-senescent MRC5 cells resulted in an ~10% increase in the number of senescent cells (as assessed by SA-β-Gal staining) after 20 days, suggesting a P_{bys} value within the lower range of our estimates. Even the lowest estimation for P_{bys} seems high when considering it is the probability of a positive feedback loop, (i.e. a potential runaway process) being activated by strong cellular damage.

6.2.3 A decline in immune function may be the main driver of senescent cell accumulation in tissues during ageing

With the established parameter set, the value for P_{new} was assigned to 0.5 to maximise tissue renewal uncertainty at any given time point. Since large-scale senescent-cell clearance does not result in tissue atrophy (Baker et al., 2011), it is expected that cleared senescent cells can be effectively replaced by new non-senescent cells even at old age. In order to make the senescence model more relevant to physiological ageing, the 'runaway' process simulation (Figure 6.7) was embedded into the multiscale model so that the occurrence of a runaway process would cause the molecular damage equivalent to an irradiation treatment (and so would trigger a single stochastic simulation of the Dalle Pezze model with the same threshold for senescence progression). Thus, the 3D multiscale model was simulated so that any given cell could enter senescence stochastically at any time point in the simulation. The simulated profiles for stochastic-induced senescence reach the same steady-state populations as those of simulated irradiation-induced senescence even for different values of P_{bys} (Figure 6.8). For

simulations of irradiation-induced senescence it can be seen that the initial irradiation treatment results in ~10% of cells entering senescence, but this proportion of the cellular population is enough to eventually drive the whole population into senescence.

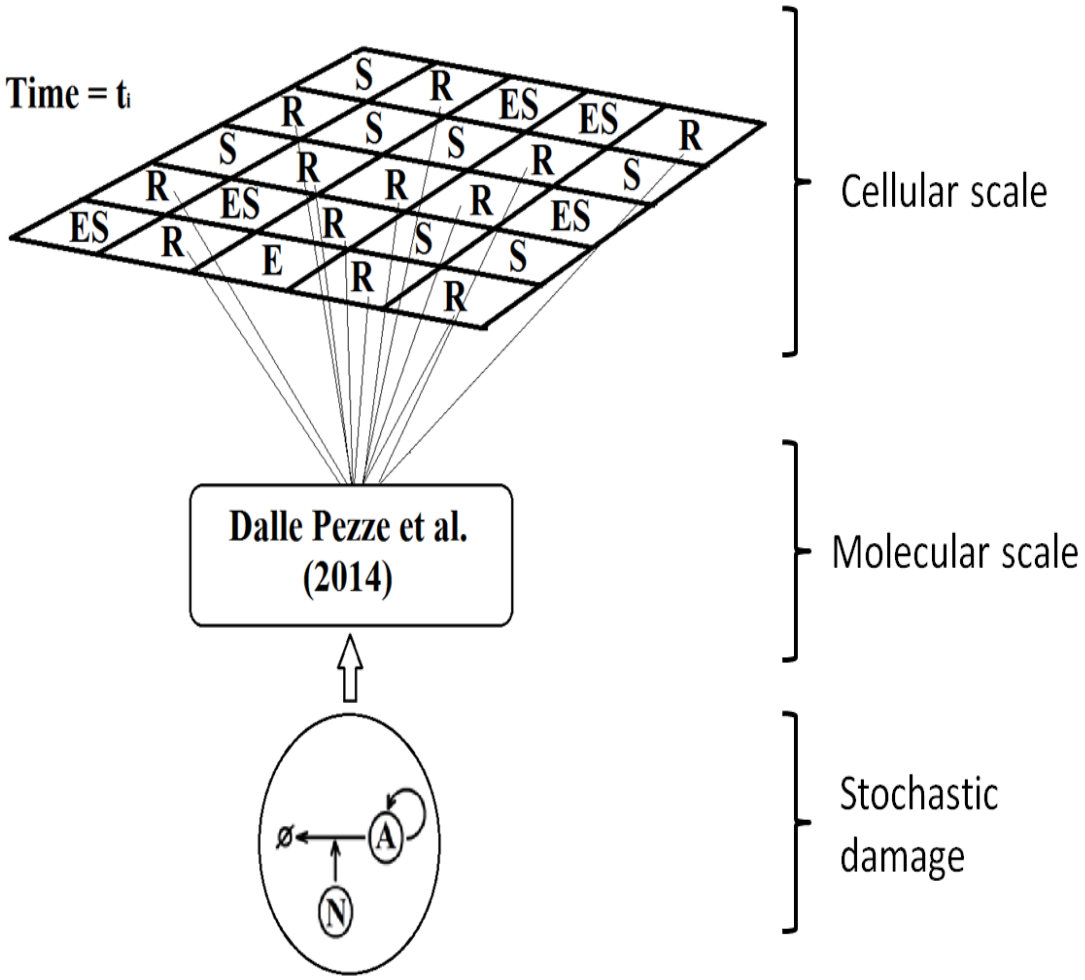

Figure 6.7. *Diagram of the multi-scale model of senescence induction by stochastic damage.*

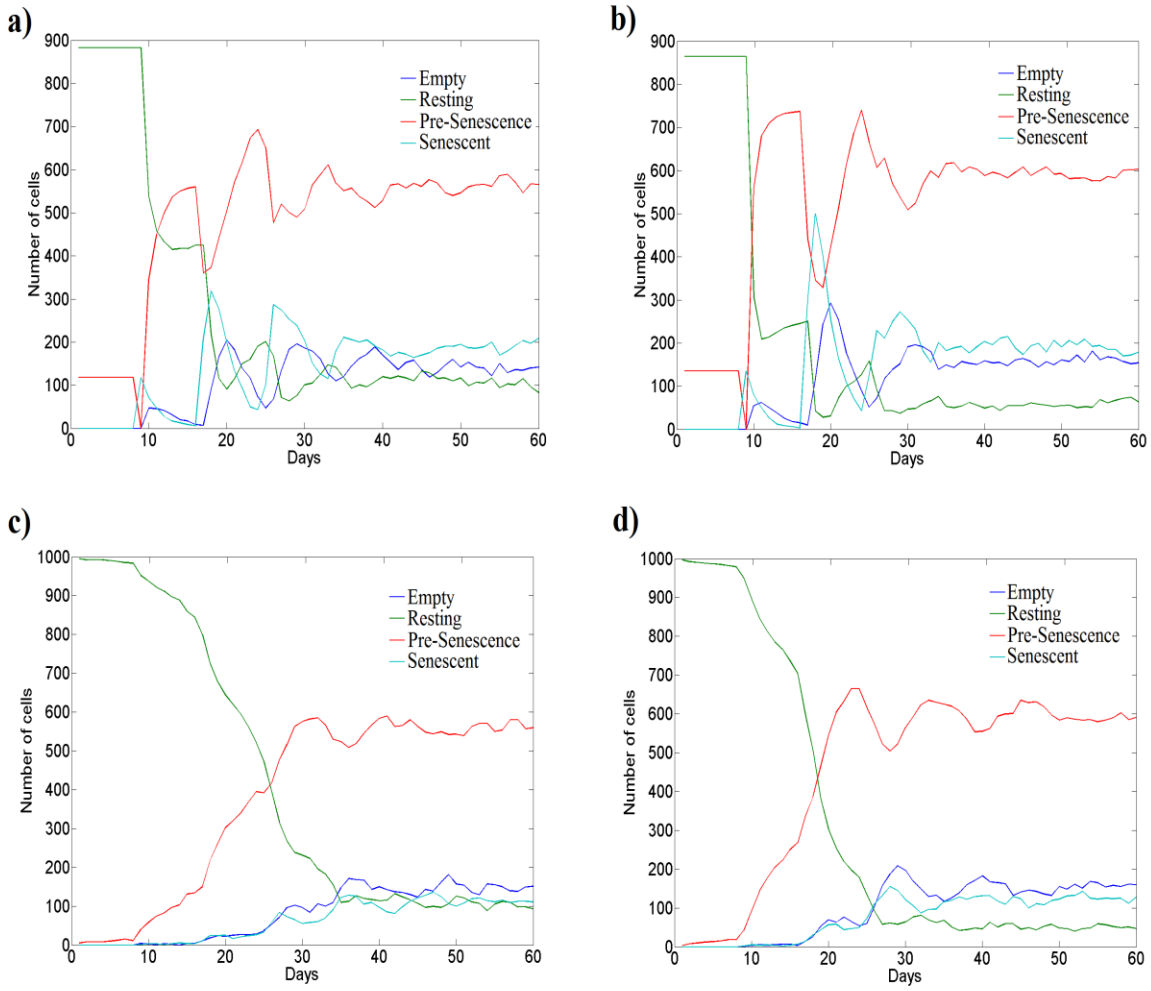

Figure 6.8. *Population dynamics of irradiation-induced senescence and stochastic senescence entry.* ***a)*** *Irradiation-induced senescence in a 10x10x10 three dimensional grid of resting cells simulated at a P_{bys} value of 0.2.* ***b)*** *Irradiation-induced senescence in a 10x10x10 three dimensional grid of resting cells simulated at a P_{bys} value of 0.4.* ***c)*** *Stochastic entry into senescence in a 10x10x10 three dimensional grid of resting cells simulated at a P_{bys} value of 0.2.* ***d)*** *Stochastic entry into senescence in a 10x10x10 three dimensional grid of resting cells simulated at a P_{bys} value of 0.4. Parameter values for all simulations are P_{clr} = 0.4, P_{new} =0.5 and P_{ind} corresponds to a single stochastic run of the Dalle Pezze et al model.*

During the ageing process, where senescent cells are known to accumulate within tissues, the immune system function is also known to decline. This could translate into a lower value for P_{clr}. Simulations of irradiation-induced senescence and stochastic senescence at a P_{clr} value of 0.1 show a higher steady state population of senescent cells arises in the 3D tissue (Figure 6.9). This is suggestive that P_{clr} bears more weight in establishing the steady state levels of senescent cells than P_{bys}.

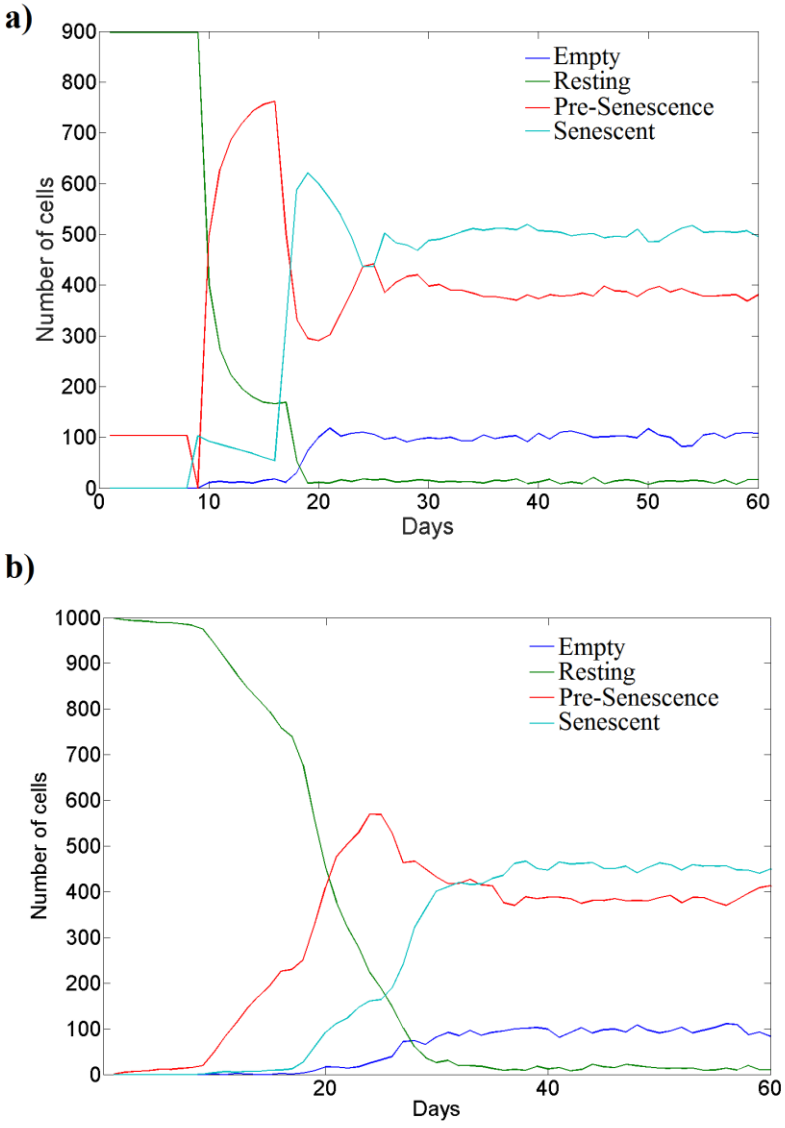

Figure 6.9. *Simulation of senescence induction in a tissue with a less effective immune system.* ***a)*** *Simulation of irradiation-induced senescence in a 10x10x10 three dimensional grid of cells.* ***b)*** *Simulation of stochastic senescence-entry in a 10x10x10 three dimensional grid of cells. Parameter values for both simulations are* P_{bys}*=0.4,* P_{clr}*=0.1,* P_{new}*=0.5 and* P_{ind} *corresponds to a single stochastic run of the Dalle Pezze et al model.*

To formally establish this observation in the adopted model topology for intercellular interactions, the model structure was translated into an ODE-framework simulated in COPASI where probability values where used as rate constants to maintain relative fluxes. Simulations of such deterministic model follow similar transition dynamics and steady state population values as the multi-scale model simulations (Figure 6.10). Parameter scans for the state transition values confirm P_{clr} as the main determinant of the senescent cell population, with P_{bys} not affecting the senescence cell attractor for multiple values of P_{clr} or P_{new} (Figure 6.11). Interestingly, altering P_{ind} in conjunction to P_{bys} did not result in a change in the attractor state for the senescent population.

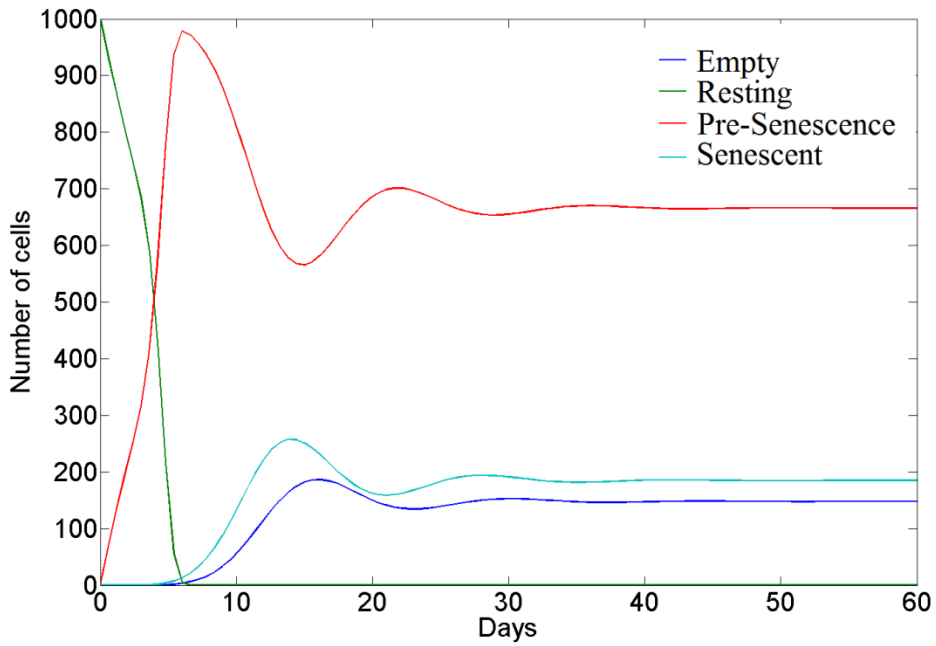

Figure 6.10. *Deterministic simulation profile of the intercellular interaction model (depicted in Figure 6.2). All reactions follow first order mass action kinetics except for that modelling the bystander effect, which follows second order kinetics. Rate constant values correspond to* $K_{ind} = 0.12$, $K_{clr}=0.4$, $K_{bys}=0.4$, $K_{new}=0.5$ *and* $K_{trans}=1$ *where the latter parameter corresponds to the transition rate from* $PS_{t=i}$ *to* $PS_{t=i+1}$.

Figure 6.11. *(Next page). Parameter scan effects on the attractor state of senescent cell populations.* ***a)*** *Deterministic simulation output of a three interval parameter scan of* P_{clr} *on top of a 100 interval scan of parameter* P_{bys}*.* ***b)*** *Stochastic simulation output of a three interval parameter scan of* P_{clr} *on top of a 100 interval scan of parameter* P_{bys}*.* ***c)*** *Deterministic simulation output of a five interval parameter scan of* P_{new} *on top of a 100 interval scan of parameter* P_{bys}*.* ***d)*** *Stochastic simulation output of a five interval parameter scan of* P_{new} *on top of a 100 interval scan of parameter* P_{bys}*.* ***e)*** *Deterministic simulation output of a ten interval parameter scan of* P_{ind} *on top of a 100 interval scan of parameter* P_{bys}*.* ***f)*** *Stochastic simulation output of a ten interval parameter scan of* P_{ind} *on top of a 100 interval scan of parameter* P_{bys}*.* ***g)*** *Deterministic simulation output of a 100 interval scan of parameter* P_{bys}*.* ***h)*** *Stochastic simulation output of a 100 interval scan of parameter* P_{bys}*. When not being scanned, rate constant values correspond to* $K_{ind} = 0.12$, $K_{clr}=0.4$, $K_{bys}=0.4$, $K_{new}=0.5$ *and* $K_{trans}=1$ *where the latter parameter corresponds to the transition rate from* $ES_{t=i}$ *to* $ES_{t=i+1}$*. Intervals in parameter scan are regular across the value range of 0 to 1.*

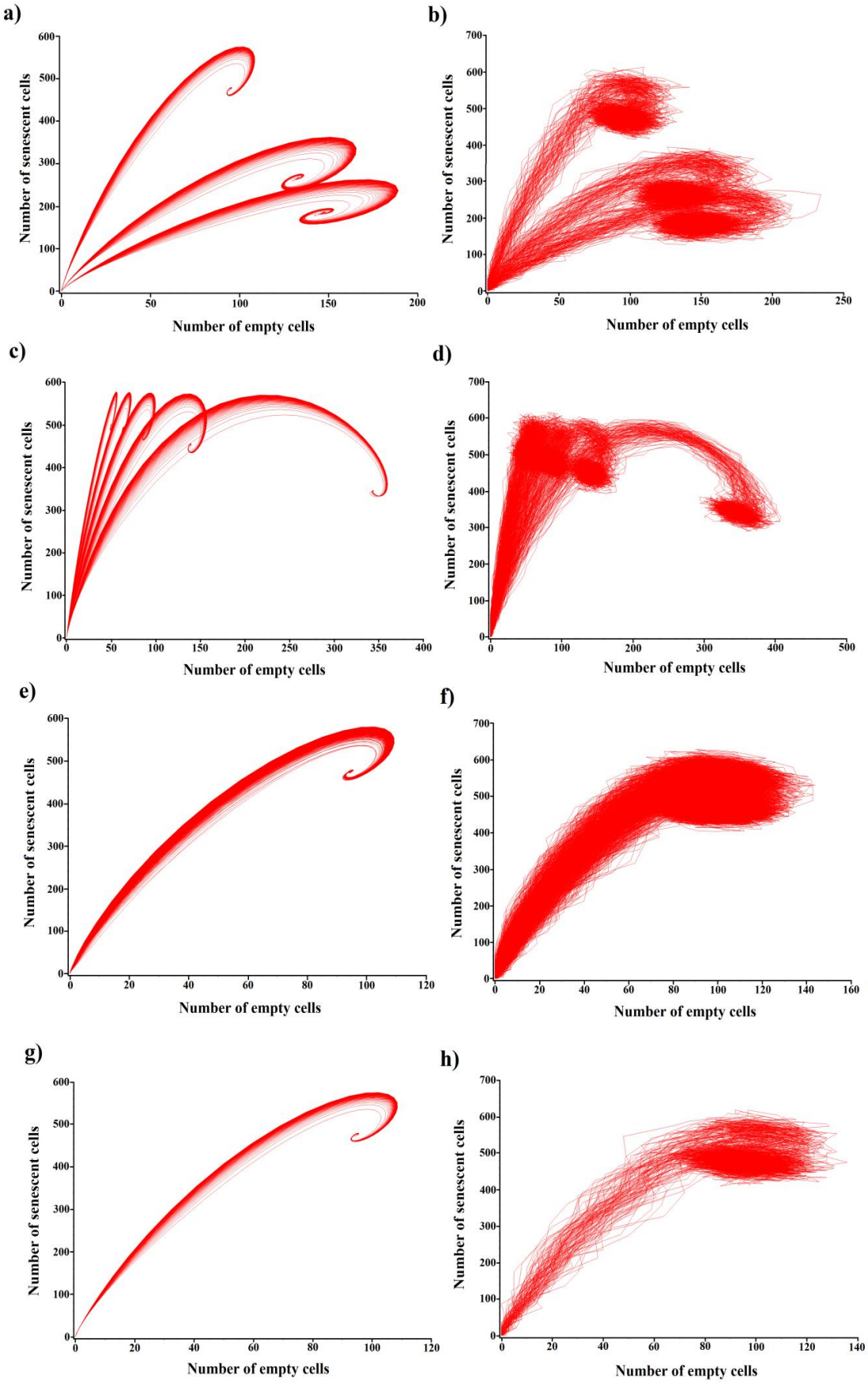
a)
Number of senescent cells
Number of empty cells
b)
Number of senescent cells
Number of empty cells
c)
Number of senescent cells
Number of empty cells
d)
Number of senescent cells
Number of empty cells
e)
Number of senescent cells
Number of empty cells
f)
Number of senescent cells
Number of empty cells
g)
Number of senescent cells
Number of empty cells
h)
Number of senescent cells
Number of empty cells

The lower weight of the bystander effect relative to senescence clearing could be an artefact of an overly-simplified model topology. The multi-scale model was adapted to more realistically represent immune cell clearance where immune cells are likely to be recruited by a group of senescence cells rather than an individual cell within a whole tissue. This was done through a statement where a senescent cell could only be cleared with probability P_{clr} if a minimum of half of the cells in the Moore neighbourhood are in a senescent state. In this setting, parameter P_{clr} is much less determinant of the senescent cell population level but is still the main determinant of the steady state population of pre-senescent cells in the tissue (Figure 6.12).

The closed model structure underlying the interaction topology at the cellular level (Figure 6.2) could lie behind the relative insensitivity of the final steady state of the senescent cell populations to the values of P_{bys} and P_{ind}. However, when the topology of the deterministic intercellular model was opened as illustrated in Figure 6.13, the same relative insensitivity of these parameters was seen, with P_{clr} being the most sensitive parameter. This was observed whether immune cell recruitment was incorporated into the opened model structure or not.

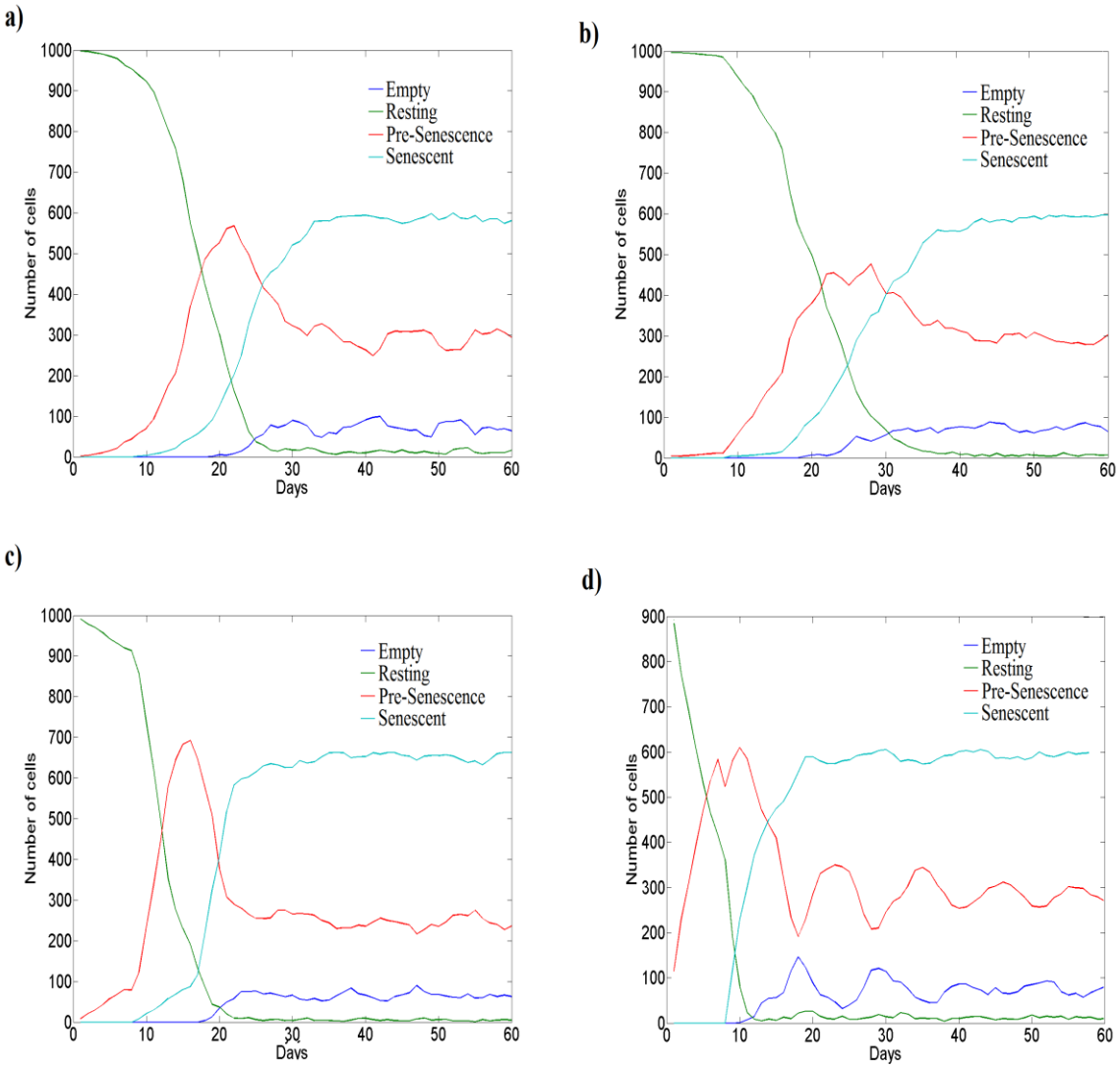

Figure 6.12. *Population dynamics of stochastic senescence entry for different values of* P_{clr} *and* P_{bys} *in a model of neighbour-dependent immune cell recruitment by senescent cells.* ***a)*** *Simulation at a* P_{bys} *value of 0.2 and* P_{clr} *value of 0.4.* ***b)*** *Simulation at a* P_{bys} *value of 0.4 and* P_{clr} *value of 0.4.* ***c)*** *Simulation at a* P_{bys} *value of 0.2 and* P_{clr} *value of 0.1.* ***d)*** *Simulation at a* P_{bys} *value of 0.2 and* P_{clr} *value of 0.4 with a ten-fold increase (0.01 to 0.1) in the probability of seeding an A molecule in a given generation during the simulation of the runaway model. All simulations were run on a 10x10x10 three dimensional grid of resting cells with the parameter value for* P_{ind} *corresponding to a single stochastic run of the Dalle Pezze et al model.*

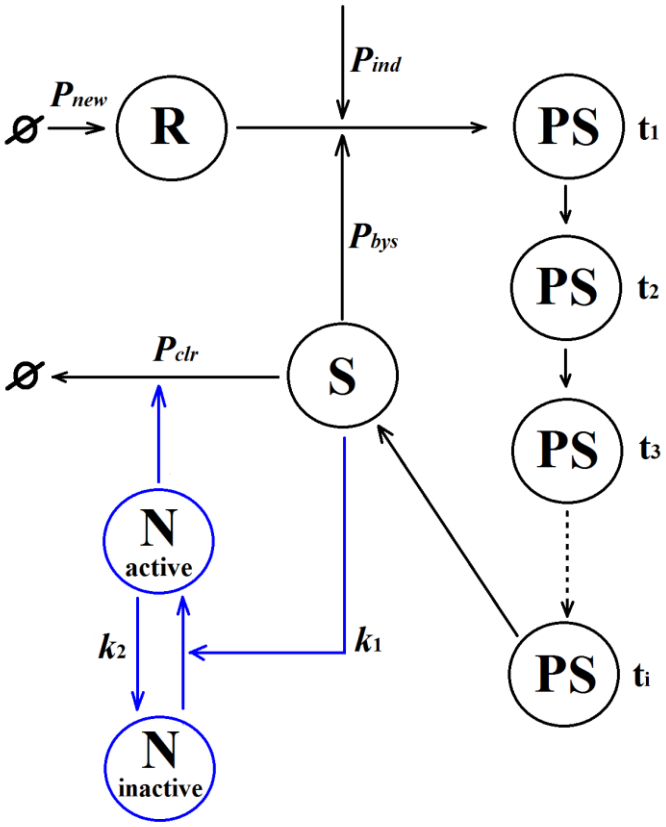

Figure 6.13. *State transitions in the deterministic model of senescence progression within a tissue. R= Resting, PS=Pre-senescence, S= Senescence, E=Empty, N=Negative regulator, t=time (days),* P_{ind}*= Rate of senescence induction,* P_{bys}*= Rate of bystander effect,* P_{clr}*=Rate of senescent cell clearance,* P_{new}*= Rate of new cell appearance. Black outline = 'open' structure of deterministic senescent model which was simulated alone or with the addition of with immune cell recruitment outlined in blue.*

6.3 Discussion

As is frequently said in Systems Biology lectures, a model must be '*as simple as possible and as complex as necessary*'. Various clues in the simulations of the developed multi-scale senescent model suggest that such model is likely to be too simple to capture the complexity of the senescent cell accumulation process. All of the simulations show an inevitable transition of all of the cells at rest into a state of senescence or pre-senescence. Whilst this might be more relatable to the population dynamics seen upon the use of a strong acute stress *in vitro* (Passos et al., 2010, Marazita et al., 2016), it is not relatable to the *in vivo* accumulation of senescence cells, where only a fraction of the cells in a tissue are observed to display markers of cellular senescence (Nelson et al., 2012, Jurk et al., 2014, Bhatia-Dey et al., 2016).

The first difficulty arises from the discrete definition of senescence employed in the multi-scale model. A cell that has undergone significant molecular damage will enter a pre-senescent state that will not be able to induce a bystander effect or recruit immune cells for the first ten days, after which the senescence programme has been fully completed. Depending on the cell type and the stress used to induce senescence, the senescence-associated secretory phenotype (SASP) has been observed as soon as five days after senescence induction (Kabir et al., 2016, Marazita et al., 2016). Furthermore, many molecular changes associated with cellular senescence are already clearly seen before the ten day time-point in irradiated human fibroblasts (Dalle Pezze et al., 2014).

The choice of a ten day time-lag before a cell becomes senescent was based on the observation in human fibroblasts that this is the earliest time-point at which the main molecular makers of cellular senescence (p21, DNA damage, ROS and SA-β-Gal) reach a steady state (Dalle Pezze et al., 2014). This steady state is associated with the new cellular state of cellular senescence and not the initial shock response from the stress treatment used to induce senescence. The time lag introduced by the 10-day rule in the cellular scale is the reason why the simulated *in vitro* senescence cell dynamics corresponded poorly with experimental data at early time points (Figure 6.5). Instead of modelling senescence as a step-entry, further work into the model would involve approaching a time-continuous increase in the P_{bys} and P_{clr} probabilities as the cells approach their maximal level of SASP release over simulated time.

The poor fit at early time points is also likely to arise due to the stringent definition of a senescence cell at the molecular level. The fact that the experimental data on the percentage senescence cells after a 20G irradiation is based on SA-β-Gal staining only (Passos et al., 2010), means that the adopted definition of a senescence cell as one that contains above average levels for four senescent markers will result in a gross underestimation of the number of senescent cells at any given time point. The problem thus lies not necessarily in an overly stringent definition of cellular senescence, but in a disagreement in the definition of senescence between the experimental dataset and the simulated model.

The aforementioned difficulties in the definition of a senescent state at both the molecular level and cellular level lies behind the inability to capture the dynamics of senescence progression at the shorter time scales as seen in Figure 6.5. However, the good fit seen at later time-points would suggest that the parameter estimation procedure has resulted in a gross-overestimation of the value of P_{bys} in order to achieve a good fit at later time points. In other words, the underestimation of senescent cells at early time-points would lead to an overestimation of their propagation to fit later time points. Thus P_{bys} is likely to be much smaller than P_{clr} in a non-aged individual.

On top of the unreliability of the estimated value for P_{bys}, the fitting landscape for this parameter seems to suggest its non-identifiability from the experimental data used for the parameter estimation process. With the exception of the P_{bys} parameter regions around 0.1 and 0.25, all of the parameter values tested resulted in very similar fits to the experimental data (Figure 6.5b). The fitting landscape in Figure 6.5b could well be viewed as a large basin with an anomalous peak at $P_{bys} \approx 0.25$. This suggests that the model parameter is non-identifiable, meaning that unique parameter values cannot be identified through an optimisation procedure utilising a given dataset (Raue et al., 2009, Chis et al., 2011).

Whether such a non-identifiability could be resolved by the use of a more extensive dataset (practical non-identifiability) or is inherent in the model structure (structural non-identifiability) is unclear. However, insensitivity of the simulated output to variations in the values for P_{ind} and P_{bys} suggest a lack of identifiability originating from model structure, or potentially an instance of model sloppiness (Chis et al., 2016). With regards to the ODE-based model of cell-to-cell interactions, alterations to model structure did not resolve the lack of influence of the P_{bys} value on the simulation output.

The conserved element in all of the different intercellular ODE models simulated is the structural relationship between *resting* cells and *senescent* cells (and thus P_{ind} and P_{bys}). Both these cellular populations are related by a linear cascade where any change through P_{ind} will proportionally feed through P_{bys} after a time lag arising from the progression of cells through pre-senescent (PS) states. This simple structure is likely to result in a strong positive correlation between the P_{ind} and P_{bys} parameters, rendering them non-identifiable.

In the formalisation of the ODE-based model of intercellular interactions, the probabilities used in the cellular scale model were used as rate constants in order to model the transition of cellular populations as fluxes following mass action kinetics. The fact that such model reproduced to a good extent the steady state cell populations of the multi-scale model suggests that treating cells in a lattice as entities that will invariably (homogenously) undergo a set of rules with probabilistic outcomes will result in a largely deterministic behaviour. This is especially true for a large cell lattice as that simulated in this study. The multi-scale model indeed treated each type of cell as being part of a perfectly homogenous population that uniformly underwent the same set of rules. This is the reason why, even in the simulations for stochastic senescence-entry, the entirety of the *resting* cell population quickly disappeared. An extra layer of uncertainty could be added where any given cell at any given time may or may not undertake its relevant rule as defined by another probabilistic parameter. This level of uncertainty is already provided for the P_{ind} parameter in the model by its coupling to the simulation of the 'runaway' model.

Upon a closer inspection of the chain of causality within the model it can be appreciated that the causal flow is unidirectional from the lower biological scales ('runaway' and Dalle Pezze *et al.* model) to the cellular scale. However, both the bystander effect and the immune-clearance of senescent cells are able to induce cellular damage. Thus, parametric relationships should exist between the number of senescence cells at the cellular scale and the lower scale levels of the multi-scale model. The sort of experimental data that would inform these parameters and how they feed across scales would need careful consideration.

Even the smallest seeding probability of *A* molecules (1%) in the 'runaway' model, as determined by an otherwise prohibitive simulation time, resulted in a steady state with no *resting* cells. This did not allow the testing of acute perturbations to this parameter under different baseline values to examine the feeding of any effects to the cellular

scale. In addition to the aforementioned limitations, the context-specificity of the adopted parameter values renders them valuable for little more than as working proxies for a posterior iteration exercise of model calibration and validation.

6.4 Concluding remarks

Overall, it is evident from the simulated output of the developed multi-scale model that it is yet of an insufficient complexity to capture any behaviour beyond a simple transition to a steady state cell population. This work has nonetheless helped identify important issues with the development of an effective multi-scale model and provided groundwork for further model development to capture the complexity of senescent cell progression within ageing tissues. Such a model could capture some facets of the alteration of tissue homeostasis with ageing through time-dependent changes in parameter P_{clr} to model immune-decline or through modelled age-related changes at the molecular level percolating to the cellular scale through cell-heterogeneous changes in P_{ind}. The main problem identified in the formalisation of what would be the first multi-scale model of cellular senescence progression within a tissue is the over-simplicity of the model structure that mostly arises from: *i)* the lack of relevant biological information and *ii)* the definition of a senescent cell (Matjusaitis et al., 2016). Other than outlining the current areas of difficulty in establishing what would be the first multi-scale model of cellular senescence, another important insight is gained from this analysis. Namely, that the magnitude of the effect of constitutive signals at the molecular level on cellular interaction networks will depend on the sensitivity of the parameter at the higher level of biological organisation through which the effect would percolate.

Chapter 7

General discussion

It is apparent from the undertaken analysis that constitutive signals in the cellular environment should be viewed as a potential source of reduced signalling responsiveness. The reason for this being that a constant signal feeding into the cell has the potential to result in a sustained activation of negative regulators that will provoke the damping of the response to subsequent acute physiological signals. This observation of a 'blunting' effect by constitutive signals seems to be able to occur in different biological signalling pathways of varying complexities and across different modelling frameworks (Section 3). Indeed, this phenomenon is predicted to be able to arise in a wide variety of possible network structures (Section 4).

Initial work (Section 3) on abstract network structures and agent-based models suggests such a phenomenon could potentially apply to higher levels of biological organisation such as intercellular signalling. However, an attempt to further explore this possibility in the context of biological ageing through the use of a multi-scale model of cellular senescence progression in a tissue proved to require extensive further work (Section 6). Experimental work on the effect of a constitutive signal in the form of oxidative stress on the activation of the Nrf2 signalling pathway by an acute redox signal yielded no indications of a 'blunting' phenomenon (Section 5).

Importantly, the theoretical analysis undertaken establishes that the 'blunting' effect can occur in a wide range of possible networks. However, another outcome of such analysis is that there are plenty of possible model structures that will not necessarily display a reduced responsiveness in the presence of a constitutive signal. The Nrf2 pathway might thus be a system that does not display this behaviour in the presence of a constitutive signal.

Whilst many studies might have involved the direct or indirect generation of constitutive signals in a biological system, for example through gene knockout or gene overexpression, it is of most physiological relevance to investigate such constitutive signals as arising spontaneously *in vivo*. Whilst this can be done for a number of conditions such as cancer, the focus of this work will be on studies relevant to the ageing process. Physiological signals such as intracellular calcium, inflammatory

factors, ROS and symphathoadrenal signals have all been reported to become elevated with age in multiple tissues and thus could provide hints as to the potential underlying occurrence of a 'blunting' effect.

Intracellular calcium is a secondary messenger molecule involved in a plethora of conserved cellular functions and also cell-specific functions like the excitable properties of cells such as neurons, cardiomyocytes or skeletal myotubes (Berridge, 2016). Calcium signalling dysregulations have been identified in all these types of excitable cells in aged tissues (Toescu and Verkhratsky, 2007, Weisleder and Ma, 2008, Zhao et al., 2008, Supnet and Bezprozvanny, 2010, Dai et al., 2012, Herraiz-Martinez et al., 2015).

In the aged brain, increased basal levels of intracellular calcium has been reported for some neurons (Kirischuk et al., 1992, Verkhratsky et al., 1994,Raza et al., 2007, Hajieva et al., 2009) but not others (Murchison and Griffith, 1998, Thibault et al., 2001, Xiong et al., 2002). Observations on the basal levels of intracellular calcium along with its spiking and buffering in aged neurons are highly cell-specific (Murchison and Griffith, 1998, Kumar et al., 2009).

One of the physiological roles of calcium during an action potential is to create a refractory period through a transient neuronal hyperpolarisation generated via the calcium-mediated shuttling of K^+ and Cl^- ions (Thibault et al., 2001, Lima and Marrion, 2007). Interestingly, hippocampal neurons have been shown to become more hyperpolarised and thus lose excitability during the ageing process, resulting in a loss in synaptic plasticity and learning ability (Oh et al., 2010). The fact that that basal intracellular calcium levels have been shown to increase with age in hippocampal neurons (Hajieva et al., 2009) and that calcium chelators or calcium channel blockers can rescue some of these age-related effects (Moyer et al., 1992, Norris et al., 1998) hints at the possibility that the constitutively elevated levels of intracellular calcium may be stabilising a state of reduced neuronal responsiveness. However, the importance of basally elevated levels of intracellular calcium to the ageing of the brain has been put into question (Toescu and Verkhratsky, 2004, Kumar et al., 2009).

Both cardiac and skeletal muscle tissue have been reported to display aberrant excitation-contraction coupling (ECC) with age (Fares and Howlett, 2010, Delbono, 2011). Calcium plays a key role in ECC since an initial calcium signal arising from the action potential at a neuromuscular junction triggers further sarcoplasmic calcium

release to activate Troponin C in myofilaments and activate the kinetics of the contraction machinery (Dai et al., 2012). In cardiac muscle ageing, changes in the calcium signal and the levels of calcium-regulating proteins have been reported to be heterogeneous and seemingly sex-specific (Feridooni et al., 2015) whilst skeletal muscle ageing has the added complexity of fibre-type specificity (Narici and Maffulli, 2010).

Whilst no substantial body of work seems to have explicitly tested for increased basal levels of intracellular calcium in aged skeletal muscle, a mouse model of muscular ageing has been reported to have leaky sarcoplasmic ryanodine receptors (RyRs) resulting from their constitutive oxidation (Andersson et al., 2011). Because the altered calcium signalling in the aged skeletal muscle was able to be rescued through RyR1 stabilisation, it is apparent that oxidative stress could be feeding in as a constant signal to actively maintain a state of calcium dysregulation and over-excitability (Andersson et al., 2011).

Interestingly, the same mouse model has been reported to have basally elevated levels of sarcoplasmic calcium that stabilises a p38 MAPK-mediated constitutive activation of NFκB and increased nitric oxide expression (Altamirano et al., 2012). Although these studies exemplify the ability of constitutive signals to propagate and cause substantial network disruption through pathway crosstalk, there seems to be no studies testing for a reduced responsiveness of p38 or NFκB to an acute stimulus in such mouse model.

In the case of aged cardiomyocytes, a number of studies report an increase in resting calcium levels (Xiao et al., 1994, , Isenberg et al., 2003, Ren et al., 2007, Qin et al., 2013) with others reporting a decrease (Grandy and Howlett, 2006) or no change (Howlett et al., 2006, Howlett, 2010, Ceylan-Isik et al., 2013, Mellor et al., 2014). There is evidence that an increase in the basal level of cardiomyocyte calcium levels can result in the chronic activation of a number of pathways (Yuan et al., 2014) and potentially the subsequent stabilisation of an aged phenotype through the chronic suppression of autophagy mediated by a sustained activation of Akt (Hua et al., 2011). However, no studies were found that examined the responsiveness of such pathways in aged vs young cardiomyocytes.

Chronic, low-level, inflammation is a wide spread observation in many aged eukaryotes which is thought to be largely mediated by the chronic activation of NFκB by a wide variety of factors (Chung et al., 2009, Tilstra et al., 2011, Balistreri et al., 2013, Jurk et

al., 2014). This chronic activation has been shown to be reduced by antioxidant treatment (Spencer et al., 1997, Kim et al., 2006), suggesting that such a state is reversible and likely to be at least partially promoted by oxidative stress. Kim *et al.* examined the basal levels of the main NFκB negative regulator, IκBα, in old rat kidneys that displayed chronic activation of NFκB and reported no evidence of increased levels of this molecule with age (Kim et al., 2006).

Work on aged rodent skeletal muscle has reported the stabilisation of a state of chronic sub-maximal NFκB activation that could not be further increased by a contraction protocol (Vasilaki et al., 2006a). However, the authors do not report an increase in the basal levels of the IκBα unit associated with the negative regulation of NFκB. Other studies that have examined the acute activation of NFκB in old vs young cells have reported a reduced activation magnitude in old cells but without observing any increase in the basal level of IκBα (Helenius et al., 1996, Trebilcock and Ponnappan, 1996, Helenius et al., 1999, Xiao and Majumdar, 2000,Helenius et al., 2001). A study by Tan *et al.* reported the opposite effect, where the constitutive activation of NFκB was actually more sensitive to TNFα stimulation in aged vs new-born smooth muscle cells (Yan et al., 1999). Other studies have shown that constitutive activation of NFκB in the rat brain is region-dependent and not associated with any change in IκBα levels (Korhonen et al., 1997).

It thus seems that the observation of a constitutive activation of NFκB in ageing is widely conserved and can potentially display a reduced responsiveness to acute stimuli. However, there is no evidence for this constitutive activation being accompanied by an increase in the basal level of the negative regulators of this pathway. It is worth noticing that IκBα is the only negative regulator that seems to be investigated alongside the constitutive activation of NFκB. This leaves out many other negative regulators such as A20 or miRNAs that might become chronically activated under conditions of constitutive NFκB activation.

The increase in oxidative stress observed in a number of tissues with age suggests that oxidant-sensitive redox signalling pathways would be expected to become chronically active with age. This has indeed been shown in mouse skeletal muscle for NFκB and AP-1 (Vasilaki et al., 2006a), for Nrf2 in mice cerebellum, liver and lungs (Zhang et al., 2012) and HSF1 in rat hepatocytes (Heydari et al., 2000). Whilst all of these studies reported a reduced activation of the redox-activated transcription factors to an acute

stimulus alongside their constitutive activation, none of them looked at the basal levels of negative regulator molecules.

Whilst there is consensus on the tendency of Nrf2 to become less responsive with age, age-related changes in its basal levels seem to be cell and tissue-specific (Zhang et al., 2015a). Safdar *et al.* examined the basal levels of both Nrf2 and its main inhibitor Keap1 in the *vastus lateralis* muscle of old individuals and reported that basal Keap1 levels decreased with age, with the Nrf2:Keap1 ratio not changing significantly (Safdar et al., 2010). Other studies have reported a reduced Nrf2 activation to an acute stimulus alongside no change (Ungvari et al., 2011a, Done et al., 2016) or even a reduction (Ungvari et al., 2011b, Gounder et al., 2012) in the basal levels of Nrf2. Evidence thus suggests that the constitutive activation of Nrf2 is not ubiquitous and not necessary to observe a reduced activation of the pathway. This could hint at the possibility that Nrf2 is being actively inhibited through crosstalk by another pathway with age (Wardyn et al., 2015). Another possibility could be that the redox signal is not being properly elicited in aged tissues as has been shown in skeletal muscle (Palomero et al., 2013).

The expression and inducibility of HSP70 has been shown to decrease with age by various studies (Kregel, 2002, Kayani et al., 2008). This might suggest a decrease in the transcriptional activity of HSF-1 with age but also an increase in the HSF1 basal levels, since HSP70 is one of its main negative regulators. In accordance with this, Lee *et al.* report a constitutive elevation in the basal levels of HSF-1 in aged human fibroblasts which are less responsive to an acute stimulation by heat shock conditions (42^{o}C) (Lee et al., 2009). In contrast, aged rat skeletal muscle displayed low basal levels of HSP70 and a blunted activation of this molecule by a muscular contraction protocol but showed no change in HSF1 activation between young and old rats (Vasilaki et al., 2002, Vasilaki et al., 2006a). A study in senescent fibroblasts revealed these to have a blunted HSF1 activation but no difference in the basal levels of this molecule was seen between senescent and pre-senescent cells (Lu et al., 2000).

Beyond the cellular level, hormonal imbalances have also been reported to occur with age (Chahal and Drake, 2007, Jones and Boelaert, 2015). There is a large body of work that has reported the sympathetic nervous system (SNS) to become persistently elevated in aged individuals, albeit in a tissue-specific manner (Seals and Esler, 2000, Pascale and Govoni, 2016). Whilst some studies report a decrease in the responsiveness of the SNS to acute stressors in rats (Margiocco et al., 2010) and humans (Grassi et al., 2003), these observations seem to be stimulus-specific (Grassi et al., 2003, Greaney et al.,

2014, Gagnon et al., 2015). The age-related loss in responsiveness of the skin sympathetic nerve traffic (SSNA) activation by cold stress has been reported in a context where its basal levels are decreased in aged individuals (Grassi et al., 2003). In contrast, the constitutive elevation of muscle sympathetic nerve traffic (MSNA) was not associated with a reduced responsiveness to heat stress by Greaney *et al.* (Greaney et al., 2014). In fact, some authors report no changes in the basal levels of MSNA between young and old individuals (Gagnon et al., 2015).

The Hypothalamic-Pituitary-Adrenal (HPA) axis is a major hormonal stress system in vertebrates primarily mediated by cortisol (Gaffey et al., 2016). Cortisol levels fluctuate during the day through the activation of a negative feedback loop primarily mediated by glucocorticoid receptors at various anatomical sites (Herman et al., 2012). However, cortisol levels have been proved to become constitutively elevated under conditions of chronic stress (Miller et al., 2007). Evidence exists that chronic stress can result in a reduced HPA sensitivity to a posterior acute stress due to the constitutive activation of negative feedback mechanisms that induce a stress-habituation response (Mizoguchi et al., 2001, Jaferi et al., 2003). However, the reduced sensitivity of HPA to acute stress does not always map to a prolonged suppressive state (Ostrander et al., 2006). In fact, chronic stress has also been associated with the sensitisation of the activation of the HPA pathway to a posterior acute stress (McGuire et al., 2010). A number of studies have related elevated cortisol levels under conditions of chronic stress to weakened feedback mechanisms whilst others, mainly from models of post-traumatic stress disorder, report a decrease in the basal cortisol levels due to the permanent activation of negative feedback (Herman et al., 2012).

The levels of cortisol release have been reported to increase with age whilst the strength of the glucocorticoid-mediated negative feedback has been reported to be diminished with age (Gupta and Morley, 2014). However, studies in primates seem to show a lowering of cortisol levels with age accompanied with an increased sensitivity to acute stress (Goncharova, 2014). Interestingly, Goncharova *et al.* still reproduced a chronic cortisol activation under constitutive stress in primates, evidencing the disparity between the ageing process and chronic stress (Goncharova, 2014). The collation of studies examining changes in the HPA axis with age reveals inconsistent results which are furthermore gender-specific (Goncharova, 2013, Gaffey et al., 2016).

The literature seems to balance in favour of increased cortisol levels with age in mice and humans, with dysfunctional negative feedback evidenced by flattened diurnal

fluctuations in cortisol levels and reduced sensitivity to glucocorticoid-mediated negative feedback (Goncharova, 2013, Gaffey et al., 2016). However, there is conflicting evidence on whether the HPA system might be less responsive to an acute stimulus in older individuals (Goncharova, 2013). It should be noted that there is a substantial difficulty in separating intrinsic biological changes in the HPA components with age from life history. Namely, the individual-specific history of extrinsic stress factors concerning the nature and timing of the stress on the particular state of the individual organism at the time of the stress (Miller et al., 2007).

Overall, it is apparent that the presence of different constitutive signals in the context of biological ageing and their association with a reduction in system responsiveness is highly tissue- and cell- specific. This is in line with the established heterogeneous nature of ageing as a biological process. Whilst examples can be found where there is a 'blunted' activation of signalling systems, many of them occur in a context where there is no underlying constitutive activation. This is expected since, as mentioned previously, the persistent activation of negative regulators can only be one of multiple mechanisms of reduced pathway responsiveness. However, of the pathways that did display a constitutive activation but reduced response to an acute stimulus, few could be related to an increase in the basal levels of negative regulators.

This is likely to be due to two main reasons. Firstly, it seems likely that the pathways are constitutively active in the first place due to a decrease in the basal levels of the negative regulators (although most studies did not explicitly test for this). Secondly, many studies did not look at the levels of negative regulator molecules when they reported the constitutive activation of pathways alongside their reduced responsiveness. Those that did, examined the levels of the main negative regulator of the pathway, without examining alternative routes of response dampening like the chronic elevation of inhibitory miRNA molecules. Thus, whilst mechanistic evidence exists for the persistent activation of negative regulators driving a loss in pathway responsiveness, current experimental data does not provide any conclusive evidence that such a phenomenon may indeed be occurring in aged tissues.

Investigating the relevance of the reported 'blunting' effect of constitutive signals to the ageing process thus requires of a yet lacking experiment that directly tests this hypothesis. The constitutive activation of the NFκB pathway seems to be well conserved across ageing tissues. The use of the literature to identify in what tissue this pathway has been reported to lose responsiveness in addition to being chronically

activated will lead the way to the testing for the basal levels of a wider number of potential inhibitory molecules of this pathway. If any was found to be elevated, the rescuing of pathway responsiveness could be attempted through the targeted inhibition of the main negative regulator entities identified.

A finding of particular interest is the ability of constitutive signals to reduce information flow through signalling pathways. This means that downstream effectors in signalling pathways will be less able to accurately reflect changes in the upstream signalling molecules. This translates into an increased heterogeneity in the cellular responses to physiological signals and therefore a greater proportion of cells that fail to respond appropriately. This increase in heterogeneity has been associated with a reduced system-level responsiveness and reduced effectiveness of interventions in senescent cells (Dalle Pezze et al., 2014). The ability of constitutive signals to reduce information flow across signalling pathways is a new perspective on how signalling dysfunctionality may propagate across biological networks.

Importantly, a loss in information flow through signalling pathways means that cells will likely respond to signals with an altered magnitude, duration and/or timing. This state of quasi-functionality will likely be sufficient to maintain function, but sub-optimal responses will also be likely to prime the cell for further damage and dysregulation and potentially drive a gradual loss of function typical of ageing processes. Such a state of quasi-functionality can result in subtle cellular- and tissue-level changes in the short term that only develop into an obvious loss of homeostasis in the long term.

Other age-related changes that may affect the cellular regulatory machinery, such as altered expression of key sensor molecules or altered intermolecular binding affinities, are also likely to reduce information flow through signalling pathways. This suggests that information theory is an intuitive framework from which to understand loss of function and regulation during the process of biological ageing. Such a perspective has so far been overlooked and seems likely to apply to a wide range of biological systems that display age-related alterations. It is thus a possibility that a loss in information flow through regulatory pathways is a yet unrecognised hallmark of the ageing process. Such a conceptual framework based on information theory could mechanistically bridge the gap between the concept of stochastic damage during organism lifetime and the gradual homeostatic decline observed with age.

A clear limitation of the presented work is the use of abstract models to represent 'a given biological network' whether redox or otherwise. The aim of this approach was to test for the generality of an observation which in its abstract nature lent itself to such an analysis. That is, that constitutive signals can promote a submaximal activation of negative feedback loops and promote a loss in system responsiveness. However, when models are not calibrated with experimental data and validated through experimentation or other procedures such as identifiability analysis, they remain mathematical constructs. In such a way, this work has examined the property of mathematical objects (aka. Networks), not "grounded" or "mapped" to a real system by experimental data. This is also applicable to our simulations that do not explicitly involve mathematical objects in the form of differential equations, since the undertaken Molecular Dynamics simulations and the Agent-based models are themselves virtual objects with statistical dependencies between the underlying components.

An attempt was made to validate the theoretical observation through experimentation although this proved to be challenging (Section 5). Further work to be undertaken would require the formalisation and calibration of a model of a specific cellular signalling system. As previously mentioned, the NFκB system could be a good model system of relevance to ageing. Time course measurements with a stimulant like TNF in a healthy system would be needed to obtain the activation dynamics of the system components. Such experimental data would then be used to calibrate the model through a parameter estimation procedure. The derivation of model parameters from experimental data will mean the mathematical object has been mapped onto the biological system of interest. If the developed model displays the same 'blunting' behaviour under the presence of a constitutive signal, it will provide a powerful explanation for the clinical observations of constitutive inflammation in aged tissues alongside a loss in responsiveness to infection.

Theoretical perturbations in the model, like the alteration of species abundances by 90% could be validated through knockout/over-expression experimental studies not only to validate model behaviour but to confirm any theoretical model predictions on the alteration of model parameters that could alleviate the effect of constitutive signals. In such a way, the model would act as an exploratory platform to attempt to reverse any identified homeostatic dysregulation. It can be anticipated that for the NFκB system this methodology is likely not to be a simple task since the system oscillates in response to stimulation. This means that the measurement time points need to be chosen carefully

and changes in signal transduction may affect the information transmitted in the frequency domain as well as the time domain.

The field of biogerontology ultimately has to provide an explanation that bridges two observations. On the one hand, a healthy and tightly regulated biological system. On the other hand, a loss of homeostasis. It is evident that this loss of homeostasis is gradual and current thinking places the concept of stochastic damage as the cause of this observation. But what is the mechanistic basis via which stochastic damage promotes a gradual homeostatic decline? The answer to this question remains unclear. However, this work sheds light as to how the observed decline may evolve. Biological systems do not suddenly collapse during ageing. Rather, different subsystems may be heterogeneously affected by the stochastic nature of damage. Since homeostasis is defined as a property where an internal state can be maintained in spite of perturbations then if homeostasis fails, even in a sub-system, there should be a constitutive elevation or decrease in the level of biological entities involved in the system. These are changes recognisable by baseline measurements. Constitutively elevated or diminished biological entities will be likely to serve as inputs or signals to other cellular pathways through cross-talk. This work establishes that if this is the case, dysfunctionality can propagate from the disrupted network sub-system to other biological pathways by interfering with their information-processing capabilities. This would be expected in turn to prime for further damage to occur, as the cell loses its ability to accurately sense and respond to its environment. A gradual functional decline arising from diminished information processing capabilities of cells with age intuitively bridges the molecular with the cellular scale. The importance of constitutive signals in other homeostatic dysregulations such as cancer suggests this work might be applicable to other diseases.

Should an attempt be made to further bridge the concept of damage and the proposed mechanism of dysfunctionality propagation, the question would remain as to how exactly does damage result in the constitutive signals. One possibility is that damage to the genome results in a mutation or set of mutations that causes the loss of system homeostasis. However, such a simple explanation as proposed by the somatic mutation theory of ageing has not been proven to be the main driver of the ageing process. The simulation of a ‘runaway’ process in this work suggests that positive feedback loops can potentially provide an architectural weak point in biological networks. Positive feedback loops often display a threshold activation and stochastic perturbations to the parameters of the system by random damage might promote their stochastic activation

with a certain frequency. In such a way, stochastic damage manifests as a substantial homeostatic perturbation to the system in the form of a constitutive signal.

To confirm such a hypothesis one could take a signalling system that employs positive feedback loops such as calcium signalling (calcium-induced calcium release) and perform single cell live microscopy using a fluorescent probe for calcium. It would be expected that older cells, or cells exposed to a damaging environment should display a greater frequency of fluorescence sparks when at resting conditions. Such sparks would be spontaneous and unpredictable. Other published work has been able to measure information transmission in mammalian signalling pathways (Uda et al., 2013). An important validation of the ideas put forward in this work would involve repeating those experiments in aged mammalian cells to confirm that there is a generalised loss of information transmission in most pathways. Due to the predicted generality of the hypothesis, a large collective effort would be needed to test for this loss in information transmission with age in different pathways and in different cell types.

Chapter 8

Conclusion

Aberrant signalling in the form of reduced pathway responsiveness to physiological stimuli is a common observation in many aged biological systems. A number of mechanisms could underlie such a state. For example, a reduction in the expression of key sensor molecules or altered intermolecular binding affinities. This work proposes another possible mechanism via which such system-level loss in responsiveness may arise. Namely that constitutive signals in the cellular environment can actively maintain a state of reduced responsiveness through the persistent, sub-maximal, activation of negative regulators within a signalling system. This effect would exist as a sustained habituation response or a constant semi-refractory period within a signalling pathway in a manner similar to those of antagonistic hallmarks of ageing (Lopez-Otin et al., 2013).

The reported phenomenon should be easily identifiable experimentally since it predicts a seemingly paradoxical observation of signalling pathways being constitutively active but also displaying basally elevated levels of at least some of the pathway's negative regulators. The theoretical analysis undertaken predicts such an effect to be able to occur in a wide variety of biological systems. This suggests its relevance transcends the field of ageing biology alone and is in principle likely to occur in other homeostatic dysregulations such as cancer. This is especially since constitutive signals are hallmarks of a loss of homeostasis. The generality of the observation in pseudo-randomly generated networks raises the possibility that this phenomenon could potentially be applicable to non-biological systems. It is important to highlight at this point that whilst this work has focused on the potential disruptive effects of constitutive signals in aged systems, genetic and dietary interventions proved to increase the lifespan in various organisms can be viewed as being constitutive signals in themselves.

It is worth of mention that the mechanism put forward in this work is not the only way constitutive signals could maintain a state of reduced responsiveness in a biological system. Persistent signals can make biological systems enter a new steady state through the chronic activation of network sub-structures, like positive feedback loops, that display a bistable behaviour (Shiraishi et al., 2010). Such structures have been shown to be able to be stochastically activated and could well serve as the sources of the

constitutive signals themselves (Faucon et al., 2014). It would be an interesting possibility that these structures could provide an architectural weak-point within biological networks. This is especially since our simulations of a stochastic 'runaway' process indicate that intracellular overcrowding may prime for such homeostatic dysregulations to occur.

Biological ageing is a process that encompasses observations often too heterogeneous to draw coherent conceptual frameworks that may shed light into the generality of the underlying gradual loss of function. How a widespread loss of biological homeostasis is triggered and evolves lies as a core question in biogerontology and is of great relevance to addressing age-related diseases. Computational modelling provides a means for the theoretical formulation of novel ideas to educate our intuition on how the ageing process may unfold. This work has made use of this methodology to examine how constitutive signals, exemplified by oxidative stress, can promote states of quasi-functionality in cellular signalling systems which would be expected to prime for a gradual loss in homeostasis.

Theoretical findings were tested across different model topologies, parameter values and modelling frameworks. Multiple examples are drawn from the literature to put forward that constitutive signals, as manifestations of homeostatic disruptions in biological systems, should be viewed as potential sources of wide-spread network dysfunctionality. This can be deemed to be a useful concept to bear in mind for any life science researcher that encounters a phenotype of dysregulated signalling in their studies of ageing and disease. In summary, this work reports a process of 'molecular habituation' within biological signalling pathways as a potential mechanism of signalling dysregulation during biological ageing.

Chapter 9

Appendix

9.1 Supplementary Figures

Supplementary Figure 1 (S1). *(Next page). Sample network topologies produced by the random network generation algorithm under constant configuration settings. Grey arrows correspond to the utilization of the product synthesized by a reaction node by another reaction node. Red arrows correspond to inhibitory interactions where the product synthesized by a reaction node promotes the degradation of the substrate of another reaction node. Network size = 20.*

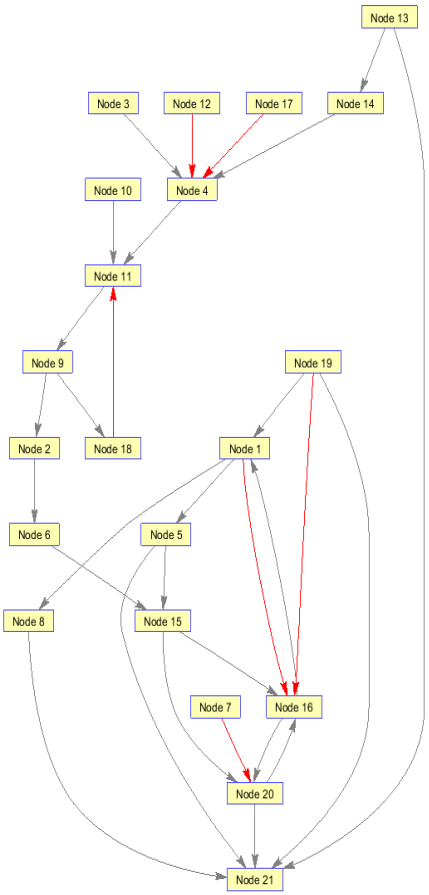
Node 13
Node 3
Node 12
Node 17
Node 14
Node 10
Node 4
Node 11
Node 9
Node 19
Node 2
Node 18
Node 1
Node 6
Node 5
Node 8
Node 15
Node 7
Node 16
Node 20
Node 21

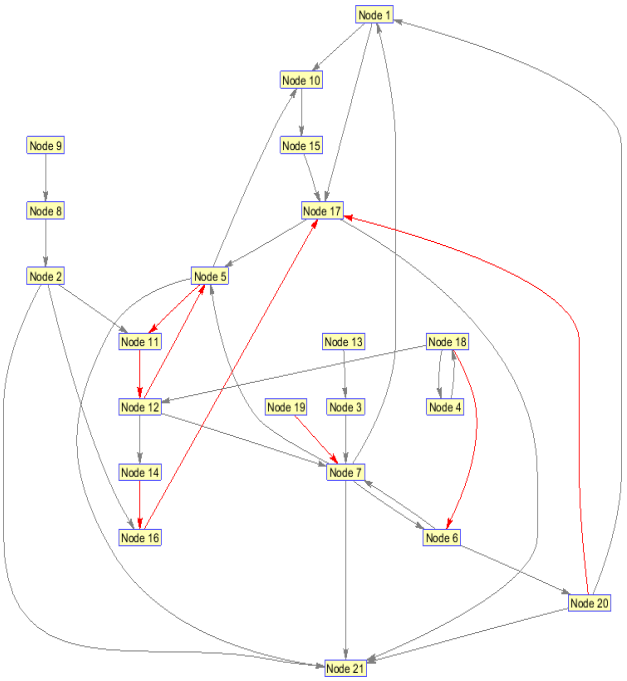
Node 1
Node 10
Node 9
Node 15
Node 8
Node 17
Node 2
Node 5
Node 11
Node 13
Node 18
Node 12
Node 19
Node 3
Node 4
Node 14
Node 7
Node 16
Node 6
Node 20
Node 21

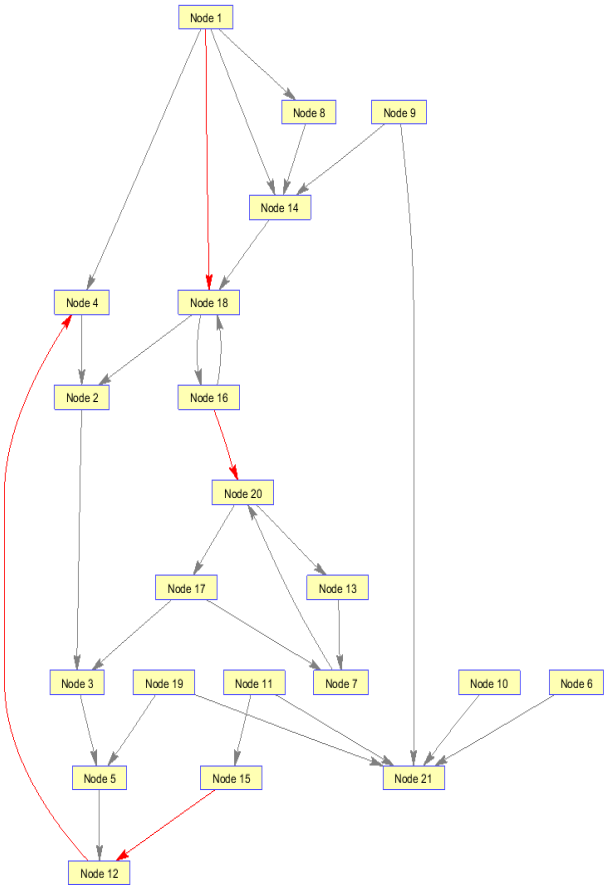
Node 1
Node 8
Node 9
Node 14
Node 4
Node 18
Node 2
Node 16
Node 20
Node 17
Node 13
Node 3
Node 19
Node 11
Node 7
Node 10
Node 6
Node 5
Node 15
Node 21
Node 12

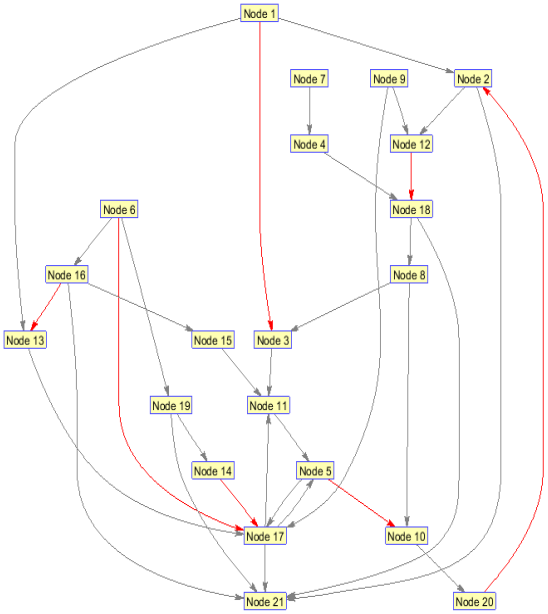
Node 1
Node 7
Node 9
Node 2
Node 4
Node 12
Node 6
Node 18
Node 16
Node 8
Node 13
Node 15
Node 3
Node 19
Node 11
Node 14
Node 5
Node 17
Node 10
Node 21
Node 20

9.2 Supplementary tables

Supplementary Table 1 (ST1). *Ordinary differential equations in Model 1.*

Variable	Equation
$d(\text{Oxidant})/dt$	$k_1 - k_2 \cdot AOX \cdot Oxidant - k_3 \cdot Sensor \cdot Oxidant$
$d(\text{Sensor})/dt$	$k_8 \cdot Inhibitor \cdot Activator - k_3 \cdot Sensor \cdot Oxidant$
$d(Sensor_{OX})/dt$	$k_3 \cdot Sensor \cdot Oxidant - k_6 \cdot Sensor_{OX} \cdot Reductant$
$d(Activator)/dt$	$k_3 \cdot Sensor \cdot Oxidant - k_8 \cdot Inhibitor \cdot Activator$
$d(Function)/dt$	$k_4 \cdot Activator \cdot Relay - k_5 \cdot Function$
$d(Reductant)/dt$	$k_9 \cdot Reductant_{OX} - k_6 \cdot Sensor_{OX} \cdot Reductant$
$d(Intermediate)/dt$	$k_6 \cdot Sensor_{OX} \cdot Reductant - k_7 \cdot Intermediate$
$d(Inhibitor)/dt$	$k_7 \cdot Intermediate - k_8 \cdot Inhibitor \cdot Activator$
$d(Reductant_{OX})/dt$	$k_7 \cdot Intermediate - k_9 \cdot Reductant_{OX}$

Supplementary Table 2 (ST2). *Kinetic parameters in Model 1*

Rate Constant	Value	Reaction
k_1	0	Oxidant generation
k_2	0.1	Oxidant scavenging
k_3	0.1	Sensor oxidation
k_4	0.1	Relay reaction
k_5	0.1	Function decay
k_6	0.1	Sensor reduction
k_7	0.01	Resolving of intermediate
k_8	0.1	Inhibitory complex formation 1
k_9	0.1	Reductant reduction

Supplementary Table 3 (ST3). *Species initial abundances in Model 1*

Name	Initial abundance (AU)
Oxidant	0 ǂ
Sensor	10
$Sensor_{OX}$	0
Activator	0
Function	0
Reductant	100
Intermediate	0
Inhibitor	0
$Reductant_{OX}$	0
AOX	*100 (fixed)*
Relay	*10 (fixed)*

ǂ Value raised to 100 during acute stimulus

Supplementary Table 4 (ST4). *Ordinary differential equations in Model 2*

Variable	Equation
$d(\text{Oxidant})/dt$	$k_1 - k_2 \cdot AOX \cdot Oxidant - k_3 \cdot Sensor \cdot Oxidant$
$d(\text{Sensor})/dt$	$k_7 \cdot Inhibitor \cdot Activator + k_{11} \cdot Inhibitor \cdot Inactive - k_3 \cdot Sensor \cdot Oxidant$
$d(Sensor_{OX})/dt$	$k_3 \cdot Sensor \cdot Oxidant - k_5 \cdot Sensor_{OX} \cdot Reductant$
$d(Activator)/dt$	$k_3 \cdot Sensor \cdot Oxidant - k_7 \cdot Inhibitor \cdot Activator$
$d(Function)/dt$	$k_4 \cdot Activator \cdot Relay - k_9 \cdot Function \cdot Relay2$
$d(Reductant)/dt$	$k_8 \cdot Reductant_{OX} - k_5 \cdot Sensor_{OX} \cdot Reductant$
$d(Intermediate)/dt$	$k_5 \cdot Sensor_{OX} \cdot Reductant - k_6 \cdot Intermediate$
$d(Inhibitor)/dt$	$k_6 \cdot Intermediate - k_7 \cdot Inhibitor \cdot Activator - k_{11} \cdot Inhibitor \cdot Inactive$
$d(Reductant_{OX})/dt$	$k_6 \cdot Intermediate - k_8 \cdot Reductant_{OX}$
$d(NegReg)/dt$	$k_9 \cdot Function \cdot Relay2 - k_{12} \cdot NegReg$
$d(Inactive)/dt$	$k_{10} \cdot Activator \cdot NegReg - k_{11} \cdot Inhibitor \cdot Inactive$

Supplementary Table 5 (ST5). *Kinetic parameters in Model 2*

Rate Constant	Value	Reaction
k_1	0	Oxidant generation
k_2	0.1	Oxidant scavenging
k_3	0.1	Sensor oxidation
k_4	0.1	Relay reaction
k_5	0.1	Sensor reduction
k_6	0.1	Resolving of intermediate
k_7	0.01	Inhibitory complex formation 1
k_8	0.1	Reductant reduction
k_9	0.1	Relay reaction 2
k_{10}	0.1	Inactivation of activator
k_{11}	0.1	Inhibitory complex formation 2
k_{12}	0.1	Degradation of negative regulator

Supplementary Table 6 (ST6). *Species initial abundances in Model 2.*

Name	Initial abundance (AU)
Oxidant	0 ǂ
Sensor	10
Sensor$_{OX}$	0
Activator	0
Function	0
Reductant	100
Intermediate	0
Inhibitor	0
Reductant$_{OX}$	0
NegReg	0
Inactive	0
AOX	*100 (fixed)*
Relay	*10 (fixed)*
Relay2	*10 (fixed)*

ǂ Value raised to 100 during acute stimulus

Supplementary Table 7 (ST7) . *Ordinary differential equations in Model 3*

Variable	Equation
$d(\text{Oxidant})/dt$	$k_1 - k_2 \cdot AOX \cdot Oxidant - k_3 \cdot Sensor \cdot Oxidant$
$d(\text{Sensor})/dt$	$k_8 \cdot Inhibitor \cdot Activator + k_{14} \cdot Inhibitor \cdot Inactive - k_3 \cdot Sensor \cdot Oxidant$
$d(Sensor_{OX})/dt$	$k_3 \cdot Sensor \cdot Oxidant - k_6 \cdot Sensor_{OX} \cdot Reductant$
$d(Activator)/dt$	$k_3 \cdot Sensor \cdot Oxidant - k_8 \cdot Inhibitor \cdot Activator - k_{11} \cdot NegReg \cdot Activator$
$d(Function)/dt$	$k_4 \cdot Activator \cdot Relay - k_5 \cdot Function$
$d(Reductant)/dt$	$k_9 \cdot Reductant_{OX} - k_6 \cdot Sensor_{OX} \cdot Reductant$
$d(Intermediate)/dt$	$k_6 \cdot Sensor_{OX} \cdot Reductant - k_7 \cdot Intermediate$
$d(Inhibitor)/dt$	$k_7 \cdot Intermediate - k_8 \cdot Inhibitor \cdot Activator - k_{14} \cdot Inhibitor \cdot Inactive$
$d(Reductant_{OX})/dt$	$k_7 \cdot Intermediate - k_9 \cdot Reductant_{OX}$
$d(Parallel)/dt$	$k_{10} \cdot Oxidant \cdot Sensor2 - k_{13} \cdot Parallel \cdot ParRelay$
$d(NegReg)/dt$	$k_{13} \cdot Parallel \cdot ParRelay - k_{12} \cdot NegReg$
$d(Inactive)/dt$	$k_{11} \cdot NegReg \cdot Activator - k_{14} \cdot Inhibitor \cdot Inactive$

Supplementary Table 8 (ST8). *Kinetic parameters in Model 3*

Rate Constant	Value	Reaction
k_1	0	Oxidant generation
k_2	0.1	Oxidant scavenging
k_3	0.1	Sensor oxidation
k_4	0.1	Relay reaction
k_5	0.1	Function decay
k_6	0.1	Sensor reduction
k_7	0.01	Resolving of intermediate
k_8	0.1	Inhibitory complex formation 1
k_9	0.1	Reductant reduction
k_{10}	0.1	Sensor2 oxidation
k_{11}	0.1	Inactivation of activator
k_{12}	0.1	Degradation of negative regulator
k_{13}	0.1	Parallel relay reaction
k_{14}	0.1	Inhibitory complex formation 2

Supplementary Table 9 (ST9). *Species initial abundances in Model 3.*

Name	Initial abundance (AU)
Oxidant	0 ǂ
Sensor	10
$Sensor_{OX}$	0
Activator	0
Function	0
Reductant	100
Intermediate	0
Inhibitor	0
$Reductant_{OX}$	0
Parallel	0
NegReg	0
Inactive	0
AOX	*100 (fixed)*
Relay	*10 (fixed)*
Sensor2	*10 (fixed)*
ParRelay	*10 (fixed)*

ǂ Value raised to 100 during acute stimulus

Supplementary Table 10 (ST10). *Ordinary differential equations in Model 4*

Variable	Equation
dO/dt	$k_1 - k_2 \cdot O$
dS/dt	$k_3 - k_4 \cdot S - k_5 \cdot O \cdot S$
dA/dt	$k_5 \cdot O \cdot S - k_6 \cdot A - k_8 \cdot A \cdot N$
dF/dt	$k_6 \cdot A - k_7 \cdot F$
dN/dt	$k_7 \cdot F - k_9 \cdot N$

Supplementary Table 11 (ST11). *Kinetic parameters in Model 4*

Rate Constant	Value
k_1	0
k_2	0.1
k_3	0.1
k_4	0.01
k_5	0.1
k_6	0.1
k_7	0.01
k_8	0.1
k_9	0.01

Supplementary Table 12 (ST12). *Species initial abundances in Model 4*

Name	Initial abundance (AU)
O	0 ǂ
S	10
A	0
F	0
N	0

ǂ Value raised to 100 during acute stimulus

Supplementary Table 13 (ST13). *Ordinary differential equations in Model 5*

Variable	Equation
dO/dt	$k_1 - k_2 \cdot O$
dS/dt	$k_3 - k_4 \cdot S - k_5 \cdot O \cdot S$
dA/dt	$k_5 \cdot O \cdot S - k_6 \cdot A - k_8 \cdot A \cdot N$
dF/dt	$k_6 \cdot A - k_7 \cdot F$
$dS2/dt$	$k_{12} - k_{13} \cdot S2 - k_{10} \cdot O \cdot S2$
dR/dt	$k_{10} \cdot O \cdot S2 - k_{11} \cdot R$
dN/dt	$k_{11} \cdot R - k_9 \cdot N$

Supplementary Table 14 (ST14). *Kinetic parameters in Model 5*

Rate Constant	Value
k_1	0
k_2	0.1
k_3	0.1
k_4	0.01
k_5	0.1
k_6	0.1
k_7	0.1
k_8	0.1
k_9	0.01
k_{10}	0
k_{11}	0
k_{12}	0
k_{13}	0.01

Supplementary Table 15 (ST15). *Species initial abundances in Model 5*

Name	Initial abundance (AU)
O	0 ǂ
S	10
A	0
F	0
S2	10
R	0
N	0

ǂ Value raised to 100 during acute stimulus

9.3 Supplementary text

The model published by Schilling et al. (Schilling et al., 2009) was used for the testing of the hypothesis on a model developed independently by a third party not involved in the work being undertaken. Such a model of Epo signalling was originally developed to map cell proliferation states to underlying network dynamics regarding the phosphorylation state of ERK1 and ERK2 molecules. This published model displayed the following features which led to its selection as an independent testing platform for our hypothesis:

-It was available as an SBML file online through the BioModels database

-It is published in a reputable, peer-reviewed journal

-Its an ODE-based model of a signalling system which is different to our redox signalling models in its overall topology (phosphorylation cascades) and its physiological role

-The system was modelled in a way that the basal level of the signal can be altered by the introduction of two simple synthesis/degradation reactions without modifying the reactions calibrated and originally established by the authors

Chapter 10

References

ADAMSON, A., BODDINGTON, C., DOWNTON, P., ROWE, W., BAGNALL, J., LAM, C., MAYA-MENDOZA, A., SCHMIDT, L., HARPER, C. V., SPILLER, D. G., RAND, D. A., JACKSON, D. A., WHITE, M. R. H. & PASZEK, P. 2016. Signal transduction controls heterogeneous NF-κB dynamics and target gene expression through cytokine-specific refractory states. *Nature Communications,* 7**,** 12057.

ADIMORA, N. J., JONES, D. P. & KEMP, M. L. 2010. A model of redox kinetics implicates the thiol proteome in cellular hydrogen peroxide responses. *Antioxid Redox Signal,* 13**,** 731-43.

AHO, T., SMOLANDER, O. P., NIEMI, J. & YLI-HARJA, O. 2007. RMBNToolbox: random models for biochemical networks. *BMC Syst Biol,* 1**,** 22.

ALDRIDGE, B. B., BURKE, J. M., LAUFFENBURGER, D. A. & SORGER, P. K. 2006. Physicochemical modelling of cell signalling pathways. *Nat Cell Biol,* 8**,** 1195-203.

ALON, U. 2007. Network motifs: theory and experimental approaches. *Nat Rev Genet,* 8**,** 450-461.

ALTAMIRANO, F., LOPEZ, J. R., HENRIQUEZ, C., MOLINSKI, T., ALLEN, P. D. & JAIMOVICH, E. 2012. Increased resting intracellular calcium modulates NF-kappaB-dependent inducible nitric-oxide synthase gene expression in dystrophic mdx skeletal myotubes. *J Biol Chem,* 287**,** 20876-87.

ANDERSSON, D. C., BETZENHAUSER, M. J., REIKEN, S., MELI, A. C., UMANSKAYA, A., XIE, W., SHIOMI, T., ZALK, R., LACAMPAGNE, A. & MARKS, A. R. 2011. Ryanodine receptor oxidation causes intracellular calcium leak and muscle weakness in aging. *Cell Metab,* 14**,** 196-207.

AOI, W. & SAKUMA, K. 2011. Oxidative stress and skeletal muscle dysfunction with aging. *Curr Aging Sci,* 4**,** 101-9.

ARCHER, C. R. & HOSKEN, DAVID J. 2016. Evolution: Escaping the Inevitability of Ageing. *Current Biology,* 26**,** R202-R204.

AZZAM, E. I., JAY-GERIN, J. P. & PAIN, D. 2012. Ionizing radiation-induced metabolic oxidative stress and prolonged cell injury. *Cancer Lett,* 327**,** 48-60.

BAEZ, A. & SHILOACH, J. 2014. Effect of elevated oxygen concentration on bacteria, yeasts, and cells propagated for production of biological compounds. *Microb Cell Fact,* 13**,** 181.

BAGNALL, J., LEEDALE, J., TAYLOR, S. E., SPILLER, D. G., WHITE, M. R., SHARKEY, K. J., BEARON, R. N. & SEE, V. 2014. Tight control of hypoxia-inducible factor-alpha transient dynamics is essential for cell survival in hypoxia. *J Biol Chem,* 289**,** 5549-64.

BAKER, D. J., CHILDS, B. G., DURIK, M., WIJERS, M. E., SIEBEN, C. J., ZHONG, J., A. SALTNESS, R., JEGANATHAN, K. B., VERZOSA, G. C., PEZESHKI, A., KHAZAIE, K., MILLER, J. D. & VAN DEURSEN, J. M. 2016. Naturally occurring p16Ink4a-positive cells shorten healthy lifespan. *Nature,* 530**,** 184-189.

BAKER, D. J., WIJSHAKE, T., TCHKONIA, T., LEBRASSEUR, N. K., CHILDS, B. G., VAN DE SLUIS, B., KIRKLAND, J. L. & VAN DEURSEN, J. M. 2011. Clearance of p16Ink4a-

positive senescent cells delays ageing-associated disorders. *Nature,* 479**,** 232-236.

BALAMURUGAN, K. 2016. HIF-1 at the crossroads of hypoxia, inflammation, and cancer. *Int J Cancer,* 138**,** 1058-66.

BALISTRERI, C. R., CANDORE, G., ACCARDI, G., COLONNA-ROMANO, G. & LIO, D. 2013. NF-κB pathway activators as potential ageing biomarkers: targets for new therapeutic strategies. *Immunity & Ageing,* 10**,** 24.

BARABASI, A. L. & OLTVAI, Z. N. 2004. Network biology: understanding the cell's functional organization. *Nat Rev Genet,* 5**,** 101-13.

BARBIERI, E. & SESTILI, P. 2012. Reactive oxygen species in skeletal muscle signaling. *J Signal Transduct,* 2012**,** 982794.

BARJA, G. 2013. Updating the mitochondrial free radical theory of aging: an integrated view, key aspects, and confounding concepts. *Antioxid Redox Signal,* 19**,** 1420-45.

BARREIRO, E., GARCIA-MARTINEZ, C., MAS, S., AMETLLER, E., GEA, J., ARGILES, J. M., BUSQUETS, S. & LOPEZ-SORIANO, F. J. 2009. UCP3 overexpression neutralizes oxidative stress rather than nitrosative stress in mouse myotubes. *FEBS Lett,* 583**,** 350-6.

BARTOSZEWSKA, S., KOCHAN, K., PIOTROWSKI, A., KAMYSZ, W., OCHOCKA, R. J., COLLAWN, J. F. & BARTOSZEWSKI, R. 2015. The hypoxia-inducible miR-429 regulates hypoxia-inducible factor-1alpha expression in human endothelial cells through a negative feedback loop. *FASEB J,* 29**,** 1467-79.

BATES, G., TABRIZI, S. & JONES, L. 2014. *Huntingtons disease*, Oxford University Press.

BATESON, P. & LALAND, K. N. 2013. Tinbergen's four questions: an appreciation and an update. *Trends Ecol Evol,* 28**,** 712-8.

BEBER, M. E., FRETTER, C., JAIN, S., SONNENSCHEIN, N., MÜLLER-HANNEMANN, M. & HÜTT, M.-T. 2012. Artefacts in statistical analyses of network motifs: general framework and application to metabolic networks. *Journal of The Royal Society Interface,* 9**,** 3426-3435.

BELL, E. L., KLIMOVA, T. A., EISENBART, J., SCHUMACKER, P. T. & CHANDEL, N. S. 2007. Mitochondrial reactive oxygen species trigger hypoxia-inducible factor-dependent extension of the replicative life span during hypoxia. *Mol Cell Biol,* 27**,** 5737-45.

BENFEITAS, R., SELVAGGIO, G., ANTUNES, F., COELHO, P. M. & SALVADOR, A. 2014. Hydrogen peroxide metabolism and sensing in human erythrocytes: a validated kinetic model and reappraisal of the role of peroxiredoxin II. *Free Radic Biol Med,* 74**,** 35-49.

BERRIDGE, M. J. 2016. The Inositol Trisphosphate/Calcium Signaling Pathway in Health and Disease. *Physiol Rev,* 96**,** 1261-96.

BESSE-PATIN, A. & ESTALL, J. L. 2014. An Intimate Relationship between ROS and Insulin Signalling: Implications for Antioxidant Treatment of Fatty Liver Disease. *Int J Cell Biol,* 2014**,** 519153.

BHAT, R. V., SHANLEY, J., CORRELL, M. P., FIELES, W. E., KEITH, R. A., SCOTT, C. W. & LEE, C. M. 2000. Regulation and localization of tyrosine216 phosphorylation of glycogen synthase kinase-3beta in cellular and animal models of neuronal degeneration. *Proc Natl Acad Sci U S A,* 97**,** 11074-9.

BHATIA-DEY, N., KANHERKAR, R. R., STAIR, S. E., MAKAREV, E. O. & CSOKA, A. B. 2016. Cellular Senescence as the Causal Nexus of Aging. *Front Genet,* 7**,** 13.

BJORKSTEN, J. 1968. The crosslinkage theory of aging. *J Am Geriatr Soc,* 16**,** 408-27.

BLAGOSKLONNY, M. V. 2006. Aging and immortality: quasi-programmed senescence and its pharmacologic inhibition. *Cell Cycle,* 5**,** 2087-102.

BLUWSTEIN, A., KUMAR, N., LEGER, K., TRAENKLE, J., OOSTRUM, J., REHRAUER, H., BAUDIS, M. & HOTTIGER, M. O. 2013. PKC signaling prevents irradiation-induced apoptosis of primary human fibroblasts. *Cell Death Dis,* 4**,** e498.

BOIS, F. Y. & GAYRAUD, G. 2015. Probabilistic Generation of Random Networks Taking into Account Information on Motifs Occurrence. *Journal of Computational Biology,* 22**,** 25-36.

BORTZ, W. M., 2ND 1986. Aging as entropy. *Exp Gerontol,* 21**,** 321-8.

BRANDMAN, O. & MEYER, T. 2008. Feedback loops shape cellular signals in space and time. *Science,* 322**,** 390-5.

BRIOCHE, T. & LEMOINE-MOREL, S. 2016. Oxidative Stress, Sarcopenia, Antioxidant Strategies and Exercise: Molecular Aspects. *Curr Pharm Des,* 22**,** 2664-78.

BRITO, P. M. & ANTUNES, F. 2014. Estimation of kinetic parameters related to biochemical interactions between hydrogen peroxide and signal transduction proteins. *Front Chem,* 2**,** 82.

BURATTINI, S., FERRI, P., BATTISTELLI, M., CURCI, R., LUCHETTI, F. & FALCIERI, E. 2004. C2C12 murine myoblasts as a model of skeletal muscle development: morpho-functional characterization. *Eur J Histochem,* 48**,** 223-33.

BÜRKLE, A., MORENO-VILLANUEVA, M., BERNHARD, J., BLASCO, M., ZONDAG, G., HOEIJMAKERS, J. H. J., TOUSSAINT, O., GRUBECK-LOEBENSTEIN, B., MOCCHEGIANI, E., COLLINO, S., GONOS, E. S., SIKORA, E., GRADINARU, D., DOLLÉ, M., SALMON, M., KRISTENSEN, P., GRIFFITHS, H. R., LIBERT, C., GRUNE, T., BREUSING, N., SIMM, A., FRANCESCHI, C., CAPRI, M., TALBOT, D., CAIAFA, P., FRIGUET, B., SLAGBOOM, P. E., HERVONEN, A., HURME, M. & ASPINALL, R. 2015. MARK-AGE biomarkers of ageing. *Mechanisms of Ageing and Development,* 151**,** 2-12.

CAMPISI, J. 2003. Cellular senescence and apoptosis: how cellular responses might influence aging phenotypes. *Experimental Gerontology,* 38**,** 5-11.

CAMPISI, J. 2013. Aging, cellular senescence, and cancer. *Annu Rev Physiol,* 75**,** 685-705.

CERVELLATI, F., CERVELLATI, C., ROMANI, A., CREMONINI, E., STICOZZI, C., BELMONTE, G., PESSINA, F. & VALACCHI, G. 2014. Hypoxia induces cell damage via oxidative stress in retinal epithelial cells. *Free Radic Res,* 48**,** 303-12.

CEYLAN-ISIK, A. F., DONG, M., ZHANG, Y., DONG, F., TURDI, S., NAIR, S., YANAGISAWA, M. & REN, J. 2013. Cardiomyocyte-specific deletion of endothelin receptor A rescues aging-associated cardiac hypertrophy and contractile dysfunction: role of autophagy. *Basic Res Cardiol,* 108**,** 335.

CHAHAL, H. S. & DRAKE, W. M. 2007. The endocrine system and ageing. *J Pathol,* 211**,** 173-80.

CHANDEL, N. S., MCCLINTOCK, D. S., FELICIANO, C. E., WOOD, T. M., MELENDEZ, J. A., RODRIGUEZ, A. M. & SCHUMACKER, P. T. 2000. Reactive oxygen species generated at mitochondrial complex III stabilize hypoxia-inducible factor-1alpha during hypoxia: a mechanism of O2 sensing. *J Biol Chem,* 275**,** 25130-8.

CHANDRA, N. 2009. Computational systems approach for drug target discovery. *Expert Opin Drug Discov,* 4**,** 1221-36.

CHANDRASEKARAN, A., IDELCHIK, M. D. & MELENDEZ, J. A. 2016. Redox control of senescence and age-related disease. *Redox Biol,* 11**,** 91-102.

CHANG, H. & LEVCHENKO, A. 2013. Adaptive molecular networks controlling chemotactic migration: dynamic inputs and selection of the network architecture. *Philos Trans R Soc Lond B Biol Sci,* 368**,** 20130117.

CHARBONEAU, L., TORY, H., CHEN, T., WINTERS, M., PETRICOIN, E. F., 3RD, LIOTTA, L. A. & PAWELETZ, C. P. 2002. Utility of reverse phase protein arrays: applications to signalling pathways and human body arrays. *Brief Funct Genomic Proteomic,* 1**,** 305-15.

CHILDS, B. G., DURIK, M., BAKER, D. J. & VAN DEURSEN, J. M. 2015. Cellular senescence in aging and age-related disease: from mechanisms to therapy. *Nat Med,* 21**,** 1424-1435.

CHIS, O. T., BANGA, J. R. & BALSA-CANTO, E. 2011. Structural identifiability of systems biology models: a critical comparison of methods. *PLoS One,* 6**,** e27755.

CHIS, O. T., VILLAVERDE, A. F., BANGA, J. R. & BALSA-CANTO, E. 2016. On the relationship between sloppiness and identifiability. *Math Biosci,* 282**,** 147-161.

CHUNG, H. Y., CESARI, M., ANTON, S., MARZETTI, E., GIOVANNINI, S., SEO, A. Y., CARTER, C., YU, B. P. & LEEUWENBURGH, C. 2009. Molecular inflammation: underpinnings of aging and age-related diseases. *Ageing Res Rev,* 8**,** 18-30.

CILDIR, G., LOW, K. C. & TERGAONKAR, V. 2016. Noncanonical NF-kappaB Signaling in Health and Disease. *Trends Mol Med,* 22**,** 414-29.

CLAFLIN, D. R., JACKSON, M. J. & BROOKS, S. V. 2015. Age affects the contraction-induced mitochondrial redox response in skeletal muscle. *Front Physiol,* 6**,** 21.

CLANTON, T. 2005. Yet another oxygen paradox. *J Appl Physiol (1985),* 99**,** 1245-6.

CLANTON, T. L. 2007. Hypoxia-induced reactive oxygen species formation in skeletal muscle. *J Appl Physiol (1985),* 102**,** 2379-88.

CLOSE, G. L., ASHTON, T., MCARDLE, A. & JACKSON, M. J. 2005. Microdialysis studies of extracellular reactive oxygen species in skeletal muscle: factors influencing the reduction of cytochrome c and hydroxylation of salicylate. *Free Radic Biol Med,* 39**,** 1460-7.

CLOUTIER, M. & WANG, E. 2011. Dynamic modeling and analysis of cancer cellular network motifs. *Integr Biol (Camb),* 3**,** 724-32.

COBLEY, J. N., MOULT, P. R., BURNISTON, J. G., MORTON, J. P. & CLOSE, G. L. 2015. Exercise improves mitochondrial and redox-regulated stress responses in the elderly: better late than never! *Biogerontology,* 16**,** 249-64.

COHEN-SAIDON, C., COHEN, A. A., SIGAL, A., LIRON, Y. & ALON, U. 2009. Dynamics and variability of ERK2 response to EGF in individual living cells. *Mol Cell,* 36**,** 885-93.

COLLINS-UNDERWOOD, J. R., ZHAO, W., SHARPE, J. G. & ROBBINS, M. E. 2008. NADPH oxidase mediates radiation-induced oxidative stress in rat brain microvascular endothelial cells. *Free Radic Biol Med,* 45**,** 929-38.

COLLOCA, M., BLANCHARD, R., HELLMICH, C., ITO, K. & VAN RIETBERGEN, B. 2014. A multiscale analytical approach for bone remodeling simulations: linking scales from collagen to trabeculae. *Bone,* 64**,** 303-13.

CORREIA-MELO, C., HEWITT, G. & PASSOS, J. F. 2014. Telomeres, oxidative stress and inflammatory factors: partners in cellular senescence? *Longev Healthspan,* 3**,** 1.

CORREIA-MELO, C., MARQUES, F. D., ANDERSON, R., HEWITT, G., HEWITT, R., COLE, J., CARROLL, B. M., MIWA, S., BIRCH, J., MERZ, A., RUSHTON, M. D., CHARLES, M., JURK, D., TAIT, S. W., CZAPIEWSKI, R., GREAVES, L., NELSON, G., BOHLOOLY, Y. M., RODRIGUEZ-CUENCA, S., VIDAL-PUIG, A., MANN, D., SARETZKI, G., QUARATO, G., GREEN, D. R., ADAMS, P. D., VON ZGLINICKI, T., KOROLCHUK, V.

I. & PASSOS, J. F. 2016. Mitochondria are required for pro-ageing features of the senescent phenotype. *EMBO J,* 35**,** 724-42.

CORREIA-MELO, C. & PASSOS, J. F. 2015. Mitochondria: Are they causal players in cellular senescence? *Biochim Biophys Acta,* 1847**,** 1373-9.

COVAS, G., MARINHO, H. S., CYRNE, L. & ANTUNES, F. 2013. Activation of Nrf2 by H2O2: de novo synthesis versus nuclear translocation. *Methods Enzymol,* 528**,** 157-71.

CUADRADO, A. 2015. Structural and functional characterization of Nrf2 degradation by glycogen synthase kinase 3/beta-TrCP. *Free Radic Biol Med,* 88**,** 147-57.

CUNNINGHAM, G. M., ROMAN, M. G., FLORES, L. C., HUBBARD, G. B., SALMON, A. B., ZHANG, Y., GELFOND, J. & IKENO, Y. 2015. The paradoxical role of thioredoxin on oxidative stress and aging. *Archives of Biochemistry and Biophysics,* 576**,** 32-38.

DADA, J. O. & MENDES, P. 2011. Multi-scale modelling and simulation in systems biology. *Integr Biol (Camb),* 3**,** 86-96.

DAI, D. F., CHEN, T., JOHNSON, S. C., SZETO, H. & RABINOVITCH, P. S. 2012. Cardiac aging: from molecular mechanisms to significance in human health and disease. *Antioxid Redox Signal,* 16**,** 1492-526.

DAI, D. F., CHIAO, Y. A., MARCINEK, D. J., SZETO, H. H. & RABINOVITCH, P. S. 2014. Mitochondrial oxidative stress in aging and healthspan. *Longev Healthspan,* 3**,** 6.

DALLE PEZZE, P., NELSON, G., OTTEN, E. G., KOROLCHUK, V. I., KIRKWOOD, T. B., VON ZGLINICKI, T. & SHANLEY, D. P. 2014. Dynamic modelling of pathways to cellular senescence reveals strategies for targeted interventions. *PLoS Comput Biol,* 10**,** e1003728.

DAY, A. M., SMITH, D. A., IKEH, M. A., HAIDER, M., HERRERO-DE-DIOS, C. M., BROWN, A. J., MORGAN, B. A., ERWIG, L. P., MACCALLUM, D. M. & QUINN, J. 2017. Blocking two-component signalling enhances Candida albicans virulence and reveals adaptive mechanisms that counteract sustained SAPK activation. *PLoS Pathog,* 13**,** e1006131.

DE MARCHI, E., BALDASSARI, F., BONONI, A., WIECKOWSKI, M. R. & PINTON, P. 2013. Oxidative stress in cardiovascular diseases and obesity: role of p66Shc and protein kinase C. *Oxid Med Cell Longev,* 2013**,** 564961.

DE SILVA, E. & STUMPF, M. P. 2005. Complex networks and simple models in biology. *J R Soc Interface,* 2**,** 419-30.

DELBONO, O. 2011. Expression and regulation of excitation-contraction coupling proteins in aging skeletal muscle. *Curr Aging Sci,* 4**,** 248-59.

DESAI, L. P., ZHOU, Y., ESTRADA, A. V., DING, Q., CHENG, G., COLLAWN, J. F. & THANNICKAL, V. J. 2014. Negative regulation of NADPH oxidase 4 by hydrogen peroxide-inducible clone 5 (Hic-5) protein. *J Biol Chem,* 289**,** 18270-8.

DJORDJEVIC, T., BELAIBA, R. S., BONELLO, S., PFEILSCHIFTER, J., HESS, J. & GORLACH, A. 2005. Human urotensin II is a novel activator of NADPH oxidase in human pulmonary artery smooth muscle cells. *Arterioscler Thromb Vasc Biol,* 25**,** 519-25.

DONE, A. J., GAGE, M. J., NIETO, N. C. & TRAUSTADOTTIR, T. 2016. Exercise-induced Nrf2-signaling is impaired in aging. *Free Radic Biol Med,* 96**,** 130-8.

DOU, T., YAN, M., WANG, X., LU, W., ZHAO, L., LOU, D., WU, C., CHANG, X. & ZHOU, Z. 2016. Nrf2/ARE Pathway Involved in Oxidative Stress Induced by Paraquat in Human Neural Progenitor Cells. *Oxid Med Cell Longev,* 2016**,** 8923860.

DUES, D. J., ANDREWS, E. K., SCHAAR, C. E., BERGSMA, A. L., SENCHUK, M. M. & VAN RAAMSDONK, J. M. 2016. Aging causes decreased resistance to multiple stresses and a failure to activate specific stress response pathways. *Aging (Albany NY),* 8**,** 777-95.

ELKALAAWY, N. & WASSAL, A. 2015. Methodologies for the modeling and simulation of biochemical networks, illustrated for signal transduction pathways: a primer. *Biosystems,* 129**,** 1-18.

ELOWITZ, M. B. & LEIBLER, S. 2000. A synthetic oscillatory network of transcriptional regulators. *Nature,* 403**,** 335-8.

ENDO, M. 2009. Calcium-induced calcium release in skeletal muscle. *Physiol Rev,* 89**,** 1153-76.

ESPINOSA-DIEZ, C., MIGUEL, V., MENNERICH, D., KIETZMANN, T., SANCHEZ-PEREZ, P., CADENAS, S. & LAMAS, S. 2015. Antioxidant responses and cellular adjustments to oxidative stress. *Redox Biol,* 6**,** 183-97.

FAILLA, G. 1958. The aging process and cancerogenesis. *Ann N Y Acad Sci,* 71**,** 1124-40.

FARES, E. & HOWLETT, S. E. 2010. Effect of age on cardiac excitation-contraction coupling. *Clin Exp Pharmacol Physiol,* 37**,** 1-7.

FAUCON, P. C., PARDEE, K., KUMAR, R. M., LI, H., LOH, Y. H. & WANG, X. 2014. Gene networks of fully connected triads with complete auto-activation enable multistability and stepwise stochastic transitions. *PLoS One,* 9**,** e102873.

FERIDOONI, H. A., DIBB, K. M. & HOWLETT, S. E. 2015. How cardiomyocyte excitation, calcium release and contraction become altered with age. *J Mol Cell Cardiol,* 83**,** 62-72.

FERRELL, J. E., JR. 2013. Feedback loops and reciprocal regulation: recurring motifs in the systems biology of the cell cycle. *Curr Opin Cell Biol,* 25**,** 676-86.

FERRELL, J. E., JR. 2016. Perfect and Near-Perfect Adaptation in Cell Signaling. *Cell Syst,* 2**,** 62-7.

FIELDING, R. A., VELLAS, B., EVANS, W. J., BHASIN, S., MORLEY, J. E., NEWMAN, A. B., ABELLAN VAN KAN, G., ANDRIEU, S., BAUER, J., BREUILLE, D., CEDERHOLM, T., CHANDLER, J., DE MEYNARD, C., DONINI, L., HARRIS, T., KANNT, A., KEIME GUIBERT, F., ONDER, G., PAPANICOLAOU, D., ROLLAND, Y., ROOKS, D., SIEBER, C., SOUHAMI, E., VERLAAN, S. & ZAMBONI, M. 2011. Sarcopenia: an undiagnosed condition in older adults. Current consensus definition: prevalence, etiology, and consequences. International working group on sarcopenia. *J Am Med Dir Assoc,* 12**,** 249-56.

FISHER, A. B. 2009. Redox signaling across cell membranes. *Antioxid Redox Signal,* 11**,** 1349-56.

FISHER, J. & HENZINGER, T. A. 2007. Executable cell biology. *Nat Biotechnol,* 25**,** 1239-49.

FLANDIN, P., DONATI, Y., BARAZZONE-ARGIROFFO, C. & MUZZIN, P. 2005. Hyperoxia-mediated oxidative stress increases expression of UCP3 mRNA and protein in skeletal muscle. *FEBS Lett,* 579**,** 3411-5.

FRANCESCHI, C. 1989. Cell proliferation, cell death and aging. *Aging (Milano),* 1**,** 3-15.

FRANCESCHI, C., BONAFE, M., VALENSIN, S., OLIVIERI, F., DE LUCA, M., OTTAVIANI, E. & DE BENEDICTIS, G. 2000. Inflamm-aging. An evolutionary perspective on immunosenescence. *Ann N Y Acad Sci,* 908**,** 244-54.

FRICK, C. L., YARKA, C., NUNNS, H. & GOENTORO, L. 2017. Sensing relative signal in the Tgf-beta/Smad pathway. *Proc Natl Acad Sci U S A,* 114**,** E2975-E2982.

FULLE, S., PROTASI, F., DI TANO, G., PIETRANGELO, T., BELTRAMIN, A., BONCOMPAGNI, S., VECCHIET, L. & FANO, G. 2004. The contribution of reactive oxygen species to sarcopenia and muscle ageing. *Exp Gerontol,* 39**,** 17-24.

FULOP, T., LE PAGE, A., FORTIN, C., WITKOWSKI, J. M., DUPUIS, G. & LARBI, A. 2014. Cellular signaling in the aging immune system. *Curr Opin Immunol,* 29**,** 105-11.

FUNAHASHI, A., MOROHASHI, M., KITANO, H. & TANIMURA, N. 2003. CellDesigner: a process diagram editor for gene-regulatory and biochemical networks. *BIOSILICO,* 1**,** 159-162.

GAFFEY, A. E., BERGEMAN, C. S., CLARK, L. A. & WIRTH, M. M. 2016. Aging and the HPA axis: Stress and resilience in older adults. *Neuroscience & Biobehavioral Reviews,* 68**,** 928-945.

GAGNON, D., SCHLADER, Z. J. & CRANDALL, C. G. 2015. Sympathetic activity during passive heat stress in healthy aged humans. *J Physiol,* 593**,** 2225-35.

GANESAN, A. & ZHANG, J. 2012. How cells process information: quantification of spatiotemporal signaling dynamics. *Protein Sci,* 21**,** 918-28.

GAUTHIER, L. D., GREENSTEIN, J. L., O'ROURKE, B. & WINSLOW, R. L. 2013. An integrated mitochondrial ROS production and scavenging model: implications for heart failure. *Biophys J,* 105**,** 2832-42.

GAVRILOV, L. A. & GAVRILOVA, N. S. 2001. The reliability theory of aging and longevity. *J Theor Biol,* 213**,** 527-45.

GEMS, D. 2015. The aging-disease false dichotomy: understanding senescence as pathology. *Front Genet,* 6**,** 212.

GLADYSHEV, V. N. 2014. The free radical theory of aging is dead. Long live the damage theory! *Antioxid Redox Signal,* 20**,** 727-31.

GOENTORO, L., SHOVAL, O., KIRSCHNER, M. W. & ALON, U. 2009. The incoherent feedforward loop can provide fold-change detection in gene regulation. *Mol Cell,* 36**,** 894-9.

GONCHAROVA, N. D. 2013. Stress responsiveness of the hypothalamic-pituitary-adrenal axis: age-related features of the vasopressinergic regulation. *Front Endocrinol (Lausanne),* 4**,** 26.

GONCHAROVA, N. D. 2014. Age-related changes in the hypothalamic-pituitary-adrenal axis: Experimental studies in primates. *Advances in Gerontology,* 4**,** 269-273.

GORLACH, A., BERTRAM, K., HUDECOVA, S. & KRIZANOVA, O. 2015. Calcium and ROS: A mutual interplay. *Redox Biol,* 6**,** 260-71.

GOUNDER, S. S., KANNAN, S., DEVADOSS, D., MILLER, C. J., WHITEHEAD, K. J., ODELBERG, S. J., FIRPO, M. A., PAINE, R., 3RD, HOIDAL, J. R., ABEL, E. D. & RAJASEKARAN, N. S. 2012. Impaired transcriptional activity of Nrf2 in age-related myocardial oxidative stress is reversible by moderate exercise training. *PLoS One,* 7**,** e45697.

GRANDY, S. A. & HOWLETT, S. E. 2006. Cardiac excitation-contraction coupling is altered in myocytes from aged male mice but not in cells from aged female mice. *Am J Physiol Heart Circ Physiol,* 291**,** H2362-70.

GRASSI, G., SERAVALLE, G., TURRI, C., BERTINIERI, G., DELL'ORO, R. & MANCIA, G. 2003. Impairment of thermoregulatory control of skin sympathetic nerve traffic in the elderly. *Circulation,* 108**,** 729-35.

GREANEY, J. L., STANHEWICZ, A. E., KENNEY, W. L. & ALEXANDER, L. M. 2014. Muscle sympathetic nerve activity during cold stress and isometric exercise in healthy older adults. *J Appl Physiol (1985),* 117**,** 648-57.

GRISSOM, N. & BHATNAGAR, S. 2009. Habituation to repeated stress: get used to it. *Neurobiol Learn Mem,* 92**,** 215-24.

GULDEN, M., JESS, A., KAMMANN, J., MASER, E. & SEIBERT, H. 2010. Cytotoxic potency of H2O2 in cell cultures: impact of cell concentration and exposure time. *Free Radic Biol Med,* 49**,** 1298-305.

GUNAWARDENA, J. 2014. Models in biology: 'accurate descriptions of our pathetic thinking'. *BMC Biol,* 12**,** 29.

GUPTA, D. & MORLEY, J. E. 2014. Hypothalamic-pituitary-adrenal (HPA) axis and aging. *Compr Physiol,* 4**,** 1495-510.

HAJIEVA, P., KUHLMANN, C., LUHMANN, H. J. & BEHL, C. 2009. Impaired calcium homeostasis in aged hippocampal neurons. *Neurosci Lett,* 451**,** 119-23.

HALDANE, J. B. S. 1941. New paths in genetics. *New Paths in Genetics.*

HARDEE, J. P., PUPPA, M. J., FIX, D. K., GAO, S., HETZLER, K. L., BATEMAN, T. A. & CARSON, J. A. 2014. The effect of radiation dose on mouse skeletal muscle remodeling. *Radiol Oncol,* 48**,** 247-56.

HARMAN, D. 1955. Aging: a theory based on free radical and radiation chemistry.

HART, Y., MAYO, A. E., SHOVAL, O. & ALON, U. 2013. Comparing apples and oranges: fold-change detection of multiple simultaneous inputs. *PLoS One,* 8**,** e57455.

HAYAKAWA, R., HAYAKAWA, T., TAKEDA, K. & ICHIJO, H. 2012. Therapeutic targets in the ASK1-dependent stress signaling pathways. *Proc Jpn Acad Ser B Phys Biol Sci,* 88**,** 434-53.

HAYES, J. D., CHOWDHRY, S., DINKOVA-KOSTOVA, A. T. & SUTHERLAND, C. 2015. Dual regulation of transcription factor Nrf2 by Keap1 and by the combined actions of beta-TrCP and GSK-3. *Biochem Soc Trans,* 43**,** 611-20.

HAYFLICK, L. 1965. The Limited in Vitro Lifetime of Human Diploid Cell Strains. *Exp Cell Res,* 37**,** 614-36.

HELENIUS, M., HANNINEN, M., LEHTINEN, S. K. & SALMINEN, A. 1996. Changes associated with aging and replicative senescence in the regulation of transcription factor nuclear factor-kappa B. *Biochem J,* 318 (Pt 2)**,** 603-8.

HELENIUS, M., KYRYLENKO, S., VEHVILAINEN, P. & SALMINEN, A. 2001. Characterization of aging-associated up-regulation of constitutive nuclear factor-kappa B binding activity. *Antioxid Redox Signal,* 3**,** 147-56.

HELENIUS, M., MÄKELÄINEN, L. & SALMINEN, A. 1999. Attenuation of NF-κB Signaling Response to UVB Light during Cellular Senescence. *Experimental Cell Research,* 248**,** 194-202.

HERMAN, J. P. 2013. Neural control of chronic stress adaptation. *Front Behav Neurosci,* 7**,** 61.

HERMAN, J. P., MCKLVEEN, J. M., SOLOMON, M. B., CARVALHO-NETTO, E. & MYERS, B. 2012. Neural regulation of the stress response: glucocorticoid feedback mechanisms. *Braz J Med Biol Res,* 45**,** 292-8.

HERRAIZ-MARTINEZ, A., ALVAREZ-GARCIA, J., LLACH, A., MOLINA, C. E., FERNANDES, J., FERRERO-GREGORI, A., RODRIGUEZ, C., VALLMITJANA, A., BENITEZ, R., PADRO, J. M., MARTINEZ-GONZALEZ, J., CINCA, J. & HOVE-MADSEN, L. 2015. Ageing is associated with deterioration of calcium homeostasis in isolated human right atrial myocytes. *Cardiovasc Res,* 106**,** 76-86.

HEYDARI, A. R., YOU, S., TAKAHASHI, R., GUTSMANN-CONRAD, A., SARGE, K. D. & RICHARDSON, A. 2000. Age-related alterations in the activation of heat shock transcription factor 1 in rat hepatocytes. *Exp Cell Res,* 256**,** 83-93.

HOESEL, B. & SCHMID, J. A. 2013. The complexity of NF-kappaB signaling in inflammation and cancer. *Mol Cancer,* 12**,** 86.

HOLMES, B. B. & DIAMOND, M. I. 2012. Cellular mechanisms of protein aggregate propagation. *Curr Opin Neurol,* 25**,** 721-6.

HOLMSTROM, K. M. & FINKEL, T. 2014. Cellular mechanisms and physiological consequences of redox-dependent signalling. *Nat Rev Mol Cell Biol,* 15**,** 411-21.

HOOPS, S., SAHLE, S., GAUGES, R., LEE, C., PAHLE, J., SIMUS, N., SINGHAL, M., XU, L., MENDES, P. & KUMMER, U. 2006. COPASI--a COmplex PAthway SImulator. *Bioinformatics,* 22**,** 3067-74.

HOWLETT, S. E. 2010. Age-associated changes in excitation-contraction coupling are more prominent in ventricular myocytes from male rats than in myocytes from female rats. *Am J Physiol Heart Circ Physiol,* 298**,** H659-70.

HOWLETT, S. E., GRANDY, S. A. & FERRIER, G. R. 2006. Calcium spark properties in ventricular myocytes are altered in aged mice. *Am J Physiol Heart Circ Physiol,* 290**,** H1566-74.

HSIEH, W. T., TZENG, K. R., CIOU, J. S., TSAI, J. J., KURUBANJERDJIT, N., HUANG, C. H. & NG, K. L. 2015. Transcription factor and microRNA-regulated network motifs for cancer and signal transduction networks. *BMC Syst Biol,* 9 Suppl 1**,** S5.

HUA, Y., ZHANG, Y., CEYLAN-ISIK, A. F., WOLD, L. E., NUNN, J. M. & REN, J. 2011. Chronic akt activation accentuates aging-induced cardiac hypertrophy and myocardial contractile dysfunction: role of autophagy. *Basic Research in Cardiology,* 106**,** 1173-1191.

HUCKA, M., FINNEY, A., SAURO, H. M., BOLOURI, H., DOYLE, J. C., KITANO, H., ARKIN, A. P., BORNSTEIN, B. J., BRAY, D., CORNISH-BOWDEN, A., CUELLAR, A. A., DRONOV, S., GILLES, E. D., GINKEL, M., GOR, V., GORYANIN, II, HEDLEY, W. J., HODGMAN, T. C., HOFMEYR, J. H., HUNTER, P. J., JUTY, N. S., KASBERGER, J. L., KREMLING, A., KUMMER, U., LE NOVERE, N., LOEW, L. M., LUCIO, D., MENDES, P., MINCH, E., MJOLSNESS, E. D., NAKAYAMA, Y., NELSON, M. R., NIELSEN, P. F., SAKURADA, T., SCHAFF, J. C., SHAPIRO, B. E., SHIMIZU, T. S., SPENCE, H. D., STELLING, J., TAKAHASHI, K., TOMITA, M., WAGNER, J., WANG, J. & FORUM, S. 2003. The systems biology markup language (SBML): a medium for representation and exchange of biochemical network models. *Bioinformatics,* 19**,** 524-31.

INGRAM, P. J., STUMPF, M. P. & STARK, J. 2006. Network motifs: structure does not determine function. *BMC Genomics,* 7**,** 108.

ISENBERG, G., BORSCHKE, B. & RUECKSCHLOSS, U. 2003. Ca2+ transients of cardiomyocytes from senescent mice peak late and decay slowly. *Cell Calcium,* 34**,** 271-80.

JACKSON, M. J. 2015. Redox regulation of muscle adaptations to contractile activity and aging. *J Appl Physiol (1985),* 119**,** 163-71.

JACKSON, M. J. 2016. Reactive oxygen species in sarcopenia: Should we focus on excess oxidative damage or defective redox signalling? *Mol Aspects Med,* 50**,** 33-40.

JACKSON, M. J. & MCARDLE, A. 2011. Age-related changes in skeletal muscle reactive oxygen species generation and adaptive responses to reactive oxygen species. *J Physiol,* 589**,** 2139-45.

JAFERI, A., NOWAK, N. & BHATNAGAR, S. 2003. Negative feedback functions in chronically stressed rats: role of the posterior paraventricular thalamus. *Physiol Behav,* 78**,** 365-73.

JANES, K. A. & LAUFFENBURGER, D. A. 2013. Models of signalling networks - what cell biologists can gain from them and give to them. *J Cell Sci,* 126**,** 1913-21.

JANSSEN, I., SHEPARD, D. S., KATZMARZYK, P. T. & ROUBENOFF, R. 2004. The healthcare costs of sarcopenia in the United States. *J Am Geriatr Soc,* 52**,** 80-5.

JEONG, H., TOMBOR, B., ALBERT, R., OLTVAI, Z. N. & BARABASI, A. L. 2000. The large-scale organization of metabolic networks. *Nature,* 407**,** 651-4.

JI, L. L. 2015. Redox signaling in skeletal muscle: role of aging and exercise. *Adv Physiol Educ,* 39**,** 352-9.

JIANG, F., ZHANG, Y. & DUSTING, G. J. 2011. NADPH oxidase-mediated redox signaling: roles in cellular stress response, stress tolerance, and tissue repair. *Pharmacol Rev,* 63**,** 218-42.

JIANG, S., TU, K., FU, Q., SCHMITT, D. C., ZHOU, L., LU, N. & ZHAO, Y. 2015a. Multifaceted roles of HSF1 in cancer. *Tumor Biology,* 36**,** 4923-4931.

JIANG, S., TU, K., FU, Q., SCHMITT, D. C., ZHOU, L., LU, N. & ZHAO, Y. 2015b. Multifaceted roles of HSF1 in cancer. *Tumour Biol,* 36**,** 4923-31.

JONES, C. M. & BOELAERT, K. 2015. The Endocrinology of Ageing: A Mini-Review. *Gerontology,* 61**,** 291-300.

JOSEPH, A. M., ADHIHETTY, P. J. & LEEUWENBURGH, C. 2016. Beneficial effects of exercise on age-related mitochondrial dysfunction and oxidative stress in skeletal muscle. *J Physiol,* 594**,** 5105-23.

JURDANA, M., CEMAZAR, M., PEGAN, K. & MARS, T. 2013. Effect of ionizing radiation on human skeletal muscle precursor cells. *Radiol Oncol,* 47**,** 376-81.

JURK, D., WILSON, C., PASSOS, J. F., OAKLEY, F., CORREIA-MELO, C., GREAVES, L., SARETZKI, G., FOX, C., LAWLESS, C., ANDERSON, R., HEWITT, G., PENDER, S. L., FULLARD, N., NELSON, G., MANN, J., VAN DE SLUIS, B., MANN, D. A. & VON ZGLINICKI, T. 2014. Chronic inflammation induces telomere dysfunction and accelerates ageing in mice. *Nat Commun,* 2**,** 4172.

KABIR, T. D., LEIGH, R. J., TASENA, H., MELLONE, M., COLETTA, R. D., PARKINSON, E. K., PRIME, S. S., THOMAS, G. J., PATERSON, I. C., ZHOU, D., MCCALL, J., SPEIGHT, P. M. & LAMBERT, D. W. 2016. A miR-335/COX-2/PTEN axis regulates the secretory phenotype of senescent cancer-associated fibroblasts. *Aging (Albany NY),* 8**,** 1608-35.

KACZARA, P., SARNA, T. & BURKE, J. M. 2010. Dynamics of H2O2 availability to ARPE-19 cultures in models of oxidative stress. *Free Radic Biol Med,* 48**,** 1064-70.

KASPAR, J. W. & JAISWAL, A. K. 2010. An autoregulatory loop between Nrf2 and Cul3-Rbx1 controls their cellular abundance. *J Biol Chem,* 285**,** 21349-58.

KASPAR, J. W., NITURE, S. K. & JAISWAL, A. K. 2009. Nrf2:INrf2 (Keap1) signaling in oxidative stress. *Free Radic Biol Med,* 47**,** 1304-9.

KAYANI, A. C., MORTON, J. P. & MCARDLE, A. 2008. The exercise-induced stress response in skeletal muscle: failure during aging. *Appl Physiol Nutr Metab,* 33**,** 1033-41.

KENNEDY, S. R., LOEB, L. A. & HERR, A. J. 2012. Somatic mutations in aging, cancer and neurodegeneration. *Mech Ageing Dev,* 133**,** 118-26.

KHALIL, H. S., GOLTSOV, A., LANGDON, S. P., HARRISON, D. J., BOWN, J. & DEENI, Y. 2015. Quantitative analysis of NRF2 pathway reveals key elements of the regulatory circuits underlying antioxidant response and proliferation of ovarian cancer cells. *J Biotechnol,* 202**,** 12-30.

KHOKHLOV, A. N. 2014. On the immortal hydra. Again. *Moscow University Biological Sciences Bulletin,* 69**,** 153-157.

KHOLODENKO, B. N. 2006. Cell-signalling dynamics in time and space. *Nat Rev Mol Cell Biol,* 7**,** 165-76.

KIM, D. H., KIM, H. K., PARK, S., KIM, J. Y., ZOU, Y., CHO, K. H., KIM, Y. S., KIM, D. H., YU, B. P., CHOI, J. S. & CHUNG, H. Y. 2006. Short-term feeding of baicalin inhibits age-associated NF-kappaB activation. *Mech Ageing Dev,* 127**,** 719-25.

KIM, G. H., KIM, J. E., RHIE, S. J. & YOON, S. 2015. The Role of Oxidative Stress in Neurodegenerative Diseases. *Exp Neurobiol,* 24**,** 325-40.

KIM SH, S. H., KAMINKER, P. & CAMPISI, J. 2002. Telomeres, aging and cancer: in search of a happy ending. *Oncogene,* 21**,** 503-11.

KIRISCHUK, S., PRONCHUK, N. & VERKHRATSKY, A. 1992. Measurements of intracellular calcium in sensory neurons of adult and old rats. *Neuroscience,* 50**,** 947-51.

KIRK, P. D., BABTIE, A. C. & STUMPF, M. P. 2015. SYSTEMS BIOLOGY. Systems biology (un)certainties. *Science,* 350**,** 386-8.

KIRKWOOD, T. B. 1977. Evolution of ageing. *Nature,* 270**,** 301-4.

KIRKWOOD, T. B. 2005. Understanding the odd science of aging. *Cell,* 120**,** 437-47.

KIRKWOOD, T. B. 2011. Systems biology of ageing and longevity. *Philos Trans R Soc Lond B Biol Sci,* 366**,** 64-70.

KIRKWOOD, T. B. & AUSTAD, S. N. 2000. Why do we age? *Nature,* 408**,** 233-8.

KIRKWOOD, T. B. L. & KOWALD, A. 2012. The free-radical theory of ageing – older, wiser and still alive. *BioEssays,* 34**,** 692-700.

KITANO, H. 2002a. Computational systems biology. *Nature,* 420**,** 206-10.

KITANO, H. 2002b. Systems biology: a brief overview. *Science,* 295**,** 1662-4.

KLIMOVA, T. A., BELL, E. L., SHROFF, E. H., WEINBERG, F. D., SNYDER, C. M., DIMRI, G. P., SCHUMACKER, P. T., BUDINGER, G. R. & CHANDEL, N. S. 2009. Hyperoxia-induced premature senescence requires p53 and pRb, but not mitochondrial matrix ROS. *FASEB J,* 23**,** 783-94.

KOLCH, W., HALASZ, M., GRANOVSKAYA, M. & KHOLODENKO, B. N. 2015. The dynamic control of signal transduction networks in cancer cells. *Nat Rev Cancer,* 15**,** 515-27.

KONDO, H., NAKAGAKI, I., SASAKI, S., HORI, S. & ITOKAWA, Y. 1993. Mechanism of oxidative stress in skeletal muscle atrophied by immobilization. *Am J Physiol,* 265**,** E839-44.

KORHONEN, P., HELENIUS, M. & SALMINEN, A. 1997. Age-related changes in the regulation of transcription factor NF-κB in rat brain. *Neuroscience Letters,* 225**,** 61-64.

KOVAC, S., ANGELOVA, P. R., HOLMSTROM, K. M., ZHANG, Y., DINKOVA-KOSTOVA, A. T. & ABRAMOV, A. Y. 2015. Nrf2 regulates ROS production by mitochondria and NADPH oxidase. *Biochim Biophys Acta,* 1850**,** 794-801.

KOVACIC, H. N., IRANI, K. & GOLDSCHMIDT-CLERMONT, P. J. 2001. Redox regulation of human Rac1 stability by the proteasome in human aortic endothelial cells. *J Biol Chem,* 276**,** 45856-61.

KOWALD, A. & KIRKWOOD, T. B. 1996. A network theory of ageing: the interactions of defective mitochondria, aberrant proteins, free radicals and scavengers in the ageing process. *Mutat Res,* 316**,** 209-36.

KREGEL, K. C. 2002. Invited Review: Heat shock proteins: modifying factors in physiological stress responses and acquired thermotolerance. *Journal of Applied Physiology,* 92**,** 2177-2186.

KRIETE, A., LECHNER, M., CLEARFIELD, D. & BOHMANN, D. 2011. Computational systems biology of aging. *Wiley Interdiscip Rev Syst Biol Med,* 3**,** 414-28.

KRIZHANOVSKY, V., YON, M., DICKINS, R. A., HEARN, S., SIMON, J., MIETHING, C., YEE, H., ZENDER, L. & LOWE, S. W. 2008. Senescence of activated stellate cells limits liver fibrosis. *Cell,* 134**,** 657-67.

KUMAR, A., BODHINATHAN, K. & FOSTER, T. C. 2009. Susceptibility to Calcium Dysregulation during Brain Aging. *Front Aging Neurosci,* 1**,** 2.

LAWLESS, C., JURK, D., GILLESPIE, C. S., SHANLEY, D., SARETZKI, G., VON ZGLINICKI, T. & PASSOS, J. F. 2012. A stochastic step model of replicative senescence explains ROS production rate in ageing cell populations. *PLoS One,* 7**,** e32117.

LEE, J. H., TSUNADA, J. & COHEN, Y. E. 2013. A model of the differential representation of signal novelty in the local field potentials and spiking activity of the ventrolateral prefrontal cortex. *Neural Comput,* 25**,** 157-85.

LEE, R. E., WALKER, S. R., SAVERY, K., FRANK, D. A. & GAUDET, S. 2014. Fold change of nuclear NF-kappaB determines TNF-induced transcription in single cells. *Mol Cell,* 53**,** 867-79.

LEE, Y. K., LIU, D. J., LU, J., CHEN, K. Y. & LIU, A. Y. 2009. Aberrant regulation and modification of heat shock factor 1 in senescent human diploid fibroblasts. *J Cell Biochem,* 106**,** 267-78.

LEI, Y., WANG, K., DENG, L., CHEN, Y., NICE, E. C. & HUANG, C. 2015. Redox regulation of inflammation: old elements, a new story. *Med Res Rev,* 35**,** 306-40.

LEPETSOS, P. & PAPAVASSILIOU, A. G. 2016. ROS/oxidative stress signaling in osteoarthritis. *Biochim Biophys Acta,* 1862**,** 576-91.

LEWIS, K. N., WASON, E., EDREY, Y. H., KRISTAN, D. M., NEVO, E. & BUFFENSTEIN, R. 2015. Regulation of Nrf2 signaling and longevity in naturally long-lived rodents. *Proc Natl Acad Sci U S A,* 112**,** 3722-7.

LIM, J. B., LANGFORD, T. F., HUANG, B. K., DEEN, W. M. & SIKES, H. D. 2016. A reaction-diffusion model of cytosolic hydrogen peroxide. *Free Radic Biol Med,* 90**,** 85-90.

LIMA, P. A. & MARRION, N. V. 2007. Mechanisms underlying activation of the slow AHP in rat hippocampal neurons. *Brain Res,* 1150**,** 74-82.

LIOCHEV, S. I. 2015. Reflections on the Theories of Aging, of Oxidative Stress, and of Science in General. Is It Time to Abandon the Free Radical (Oxidative Stress) Theory of Aging? *Antioxid Redox Signal,* 23**,** 187-207.

LIPSITZ, L. A. & GOLDBERGER, A. L. 1992. Loss of 'complexity' and aging. Potential applications of fractals and chaos theory to senescence. *JAMA,* 267**,** 1806-9.

LOBODA, A., DAMULEWICZ, M., PYZA, E., JOZKOWICZ, A. & DULAK, J. 2016. Role of Nrf2/HO-1 system in development, oxidative stress response and diseases: an evolutionarily conserved mechanism. *Cell Mol Life Sci,* 73**,** 3221-47.

LOPEZ-OTIN, C., BLASCO, M. A., PARTRIDGE, L., SERRANO, M. & KROEMER, G. 2013. The hallmarks of aging. *Cell,* 153**,** 1194-217.

LU, J., PARK, J. H., LIU, A. Y. & CHEN, K. Y. 2000. Activation of heat shock factor 1 by hyperosmotic or hypo-osmotic stress is drastically attenuated in normal human fibroblasts during senescence. *J Cell Physiol,* 184**,** 183-90.

LUJAMBIO, A. 2016. To clear, or not to clear (senescent cells)? That is the question. *Bioessays,* 38 Suppl 1**,** S56-64.

LUSHCHAK, V. I. 2014. Free radicals, reactive oxygen species, oxidative stress and its classification. *Chem Biol Interact,* 224**,** 164-75.

MA, W., TRUSINA, A., EL-SAMAD, H., LIM, W. A. & TANG, C. 2009. Defining network topologies that can achieve biochemical adaptation. *Cell,* 138**,** 760-73.

MA, X. & GAO, L. 2012. Biological network analysis: insights into structure and functions. *Briefings in Functional Genomics,* 11**,** 434-442.

MACHADO, D., COSTA, R. S., ROCHA, M., FERREIRA, E. C., TIDOR, B. & ROCHA, I. 2011. Modeling formalisms in Systems Biology. *AMB Express,* 1**,** 45.

MADAMANCHI, N. R. & RUNGE, M. S. 2013. Redox signaling in cardiovascular health and disease. *Free Radic Biol Med,* 61**,** 473-501.

MAHER, P. 2005. The effects of stress and aging on glutathione metabolism. *Ageing Res Rev,* 4**,** 288-314.

MANABE, Y., MIYATAKE, S., TAKAGI, M., NAKAMURA, M., OKEDA, A., NAKANO, T., HIRSHMAN, M. F., GOODYEAR, L. J. & FUJII, N. L. 2012. Characterization of an acute muscle contraction model using cultured C2C12 myotubes. *PLoS One,* 7**,** e52592.

MANDA, G., ISVORANU, G., COMANESCU, M. V., MANEA, A., DEBELEC BUTUNER, B. & KORKMAZ, K. S. 2015. The redox biology network in cancer pathophysiology and therapeutics. *Redox Biol,* 5**,** 347-57.

MARAZITA, M. C., DUGOUR, A., MARQUIONI-RAMELLA, M. D., FIGUEROA, J. M. & SUBURO, A. M. 2016. Oxidative stress-induced premature senescence dysregulates VEGF and CFH expression in retinal pigment epithelial cells: Implications for Age-related Macular Degeneration. *Redox Biol,* 7**,** 78-87.

MARENGO, B., NITTI, M., FURFARO, A. L., COLLA, R., CIUCIS, C. D., MARINARI, U. M., PRONZATO, M. A., TRAVERSO, N. & DOMENICOTTI, C. 2016. Redox Homeostasis and Cellular Antioxidant Systems: Crucial Players in Cancer Growth and Therapy. *Oxid Med Cell Longev,* 2016**,** 6235641.

MARGIOCCO, M. L., BORGARELLI, M., MUSCH, T. I., HIRAI, D. M., HAGEMAN, K. S., FELS, R. J., GARCIA, A. A. & KENNEY, M. J. 2010. Effects of combined aging and heart failure on visceral sympathetic nerve and cardiovascular responses to progressive hyperthermia in F344 rats. *Am J Physiol Regul Integr Comp Physiol,* 299**,** R1555-63.

MARINHO, H. S., CYRNE, L., CADENAS, E. & ANTUNES, F. 2013. H2O2 delivery to cells: steady-state versus bolus addition. *Methods Enzymol,* 526**,** 159-73.

MARINHO, H. S., REAL, C., CYRNE, L., SOARES, H. & ANTUNES, F. 2014. Hydrogen peroxide sensing, signaling and regulation of transcription factors. *Redox Biol,* 2**,** 535-62.

MARTIN-RUIZ, C., JAGGER, C., KINGSTON, A., COLLERTON, J., CATT, M., DAVIES, K., DUNN, M., HILKENS, C., KEAVNEY, B., PEARCE, S. H., DEN ELZEN, W. P., TALBOT, D., WILEY, L., BOND, J., MATHERS, J. C., ECCLES, M. P., ROBINSON, L., JAMES, O., KIRKWOOD, T. B. & VON ZGLINICKI, T. 2011. Assessment of a large panel of candidate biomarkers of ageing in the Newcastle 85+ study. *Mech Ageing Dev,* 132**,** 496-502.

MARTINEZ-LOPEZ, N., ATHONVARANGKUL, D. & SINGH, R. 2015. Autophagy and aging. *Adv Exp Med Biol,* 847**,** 73-87.

MASOUD, G. N. & LI, W. 2015. HIF-1alpha pathway: role, regulation and intervention for cancer therapy. *Acta Pharm Sin B,* 5**,** 378-89.

MAST, F. D., RATUSHNY, A. V. & AITCHISON, J. D. 2014. Systems cell biology. *J Cell Biol,* 206**,** 695-706.

MATERI, W. & WISHART, D. S. 2007. Computational systems biology in cancer: modeling methods and applications. *Gene Regul Syst Bio,* 1**,** 91-110.

MATJUSAITIS, M., CHIN, G., SARNOSKI, E. A. & STOLZING, A. 2016. Biomarkers to identify and isolate senescent cells. *Ageing Res Rev,* 29**,** 1-12.

MAZZARELLO, P. 1999. A unifying concept: the history of cell theory. *Nat Cell Biol,* 1**,** E13-5.

MC AULEY, M. T., GUIMERA, A. M., HODGSON, D., MCDONALD, N., MOONEY, K. M., MORGAN, A. E. & PROCTOR, C. J. 2017. Modelling the molecular mechanisms of aging. *Biosci Rep,* 37.

MC AULEY, M. T. & MOONEY, K. M. 2015. Computational systems biology for aging research. *Interdiscip Top Gerontol,* 40**,** 35-48.

MCARDLE, A., PATTWELL, D., VASILAKI, A., GRIFFITHS, R. D. & JACKSON, M. J. 2001. Contractile activity-induced oxidative stress: cellular origin and adaptive responses. *Am J Physiol Cell Physiol,* 280**,** C621-7.

MCBEAN, G. J., ASLAN, M., GRIFFITHS, H. R. & TORRAO, R. C. 2015. Thiol redox homeostasis in neurodegenerative disease. *Redox Biol,* 5**,** 186-94.

MCCORD, J. M. & FRIDOVICH, I. 1969. Superoxide dismutase an enzymic function for erythrocuprein (hemocuprein). *Journal of Biological chemistry,* 244**,** 6049-6055.

MCDONAGH, B., SAKELLARIOU, G. K. & JACKSON, M. J. 2014a. Application of redox proteomics to skeletal muscle aging and exercise. *Biochem Soc Trans,* 42**,** 965-70.

MCDONAGH, B., SAKELLARIOU, G. K., SMITH, N. T., BROWNRIDGE, P. & JACKSON, M. J. 2014b. Differential cysteine labeling and global label-free proteomics reveals an altered metabolic state in skeletal muscle aging. *J Proteome Res,* 13**,** 5008-21.

MCGUIRE, J., HERMAN, J. P., HORN, P. S., SALLEE, F. R. & SAH, R. 2010. Enhanced fear recall and emotional arousal in rats recovering from chronic variable stress. *Physiol Behav,* 101**,** 474-82.

MEDAWAR, P. B. 1952. *An unsolved problem of biology*, College.

MEDVEDEV, Z. A. 1990. An attempt at a rational classification of theories of ageing. *Biol Rev Camb Philos Soc,* 65**,** 375-98.

MELLOR, K. M., CURL, C. L., CHANDRAMOULI, C., PEDRAZZINI, T., WENDT, I. R. & DELBRIDGE, L. M. 2014. Ageing-related cardiomyocyte functional decline is sex and angiotensin II dependent. *Age (Dordr),* 36**,** 9630.

MIGUEL, F., AUGUSTO, A. C. & GURGUEIRA, S. A. 2009. Effect of acute vs chronic H2O2-induced oxidative stress on antioxidant enzyme activities. *Free Radic Res,* 43**,** 340-7.

MILLER, C. J., GOUNDER, S. S., KANNAN, S., GOUTAM, K., MUTHUSAMY, V. R., FIRPO, M. A., SYMONS, J. D., PAINE, R., 3RD, HOIDAL, J. R. & RAJASEKARAN, N. S. 2012. Disruption of Nrf2/ARE signaling impairs antioxidant mechanisms and promotes cell degradation pathways in aged skeletal muscle. *Biochim Biophys Acta,* 1822**,** 1038-50.

MILLER, G. E., CHEN, E. & ZHOU, E. S. 2007. If it goes up, must it come down? Chronic stress and the hypothalamic-pituitary-adrenocortical axis in humans. *Psychol Bull,* 133**,** 25-45.

MILLONIG, G., GANZLEBEN, I., PECCERELLA, T., CASANOVAS, G., BRODZIAK-JAROSZ, L., BREITKOPF-HEINLEIN, K., DICK, T. P., SEITZ, H. K., MUCKENTHALER, M. U. & MUELLER, S. 2012. Sustained submicromolar H2O2 levels induce hepcidin via signal transducer and activator of transcription 3 (STAT3). *J Biol Chem,* 287**,** 37472-82.

MILO, R., SHEN-ORR, S., ITZKOVITZ, S., KASHTAN, N., CHKLOVSKII, D. & ALON, U. 2002. Network motifs: simple building blocks of complex networks. *Science,* 298**,** 824-7.

MITNITSKI, A. B., RUTENBERG, A. D., FARRELL, S. & ROCKWOOD, K. 2017. Aging, frailty and complex networks. *Biogerontology,* 18**,** 433-446.

MITRA, K., CARVUNIS, A.-R., RAMESH, S. K. & IDEKER, T. 2013. Integrative approaches for finding modular structure in biological networks. *Nature reviews. Genetics,* 14**,** 719-732.

MITROPHANOV, A. Y. & GROISMAN, E. A. 2008. Positive feedback in cellular control systems. *Bioessays,* 30**,** 542-55.

MIZOGUCHI, K., YUZURIHARA, M., ISHIGE, A., SASAKI, H., CHUI, D. H. & TABIRA, T. 2001. Chronic stress differentially regulates glucocorticoid negative feedback response in rats. *Psychoneuroendocrinology,* 26**,** 443-59.

MOONEY, K. M., MORGAN, A. E. & MC AULEY, M. T. 2016. Aging and computational systems biology. *Wiley Interdiscip Rev Syst Biol Med,* 8**,** 123-39.

MORGAN, M. J. & LIU, Z. G. 2011. Crosstalk of reactive oxygen species and NF-kappaB signaling. *Cell Res,* 21**,** 103-15.

MORITA, K., SAITOH, M., TOBIUME, K., MATSUURA, H., ENOMOTO, S., NISHITOH, H. & ICHIJO, H. 2001. Negative feedback regulation of ASK1 by protein phosphatase 5 (PP5) in response to oxidative stress. *EMBO J,* 20**,** 6028-36.

MORLEY, A. A. 1995. The somatic mutation theory of ageing. *Mutat Res,* 338**,** 19-23.

MOYER, J. R., JR., THOMPSON, L. T., BLACK, J. P. & DISTERHOFT, J. F. 1992. Nimodipine increases excitability of rabbit CA1 pyramidal neurons in an age- and concentration-dependent manner. *J Neurophysiol,* 68**,** 2100-9.

MUELLER, S., MILLONIG, G. & WAITE, G. N. 2009. The GOX/CAT system: a novel enzymatic method to independently control hydrogen peroxide and hypoxia in cell culture. *Adv Med Sci,* 54**,** 121-35.

MURARO, D., LARRIEU, A., LUCAS, M., CHOPARD, J., BYRNE, H., GODIN, C. & KING, J. 2016. A multi-scale model of the interplay between cell signalling and hormone transport in specifying the root meristem of Arabidopsis thaliana. *J Theor Biol,* 404**,** 182-205.

MURCHISON, D. & GRIFFITH, W. H. 1998. Increased calcium buffering in basal forebrain neurons during aging. *J Neurophysiol,* 80**,** 350-64.

NANDURI, J., VADDI, D. R., KHAN, S. A., WANG, N., MAKARENKO, V., SEMENZA, G. L. & PRABHAKAR, N. R. 2015. HIF-1alpha activation by intermittent hypoxia requires NADPH oxidase stimulation by xanthine oxidase. *PLoS One,* 10**,** e0119762.

NARICI, M. V. & MAFFULLI, N. 2010. Sarcopenia: characteristics, mechanisms and functional significance. *British Medical Bulletin,* 95**,** 139-159.

NELSON, G., WORDSWORTH, J., WANG, C., JURK, D., LAWLESS, C., MARTIN-RUIZ, C. & VON ZGLINICKI, T. 2012. A senescent cell bystander effect: senescence-induced senescence. *Aging Cell,* 11**,** 345-9.

NETTO, L. E. & ANTUNES, F. 2016. The Roles of Peroxiredoxin and Thioredoxin in Hydrogen Peroxide Sensing and in Signal Transduction. *Mol Cells,* 39**,** 65-71.

NITURE, S. K. & JAISWAL, A. K. 2009. Prothymosin-alpha mediates nuclear import of the INrf2/Cul3 Rbx1 complex to degrade nuclear Nrf2. *J Biol Chem,* 284**,** 13856-68.

NORRIS, C. M., HALPAIN, S. & FOSTER, T. C. 1998. Reversal of age-related alterations in synaptic plasticity by blockade of L-type Ca2+ channels. *Journal of Neuroscience,* 18**,** 3171-3179.

O'HARA, L., LIVIGNI, A., THEO, T., BOYER, B., ANGUS, T., WRIGHT, D., CHEN, S. H., RAZA, S., BARNETT, M. W., DIGARD, P., SMITH, L. B. & FREEMAN, T. C. 2016. Modelling the Structure and Dynamics of Biological Pathways. *PLoS Biol,* 14**,** e1002530.

O'MAHONY, F. C., NANDA, J., LAIRD, A., MULLEN, P., CALDWELL, H., OVERTON, I. M., EORY, L., O'DONNELL, M., FARATIAN, D., POWLES, T., HARRISON, D. J. &

STEWART, G. D. 2013. The use of reverse phase protein arrays (RPPA) to explore protein expression variation within individual renal cell cancers. *J Vis Exp*.

OH, M. M., OLIVEIRA, F. A. & DISTERHOFT, J. F. 2010. Learning and aging related changes in intrinsic neuronal excitability. *Front Aging Neurosci,* 2**,** 2.

OLIVEIRA-MARQUES, V., MARINHO, H. S., CYRNE, L. & ANTUNES, F. 2009. Role of hydrogen peroxide in NF-kappaB activation: from inducer to modulator. *Antioxid Redox Signal,* 11**,** 2223-43.

OSTRANDER, M. M., ULRICH-LAI, Y. M., CHOI, D. C., RICHTAND, N. M. & HERMAN, J. P. 2006. Hypoactivity of the hypothalamo-pituitary-adrenocortical axis during recovery from chronic variable stress. *Endocrinology,* 147**,** 2008-17.

PALOMERO, J., VASILAKI, A., PYE, D., MCARDLE, A. & JACKSON, M. J. 2013. Aging increases the oxidation of dichlorohydrofluorescein in single isolated skeletal muscle fibers at rest, but not during contractions. *Am J Physiol Regul Integr Comp Physiol,* 305**,** R351-8.

PAPADOPOULOS, S., JURGENS, K. D. & GROS, G. 2000. Protein diffusion in living skeletal muscle fibers: dependence on protein size, fiber type, and contraction. *Biophys J,* 79**,** 2084-94.

PAPAIAHGARI, S., ZHANG, Q., KLEEBERGER, S. R., CHO, H. Y. & REDDY, S. P. 2006. Hyperoxia stimulates an Nrf2-ARE transcriptional response via ROS-EGFR-PI3K-Akt/ERK MAP kinase signaling in pulmonary epithelial cells. *Antioxid Redox Signal,* 8**,** 43-52.

PARTRIDGE, L. 2010. The new biology of ageing. *Philosophical Transactions of the Royal Society B: Biological Sciences,* 365**,** 147-154.

PASCALE, A. & GOVONI, S. 2016. Cerebral Aging: Implications for the Heart Autonomic Nervous System Regulation. *In:* GRONDA, E., VANOLI, E. & COSTEA, A. (eds.) *Heart Failure Management: The Neural Pathways.* Cham: Springer International Publishing.

PASSOS, J. F., NELSON, G. & VON ZGLINICKI, T. 2008. Telomeres, Senescence, Oxidative Stress, and Heterogeneity. *In:* RUDOLPH, K. L. (ed.) *Telomeres and Telomerase in Ageing, Disease, and Cancer: Molecular Mechanisms of Adult Stem Cell Ageing.* Berlin, Heidelberg: Springer Berlin Heidelberg.

PASSOS, J. F., NELSON, G., WANG, C., RICHTER, T., SIMILLION, C., PROCTOR, C. J., MIWA, S., OLIJSLAGERS, S., HALLINAN, J., WIPAT, A., SARETZKI, G., RUDOLPH, K. L., KIRKWOOD, T. B. & VON ZGLINICKI, T. 2010. Feedback between p21 and reactive oxygen production is necessary for cell senescence. *Mol Syst Biol,* 6**,** 347.

PASSOS, J. F., SARETZKI, G., AHMED, S., NELSON, G., RICHTER, T., PETERS, H., WAPPLER, I., BIRKET, M. J., HAROLD, G., SCHAEUBLE, K., BIRCH-MACHIN, M. A., KIRKWOOD, T. B. & VON ZGLINICKI, T. 2007. Mitochondrial dysfunction accounts for the stochastic heterogeneity in telomere-dependent senescence. *PLoS Biol,* 5**,** e110.

PEARSON, T., KABAYO, T., NG, R., CHAMBERLAIN, J., MCARDLE, A. & JACKSON, M. J. 2014. Skeletal muscle contractions induce acute changes in cytosolic superoxide, but slower responses in mitochondrial superoxide and cellular hydrogen peroxide. *PLoS One,* 9**,** e96378.

PENDYALA, S., GORSHKOVA, I. A., USATYUK, P. V., HE, D., PENNATHUR, A., LAMBETH, J. D., THANNICKAL, V. J. & NATARAJAN, V. 2009. Role of Nox4 and Nox2 in

hyperoxia-induced reactive oxygen species generation and migration of human lung endothelial cells. *Antioxid Redox Signal,* 11**,** 747-64.

PERKINS, A., NELSON, K. J., PARSONAGE, D., POOLE, L. B. & KARPLUS, P. A. 2015. Peroxiredoxins: guardians against oxidative stress and modulators of peroxide signaling. *Trends Biochem Sci,* 40**,** 435-45.

PICKERING, A. M., VOJTOVICH, L., TOWER, J. & KJ, A. D. 2013. Oxidative stress adaptation with acute, chronic, and repeated stress. *Free Radic Biol Med,* 55**,** 109-18.

PILLAY, C. S., EAGLING, B. D., DRISCOLL, S. R. & ROHWER, J. M. 2016. Quantitative measures for redox signaling. *Free Radic Biol Med,* 96**,** 290-303.

PILLAY, C. S., HOFMEYR, J. H., MASHAMAITE, L. N. & ROHWER, J. M. 2013. From top-down to bottom-up: computational modeling approaches for cellular redoxin networks. *Antioxid Redox Signal,* 18**,** 2075-86.

POWERS, S. K. & JACKSON, M. J. 2008. Exercise-induced oxidative stress: cellular mechanisms and impact on muscle force production. *Physiol Rev,* 88**,** 1243-76.

POWERS, S. K., SMUDER, A. J. & JUDGE, A. R. 2012. Oxidative stress and disuse muscle atrophy: cause or consequence? *Curr Opin Clin Nutr Metab Care,* 15**,** 240-5.

PRATT, D. A., TALLMAN, K. A. & PORTER, N. A. 2011. Free radical oxidation of polyunsaturated lipids: New mechanistic insights and the development of peroxyl radical clocks. *Acc Chem Res,* 44**,** 458-67.

PRESCOTT, S. A. & CHASE, R. 1999. Sites of plasticity in the neural circuit mediating tentacle withdrawal in the snail Helix aspersa: implications for behavioral change and learning kinetics. *Learn Mem,* 6**,** 363-80.

PROCTOR, C. J., PIENAAR, I. S., ELSON, J. L. & KIRKWOOD, T. B. 2012. Aggregation, impaired degradation and immunization targeting of amyloid-beta dimers in Alzheimer's disease: a stochastic modelling approach. *Mol Neurodegener,* 7**,** 32.

PROMISLOW, D. E. 1994. DNA repair and the evolution of longevity: a critical analysis. *J Theor Biol,* 170**,** 291-300.

PRONK, T. E., VAN DER VEEN, J. W., VANDEBRIEL, R. J., VAN LOVEREN, H., DE VINK, E. P. & PENNINGS, J. L. 2014. Comparison of the molecular topologies of stress-activated transcription factors HSF1, AP-1, NRF2, and NF-kappaB in their induction kinetics of HMOX1. *Biosystems,* 124**,** 75-85.

QIN, F., SIWIK, D. A., LANCEL, S., ZHANG, J., KUSTER, G. M., LUPTAK, I., WANG, L., TONG, X., KANG, Y. J., COHEN, R. A. & COLUCCI, W. S. 2013. Hydrogen peroxide-mediated SERCA cysteine 674 oxidation contributes to impaired cardiac myocyte relaxation in senescent mouse heart. *J Am Heart Assoc,* 2**,** e000184.

QUARTERONI, A., LASSILA, T., ROSSI, S. & RUIZ-BAIER, R. 2017. Integrated Heart—Coupling multiscale and multiphysics models for the simulation of the cardiac function. *Computer Methods in Applied Mechanics and Engineering,* 314**,** 345-407.

RADAK, Z., CHUNG, H. Y., KOLTAI, E., TAYLOR, A. W. & GOTO, S. 2008. Exercise, oxidative stress and hormesis. *Ageing Res Rev,* 7**,** 34-42.

RAHI, SAHAND J., PECANI, K., ONDRACKA, A., OIKONOMOU, C. & CROSS, FREDERICK R. 2016. The CDK-APC/C Oscillator Predominantly Entrains Periodic Cell-Cycle Transcription. *Cell,* 165**,** 475-487.

RAINS, J. L. & JAIN, S. K. 2011. Oxidative stress, insulin signaling, and diabetes. *Free Radic Biol Med,* 50**,** 567-75.

RAMASWAMI, M. 2014. Network plasticity in adaptive filtering and behavioral habituation. *Neuron,* 82**,** 1216-29.

RATTO, M., Castelletti, A., Pagano, A. 2012. Emulation techniques for the reduction and sensitivity analysis of complex environmental models. *Environmental Modelling and Software*, 34, 1-116.

RAUE, A., KREUTZ, C., MAIWALD, T., BACHMANN, J., SCHILLING, M., KLINGMULLER, U. & TIMMER, J. 2009. Structural and practical identifiability analysis of partially observed dynamical models by exploiting the profile likelihood. *Bioinformatics,* 25**,** 1923-9.

RAZA, M., DESHPANDE, L. S., BLAIR, R. E., CARTER, D. S., SOMBATI, S. & DELORENZO, R. J. 2007. Aging is associated with elevated intracellular calcium levels and altered calcium homeostatic mechanisms in hippocampal neurons. *Neurosci Lett,* 418**,** 77-81.

REID, M. B., KHAWLI, F. A. & MOODY, M. R. 1993. Reactive oxygen in skeletal muscle. III. Contractility of unfatigued muscle. *J Appl Physiol (1985),* 75**,** 1081-7.

REN, J., LI, Q., WU, S., LI, S. Y. & BABCOCK, S. A. 2007. Cardiac overexpression of antioxidant catalase attenuates aging-induced cardiomyocyte relaxation dysfunction. *Mech Ageing Dev,* 128**,** 276-85.

RIBOU, A. C. 2016. Synthetic Sensors for Reactive Oxygen Species Detection and Quantification: A Critical Review of Current Methods. *Antioxid Redox Signal,* 25**,** 520-33.

ROEDDING, A. S., TONG, S. Y., AU-YEUNG, W., LI, P. P. & WARSH, J. J. 2013. Chronic oxidative stress modulates TRPC3 and TRPM2 channel expression and function in rat primary cortical neurons: relevance to the pathophysiology of bipolar disorder. *Brain Res,* 1517**,** 16-27.

SAFDAR, A., DEBEER, J. & TARNOPOLSKY, M. A. 2010. Dysfunctional Nrf2–Keap1 redox signaling in skeletal muscle of the sedentary old. *Free Radical Biology and Medicine,* 49**,** 1487-1493.

SAKELLARIOU, G. K., JACKSON, M. J. & VASILAKI, A. 2014. Redefining the major contributors to superoxide production in contracting skeletal muscle. The role of NAD(P)H oxidases. *Free Radic Res,* 48**,** 12-29.

SALTELLI, A., Ratto, M., Andres, T., Campolongo, F., Cariboni, J., Gatelli, D., Saisana, M., Tarantola, S. 2008. Global Sensitivity Analysis. The Primer. *John Wiley & Sons, Ltd, Hoboken, N.J*

SANZ, A. 2016. Mitochondrial reactive oxygen species: Do they extend or shorten animal lifespan? *Biochim Biophys Acta,* 1857**,** 1116-26.

SAURO, H. M. 2011. *Enzyme kinetics for systems biology*, Future Skill Software.

SAURO, H. M. & KHOLODENKO, B. N. 2004. Quantitative analysis of signaling networks. *Prog Biophys Mol Biol,* 86**,** 5-43.

SCHIEBER, M. & CHANDEL, N. S. 2014. ROS function in redox signaling and oxidative stress. *Curr Biol,* 24**,** R453-62.

SCHILLING, M., MAIWALD, T., HENGL, S., WINTER, D., KREUTZ, C., KOLCH, W., LEHMANN, W. D., TIMMER, J. & KLINGMULLER, U. 2009. Theoretical and experimental analysis links isoform-specific ERK signalling to cell fate decisions. *Mol Syst Biol,* 5**,** 334.

SCHNEIDER, C. A., RASBAND, W. S. & ELICEIRI, K. W. 2012. NIH Image to ImageJ: 25 years of image analysis. *Nat Methods,* 9**,** 671-5.

SCHNELL, S. & TURNER, T. E. 2004. Reaction kinetics in intracellular environments with macromolecular crowding: simulations and rate laws. *Prog Biophys Mol Biol,* 85**,** 235-60.

SCHRODER, K. 2014. NADPH oxidases in redox regulation of cell adhesion and migration. *Antioxid Redox Signal,* 20**,** 2043-58.

SCIALO, F., SRIRAM, A., FERNANDEZ-AYALA, D., GUBINA, N., LOHMUS, M., NELSON, G., LOGAN, A., COOPER, H. M., NAVAS, P., ENRIQUEZ, J. A., MURPHY, M. P. & SANZ, A. 2016. Mitochondrial ROS Produced via Reverse Electron Transport Extend Animal Lifespan. *Cell Metab,* 23**,** 725-34.

SEALS, D. R. & ESLER, M. D. 2000. Human ageing and the sympathoadrenal system. *J Physiol,* 528**,** 407-17.

SELMAN, C., BLOUNT, J. D., NUSSEY, D. H. & SPEAKMAN, J. R. 2012. Oxidative damage, ageing, and life-history evolution: where now? *Trends in Ecology & Evolution,* 27**,** 570-577.

SEN, C. K. & ROY, S. 2008. Redox signals in wound healing. *Biochim Biophys Acta,* 1780**,** 1348-61.

SHANKAR, P., NISHIKAWA, M. & SHIBATA, T. 2015. Adaptive Responses Limited by Intrinsic Noise. *PLoS One,* 10**,** e0136095.

SHANNON, C. E. 1997. The mathematical theory of communication. 1963. *MD Comput,* 14**,** 306-17.

SHANNON, C. E. 2001. A mathematical theory of communication. *ACM SIGMOBILE Mobile Computing and Communications Review,* 5**,** 3-55.

SHEN-ORR, S. S., MILO, R., MANGAN, S. & ALON, U. 2002. Network motifs in the transcriptional regulation network of Escherichia coli. *Nat Genet,* 31**,** 64-8.

SHIRAISHI, T., MATSUYAMA, S. & KITANO, H. 2010. Large-scale analysis of network bistability for human cancers. *PLoS Comput Biol,* 6**,** e1000851.

SIES, H. 2015. Oxidative stress: a concept in redox biology and medicine. *Redox Biol,* 4**,** 180-3.

SINGER, M. A. 2016. The Origins of Aging: Evidence that Aging is an Adaptive Phenotype. *Curr Aging Sci,* 9**,** 95-115.

SINHA, K., DAS, J., PAL, P. B. & SIL, P. C. 2013. Oxidative stress: the mitochondria-dependent and mitochondria-independent pathways of apoptosis. *Arch Toxicol,* 87**,** 1157-80.

SOBOTTA, M. C., BARATA, A. G., SCHMIDT, U., MUELLER, S., MILLONIG, G. & DICK, T. P. 2013. Exposing cells to H2O2: a quantitative comparison between continuous low-dose and one-time high-dose treatments. *Free Radic Biol Med,* 60**,** 325-35.

SOBOTTA, M. C., LIOU, W., STOCKER, S., TALWAR, D., OEHLER, M., RUPPERT, T., SCHARF, A. N. & DICK, T. P. 2015. Peroxiredoxin-2 and STAT3 form a redox relay for H2O2 signaling. *Nat Chem Biol,* 11**,** 64-70.

SOGA, M., MATSUZAWA, A. & ICHIJO, H. 2012. Oxidative Stress-Induced Diseases via the ASK1 Signaling Pathway. *Int J Cell Biol,* 2012**,** 439587.

SOHAL, R. S. & ORR, W. C. 2012. The redox stress hypothesis of aging. *Free Radic Biol Med,* 52**,** 539-55.

SOROKIN, A., LE NOVERE, N., LUNA, A., CZAUDERNA, T., DEMIR, E., HAW, R., MI, H., MOODIE, S., SCHREIBER, F. & VILLEGER, A. 2015. Systems Biology Graphical Notation: Entity Relationship language Level 1 Version 2. *J Integr Bioinform,* 12**,** 264.

SOSA, V., MOLINE, T., SOMOZA, R., PACIUCCI, R., KONDOH, H. & ME, L. L. 2013. Oxidative stress and cancer: an overview. *Ageing Res Rev,* 12**,** 376-90.

SPENCER, N. F., POYNTER, M. E., IM, S. Y. & DAYNES, R. A. 1997. Constitutive activation of NF-kappa B in an animal model of aging. *Int Immunol,* 9**,** 1581-8.

SUPNET, C. & BEZPROZVANNY, I. 2010. The dysregulation of intracellular calcium in Alzheimer disease. *Cell Calcium,* 47**,** 183-9.

SWAN, C. L. & SISTONEN, L. 2015. Cellular stress response cross talk maintains protein and energy homeostasis. *EMBO J,* 34**,** 267-9.

SZILARD, L. 1959. On the Nature of the Aging Process. *Proc Natl Acad Sci U S A,* 45**,** 30-45.

SZUMIEL, I. 2015. Ionizing radiation-induced oxidative stress, epigenetic changes and genomic instability: the pivotal role of mitochondria. *Int J Radiat Biol,* 91**,** 1-12.

TAGUCHI, K., FUJIKAWA, N., KOMATSU, M., ISHII, T., UNNO, M., AKAIKE, T., MOTOHASHI, H. & YAMAMOTO, M. 2012. Keap1 degradation by autophagy for the maintenance of redox homeostasis. *Proc Natl Acad Sci U S A,* 109**,** 13561-6.

TAN, P. L., SHAVLAKADZE, T., GROUNDS, M. D. & ARTHUR, P. G. 2015a. Differential thiol oxidation of the signaling proteins Akt, PTEN or PP2A determines whether Akt phosphorylation is enhanced or inhibited by oxidative stress in C2C12 myotubes derived from skeletal muscle. *Int J Biochem Cell Biol,* 62**,** 72-9.

TAN, P. L., SHAVLAKADZE, T., GROUNDS, M. D. & ARTHUR, P. G. 2015b. Differential thiol oxidation of the signaling proteins Akt, PTEN or PP2A determines whether Akt phosphorylation is enhanced or inhibited by oxidative stress in C2C12 myotubes derived from skeletal muscle. *The International Journal of Biochemistry & Cell Biology,* 62**,** 72-79.

TEBAY, L. E., ROBERTSON, H., DURANT, S. T., VITALE, S. R., PENNING, T. M., DINKOVA-KOSTOVA, A. T. & HAYES, J. D. 2015. Mechanisms of activation of the transcription factor Nrf2 by redox stressors, nutrient cues, and energy status and the pathways through which it attenuates degenerative disease. *Free Radic Biol Med,* 88**,** 108-46.

TERMAN, A. & BRUNK, U. T. 2004. Aging as a catabolic malfunction. *Int J Biochem Cell Biol,* 36**,** 2365-75.

THAKUR, S., SARKAR, B., CHOLIA, R. P., GAUTAM, N., DHIMAN, M. & MANTHA, A. K. 2014. APE1/Ref-1 as an emerging therapeutic target for various human diseases: phytochemical modulation of its functions. *Exp Mol Med,* 46**,** e106.

THIBAULT, O., HADLEY, R. & LANDFIELD, P. W. 2001. Elevated postsynaptic [Ca2+]i and L-type calcium channel activity in aged hippocampal neurons: relationship to impaired synaptic plasticity. *J Neurosci,* 21**,** 9744-56.

THURLEY, K., GERECHT, D., FRIEDMANN, E. & HOFER, T. 2015. Three-Dimensional Gradients of Cytokine Signaling between T Cells. *PLoS Comput Biol,* 11**,** e1004206.

THURLEY, K., TOVEY, S. C., MOENKE, G., PRINCE, V. L., MEENA, A., THOMAS, A. P., SKUPIN, A., TAYLOR, C. W. & FALCKE, M. 2014. Reliable encoding of stimulus intensities within random sequences of intracellular Ca2+ spikes. *Sci Signal,* 7**,** ra59.

TILSTRA, J. S., CLAUSON, C. L., NIEDERNHOFER, L. J. & ROBBINS, P. D. 2011. NF-kappaB in Aging and Disease. *Aging Dis,* 2**,** 449-65.

TOESCU, E. C. & VERKHRATSKY, A. 2004. Ca2+ and mitochondria as substrates for deficits in synaptic plasticity in normal brain ageing. *J Cell Mol Med,* 8**,** 181-90.

TOESCU, E. C. & VERKHRATSKY, A. 2007. The importance of being subtle: small changes in calcium homeostasis control cognitive decline in normal aging. *Aging Cell,* 6**,** 267-73.

TOMALIN, L. E., DAY, A. M., UNDERWOOD, Z. E., SMITH, G. R., DALLE PEZZE, P., RALLIS, C., PATEL, W., DICKINSON, B. C., BAHLER, J., BREWER, T. F., CHANG, C. J.,

SHANLEY, D. P. & VEAL, E. A. 2016. Increasing extracellular H2O2 produces a bi-phasic response in intracellular H2O2, with peroxiredoxin hyperoxidation only triggered once the cellular H2O2-buffering capacity is overwhelmed. *Free Radic Biol Med,* 95**,** 333-48.

TOSATO, M., ZAMBONI, V., FERRINI, A. & CESARI, M. 2007. The aging process and potential interventions to extend life expectancy. *Clin Interv Aging,* 2**,** 401-12.

TOYOSHIMA, Y., KAKUDA, H., FUJITA, K. A., UDA, S. & KURODA, S. 2012. Sensitivity control through attenuation of signal transfer efficiency by negative regulation of cellular signalling. *Nat Commun,* 3**,** 743.

TRACHOOTHAM, D., LU, W., OGASAWARA, M. A., NILSA, R. D. & HUANG, P. 2008. Redox regulation of cell survival. *Antioxid Redox Signal,* 10**,** 1343-74.

TREBILCOCK, G. U. & PONNAPPAN, U. 1996. Induction and regulation of NFkappaB during aging: role of protein kinases. *Clin Immunol Immunopathol,* 79**,** 87-91.

TRUONG, T. H. & CARROLL, K. S. 2012. Redox regulation of epidermal growth factor receptor signaling through cysteine oxidation. *Biochemistry,* 51**,** 9954-65.

TU, Y. 2013. Quantitative modeling of bacterial chemotaxis: signal amplification and accurate adaptation. *Annu Rev Biophys,* 42**,** 337-59.

TURRENS, J. F. 2003. Mitochondrial formation of reactive oxygen species. *J Physiol,* 552**,** 335-44.

UDA, S. & KURODA, S. 2016. Analysis of cellular signal transduction from an information theoretic approach. *Semin Cell Dev Biol,* 51**,** 24-31.

UDA, S., SAITO, T. H., KUDO, T., KOKAJI, T., TSUCHIYA, T., KUBOTA, H., KOMORI, Y., OZAKI, Y. & KURODA, S. 2013. Robustness and compensation of information transmission of signaling pathways. *Science,* 341**,** 558-61.

UNGVARI, Z., BAILEY-DOWNS, L., GAUTAM, T., SOSNOWSKA, D., WANG, M., MONTICONE, R. E., TELLJOHANN, R., PINTO, J. T., DE CABO, R., SONNTAG, W. E., LAKATTA, E. G. & CSISZAR, A. 2011a. Age-associated vascular oxidative stress, Nrf2 dysfunction, and NF-{kappa}B activation in the nonhuman primate Macaca mulatta. *J Gerontol A Biol Sci Med Sci,* 66**,** 866-75.

UNGVARI, Z., BAILEY-DOWNS, L., SOSNOWSKA, D., GAUTAM, T., KONCZ, P., LOSONCZY, G., BALLABH, P., DE CABO, R., SONNTAG, W. E. & CSISZAR, A. 2011b. Vascular oxidative stress in aging: a homeostatic failure due to dysregulation of NRF2-mediated antioxidant response. *Am J Physiol Heart Circ Physiol,* 301**,** H363-72.

VAN DEURSEN, J. M. 2014. The role of senescent cells in ageing. *Nature,* 509**,** 439-446.

VASILAKI, A., JACKSON, M. J. & MCARDLE, A. 2002. Attenuated HSP70 response in skeletal muscle of aged rats following contractile activity. *Muscle Nerve,* 25**,** 902-5.

VASILAKI, A., MANSOURI, A., VAN REMMEN, H., VAN DER MEULEN, J. H., LARKIN, L., RICHARDSON, A. G., MCARDLE, A., FAULKNER, J. A. & JACKSON, M. J. 2006a. Free radical generation by skeletal muscle of adult and old mice: effect of contractile activity. *Aging Cell,* 5**,** 109-17.

VASILAKI, A., MCARDLE, F., IWANEJKO, L. M. & MCARDLE, A. 2006b. Adaptive responses of mouse skeletal muscle to contractile activity: The effect of age. *Mech Ageing Dev,* 127**,** 830-9.

VEAL, E. & DAY, A. 2011. Hydrogen peroxide as a signaling molecule. *Antioxid Redox Signal,* 15**,** 147-51.

VERKHRATSKY, A., SHMIGOL, A., KIRISCHUK, S., PRONCHUK, N. & KOSTYUK, P. 1994. Age-dependent changes in calcium currents and calcium homeostasis in mammalian neurons. *Ann N Y Acad Sci,* 747**,** 365-81.

VILLAVERDE, A. F. & BANGA, J. R. 2014. Reverse engineering and identification in systems biology: strategies, perspectives and challenges. *J R Soc Interface,* 11**,** 20130505.

VINA, J., BORRAS, C., ABDELAZIZ, K. M., GARCIA-VALLES, R. & GOMEZ-CABRERA, M. C. 2013. The free radical theory of aging revisited: the cell signaling disruption theory of aging. *Antioxid Redox Signal,* 19**,** 779-87.

VIZAN, P., MILLER, D. S., GORI, I., DAS, D., SCHMIERER, B. & HILL, C. S. 2013. Controlling long-term signaling: receptor dynamics determine attenuation and refractory behavior of the TGF-beta pathway. *Sci Signal,* 6**,** ra106.

VON ZGLINICKI, T., SARETZKI, G., DOCKE, W. & LOTZE, C. 1995. Mild hyperoxia shortens telomeres and inhibits proliferation of fibroblasts: a model for senescence? *Exp Cell Res,* 220**,** 186-93.

WAGNER, B. A., WITMER, J. R., VAN 'T ERVE, T. J. & BUETTNER, G. R. 2013. An Assay for the Rate of Removal of Extracellular Hydrogen Peroxide by Cells. *Redox Biol,* 1**,** 210-217.

WANG, H. X., WU, X. R., YANG, H., YIN, C. L., SHI, L. J. & WANG, X. J. 2013. Urotensin II inhibits skeletal muscle glucose transport signaling pathways via the NADPH oxidase pathway. *PLoS One,* 8**,** e76796.

WANG, M., WEISS, M., SIMONOVIC, M., HAERTINGER, G., SCHRIMPF, S. P., HENGARTNER, M. O. & VON MERING, C. 2012a. PaxDb, a database of protein abundance averages across all three domains of life. *Mol Cell Proteomics,* 11**,** 492-500.

WANG, X. & HAI, C. 2016. Novel insights into redox system and the mechanism of redox regulation. *Mol Biol Rep,* 43**,** 607-28.

WANG, Y., LIU, Q., ZHAO, W., ZHOU, X., MIAO, G., SUN, C. & ZHANG, H. 2017. NADPH Oxidase Activation Contributes to Heavy Ion Irradiation-Induced Cell Death. *Dose Response,* 15**,** 1559325817699697.

WANG, Y., PASZEK, P., HORTON, C. A., YUE, H., WHITE, M. R., KELL, D. B., MULDOON, M. R. & BROOMHEAD, D. S. 2012b. A systematic survey of the response of a model NF-kappaB signalling pathway to TNFalpha stimulation. *J Theor Biol,* 297**,** 137-47.

WANG, Z., BUTNER, J. D., KERKETTA, R., CRISTINI, V. & DEISBOECK, T. S. 2015. Simulating cancer growth with multiscale agent-based modeling. *Semin Cancer Biol,* 30**,** 70-8.

WARDYN, J. D., PONSFORD, A. H. & SANDERSON, C. M. 2015. Dissecting molecular cross-talk between Nrf2 and NF-kappaB response pathways. *Biochem Soc Trans,* 43**,** 621-6.

WARMFLASH, A., FRANCOIS, P. & SIGGIA, E. D. 2012. Pareto evolution of gene networks: an algorithm to optimize multiple fitness objectives. *Phys Biol,* 9**,** 056001.

WEISLEDER, N. & MA, J. 2008. Altered Ca2+ sparks in aging skeletal and cardiac muscle. *Ageing Res Rev,* 7**,** 177-88.

WEISMANN, A., POULTON, E. B., SCHÖNLAND, S. & SHIPLEY, A. E. 1891. *Essays upon heredity and kindred biological problems, by Dr. August Weismann. Ed. by Edward B. Poulton, Selmar Schönland, and Arthur E. Shipley. Authorised translation,* Oxford, Clarendon Press.

WILLIAMS, G. C. 1957. Pleiotropy, Natural Selection, and the Evolution of Senescence. *Evolution***,** 398-411.

WILLIAMS, R., TIMMIS, J. & QWARNSTROM, E. 2014. Computational Models of the NF-KB Signalling Pathway. *Computation,* 2**,** 131.

WINTERBOURN, C. C. 2008. Reconciling the chemistry and biology of reactive oxygen species. *Nat Chem Biol,* 4**,** 278-86.

WINTERBOURN, C. C. 2015. Are free radicals involved in thiol-based redox signaling? *Free Radic Biol Med,* 80**,** 164-70.

WOO, H. A., YIM, S. H., SHIN, D. H., KANG, D., YU, D. Y. & RHEE, S. G. 2010. Inactivation of peroxiredoxin I by phosphorylation allows localized H(2)O(2) accumulation for cell signaling. *Cell,* 140**,** 517-28.

WOOLLEY, J. F., STANICKA, J. & COTTER, T. G. 2013. Recent advances in reactive oxygen species measurement in biological systems. *Trends Biochem Sci,* 38**,** 556-65.

XI, J. Y. & OUYANG, Q. 2016. Using Sub-Network Combinations to Scale Up an Enumeration Method for Determining the Network Structures of Biological Functions. *PLoS One,* 11**,** e0168214.

XIAO, R. P., SPURGEON, H. A., O'CONNOR, F. & LAKATTA, E. G. 1994. Age-associated changes in beta-adrenergic modulation on rat cardiac excitation-contraction coupling. *J Clin Invest,* 94**,** 2051-9.

XIAO, Z. Q. & MAJUMDAR, A. P. 2000. Induction of transcriptional activity of AP-1 and NF-kappaB in the gastric mucosa during aging. *Am J Physiol Gastrointest Liver Physiol,* 278**,** G855-65.

XIONG, J., VERKHRATSKY, A. & TOESCU, E. C. 2002. Changes in mitochondrial status associated with altered Ca2+ homeostasis in aged cerebellar granule neurons in brain slices. *J Neurosci,* 22**,** 10761-71.

YAN, Z. Q., SIRSJO, A., BOCHATON-PIALLAT, M. L., GABBIANI, G. & HANSSON, G. K. 1999. Augmented expression of inducible NO synthase in vascular smooth muscle cells during aging is associated with enhanced NF-kappaB activation. *Arterioscler Thromb Vasc Biol,* 19**,** 2854-62.

YOO, H. J., IM, C. N., YOUN, D. Y., YUN, H. H. & LEE, J. H. 2014. Bis is Induced by Oxidative Stress via Activation of HSF1. *Korean J Physiol Pharmacol,* 18**,** 403-9.

YU, X., WANG, P., SHI, Z., DONG, K., FENG, P., WANG, H. & WANG, X. 2015. Urotensin-II-Mediated Reactive Oxygen Species Generation via NADPH Oxidase Pathway Contributes to Hepatic Oval Cell Proliferation. *PLoS One,* 10**,** e0144433.

YUAN, Q., CHEN, Z., SANTULLI, G., GU, L., YANG, Z.-G., YUAN, Z.-Q., ZHAO, Y.-T., XIN, H.-B., DENG, K.-Y., WANG, S.-Q. & JI, G. 2014. Functional Role of Calstabin2 in Age-related Cardiac Alterations. 4**,** 7425.

ZHANG, H., DAVIES, K. J. & FORMAN, H. J. 2015a. Oxidative stress response and Nrf2 signaling in aging. *Free Radic Biol Med,* 88**,** 314-36.

ZHANG, H., LIU, H., DAVIES, K. J., SIOUTAS, C., FINCH, C. E., MORGAN, T. E. & FORMAN, H. J. 2012. Nrf2-regulated phase II enzymes are induced by chronic ambient nanoparticle exposure in young mice with age-related impairments. *Free Radic Biol Med,* 52**,** 2038-46.

ZHANG, M., AN, C., GAO, Y., LEAK, R. K., CHEN, J. & ZHANG, F. 2013. Emerging roles of Nrf2 and phase II antioxidant enzymes in neuroprotection. *Prog Neurobiol,* 100**,** 30-47.

ZHANG, Q., BHATTACHARYA, S., PI, J., CLEWELL, R. A., CARMICHAEL, P. L. & ANDERSEN, M. E. 2015b. Adaptive Posttranslational Control in Cellular Stress Response Pathways and Its Relationship to Toxicity Testing and Safety Assessment. *Toxicol Sci,* 147**,** 302-16.

ZHAO, X., WEISLEDER, N., THORNTON, A., OPPONG, Y., CAMPBELL, R., MA, J. & BROTTO, M. 2008. Compromised store-operated Ca2+ entry in aged skeletal muscle. *Aging Cell,* 7**,** 561-8.

ZOROV, D. B., JUHASZOVA, M. & SOLLOTT, S. J. 2014. Mitochondrial reactive oxygen species (ROS) and ROS-induced ROS release. *Physiol Rev,* 94**,** 909-50.